Radiation dose and radionuclide inventory characterization following a hypothetical nuclear criticality accident at a uranium processing facility

T.E. Sibiya

orcid.org/0000-0003-2042-978X

Dissertation accepted in partial fulfilment of the requirements for the degree *Master of Engineering in Nuclear Engineering* at the Potchefstroom Campus North-West University, South Africa

Supervisor Co-supervisor	Prof V.V. Naicker Mr T.J. van Rooyen
Graduation	June 2021
Student number	23291958

Declaration

I declare that this research manuscript is my own, unaided work. In early 2019, I received 5 days of initial guidance in the development of the MCNP calculation models, from my co-supervisor, Mr Johann van Rooyen based at the Radiation and Reactor Theory (RRT) department, Necsa[1]; he also assisted with the presentation in Appendix A. This dissertation is being submitted in partial fulfilment of the requirement for the degree Master of Engineering in the Unit of Energy and Technology systems in the Faculty of Engineering at the North West University, Potchefstroom Campus, South Africa. It has not been submitted before for any degree or examination in any other university.

Signature  Date 22 June 2021

[1] Necsa — the South African Nuclear Energy Corporation

Abstract

This study focused on a hypothetical nuclear criticality excursion in a **P**lutonium **U**ranium **R**eduction **EX**traction (PUREX) processing facility for the recovery of non-irradiated enriched uranium, which are present in scrap material from historical operations. The entire facility, including the fissile process-mass in the workstation where the hypothetical excursion takes place and, the concrete biological shielding walls and roof, was modelled in a series of calculation models using the radiation transport code, MCNP6.2. ENDF/B-8.0 nuclear data was used, and special thermal treatment of scattering kinetics was requested wherever possible, to accurately quantify the impact of the bound state of nuclides, on the thermal neutron energy spectrum. The calculation models were developed to quantify the neutron and photon doses resulting from the criticality excursion at a number of "human detector"[2] positions placed inside and around the PUREX facility. The design basis criticality accident is an excursion involving 10^{17} fission events, which is denoted as a $\mathrm{CA}(10^{17}\mathrm{f})$ accident.

The calculation model of a "naïve", baseline facility design was used to quantify the neutron and photon doses. This design was denoted as "modification zero" or MOD0. The conclusion was that the baseline design carries an unacceptable radiological risk — a nuclear criticality excursion inside this baseline facility design was shown to be lethal for every person within a circa 10 m radius from the epicentre of the fissile process mass where the excursion takes place, and also lead to acute radiation syndrome and a substantially elevated cancer risk in all survivors. This baseline design was unable to contain the pulse of ionising radiation, because there was a lack of partitioning shielding walls inside the facility. Radiation therefore streamed freely between processing workstations. Step-by-step facility design modifications, denoted as MOD1, MOD2, until MOD6, were then introduced in order to arrive at a significantly safer facility design, from a personnel exposure perspective. The goal of the stepwise improvements was to compartmentalise the facility into well shielded cubicles, with a shielding wall geometry and thickness able to localise the lethal dose to a single workstation compartment or cubicle, whilst maintaining the doses in all other compartments near or below the International Commission on Radiological Protection's (ICRP's) recommended annual dose limit of 20 mSv for occupational exposure, which is a factor 50 times below the threshold dose of 1000 mSv for the onset of acute radiation syndrome. It is practically unavoidable that the person(s) in the cubicle where the excursion takes place, will receive a lethal dose. Instead, the aim of the improvements was to ensure that staff in adjacent workstations, the control room, workshop and ablution facilities, as well as persons outside the main processing hall, at the position directly opposite the fissile volume hosting the excursion, would receive effective doses at or below the annual dose limit for normal occupational exposure. The analysis also showed that all the inner partitioning walls must extend all the way to the roof; if this is not done, a significant amount of streaming from the accident cubicle to adjacent

[2] A detector modelled in MCNP with human tissue equivalent material.

cubicles, was observed. This shielding design methodology that proved fruitful and ultimately successful, can be called the radiological de-coupling of process workstations from each other, via an improved placement of inner partitioning concrete walls of adequate thickness and height. The shielded workstations are designed so that the radiation from a criticality excursion is contained and confined to the accident workstation; lethality is localised and the PUREX plant is rescued from being "one large coffin".

In the final design of the facility, the highest effective dose recorded in passages and workstation cubicles adjacent to the accident cubicle, ranged from a minimum of 1 mSv to a maximum of 50 mSv, that is, the design modifications to achieve radiological decoupling of sub-spaces, via an improved design of partitioning walls, was successful. In the control room, workshop and ablution cubicle, doses were well below 20 mSv — the present dose limit on effective dose for radiation workers. The dose on top of the concrete roof, directly overhead the vessel hosting the postulated $\mathrm{CA}(10^{17}\mathrm{f})$ excursion, was just below 40 mSv; this is considered acceptable because the human occupancy factor on the roof is essentially zero. The above radiological compartmentalisation was achieved with ordinary concrete shielding walls, namely, the cheapest possible concrete, with which structural engineers and building contractors are also most familiar.

The next step was to quantify the inventory of fission products produced in the 10^{17} fission events. The neutron fluence spectrum as well as the integral neutron fluence inside the fissile process mass, were ported to the code FISPACT-II 3.00 to calculate the inventory of radioactive fission products produced by the excursion; the latter code was executed using TENDL-2019 nuclear data.

As a last step, the inventory of radioisotopes products produced by neutron activation from the $\mathrm{CA}(2.5 \times 10^{17}\mathrm{n})$ excursion, was calculated. The neutron fluence-rate spectrum $\varphi_n(E)$ as well as the integral neutron fluence-rate $\varphi_n = \int_0^\infty \varphi_n(E)\, dE$ inside the stainless-steel (SS-316L) vessel containing the fissile process mass, were calculated and ported to FISPACT-II, to calculate the inventory of radioactive isotopes that would be produced in the SS-316L alloy by neutron activation. As before, FISPACT-II was executed with TENDL-2019 nuclear data. Results showed that the activities of, and dose-rates from, fission products will completely dominate the neutron activation source-term. It is also shown that the facility may have to be sealed off for as long as 1 year before decontamination and either decommissioning or re-commissioning work should commence. If human entry is allowed before $T_{cool} \approx 1\,\mathrm{yr}$, an unnecessarily high dose will be received by the decontamination crew.

A corollary (associated truth) of this investigation is that the local nuclear sector will struggle to survive the social and political trauma posed by a nuclear criticality accident, and that it is therefore imperative

to prevent such events by designing systems, structures and components as well as administrative processes so that the probability for criticality accidents is driven to practically zero.

Dedication

This dissertation is dedicated to my family, especially my wife and kids. How can I forget to specially mention my son, Wandile Sibiya, who always competed with this work for attention while asking me, "*daddy how far with your chapters?"* Pursuing this logic further, he invented a practical suggestion, *"daddy maybe you should work more and sleep less so that you can complete your chapters faster".*

This work, which is my second MSc dissertation, is a true reflection of the fact that one can never be over-educated and should never miss an opportunity to enrol for further academic education in order to gain more domain-knowledge and competence. In addition to having to delve deeply in the sub-discipline of nuclear criticality safety, within the wider domain of nuclear engineering, the necessity to compose this dissertation to a good standard also forced me to learn how to use MS Word 2016 for scientific technical writing. It was a pleasant surprise to see how far this software had advanced since my disastrous historical encounter with Word-97 around the year 2002; in those years, MS Word was, with good reason, vehemently resented and avoided by most scientists and engineers.

Education is the most powerful weapon which can be used to change the world. Nelson Rolihlahla Mandela (18 July 1918 – 05 December 2013) could not have put it better.

Acknowledgements

I would like to express gratitude to my supervisors, Mr Johann van Rooyen and Prof Vishana Naicker for mentoring and advising me both in my academic and personal life. I thank them for providing a great opportunity to work under their supervision during my studies towards a second MSc in Nuclear Engineering. Their continuous support, encouragement and patient guidance have motivated me to tackle and complete this MSc project.

A special thanks also goes to Mr Bolade Adetula for his assistance with the sharing of informative material and viewpoints regarding nuclear criticality safety.

I would like to acknowledge North-West University, Potchefstroom Campus, in particular the Unit for Energy and Technology Systems for permitting me to be based at Necsa during the period of my research work.

The steadfast financial support provided by Necsa through its study assistance scheme throughout the duration required for the completion of my research work, is an important factor, for which I remain grateful.

Who am I without my lovely family and friends? They continuously reminded me how enjoyable and encouraging it is to have continuous support from them. To all, I express deep gratitude!

TABLE OF CONTENTS

List of figures

Page

List of tables

Page

Abbreviations and symbols

ACE ..... A Compact ENDF (nuclear data format read by the code MCNP6)

ALARA..... As Low As Reasonably Achievable, that is, the principle that a radiation shielding design and a radiation protection programme, must be optimised, i.e. if an affordable design or process improvement that lowers worker exposure to ionising radiation can be made, then that improvement must be approved and funded

ARS ..... Acute Radiation Syndrome

BAT ..... Best Available Technology

BE..... Binding Energy

CA ..... Criticality Accident

$\mathrm{CA}(10^{17}\mathrm{f})$ ..... Criticality Accident involving 10^{17} fissions (this being an example)

$\mathrm{CA}(\mathrm{MOD0}, 10^{17}\mathrm{f})$ ..... Criticality Accident in PUREX facility design modification MOD0, involving 10^{17} fissions (example)

$\mathrm{CA}(\nu \times 10^{17}\mathrm{n})$ ..... Criticality Accident involving the emission of $\nu \times 10^{17}$ neutrons from fission (example)

CAAS..... Criticality Accident Alarm System

CCC..... Computer Code Collection (of the RSICC)

CI..... Confidence Interval

D ..... Dose (generic) or absorbed dose (depending on context)

DFN ..... Delayed Fission Neutron

DL..... Dose Limit

DOE..... Department of Energy

DSB ..... Double Strand Break in DNA

E ..... Energy (the meaning of the symbol depends on the context)

E ..... Effective dose (the meaning of the symbol depends on the context)

ENDF ..... Evaluated Nuclear Data File

ENDF/B ..... Evaluated Nuclear Data File, type B

ENDF/B-8.1 ..... Evaluated Nuclear Data File, type B, release 8.1 (example)

EPD ..... Electronic Personal Dosimeter

FDCF ..... Fluence-to-Dose Conversion Factor

FoS ..... Factor of Safety

FRDRCF ..... Fluence-Rate to Dose-Rate Conversion Factor

GUI ..... Graphical User Interface

H ..... Equivalent dose

HEU ..... High Enrichment Uranium

HEU_{90} ..... High Enrichment Uranium containing 90% ^{235}U by mass (example)

HPC ..... High Performance Computing

IAEA ..... International Atomic Energy Agency

ICRP ..... International Commission on Radiological Protection

ICRU ..... International Commission on Radiation Units and Measurements

JAEA ..... Japan Atomic Energy Agency

JAERI ..... Japan Atomic Energy Research Institute

JANIS ..... Java-based Nuclear Information Software — a GUI to access and plot data in ENDF/B and other nuclear data collections.

k_{eff} ..... Effective neutron multiplication of a system containing fissile and fissionable material

LANL ..... Los Alamos National Laboratory

$LD_{50/30}$ ..... Lethal dose that will kill 50% of exposed people within 30 days

$LD_{50/60}$ ..... Lethal dose that will kill 50% of exposed people within 60 days

LET ..... Linear Energy Transfer, i.e., $\frac{dE}{dx}$, where E denotes the particle's energy and x denotes the spatial variable

LEU ..... Low Enrichment Uranium

$LEU_{19.75}$ ..... Low Enrichment Uranium with a (nominal) mass-enrichment of 19.75% ^{235}U (example)

$LEU_{4.75}$ ..... Low Enrichment Uranium with a (nominal) mass-enrichment of 4.75% ^{235}U (example)

LLNL ..... Lawrence Livermore National Laboratory

MAGIC MERV ..... Mass, Absorption, Geometry, Interactions, Concentration, Moderation, Enrichment, Reflection and Volume

MCNP ..... Monte Carlo N-Particle Transport Code

MERMAIDS ..... Mass, Enrichment, Reflection, Moderation, Absorption, Interactions, Density and Shape

ν ..... Fission neutron multiplicity, the average yield of fission neutrons per fission event

NAB ..... Natural Abundance

NABD ..... Natural Annual Background Dose

NAB ..... Natural Abundance

NAD ..... Neutron Absorbed Dose

NBDR ..... Natural Background Dose Rate

NBD ..... Natural Background Dose

NC ..... Nuclear Criticality

NCA ..... Nuclear Criticality Accident

NCE ..... Nuclear Criticality Excursion

NCS ..... Nuclear Criticality Safety

NCST..... Nuclear Criticality Safety Training

NED..... Neutron Equivalent Dose

$\mathrm{NED(x,y)}$..... The Neutron Equivalent Dose (NED) as a function of the spatial coordinates x and y (example)

NEDR ..... Neutron Equivalent Dose Rate

$NEDR(x,y)$ ..... The Neutron Equivalent Dose Rate (NEDR) as a function of the spatial coordinates x and y (example)

NRC..... Nuclear Regulatory Commission

NSSS..... Nuclear Steam Supply System

ORNL ..... Oak Ridge National Laboratory

PED ..... Photon Equivalent Dose[3]

$\mathrm{PED(x,y)}$ ..... The Photon Equivalent Dose (PED) as a function of the spatial coordinates x and y (example)

PEDR ..... Photon Equivalent Dose Rate

$PEDR(x,y)$ ..... The Photon Equivalent Dose Rate (PEDR) as a function of the spatial coordinates x and y (example)

PFG ..... Prompt Fission Gamma

PDN..... Prompt Fission Neutron

PUREX ..... Plutonium Uranium Reduction Extraction

ρ ..... Mass-density (meaning depends on the context)

ρ ..... Reactivity (meaning depends on the context)

R ..... Radius (meaning depends on the context)

R ..... Response (meaning depends on the context)

[3] For ionizing photons, the radiation weighting factor is 1, that is, the absorbed dose and equivalent dose are identical.

$\mathfrak{R}(E)$ ..... Response function (generic)

$\mathfrak{R}_n(E)$ ..... The response function, which figures in a linear functional of the form $\langle \varphi_n, \mathfrak{R}_n \rangle$, which converts neutron fluence to neutron equivalent dose; the fluence-to-dose (conversion) function

RBE ..... Relative Biological Effectiveness

RCC ..... Right Circular Cylinder

REMM ..... Relative Elemental Molar Mass, e.g., $\mathrm{REMM(C)} = 12.011\ \mathrm{g\ mole^{-1}}$

RIMM ..... Relative Isotopic Molar Mass, e.g. $\mathrm{RIMM}\left({}^{235}_{92}\mathrm{U}\right) = 235.0439282\ \mathrm{g\ mole^{-1}}$

RP ..... Radiation Protection

RPO ..... Radiation Protection Officer

RSICC ..... Radiation Safety Information Computational Centre

RWF ..... Radiation Weighting Factor (w_R)

SSB ..... Single Strand Break (in DNA)

SSC ..... Structures, Systems and Components

TBP ..... Tributyl Phosphate

TED ..... Total Equivalent Dose $(\mathrm{TED} = \mathrm{NED} + \mathrm{PED})$

TEM ..... Tissue-Equivalent Material (for calculational radiation detectors)

TLD ..... Thermoluminescent Dosimeter

TWF ..... Tissue Weighting Factor

UK ..... United Kingdom

USA ..... United State of America

USSR ..... Union of Soviet Socialist Republics

w_R ..... Radiation weighting factor

w_T ..... Tissue weighting factor

A note regarding the use of units in this work

Practically all radiation transport codes use the centimetre-gram-second (CGS) system of units. The radiation transport code used in this work — MCNP — uses the unit centimetre for length and gram for mass. To avoid confusion, this work therefore freely uses the CGS unit system and expresses the dimensions of radiation shields in the unit cm, fluence-rate in the units $\mathrm{cm}^{-2}.\mathrm{s}^{-1}$, fluence in the unit cm^{-2} and mass-density in the units $\mathrm{g\,cm}^{-3}$. The standard engineering practice of reporting the dimensions of structures and components in the unit mm is not followed in this dissertation.

Both the ICRP and ICRU do not permit the use of the term “flux” for the quantity $\varphi = Nv$ where N is the number of particles per unit volume, and v is the velocity of these particles — this is explained in for example, ICRP (2007) and ICRU (2011). Instead, these two authoritative international commissions enforce the use of the terms *fluence-rate* for φ and *fluence* for the time-integral $\Phi = \int_0^\infty \varphi(t)\,dt$. Because this dissertation deals with radiation protection and radiation dose — quantities for which the ICRP and ICRU act as international custodians — the terminology recommended by these two commissions will be used.

1 Introduction and literature review

1.1 Introduction to the PUREX process and concerns about nuclear criticality safety—the possibility of criticality excursions

At nuclear facilities, there is often a need to recover enriched uranium from liquid effluent as well as uranium-containing scrap materials. One example of uranium bearing scrap material available from historical processes in South Africa, is filters from a decommissioned uranium enrichment facility, which have been found to contain recoverable amounts of enriched uranium in the chemical form UF_4 (Badenhorst *et al*., 2016). Other examples of immediate relevance to the South African nuclear industry, are discussed in Fourie *et al.* (2016); Gama *et al*. (2018); Mathuthu *et al*. (2019); Potgieter *et al*. (2020; 2019) and Stassen & Suthiram (2015).

As a rule, chemical processing is required to recover such enriched uranium. Facilities using chemical processes to extract and recover fissile material such as enriched uranium, have to employ a multi-stage recovery process. The recovery pathway typically proceeds through dissolution in an aqueous process, to a final product, which is normally metallic uranium ingots. The PUREX (**P**lutonium **U**ranium **R**eduction **EX**traction) process is a well-established methodology to recover enriched uranium from uranium-bearing waste material (IAEA, 1999). In other words, the enriched uranium will be dissolved into hydrogen-rich moderator materials, and this leads to nuclear criticality safety concerns.

A facility that uses the PUREX chemical process to extract uranium fissile nuclear material from miscellaneous scrap-material presents possible hazards such as the prompt nuclear criticality accident, also termed a nuclear criticality excursion. A criticality excursion typically involves at least $N_f \approx 10^{16}$ fission events, which will release in the order of $2.5N_f$ fission neutrons and around $8N_f$ ionising photons, which will impart a substantial radiation dose to any person who may be nearby. If the input-material into the PUREX process is non-irradiated enriched uranium, practically no fission-products will be present during normal operation (NO), so that the dominant operational safety concern will be the risk of a nuclear criticality accident.

1.2 Lethal potential of criticality excursions

Before delving into the literature regarding criticality excursions and their consequences, the lethal potential of such excursions is derived on the basis of the ICRP's published fluence-to-dose conversion factors (ICRP and ICRU, 2017), as well as the published ballpark magnitude of fission yields of criticality excursions happening in solutions or slurries of fissile isotopes in water or organic solution systems. Using the fluence-to-dose factors together with the typical frontal area of an adult

human body $(\sim 0.5\ \mathrm{m}^2)$, the information plotted in Figure 1.1 was calculated using a simple MathCAD-15 worksheet. The graph shows the number of radiation particles, at different energies, in an expanded and aligned radiation field, which has to be incident upon an adult human body, to impart an effective dose of 1000 mSv — the threshold dose for acute radiation syndrome (ARS).

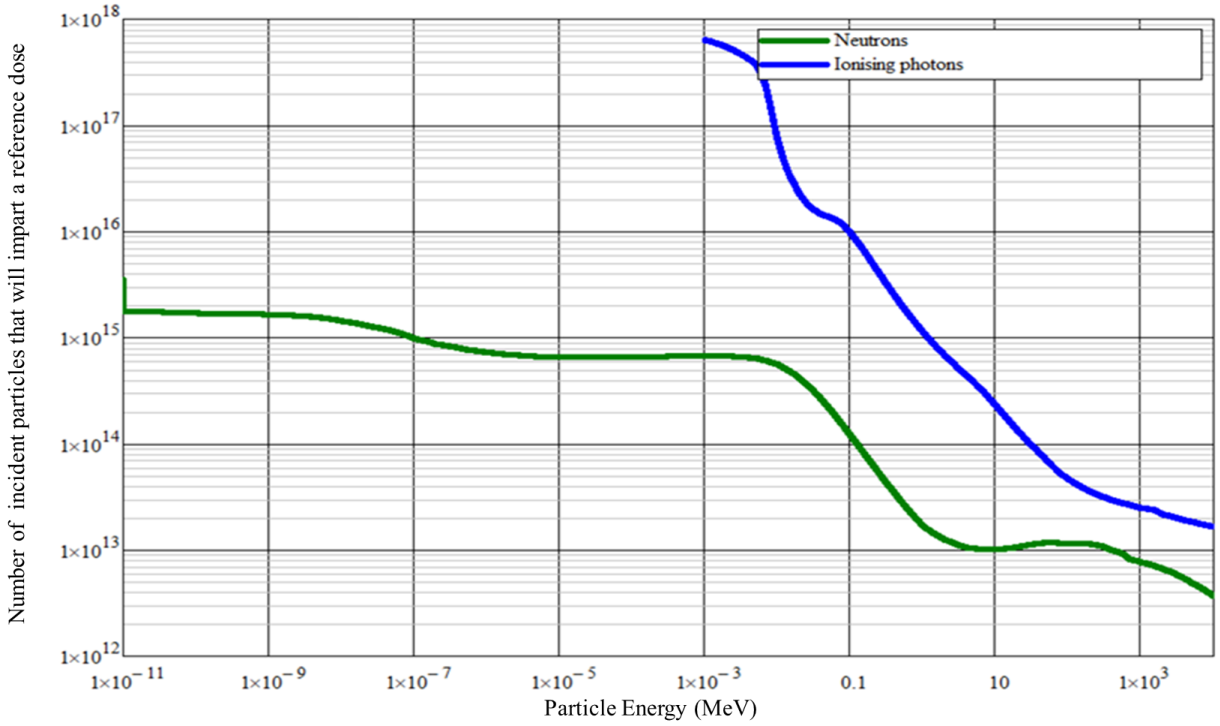

Figure 1.1: Number of neutrons and ionizing photons that will impart an effective dose of 1000 mSv to the body, at different incident particle energies.

Figure 1.1 makes it clear that the neutron is a more dangerous particle than the photon. In the rest of this section, the focus will therefore be on the neutron dose, and the photon dose will be neglected for the purposes of the intuitive argument.

The average energy at which prompt fission neutrons (PFNs) are emitted when the fissile isotope $^{235}\mathrm{U}$ fissions, is in the order of 2 MeV, as is easily calculated from the Watt spectrum (Watt, 1952) using coefficients determined by Cranberg *et al.* (1956). Consider a hypothetical criticality accident that involves 10^{16} fissions and emits $\nu \times 10^{16} \approx 2.5 \times 10^{16}$ neutrons at an energy of 2 MeV, where ν is the yield or multiplicity of fission neutrons per fission of $^{235}\mathrm{U}$. A Criticality Accident (CA) of this magnitude is denoted symbolically as $\mathrm{CA}(10^{16}\mathrm{f})$ and, equivalently, as $\mathrm{CA}(2.5 \times 10^{16}\mathrm{n})$. In the literature survey, as expounded below, it will be shown that a $\mathrm{CA}(10^{16}\mathrm{f})$ excursion is the minimum magnitude of typical, that is, normative criticality excursions in aqueous solutions or slurries of fissile material.

Using the 2017 values of the fluence-to-dose factors published jointly by the ICRP and ICRU (ICRP and ICRU, 2017), it can easily be calculated that 1.3×10^{13} neutrons of $E \approx 2\ \mathrm{MeV}$ striking the human body will impart an effective dose of 1000 mSv, namely, the threshold dose at which acute radiation syndrome will be clinically manifest. Likewise, approximately 6.3×10^{13} neutrons of $E \approx 2\ \mathrm{MeV}$ striking the human body will impart an effective dose of 5000 mSv, that is, a radiation dose in the non-survivable, lethal range. Working with this fact, namely that $\sim 6 \times 10^{13}$ fission neutrons striking the human body will typically cause death, it follows immediately that a $\mathrm{CA}(10^{16}\mathrm{f})$ excursion, namely, a $\mathrm{CA}(2.5 \times 10^{16}\mathrm{n})$ event, undoubtedly has lethal potential — 2.5×10^{16} fast neutrons is around 150 times higher than the number of neutrons that can be fatal, if they should strike a human body. Based on the above, along with a geometric ratio analysis, the approximate *radius of non-survivability* for human bystanders around an unshielded criticality excursion, can be calculated, using the approximate solid angle subtended by a human body at different radii R, as a fraction of the surface area $4\pi R^2$ of a sphere with radius R; results are summarized in Table 1.1.

Table 1.1: Approximate radii of non-survivability around unshielded nuclear criticality accidents of different magnitudes.

Magnitude of criticality excursion (i.e. number of fissions)	**Approximate radius of non-survivability** (m)
$1{\times}10^{16}$	4.0
$5{\times}10^{16}$	8.5
$1{\times}10^{17}$	12.5
$5{\times}10^{17}$	27.0
$1{\times}10^{18}$	40.0

1.3 Criticality controls: MERMAIDS and MAGIC MERV

Factors that must be controlled to prevent a Nuclear Criticality (NC) excursion, can be remembered by the initialism **MERMAIDS** (McKenzie, 2019):

M	**M**ass
E	**E**nrichment
R	**R**eflection
M	**M**oderation
A	**A**bsorption
I	**I**nteractions
D	**D**ensity
S	**S**hape

An alternative initialism that can serve as a memory-help, is **MAGIC MERV** (Putman, 1999, 2012):

M	**M**ass
A	**A**bsorption
G	**G**eometry
I	**I**nteractions
C	**C**oncentration
M	**M**oderation
E	**E**nrichment
R	**R**eflection
V	**V**olume

1.4 Historical background on nuclear criticality safety (NCS) and NCS accidents

The PUREX chemical process employs tributyl phosphate (TBP) as the solvent and nitric acid as the salting agent — this therefore includes both aqueous (watery) slurry and organic phases. The likelihood of nuclear criticality accidents in aqueous fissile media is narrated by Barbry *et al*. (2009), Barbry and Fouillaud (2002), and Barbry (1993), through experimental work using a SILENE reactor fuelled with fissile solution of 93% enriched uranyl nitrate — this was to study nuclear criticality safety especially for facilities that process fissile material in aqueous media. Moreover, McLaughlin (2003) emphasised a higher probability of criticality accidents in solutions such as slurries than in dry forms in a paper presented at the 2003 Japan Atomic Energy Research Institute (JAERI) conference.

According to Vargo (1999) and McLaughlin *et al.* (2000), a nuclear criticality accident could occur as a result of wrong execution of authorised operational procedures, accumulation of fissile mass, operators' knowledge to operate the plant and unexpected transfer of uranyl nitrate solution to unsafe geometry tanks.

A nuclear criticality accident that takes place in a liquid solution or slurry of fissile actinides, will lead to circa 10^{16} to 3×10^{18} fission events (Nakajima, 2003), i.e., this is the normal range of the magnitude of excursions for aqueous fissile solutions. In fissile systems dominated by $^{235}\mathrm{U}$, every fission event typically releases $\nu \approx 2.4355$ fission neutrons; in fissile systems dominated by $^{239}\mathrm{Pu}$, every fission event normally releases $\nu \approx 2.8836$ fission neutrons (Lamarsh and Baratta, 2017). For all fissioning isotopes, circa 8 prompt gamma-photons are released per fission event. In addition, the fission products produced by the fission events, will continue to emit gamma-photons plus intense beta-electrons, long after the end of the criticality excursion. The emitted ionising radiation is most likely to cause severe damage and fatality to the operators and workers in the vicinity. The approximate radii of non-survivability for unshielded criticality excursions have been summarised in Table 1.1. As a general rule, all people closer than circa 4 metres from a vessel where a criticality

excursion takes place, are likely to die from acute radiation syndrome, i.e., days to weeks. It is therefore imperative to introduce both engineered criticality controls and administrative criticality controls. Rigorous safety evaluations are required for every facility handling enriched fissile material. It is necessary to install a Criticality Accident Alarm System (CAAS) in such facilities (Miller and Peplow, 2013). The CAAS serves as an area monitoring system for warning the operators and workers to immediately evacuate the affected area (Baker *et al.*, 1994; Greenfield, 2009; Gross, 2018). A CAAS will reduce the likelihood of workers incurring lethal radiation doses (McKenzie, 2019). Criticality excursions in liquid media are, generally, non-explosive, but intensely radiative.

In the aftermath of a criticality excursion, the affected vessel will contain a substantial amount of highly radioactive fission products. It is important to be able to quantify the time-evolution of the inventory of radionuclides produced by a criticality excursion, so that a responsible waiting-time between the excursion and subsequent clean-up-operations, can be ascertained in advance and be incorporated in emergency plans.

1.5 The PUREX chemical process

Only a very short overview of the PUREX process is given here; more detail is given in Chapter 3 on page 50.

The PUREX process is a multi-stage process (IAEA, 1999) for extracting Plutonium (Pu) and Uranium (U). A PUREX plant will always have several interconnected workstations of operations with homogeneous fissile solutions. PUREX is the de-facto standard aqueous nuclear reprocessing method for the recovery of uranium (and plutonium) from irradiated uranium-bearing materials (Irish and Reas, 1957). It is based on liquid–liquid extraction ion-exchange. The uranic material is first dissolved in nitric acid. An organic solvent consists of 30% tributyl phosphate (TBP) in a hydrocarbon, such as kerosene, is also used. Uranium ions are extracted as $UO_2(NO_3)_2(TBP)_2$ complexes, and plutonium as similar chemical complexes (Anand *et al.*, 2018). Other fission products remain in the aqueous phase, as do the actinides americium and curium.

The PUREX process is compartmentalized into unit-operations (Baumgärtner and Ertel, 1980; Durazzo *et al.,* 2017; Mathur *et al.*, 1993; McKibben, 1984) that include:

1. Preparatory, i.e., “head-end” processes such as de-cladding, dissolution, filtration, and adjustment of acidity and salting (Ramanujam, 1998).
2. Solvent extraction with TBP (Aneheim, 2012) which partitions and decontaminates the U and Pu from the fission products. TBP is highly selective for U and Pu. As a commercial product, it is cheaply available and can be purified easily. It has a high boiling point (266°C) and is non-volatile. Its solubility in water is very low, its chemical, thermal and radiation

stabilities are high, it selects against fission products but selects for Pu and U, resulting in excellent purification of these two actinides (Ramanujam, 1998).

3. The final purification and beneficiation cycle for U, which involves:
    - Evaporation
    - Ion-exchange concentration
    - De-nitration
    - Fluoride precipitation
    - Reduction to metallic uranium.

Each unit-operation has its own, specific nuclear criticality safety (NCS) issues. This is expounded in Chapter 3.

1.6 Nuclear criticality safety systems

The facilities housing PUREX uranium recovery technology, must always be designed with nuclear criticality safety considerations in mind. Nuclear criticality safety (NCS) means that the effective neutron multiplication factor, k_{eff}, of all systems and subsystems containing fissile material such as ^{235}U, must always be maintained well below $k_{\text{eff}} < 0.95$, that is, maintained at subcritical conditions, with an adequate margin of subcriticality. This is attained by (1) engineered controls and (2) administrative controls. Examples of engineered controls are, for example, vessels designed to be small enough to prevent nuclear criticality accidents. Furthermore, the shapes of storage and mixing vessels are selected to be high-leakage geometries, in order to allow neutrons to leak out of the system before a substantial fraction of the neutrons have been moderated to thermal neutron energies. Shapes, sizes and placement of pipes and vessels also seek to discourage the reflection of neutrons back into the system. Another example of engineered NCS control is that storage tanks are separated by adequate separation distances plus partitioning neutron-shields such as concrete walls between the tanks, so as to neutronically de-couple the tanks containing fissile material, from each other. Each tank must also be adequately *bunded* so that material from multiple leaking tanks do not flow together into one supercritical configuration of fissile material and moderator-reflector, in the event of leakages or ruptures of the storage tanks. Examples of administrative controls are (1) limiting the mass-concentration of uranium, (2) measuring the uranium enrichment grade by sampling and analyses, and (3) rinsing tanks thoroughly at prescribed intervals, to prevent the build-up of uranic sludge in vessels.

It is not possible to up-front design any industrial-scale uranium-chemistry facility to be absolute safe. One can, for example, design a facility to be safe for handling uranium enrichments up to 5% and

uranium concentrations up to 100 gram of uranium per 1 litre of solvent, but if 93% enriched uranium (i.e., HEU_{93}) accidentally enters such a facility, undetected by routine measurements, it is almost certain that a nuclear criticality excursion will happen. If a facility is designed to be 100% safe for 99% enriched HEU (i.e., HEU_{99}), the facility throughput and cost will suffer greatly — no industrial scale facility for reprocessing Pressurised Water Reactor (PWR) fuel, can, for example, operate economically with diminutive 1.5 litre sized storage tanks and dwarf-pipes with 1 cm inner diameters. It is therefore for this reason, all real-life uranium recovery facilities are engineered to be safe within a specified safe operating envelope (for example, limitation of uranium mass per vessel), and with added administrative measures (for example, rules, inspection, sampling, laboratory analyses and periodic flushing to prevent fissile sludge from building up in vessels).

In spite of the safety design, the historical operational experience of plutonium and uranium processing facilities reveals a non-negligible possibility of serious nuclear criticality accidents (McLaughlin, 2003, 2001; McLaughlin *et al.*, 2000; Stratton and Smith, 1989). This is highlighted by the 22 nuclear criticality accidents reported to have occurred worldwide by the year 2020, with the September 1999 Tokaimura criticality accident in Japan being the most recent of these (Endo, 2010; Ishigure *et al.,* 2001; Mechitoua, 2001; Takada, 2012).

1.7 The PUREX facility under analysis

The facility under investigation uses PUREX technology to recover uranium from waste or scrap material. The uranium-bearing waste materials are un-irradiated, and therefore contain no fission products. The uranium-bearing carrier materials are of different enrichment grades, with a maximum possible enrichment of HEU_{90}.

The uranium-bearing scrap material is first dissolved in nitric acid inside a “wet” glovebox. The uranium solution is extracted from the dissolved material and purified using a tributyl phosphate (TBP) organic solution.

The facility has concrete walls which will act as a biological shield if a situation such as a criticality excursion causes a spike in the dose-rate. The US NRC (Nuclear Regulatory Commission) specifies that, in safety assessments, all Ordinary Concrete must be modelled with a standard composition and mass-density, known as *Regulatory Concrete* (Rearden and Jessee, 2020) and this practice has been followed in this dissertation. The prescribed mass-density of regulatory concrete is $\rho = 2.30\ \text{g cm}^{-3}$. Its elemental composition is essentially SiO_2 plus circa 4.4% Ca and 1.4% Fe by mass (Rearden and Jessee, 2020). The elemental composition of regulatory concrete is shown on page 8, Table 1.2. The elemental composition of US NRC concrete for the MCNP calculation models is presented on page 130, Table A-5.

Table 1.2: The elemental composition of US NRC regulatory concrete.

Element identification	**Weight** (%)
26000	1.4
1000	1.0
13000	3.4
20000	4.4
8000	53.2
14000	33.7
11000	2.9

The facility is applying for a *nuclear authorising license* in order to operate a process for the recovery of uranium from un-irradiated uranium-bearing scrap-materials. The recovered uranium material is subsequently used to manufacture uranium metal ingots earmarked for use in target-plates for medical radioisotope production. A detail information about the local PUREX facility is expounded in § 3.2 on page 50.

1.8 Purpose and problem statement

The purpose of this study is to perform a radiological analysis of a PUREX facility for uranium-recovery from scrap-material, in the event of a hypothetical nuclear criticality excursion happening in one of the PUREX processes. The scrap uranium-bearing materials used as feedstock in the PUREX plant under assessment, are unirradiated, so that there are no fission products present initially. This means that dose-rates during normal operation will be low, that is, the dominant radiological concern is personnel doses caused by a criticality excursion, i.e., an abnormal, accidental event. A criticality excursion will typically lead to a minimum of 10^{16} fission events (McLaughlin, 2003), which will release circa 2.5×10^{16} fission neutrons and approximately 8×10^{17} ionising photons, the latter largely as prompt-fission gamma-rays (PFGs). During a criticality excursion, a considerable inventory of fission-products will be formed, leading to subsequent radioactive contamination issues and elevated dose-rates in the facility. The “flash” of neutrons emitted during the criticality excursion will, furthermore, induce a small yet non-negligible inventory of radio-isotopes via neutron-activation, which will be an additional source term for some months. In the facility under analysis, the uranium present in feedstock materials, has different enrichment grades, ranging up to high enrichment uranium of grade HEU_{90} in the fissile isotope ^{235}U.

The facility under assessment is applying to the nuclear safety regulator for a nuclear license granting authorization to routinely recover enriched uranium from uranium-bearing scrap materials; the final product takes the form of enriched uranium as metal ingots. An application for a nuclear license requires the submission of extensive and in-depth safety-case documentation, which involves risk assessment and risk quantification. Dose quantification and facility layout optimisation are important facets of the application that must be made to the regulator. This study will, in a slightly amended form, be part of the licensing-case documentation submitted to the regulator — this is the *raison d'être* for this project.

1.9 Research aims and objectives

The following research aims have been selected to (1) arrive at a radiologically robust design and to (2) formulate a kernel of documentation in support of the licensing-case for the PUREX facility, which will have to be submitted to the nuclear safety regulator as part of the application for a nuclear operating license. These research objectives are conveniently numbered RO_1, RO_2, to RO_{11}, and are as follows:

RO_1 Conduct a literature survey of nuclear criticality safety principles as well as historical criticality accidents (CAs).

RO_2 Describe the PUREX process in general, and its specific implementation at the facility under assessment, in a format useful for incorporation into a license-application submission to a nuclear safety regulator. The emphasis will not be on process chemistry, but on factors impacting criticality safety — enrichment, moderation, reflection, etc., as expounded in § 2.2.

RO_3 Summarize the physics of nuclear fission, fission neutron energy spectrum and yield. Present the concept effective neutron multiplication factor (k_{eff}) as well as reactivity, ρ.

RO_4 Summarize the theory and practice of dose calculations with a radiation transport code, in a digestible, intuitive presentation, without drowning the reader under a mountain of mathematical formulas.

RO_5 Summarize the theory and practice of fission product inventory calculations as well as neutron activation calculations, with the nuclide inventory code FISPACT-II, in a digestible, intuitive presentation.

RO_6 Develop an MCNP calculation model of the “naïve”, baseline design of a PUREX facility. Identify the process-mass and position in the facility at the highest risk of a criticality excursion. Calculate and plot a dose-map for a criticality excursion in this “baseline” facility design, called design modification zero and denoted as MOD0. Based on the dose-map, design more effective radiation shielding. Improve the geometry and thickness of shielding structures. Do this step-by-step, proceeding through design modification MOD1, then MOD2,

until the last modification which brings the required safety. Arrive at a functional and ethical facility design that will confine and contain the dose from a CA in a small subsection of the facility, whilst ensuring that all workers in adjacent workstations receive doses that are at or below the ICRP's recommended annual dose limit of 20 mSv, i.e., a factor 50 times lower than the threshold dose for the onset of acute radiation syndrome (ARS). In other words, in the final facility design, the different processing stations must be radiologically decoupled, i.e., a NCA in one processing sub-area must not kill or seriously injure workers in adjacent areas, this to say, damage to health must be highly localized.

RO_7 Modify the base-line floorplan, specifically the extent and thicknesses of inner concrete walls, until the above dose constraint of $\mathrm{TED} \leq 20$ mSv for adjacent areas is met[4].

RO_8 Quantify the dose to operators inside the workstation where the CA is hypothesised to occur, as well as in adjacent workstations. Construct top-view $NED(x,y)$, $PED(x,y)$, $TED(x,y)$ as well as side-view $NED(x,z)$, $PED(x,z)$ and $TED(x,z)$ contour plots to visualise dose distributions and to diagnose shortcomings in the shielding design.

RO_9 Quantify the radionuclide inventory present in the fissile mass in which the excursion took place, at several post-accident cooling times. Graph $A_{\mathrm{tot}}(t)$ as well as $PEDR(t)$ for $t \in [1\ day; 1\ yr]$ post-excursion.

RO_{10} Quantify the neutron-activation source-term in the most highly irradiated structure, i.e., the stainless-steel wall of the process vessel in which the excursion had taken place, which would have been exposed to a high neutron fluence, Φ. This activation source-term will remain, even after the complete removal of fission-product contamination after the excursion.

RO_{11} Based on the calculated dose maps, $NED(x,y,z)$ and $PED(x,y,z)$, make some tentative conclusions and recommendations for the placement and dose measurement range of Criticality Accident Alarm System (CAAS) detectors in the plant.

1.10 Literature review: nuclear criticality, criticality accidents, criticality standards and control measures

The theory and practice of nuclear criticality safety is presented in the next chapter — in Chapter 2 on page 19.

1.10.1 Concise overview of historical criticality accidents

A total of 22 nuclear criticality accidents (CAs) are known to have occurred in fissile material processing facilities (Hodges and Sanders, 2014; McLaughlin, 2003; McLaughlin *et al.,* 2000;

[4] $TED = NED + PED$; as highlighted in the abbreviations exercise.

Skinner, 2017; Stratton and Smith, 1989; Vargo, 1999). Most of these accidents occurred in the USSR between 1953 and 1997, while relatively few occurred in the USA, Western Europe and Japan. The latest criticality accident occurred in Japan at the Tokai-mura nuclear fuel processing facility, on 30 September 1999. Of the 22 recorded CAs, 21 occurred with fissile material in aqueous, i.e., "watery slurry" solution, whilst only one accident occurred with metal ingots (Nakajima, 2003). The total *number of fissions* per CA reported by Nakajima (2003), McLaughlin (2003) and McLaughlin *et al.* (2000), ranges between 1×10^{15} and 1×10^{19}, while the majority of excursions fall in the range from 10^{16} to 3×10^{18} fissions per excursion. A notable exception is the nuclear criticality accident at the Idaho chemical processing plant in the USA (Skinner, 2017) — where the total fission yield, was massively high at 4×10^{19} fissions. The fission yield expresses the magnitude of the nuclear criticality excursion and the number of neutrons and gamma-photons; radiation doses are directly proportional to the number of fissions.

Several investigating teams have used a variety of methods to retrospectively quantify radiation doses following a nuclear criticality accident. Here below follows an overview of authors and methods.

Kerr and Tankersley (2006) used the sodium-24 ($^{24}\mathrm{Na}$) activity in the body or irradiated persons to evaluate the dose distribution for the 8 most highly exposed personnel during the criticality accident in 1958 at the Y-12 plant in Oak Ridge, Tennessee, USA. These men were not wearing any personal dosimetry badges during the event. They were located quite close to the epicentre of the volume in which the criticality accident occurred. To estimate the first collision absorbed dose from neutron and γ-radiation, the author used a small donkey (a "burro") as a surrogate for a human and a value for the relative biological effectiveness of $RBE = 2$, based on deterministic effects related to fatality. The dose results showed an uncertainty of about 20%. This method is based on the neutron activation reaction,

$$\boxed{^{23}\mathrm{Na} + n \underset{(n,\gamma)}{\longrightarrow} {}^{24}\mathrm{Na}} \; (T_{\mathrm{half}}(^{24}\mathrm{Na}) = \; 14.957 \; \mathrm{hr})$$

with the "salt" in human blood. The "burro" experiment consisted of exposing a large mammal to a mock-up nuclear reactor which was assumed to give the same neutron spectrum as the accidental excursion. First, the ratio $\frac{\gamma\text{-dose}}{\text{neutron dose}}$ was determined. Next, the relationship between the activity concentration of $^{24}\mathrm{Na}$ in blood sodium and the dose from fast neutrons, was determined (Union Carbide Nuclear Company, 1958).

Endo (2010) employed the prodromal biological sample, chromosomes, lymphocyte and $^{24}\mathrm{Na}$ measurement to estimate the doses of the three heavily exposed personnel in the 2009 criticality accident at the Tokai-mura fuel processing facility in Japan. An anthopomorphic calculational model

of an exposed human, modelled with the Monte Carlo radiation transport codes[5] MCNP5 and MCNPX, was used to reconstruct the 3D dose deposition pattern. The highest dose was found to be $67\ \mathrm{Gy}$, where $29\ \mathrm{Gy}$ was from neutrons and $38\ \mathrm{Gy}$ was received from ionising photons. In general, radiation doses above circa 4 Gy are non-survivable (ICRP, 2007).

Sono *et al.* (2001) employed thermoluminescent dosimeters (TLDs) employing the thermo-luminescent salt, lithium tetra-borate, as well as modelling with a continuous-energy Monte Carlo code, MVP[6], to evaluate the gamma-ray doses during the criticality accident situation at the Transient Experiment Criticality Facility (TRACY) in Japan. The facility used uranyl nitrate solution inside a stainless steel cylinder tank. The discrepancies between the calculated and measured γ-doses increased with increased distance — from the epicentre of the uranic tank, discrepancies ranged from 16% to 40%.

Murazaki *et al.,* (2009) also used TLDs dosimeters to measure the neutron dose under deliberate criticality accident conditions achieved TRACY. The experiments were carried out with and without a water reflector. The resulted neutron doses were converted to tissue kerma, employing dose conversion factors calculated with the Monte Carlo code MCNP5, using continuous-energy nuclear data. The neutron tissue kerma values calculated using MCNP5, were compared to the measurements; the discrepancy was within 25%, indicating that TLD dosimeters are fit for use to measure neutron doses, as well as γ-doses, under criticality accident conditions.

Nakamura *et al.,* (2004) used TLDs made of alanine dosimetry[7], developed by then Japan Atomic Energy Research Institute (JAERI), to measure the neutron dose in the nuclear criticality accident situations from the Transient Experiment criticality facility housing a TRACY reactor. TRACY is a pulse-type reactor using 10% enriched uranyl nitrate solution. The uranium concentration is in the cylindrical tank of diameter 50 cm and height 200 cm, and the limiting uranium concentration is 500 gram per litre. The doses were also analytic calculated and the calculation took consideration of the calibration constant of TLDs and the dose conversion coefficients. The calculations and measurements were within 15% discrepancy, and such was attributed to the radiation field that impinge the TLDs.

---

[5] These codes (MCNP5 and MCNPX) were merged into MCNP6, which replaced both these codes by circa 2012.

[6] The Monte Carlo code MVP is under continuous development at the Japan Atomic Energy Agency (JAEA).

[7] The amino acid L-alanine forms a very stable free radical when exposed to ionising radiation, and the concentration of this free radical is dose dependent, having a dependency characterised by high accuracy and low error. For this reason, L-alanine has thus become a favoured dosimetry technique in radiation facilities. The positive characteristics of EPR/alanine dosimetry, such as, stability, reproducibility, cumulatively and in-dependency to the variations in dose rate make it a reliable technique for dose measurements in industrial as well as medical irradiation processes (Morsy, 2012).

Abrefah *et al.* (2018) employed the codes MCNP6 and ORIGEN-S[8] to calculate the total reactor core radionuclide inventory and the source term; and subsequently estimate the dose rate in the vicinity of Ghana Research Reactor-1 (GHARR-1) for the process of converting the reactor from using highly enriched uranium (HEU) to low enriched uranium (LEU). The ORIGEN-S code was used to calculate the activities of radioisotopes (i.e., the total radionuclide inventory) and radiation emission source-term. This source-term was then fed to the code MCNP6 to compute dose rates. A stepwise calculational method was used: first, MCNP6 was used to compute the neutron fluence-rate and the effective neutron multiplication factor, k_{eff}. The computed neutron fluence-rate spectrum $\varphi(E)$ was passed to an ORIGEN-S calculation model and used to deplete the nuclear fuel in the core, and calculate the radionuclide inventory in the core (i.e., (N_i, A_i) matrices, where N_i denotes nuclide identity and A_i the corresponding activity of that radionuclide species. The source term, i.e., the radiation emission, from the core depletion calculation was then used to calculate photon dose rates. The relative 1σ statistical errors of the MCNP6 dose-rate calculations were very low — in the range from $0.06\% - 0.3\%$ (Abrefah *et al.,* 2018).

Miller *et al.,* (2018) used modern radiation transport computer codes such as SCALE and MCNP to model the critical uranium system of the 1997 Slide Rule[9]. Three scenarios, namely, enriched uranyl nitrate, uranium dioxide and enriched uranium metal, were modelled to quantify prompt doses and delayed gamma-ray doses with acceptable accuracy. The relative error between the codes was in the order of 5%. Despite the fact that calculated doses showed good comparative agreement, the impact of the shield thickness and the latest values of fluence-to-dose conversion factors[10] (ICRP and ICRU, 2017) were not considered.

---

[8] In 2016, the ORIGEN-S code was renamed to the simpler designation, ORIGEN, because the competing code ORIGEN-2 was abandoned and orphaned around 2002.

[9] The "Slide Rule" contains correlated technical information about the following quantities of importance to nuclear criticality accidents: (1) fission yield estimation, (2) direct and indirect prompt neutron and gamma radiation dose estimates at variable distances from the accident, (3) dose rates from the decay-gammas from fission-products, at variable distances from and time after the fission yield, (4) time-integrated dose estimates at variable distances from, and times after, the fission excursion, (5) dose reduction factors for variable thicknesses of steel, concrete, and water.

[10] The values of fluence-to-dose factors are updated every circa 15 to 20 years, in ICRU and ICRP publications. These conversion factors are not fixed but "evolve" because their enumeration improve with, e.g., (1) advances to radiation transport codes, (2) the development of higher-fidelity medical physics voxel phantom models, (3) advances in radiobiology and (4) advances in clinical knowledge on differential organ sensitivity to radiation carcinogenesis. All these sciences progress steadily, so that there is a need to revise and improve fluence-to-dose factors at least every 20 years. In turn, all these sciences rest upon a foundation of data science and computer technology, which are also steadily progressing disciplines.

Several authors highlighted a number of methodologies for the quantification of yields and doses from nuclear criticality accidents, especially in facilities processing fissile material. Many criticality experiments have used reactors such as SILENE in France and TRACY in Japan, to quantify nuclear criticality excursions for, in particular, the processing of fissile solutions. These experiments, have provided vital domain knowledge in NCS.

Because criticality experiments cannot and may not be performed locally in the country, the focus is on using radiation transport codes such as MCNP6.2 together with a radionuclide inventory code, FISPACT-II 3.00, to compute dose-rates. These are purely neutronics codes which cannot possibly calculate the number of fission events in a criticality excursion. The number of fissions, which translates to the number of neutrons that are produced, translates to a tally multiplication factor in an MCNP calculation model. The value of this tally multiplication factor is *imposed* on the model by the user, based on the selection of a design basis accident of a chosen magnitude, which is in turn based on a survey of existing literature.

Multi-physics codes capable of modelling the detailed kinetics and dynamics of a sudden fission excursion, are not available in the public domain, for a good reason, namely that such codes can potentially be misused by "bad actors" to design fission weapons. The chosen calculational scheme, as followed in this research work, namely (1) imposing an a-priori, design-basis magnitude (i.e., 10^{17} fissions, i.e., a $\mathrm{CA}(10^{17}\mathrm{f})$ on the excursion, (2) using MCNP to calculate equivalent doses and fluence-rate spectra, and then (3) using FISPACT to quantify the radionuclide inventory of fission and activation products produced by the fission excursion, and to estimate residual post-excursion dose rates, is judged to be the best available technology (BAT) for safety assessments and the spatial positioning of CAAS detectors in a facility.

1.11 Research methodology

The following step-by-step research methodology was designed to achieve the research objectives set forth in §1.9 on page 9. This research methodology steps are conveniently numbered RM_1, RM_2, etc., and are as follows:

RM_1 Based on the literature survey, a "number of fissions" accident magnitude will be *imposed* on the criticality accident, because a neutronics code such as MCNP is inherently unable to calculate this quantity[11]. The magnitude of the excursion will be fixed at the reference value

[11] Note by co-supervisor, TJvR: Codes that can calculate this, have to couple a neutronics code with a multi-physics code that include explosion-dynamics capabilities. For non-proliferation reasons, such codes are not available in the public domain.

of $CA(10^{17}\text{f})$, i.e., 10^{17} fissions. Based on an analysis of the process and the literature, select the most likely spatial locale for a criticality excursion in the PUREX facility.

RM$_2$ Start with the "naïve", baseline design for the PUREX facility, as produced by the engineering office by a designer with no scientific training in nuclear engineering, criticality safety and radiation shielding. Develop an MCNP6.2 calculation model of this non-modified, baseline architecture of the PUREX facility, which will be termed the MOD0 design. Model a criticality excursion in which the effective neutron multiplication factor k_{eff} is in the approximate numerical range $1.01 \leq k_{\text{eff}} \leq 1.02$, i.e., a fissile system that is marginally supercritical. Place a number of calculational detectors, filled with tissue-equivalent material (TEM), at selected positions inside the facility, outside the facility walls and on the roof. Also develop MCNP FMESH mesh-tallies so as to be able to graphically display dose results as easy-to-interpret colour-coded dose-contour plots. Interpret the calculated neutron equivalent dose (NED), photon equivalent dose (PED) and total equivalent dose $(TED = NED + PED)$ in the individual tallies as well as in the mesh-tallies, and use it to diagnose the glaring shortcomings of the base-model, i.e. the MOD0 facility design.

RM$_3$ Based on the results of the MCNP calculation model, develop a MOD1 modification of the baseline floorplan and wall, and roof design for the PUREX facility, aimed at lowering doses and improving radiological safety. Develop an MCNP6.2 calculation model for this MOD1 architecture of the PUREX facility. Model the identical design-basis criticality excursion — a $\text{CA}(10^{17}\text{f})$ event at the evaporation workstation. Use the mesh-tallies to generate informative, diagnostic colour-coded dose-contour maps — horizontal as well as vertical. These dose maps are denoted as e.g., $NED(x,y)$, $PED(x,y)$, $TED(x,y)$ and $TED(x,z)$ dose distributions. Interpret the calculated doses at individual tallies as well as the dose contour maps, which will assist with the visual identification of radiation streaming paths. Use these methods to diagnose the remaining radiological imperfections of the MOD1 facility architecture.

RM$_4$ Repeat the above process another e.g., 5 times, until the design of, specifically, the inner partitioning walls inside the facility, as well as the perimeter concrete wall, has been modified to achieve the following radiological safety criteria, for the design-basis accident:

- Only the worker(s) inside the cubicle where the criticality accident occurs, may receive radiation doses in the fatal/lethal range.
- In the final facility design, the different processing stations must be radiologically decoupled, i.e., a NC accident in one processing sub-area must not kill or seriously impair workers in adjacent areas, i.e., damage must be highly localized.
- Radiation doses to workers who are not inside the cubicle where the excursion occurs, must be in the dose range where they will not suffer acute radiation syndrome (ARS).

- Radiation doses to workers positioned at their normal workstations, in the control room, in the ablution facilities, must be at or below 20 mSv, which is the ICRP's recommended annual dose limit (ICRP, 2007) for radiation workers involved in practices, this is explained in § 2.10 on page 47.

RM_5 Doses to the operator present in the cubicle where the excursion plays out, will be quantified.

RM_6 The MCNP calculation models must use current cross-section data, namely ENDF/B-8.0 nuclear data (Brown *et al.,* 2018) in ACE format (Conlin *et al.*, 2018) and must also use special bound-state low-energy scattering cross-sections (Parsons, 2018). The composition of ordinary concrete must conform to that of "Regulatory Concrete" as prescribed by the Nuclear Regulatory Commission of the United State of America (US NRC), to ensure that all licensing submissions in which concrete is modelled, are standardised.

RM_7 Dose maps must be produced to assist future investigators in making informed decisions regarding a Criticality Accident Alarm System (CAAS) for the PUREX facility. This involves the type of detector, the dose range to be covered as well as the placement of detectors.

RM_8 Develop and execute a FISPACT-II 3.00 (Sublet *et al.*, 2015) calculation model to quantify the radionuclide inventory for several post-accident "cooling" periods. The neutron fluence spectra $\Phi(E)$ inside the fissile process mass, as calculated by the MCNP model, has to be ported to FISPACT, i.e., the FISPACT calculation model is dependent on the results calculated with the MCNP calculation model.

RM_9 Use the MCNP calculation model to calculate neutron fluence spectra $\Phi(E)$ inside stainless-steel structure closest to the hypothetical criticality excursion, to calculate and present the subsequent time-dependence of the neutron-activation source-term in this structure. This activation source-term will remain, even after the complete removal of fission-product contamination after the excursion.

Another aspect of the methodology is to document the information in a form that can be readily adapted into documentation such as a Safety Assessment Report (SAR) for the facility, or an application for a nuclear operations license, directed to the nuclear safety regulator.

1.12 Outline of dissertation

The work is presented in several chapters and one Appendix.

Chapter 1 presents an introduction to the PUREX process for uranium recovery, including its process chemistry. The hypothetical potential for a criticality excursion in a PUREX process is presented, on the basis of the presence of the fissile uranium isotope, $^{235}\mathrm{U}$. The conceptual framework for preventing criticality excursions, is presented with reference to two initialisms — MERMAIDS and

MAGIC MERV. The literature about nuclear criticality accidents and nuclear criticality safety, is reviewed and briefly summarised. The problem statement and purpose of the work is formulated, as are the research objectives and research methodology.

Chapter 2 begins by presenting theoretical consideration of importance to nuclear fission, nuclear criticality events, criticality safety, criticality calculations and the radioactivity of fission products. The focus then falls on key concepts such as to it looks at the theory of radiation transport, dose calculations, nuclide inventory calculations and source-term calculations, without getting bogged down in excessive mathematical detail. The energy released in criticality excursions, as well as the typical degree of heating that will be observed when there is a criticality excursion in aqueous fissile solutions, is developed. Conceptual beacons for the interpretation of calculated doses and dose rates are presented. The concepts dose limits, dose constraints, practices and interventions, as formulated in ICRP reports, are presented. Finally, the two principal codes used for the quantitative analyses, are introduced — MCNP6.2 and FISPACT-II version 3.00. The code MCNP6.2 was used to model the criticality excursion and quantify doses at different positions in the plant. An article dealing with the normalisation of criticality excursion radiation doses with MCNP, is presented. The code FISPACT was used to calculate the inventory of additional radionuclides generated by the criticality event, whether by the production of fission products or via neutron activation.

Chapter 3 presents the PUREX process and facility layout. It is argued that the combination of fissile material and the neutron moderator $^{1}\mathrm{H}$, which is abundant in water, has the potential to cause criticality, in the unlikely event that process control goes awry.

Chapter 4 is a long chapter forming the practical core of this dissertation. As a baseline design, the first floorplan design by the drawing office, is used as a point of departure. This "naïve" design, produced by a person with no knowledge of nuclear criticality or radiation shielding, is used as a point of departure. This un-modified design is named MOD0. An MCNP6.2 calculation model of a criticality excursion taking place at a selected workstation in the MOD0 design of the PUREX facility is developed and executed. The calculated doses are evaluated and found to be dangerously high — the MOD0 design will cause the process hall to be a large death-trap in the event of a criticality excursion. Using FMESH mesh-tallies, neutron and photon doses are each calculated in approximately $140 \times 140 \approx 200{,}000$ mesh cells in both the x-y plane (for a top-view of the horizontal dose distribution) and the x-z plane (for a side-view of the vertical dose distribution) and visualised in contour plots. By inspecting the dose contours as well as doses in strategically placed tallies, the weaknesses in the design are identified, and the design is then improved to eliminate these identified weakness. This cycle of (1) modelling with MCNP6.2, (2) diagnosis and (3) improvement, is repeated a number of times, until it finally converges to a design that presents a good balance

between the (1) radiological protection of workers, and (2) affordability. Chapter 4 ends with some brief remarks about a CAAS — a criticality accident alarm system — for this PUREX plant.

Chapter 5 presents the calculation of the inventory of radionuclides inside the fissile process mass that underwent a criticality excursion, as well as the calculation of the inventory of radionuclides in the structure that underwent the most intense neutron irradiation in the criticality event, namely the vessel containing the fissile process mass. The code FISPACT-II is introduced, and the FISPACT-II calculation model is discussed. A summary of findings and accomplishments are presented in Chapter 6.

Appendix A presents an in-depth overview of radiation MCNP6 calculation models for NCS calculations and dose calculations for criticality excursions. Radiation transport theory is treated, in an intuitive and digestible manner. The code FISPACT-II and the calculation models for calculating the radionuclide inventories from (1) fission and (2) neutron activation, are discussed.

2 Theoretical background and introduction to the principal codes used for this investigation

2.1 The nuclear fission and chain reaction

2.1.1 Binding energy per nucleon

The binding energy per nucleon is lower in heavy nuclei such as the fissile and fissionable isotopes of e.g., thorium, uranium and plutonium, compared to nuclei such as isotopes of e.g., molybdenum, cesium and iodine, which are situated closer to the peak of the curve of $BE(A)$, i.e., binding energy per nucleon, shown in Figure 2.1. At the very peak of this curve one encounters isotopes of Fe and Ni, notably $^{56}\mathrm{Fe}$.

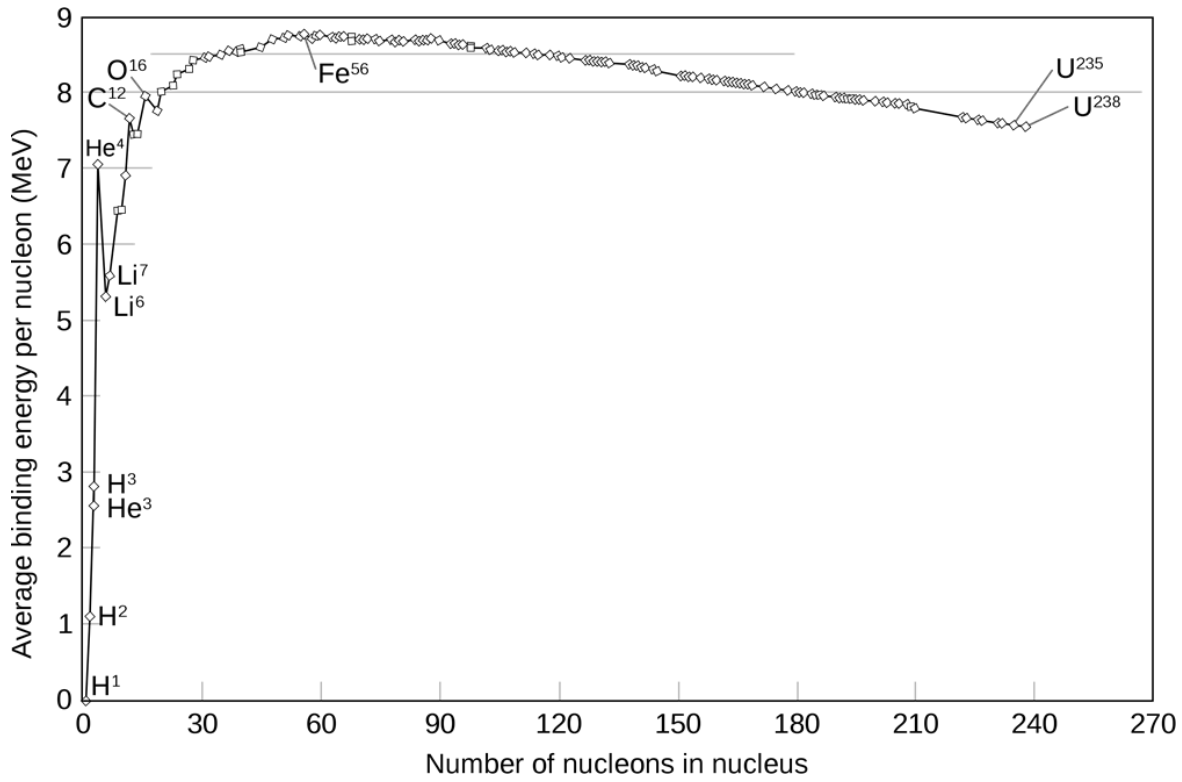

Figure 2.1: The curve of binding energy per nucleon, $\boldsymbol{BE(A)}$, is seen to peak in the region of ^{56}Fe, where it is significantly higher than for heavy nuclei such as ^{235}U and ^{238}U(Physics Stack Exchange, 2020).

A significant amount of energy (more than 200 MeV) is released when nuclear fission of heavy nuclei such as $^{235}\mathrm{U}$, $^{238}\mathrm{U}$, or $^{239}\mathrm{Pu}$ occurs. The reason is that the binding energy per nucleon, $BE(A)$ steadily decreases from $A \approx 56$ to $A \approx 92$ (uranium). If the heavy nucleus $^{235}\mathrm{U}$ fissions, the fission fragments will have higher binding energies than the "overweight" parent nuclide, and this energy difference will be released. This energy change, ΔE, is more than 1 million times larger than the

energy changes encountered in chemical reactions. As a result, the “burning” of uranium fuel presents an energy density that is more than 1 million times higher than the combustion of hydrocarbon fuel.

2.1.2 Nuclear fission

The phenomenon of nuclear fission underlies fission chain reactions and, therefore, potential criticality excursions. The energetic driving force that underlies the fission of heavy nuclei, is the higher binding energies per nucleon, of isotopes in the atomic mass number domain $90 \leq A \leq 140$, compared to $BE(A)\ \forall\ A \geq\ 230$.

The energy-dependence of the cross-sections $\sigma_f(E)$ for the neutron-induced fission of the two uranium isotopes, $^{235}\mathrm{U}$ and $^{238}\mathrm{U}$, are illustrated in Figure 2.2. The cross-section data was taken from ENDF/B-7.1 (2011) via the JANIS-4.0 GUI (Soppera *et al.*, 2013).

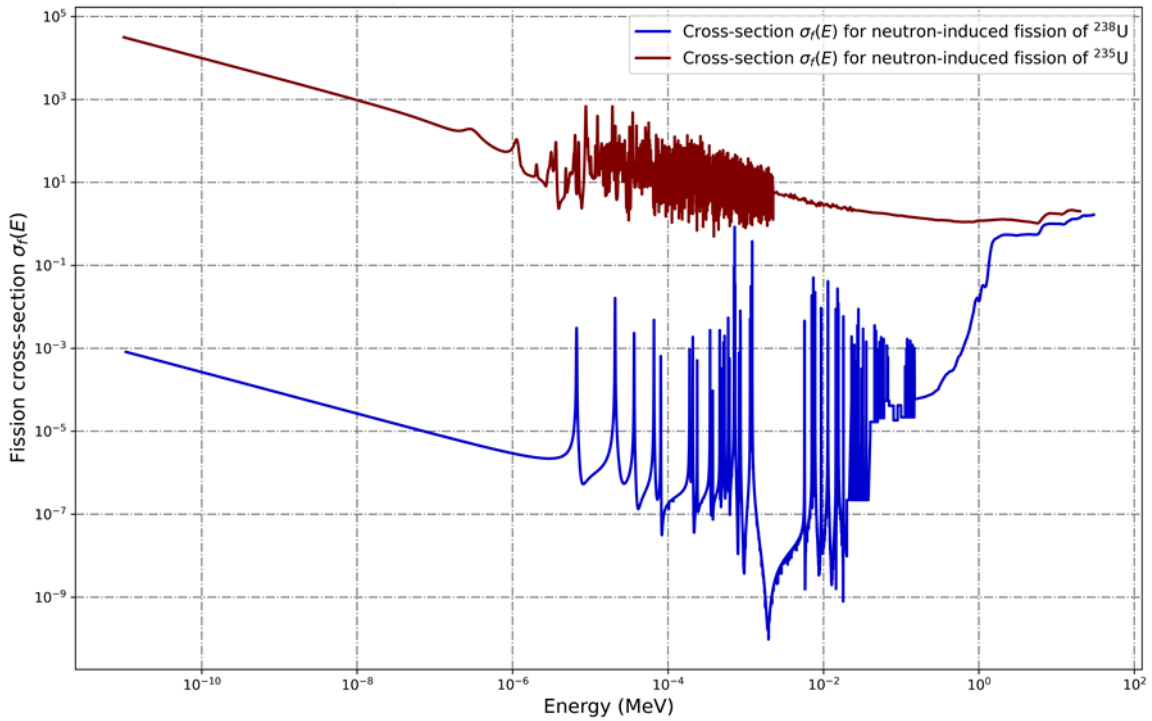

Figure 2.2: Cross-sections for the neutron-induced fission of ^{235}U and ^{238}U.

From Figure 2.2 it is evident that $^{235}\mathrm{U}$ is a ***fissile*** isotope, whereas $^{238}\mathrm{U}$ is a fissionable isotope — the cross-section for the neutron-induced fission $\sigma_f(E)$ of $^{235}\mathrm{U}$ is “usefully high” at thermal neutron energies, while that of $^{238}\mathrm{U}$ $\sigma_f(E)$ only becomes “usefully high” at $E_n \geq 1$ MeV. This means that when HEU is in a volume with a neutron moderator such as water, fast neutrons will be thermalized from high energy to lower energies of approximately 0.0253 eV because of the abundance of the

moderator isotope $^{1}\mathrm{H}$. This will in turn makes the thermalized neutrons more effective in the fission chain reaction.

The nuclear fission of a fissile isotope is initiated by an incident thermal neutron. In the case of the neutron-induced fission of $^{235}\mathrm{U}$, this nucleus absorbs the incident slow neutron to form the compound nucleus, $^{236}\mathrm{U}^{*}$, in an excited state (denoted by the superscripted symbol $\boxed{*}$). This compound nucleus enters a cyclic prolate[12]-oblate shape-oscillation, eventually overshooting the prolate shape, takes a dumbbell shape and then fissions into two fission fragments, in turn releases significant amount of energy and several instantaneously (usually within 10^{-14} seconds) neutrons per fission event . This is illustrated in Figure 2.3. This illustrative Figure 2.3 was taken from the textbook (Duderstadt and Hamilton, 1976); the text, uranium-235 symbol and arrows in blue colour was added to enhance the illustration.

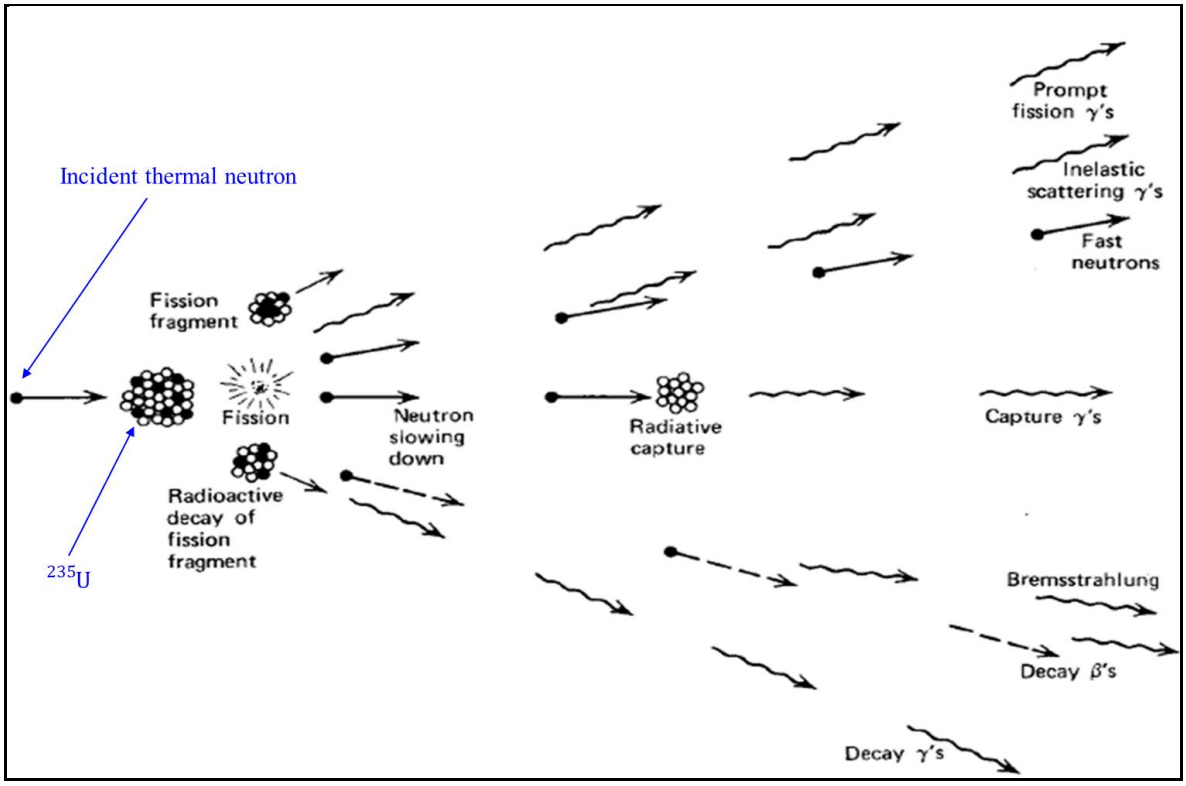

Figure 2.3: The nuclear fission reaction and subsequently fission products (Duderstadt and Hamilton, 1976).

The initial *fission fragments* are highly unstable and decay to a succession of *fission products.* During the scission and fragment-acceleration phases of fission, an average of around $\nu \approx 2.5$

[12] A prolate (elongated) spheroid is shaped like a rugby ball; an oblate (flattened) spheroid is shaped like a lentil, or some pumpkins.

neutrons are released. Additionally, β^--electrons and γ-photons are emitted. The nuclear fission reaction of ^{235}U is written as in equation (2.1).

$$ {}^{1}_{0}n + {}^{235}_{92}U \rightarrow ({}^{236}_{92}U)^{*} \rightarrow {}^{A}_{Z}X + {}^{A}_{Z}Y + 3({}^{1}_{0}n) + \text{Energy} \qquad (2.1) $$

Where:

$^{1}_{0}n$	=	Incident neutron, thermal
$^{235}_{92}$U	=	Fissile target nucleus
$(^{236}_{92}\text{U})^{*}$	=	Compound nucleus in excited state
$^{A}_{Z}X + {}^{A}_{Z}Y$	=	Two fission fragments
$3(^{1}_{0}n)$	=	Number of fission neutrons released; usually between 2 and 3

On average, a fission reaction on ^{235}U releases around 200 MeV of recoverable energy (Lamarsh and Baratta, 2017). Most of this energy is present in the high initial velocity of the fission-fragments — potential energy in the electrostatic repulsion between positive charges is converted to the kinetic energy of the fission fragments, which is then converted to atomic vibrational energy, that is, heat. A simulation of the tracks of typical fission fragments, was computed with the Monte Carlo code SRIM; this is displayed in Figure 2.4 (Ziegler and Biersack, 2008).

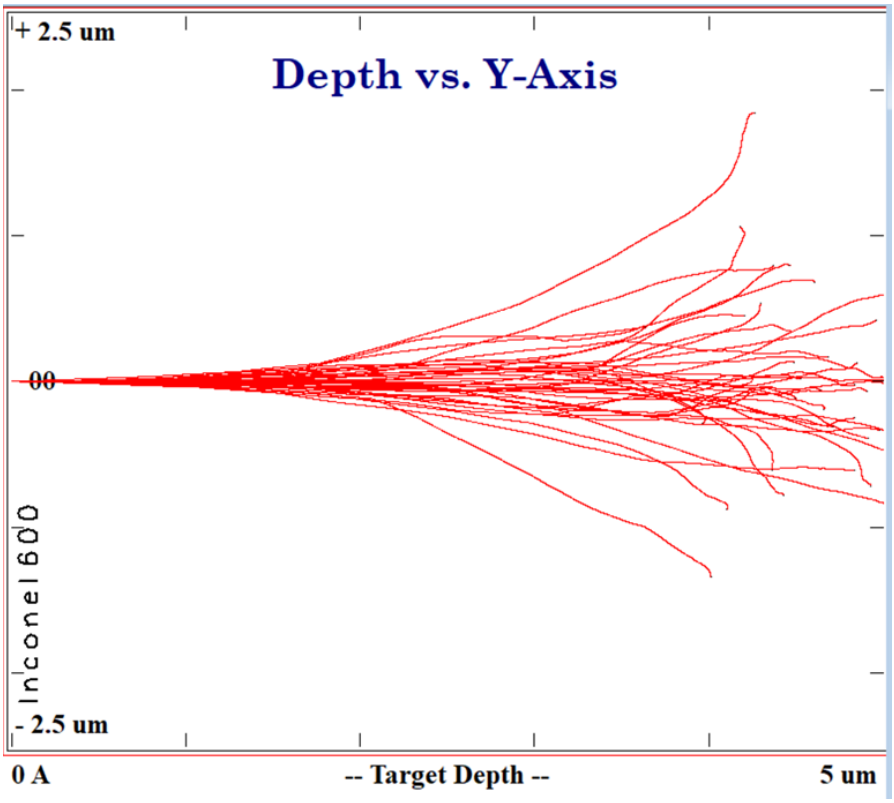

Figure 2.4: A simulation of the tracks of typical fission fragments.

It is transparent in Figure 2.4, the range of typical fission fragments in UO_2 reactor fuel, is below 10 μm; it is the kinetic energy of the fission fragments, when converted to heat (i.e., atomic vibrations) within less than 10 μm, that provides the "nuclear heat" used in the nuclear steam supply system (NSSS) of a power reactor system.

Nuclear fission and subsequent prompt fission neutron emission take place as follows. A neutron is absorbed by the fissile or fissionable nucleus, thereby adding its binding energy (circa 7 MeV) as well as practically all its kinetic energy, as internal excitation energy to the compound nucleus that is formed. The compound nucleus, formed after neutron absorption, is very unstable, with a lifetime of approximately 10^{-14} seconds. The "nuclear fluid" of the excited, large compound nucleus undergoes large oscillations and shape-deformations, because the repulsive Coulomb force in such a large, highly excited nucleus is very destabilising; in such nuclei, the short-ranged strong nuclear interaction "struggles" to keep the violently oscillating nucleus "in one piece". If the compound nucleus is sufficiently excited, it will, during one such "oblate spheroid to prolate spheroid" oscillation, "overshoot" the prolate shape and deform into an elongated dumbbell shape, the two ends of which then repel each other strongly via the long-ranged Coulomb repulsion. The strong nuclear interaction, being very short-ranged, is no longer able to hold the two positively charged ends together. The two dumbbell-shaped "blobs" scission within approximately 10^{-20} seconds into two positively charged nuclear fragments, which repel each other with such tremendous Coulombic repulsion that many of their orbital electrons are torn off as a result of the fierce acceleration of these two fission fragments. Two highly positively charged *fission fragments* are thus formed. The (usually 2) fission fragments are highly excited and excessively rich in neutrons, so that neutrons will evaporate from the accelerated fission fragments. The Coulomb barrier prevents charged particles from evaporating from the fission fragments; only neutrons can evaporate, because they are electrically neutral. The near-instantaneously released neutrons are called *prompt* fission neutrons (PFNs). On a longer timescale, ranging to more than a minute, delayed fission neutrons (DFNs) are also released; in the case of the fission of $^{235}\mathrm{U}$, circa 0.68% of fission neutrons are released as delayed neutrons, from a number of neutron-emitting radionuclides that are formed so far from the valley of β-stability that they may approach the neutron drip-line. Delayed neutrons are of the utmost importance for reactor control. In the absence of delayed neutrons, the reactor period would be in the order of $10^{-5}\ s$ (Duderstadt and Hamilton, 1976; Lamarsh and Baratta, 2017; Lewis, 2008; Stacey, 2018), that is to say, reactor power could have doubled in a mere $10\ \mu s$; it is impossible to control such a reactor — it would have been a "bomb".

2.1.3 Fission neutron spectra

The energy spectrum of prompt fission neutrons emitted by $^{235}\mathrm{U}$ is described to high accuracy by the Watt PFN spectrum formula, with fitting parameters determined by (Cranberg *et al.,* 1956); the

mathematical form is

$$Q(E) = 0.45283 \exp\left(\frac{-E}{0.965}\right) \sinh\sqrt{2.29E}$$

which is displayed in Figure 2.5.

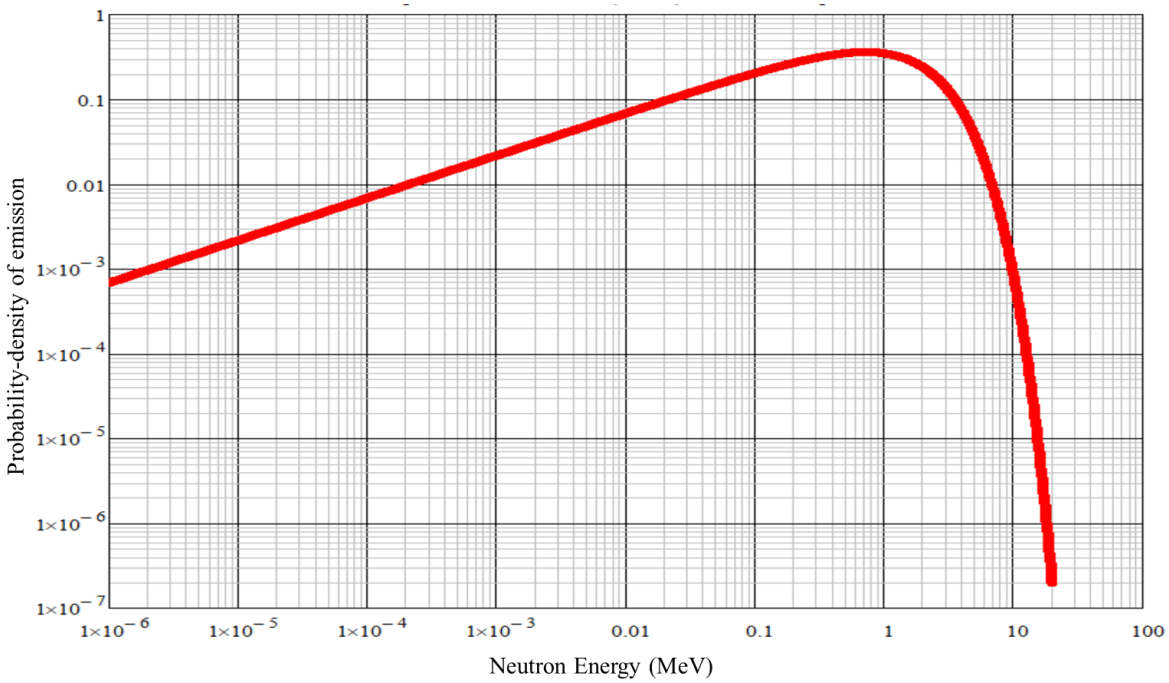

Figure 2.5: Energy-spectrum Q(E) at which prompt fission neutrons are emitted when ^{235}U fissions (Cranberg et al., 1956).

2.1.4 Neutron spectra in fissile systems containing hydrogenous material

In a material containing ^{1}H as a dominant neutron scatterer, emitted PFNs (and DFNs) are slowed down and moderated to take on the neutron spectrum $\varphi(E)$ shown in Figure 2.6, which was calculated with a long MCNP simulation of the criticality excursion.

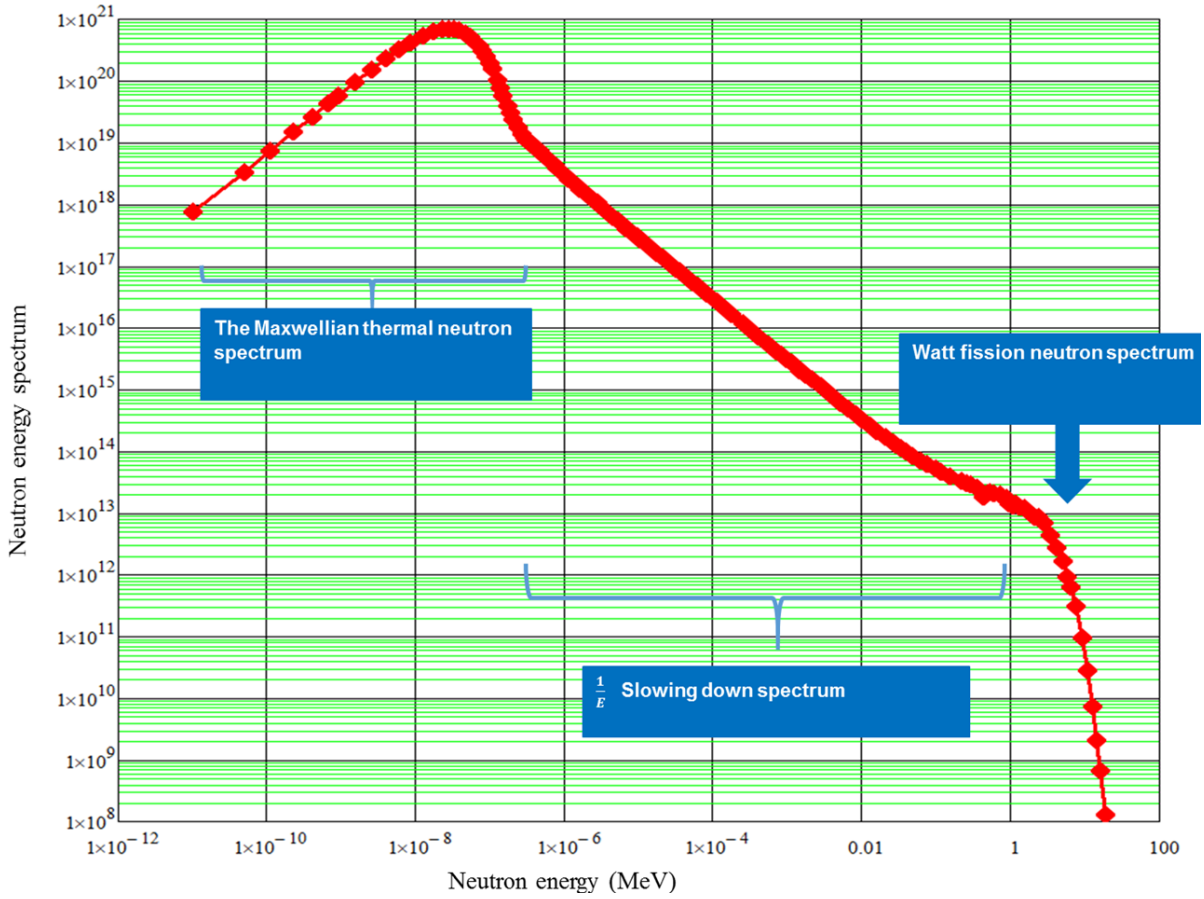

Figure 2.6: The reconstructed neutron energy spectrum in watery fissioning volume.

As indicated in the annotations, the neutron spectrum has 3 principal regions: the PFN spectrum seen on the RHS, the slowing-down spectrum in the centre and the Maxwellian thermal neutron spectrum on the LHS.

Some characteristics of the calculated neutron spectrum seen in Figure 2.6, are summarised in Table 2.1.

Table 2.1: Characteristics of the neutron spectrum inside the fissile material in which the criticality excursion takes place.

Characteristic	**Value**
Percentage of neutrons with $E \in [10^{-11}; 10^{-6}]$ MeV, i.e. thermal neutrons	40.7 %
Percentage of neutrons with $E \in [10^{-6}; 10^{-1}]$ MeV, i.e. epithermal neutrons	25.2 %
Percentage of neutrons with $E \in [10^{-1}; 20]$ MeV, i.e. fast neutrons	34.2 %
Average neutron energy	0.60 MeV

2.1.5 Fission product yield

The yield as a function of the mass number A of the fission products, is shown in Figure 2.7; this graph was produced by using the JANIS-4 GUI (Soppera *et al.*, 2013) to access ENDF/B-7.1 nuclear data, and porting the nuclear data to plotting software.

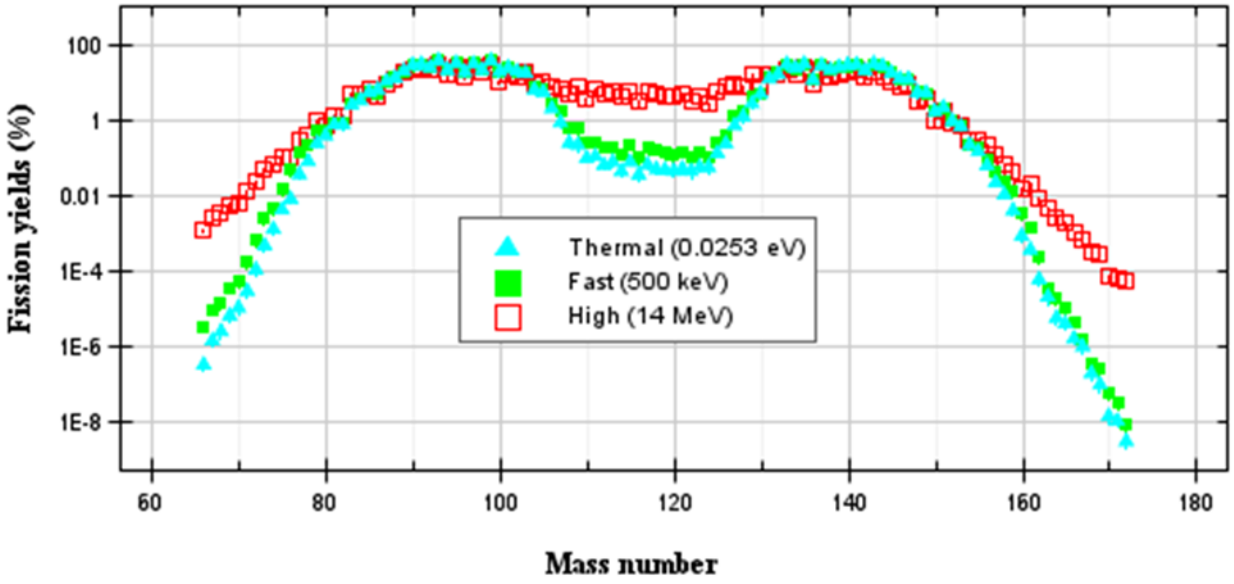

Figure 2.7: The fission product yields for thermal, fast and 14 MeV fission neutrons in uranium-235.

The $Y_{\mathrm{fp}}(A)$ fission-product yield curve in Figure 2.7 is colloquially known as the "M"-curve or the "twin-hump camel" curve, based on the two broad peaks or humps. The lower mass-number group of fission products have notable yields are from 65 to 110, whereas the heavy mass-number group has a broad peak from $A \in [125;\ 170]$.

The twin peaks seen in Figure 2.7, which has a logarithmic y-axis, are more prominent when plotted with a linear vertical axis, as shown in Figure 2.8.

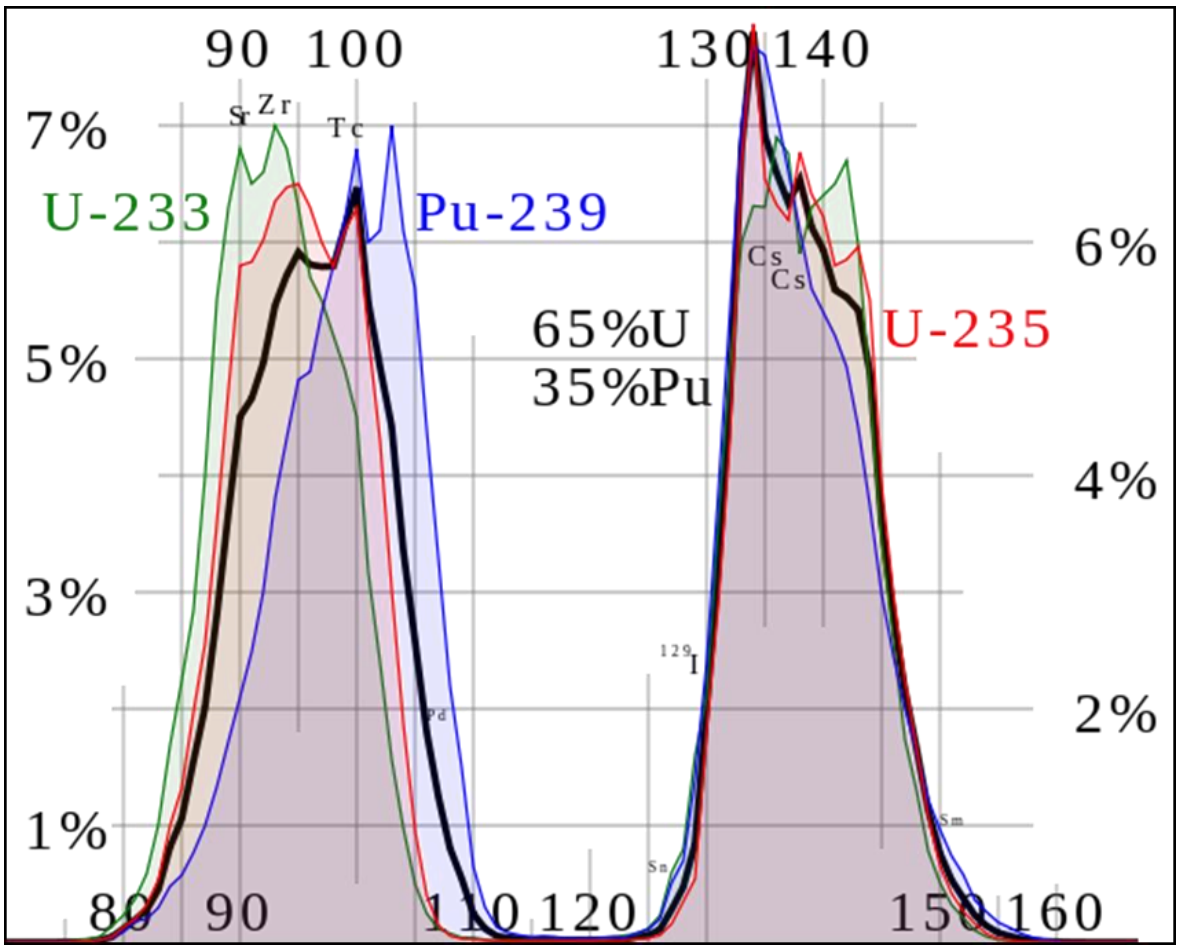

Figure 2.8: Fission product yields by mass for thermal neutron fission of ^{235}U, ^{239}Pu, a combination of the two typical of current nuclear power reactors, and ^{233}U used in the thorium cycle[13].

2.1.6 Understanding the radioactivity of fission fragments and fission products

As explained in previous sections, the initial fission fragments are very unstable and therefore decays to a succession of fission products (radionuclide inventory). The inventory of radioactive fission products produced by the criticality excursion can either decay into stable nuclides or a long radioactive decay chain which ends with stable fission products. The activity of each fission product (radionuclide) is mathematical expressed in terms of exponential decay law, as in equation (2.2).

$$A = A_0 e^{-\lambda t} \tag{2.2}$$

where:

A = activity measured in (Bq) of the fission product at time $t = t + \Delta t$

A_0 = initial activity of the fission product at time $t = 0\ second$

[13] https://en.wikipedia.org/wiki/Nuclear_fission#/media/File:ThermalFissionYield.svg

λ = decay constant of the fission product

$-$ = the minus sign represent the decay in activity of the fission product over time

Figure 2.9 on page 28 presents a colour-coded chart of the nuclides (Soppera *et al.,* 2013).

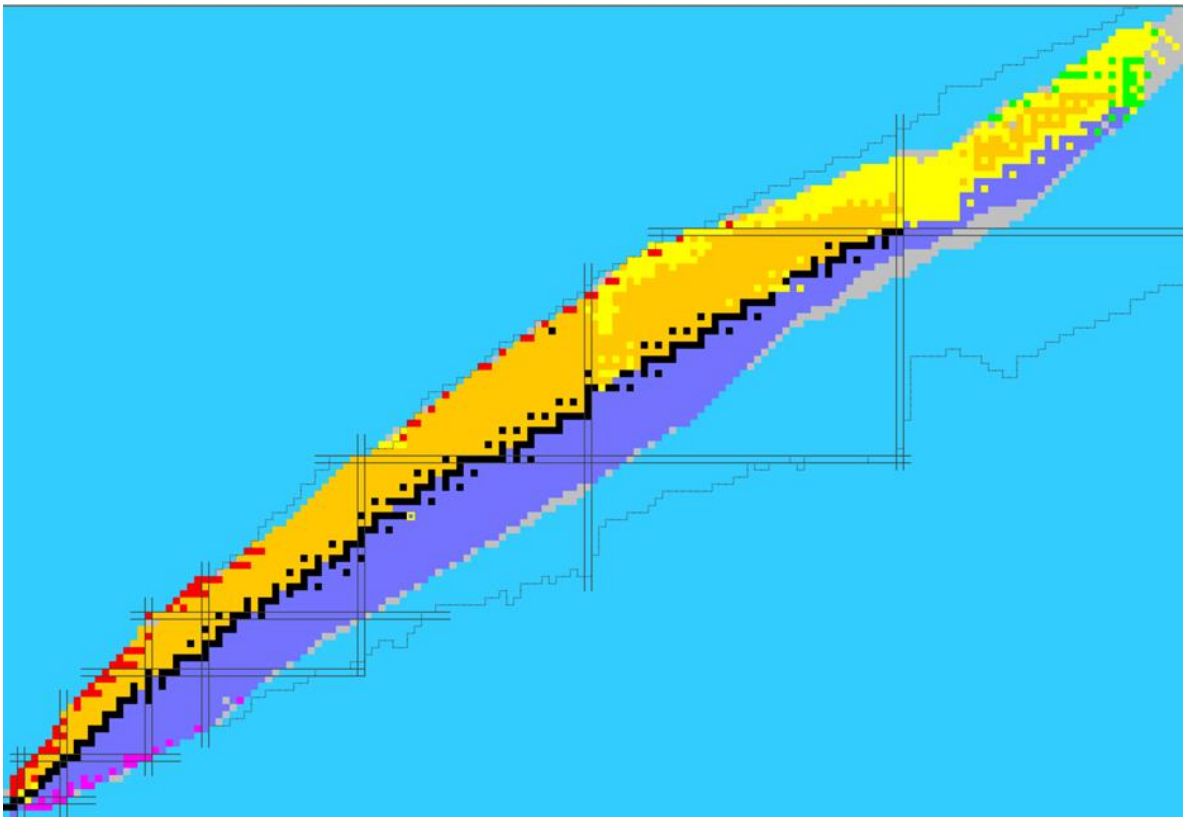

Figure 2.9: A colour-coded chart of the nuclides.

Where legend means:

	Proton drip-line
	Neutron-poor nuclei that transition via β^+ and EC
	α-particle emitting nuclei
	Stable nuclei
	Neutron-rich nuclei that transition via β^-
	Neutron drip-line
	Spontaneously fissioning heavy nuclei
	Short-lived nuclides with unknown properties

Let $BE(Z,A)$ denote the binding energy ("BE") in a nucleus with atomic number Z and mass-number A. If a 3D plot of the chart of the nuclides is made, with every isotope's $\frac{1}{BE(Z,A)}$ parameter, namely, the reciprocal of the binding energy per nucleon, plotted on the vertical z-axis, the zig-zag black line of β-stability that is seen in Figure 2.9 can be visualised as the "valley of β-stability, as seen in Figure 2.10. The higher the binding energy per nucleon, the lower the 3D vertical height of

the isotope in Figure 2.10. The highest $BE(Z,A)$ is observed in the immediate vicinity of the $^{56}_{26}\mathrm{Fe}$ nucleus, which lies at the vertical minimum of the valley of β-stability.

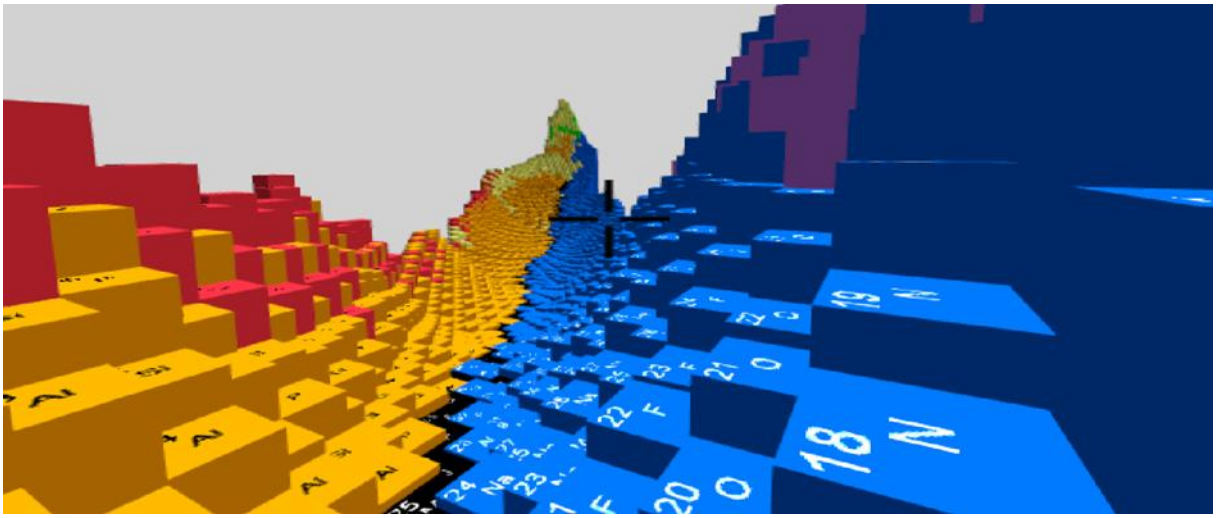

Figure 2.10: A 3D plot of the chart of the nuclides, showing the valley of β-stability amidst the surrounding hills of β-instability[14].

Where legend means:

Proton drip-line
Neutron-poor nuclei that transition via β^+ and EC
Stable nuclei
Neutron-rich nuclei that transition via β^-
Spontaneously fissioning heavy nuclei
Neutron drip-line

The proton drip-line is encountered when nuclei are so excessively neutron-poor that they spontaneously eject protons; the neutron drip-line is where nuclei are so excessively neutron-rich that they spontaneously eject neutrons. Delayed fission neutrons may be emitted by fission fragments located towards the neutron drip-line.

With reference to Figure 2.10, one can state that isotopes located on the neutron-rich side of the valley of beta-stability (colour-coded blue and purple) are unstable because they have excessively high $\frac{\text{neutron}}{\text{proton}}$ ratios.

The reason for the intense radioactivity of fission products, is now developed. The $^{235}\mathrm{U}$ nucleus has a $\frac{\text{neutron}}{\text{proton}}$ ratio of

[14] This diagram was generated using Nucleus-Win 2.1, developed at the Atomic Mass Data Centre (AMDC) in France (https://www.csnsm.in2p3.fr). Most of the activities of this organisation has since relocated to China.

$$\frac{N}{Z} = \frac{235 - 92}{92} \approx 1.55$$

whereas a stable nucleus with $A \approx 140$ requires a $\frac{\text{neutron}}{\text{proton}}$ ratio in the range

$$\frac{N}{Z} \approx 1.40;$$

a stable nucleus with $A \approx 90$ requires a $\frac{\text{neutron}}{\text{proton}}$ ratio in the range

$$\frac{N}{Z} \approx 1.25.$$

When ^{235}U fissions, the fission fragments will have a $\frac{\text{neutron}}{\text{proton}}$ ratio

$$\frac{N}{Z} \geq 1.5$$

which means that fission fragments have a very large *neutron excess.* This neutron excess makes the fission fragments highly unstable, i.e., radioactive; in Figure 2.10 these fission fragments will lie high up on the blue side of the slope/cliff, very far from the valley of β-stability. Most fission fragments are extremely unstable as a result of the large neutron excess in their nuclei, and therefore transition quickly to a large ensemble of fission products.

2.1.7 High neutron excess in fission fragments cause the emission of delayed fission neutrons (DFNs)

In the first seconds to minutes after fission, the neutron excess is so high that some fission fragments transition by the emission of neutrons; this phenomenon is termed delayed fission neutron (DFN) emission. The energy spectrum of delayed fission neutrons (reproduced from lectures presented at North West University (NWU), South Africa in 2011, by Professor Kostadin Ivanov), is shown in Figure 2.11.

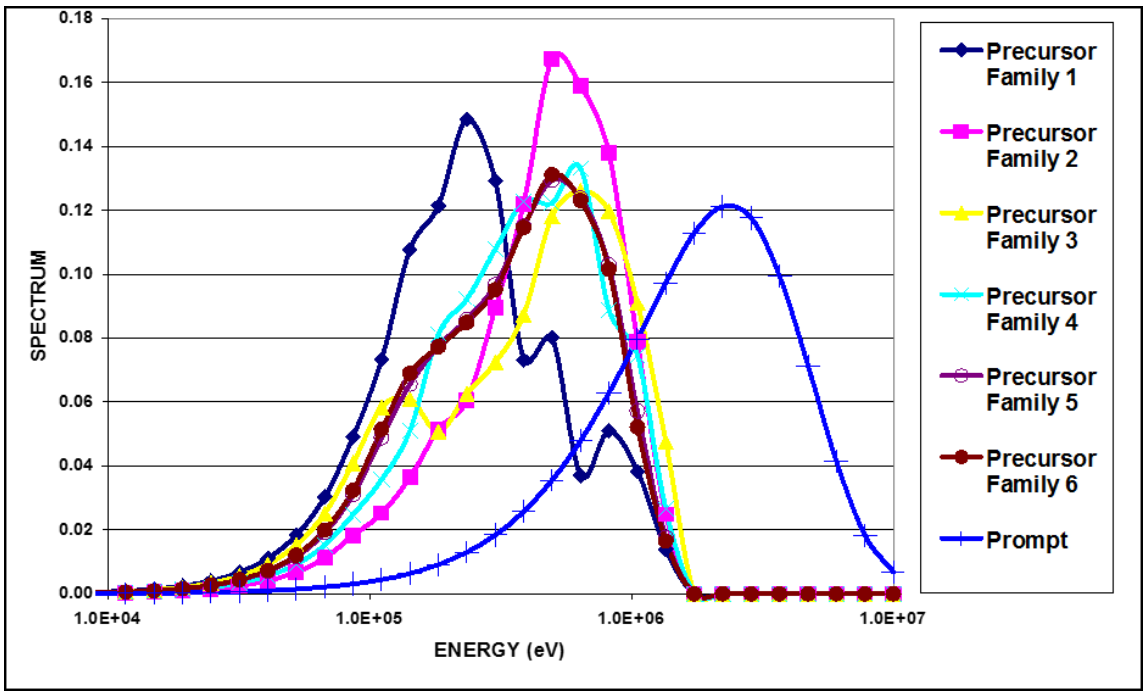

Figure 2.11: Comparison of energy spectra of delayed fission neutrons, with prompt fission neutrons.

Figure 2.11 indicates that the emission energies of DFNs are somewhat lower than that of PFNs; this makes DFNs easier to moderate and contribute to fission, compared to PFNs.

After a few hours, many of the initially produced, short-lived fission fragments will transition to fission products, which mainly transmute via β^--decay, in a quest to lower the excessively high $\frac{n}{p}$-, i.e., $\frac{N}{Z}$-ratio. This means that fission products are primarily β^--electron emitters; they will also emit ionizing photons, as a byproduct of β^--decay[15].

2.1.8 The neutron multiplication factor, k_{eff}

The nuclear fission chain reaction is fundamentally based on neutron-balance, and this can mathematical be expressed by the effective neutron multiplication factor, k_{eff}, given by Eq. (2.3).

$$k_{\text{eff}} = \frac{\text{number of neutrons in one generation}}{\text{number of neutrons in preceding generation}} \tag{2.3}$$

Figure 2.12 shows how a population of free neutrons in a reactor can either diminish $(k_{\text{eff}} < 1)$, be constant $(k_{\text{eff}} = 1)$ or grow $(k_{\text{eff}} > 1)$ as a function of time.

[15] Note by co-supervisor TJvR: In the language of astrophysics, the decay of fission products can be characterized as an S-process, because it is β^--delayed.

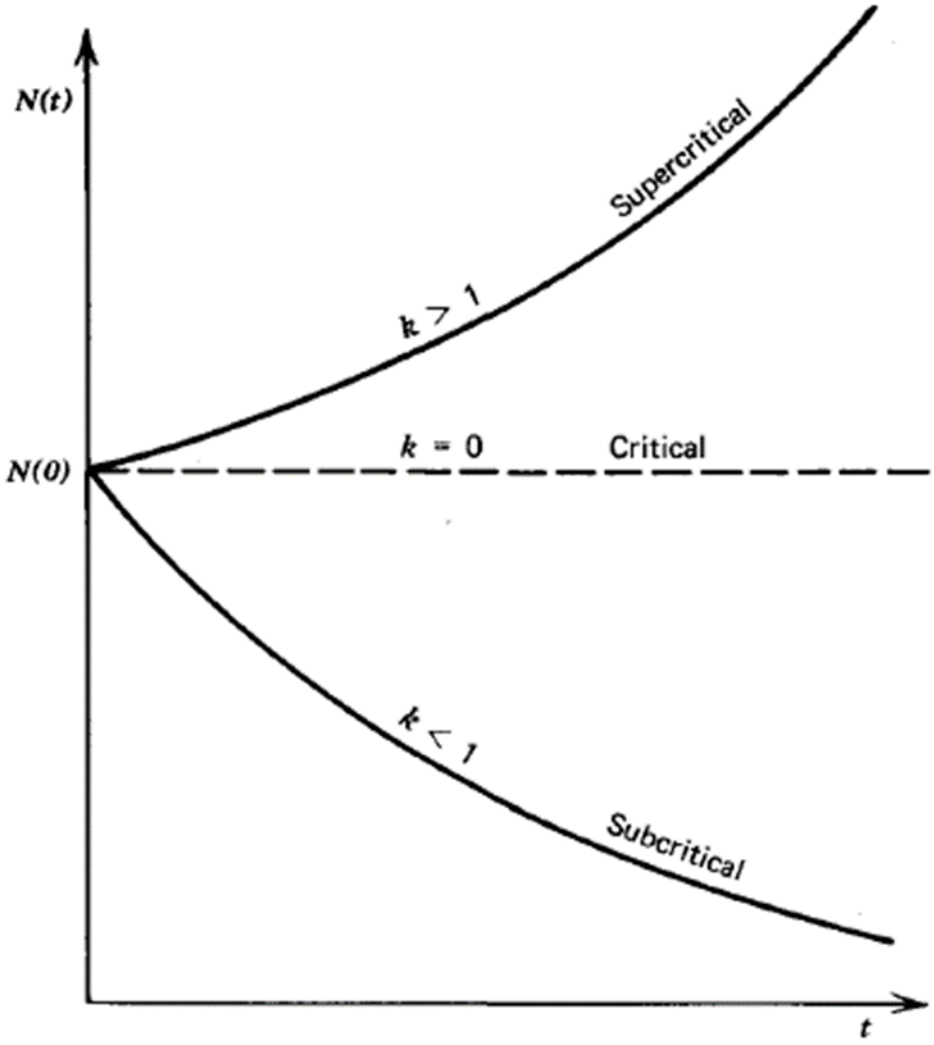

Figure 2.12: The phenomenological behaviour of the neutrons of two successive generation in a criticality system (Duderstadt and Hamilton, 1976:78).

The criticality condition of a system, expressed in terms of k_{eff} is shown in Table 2.2.

Table 2.2: The state of a system with fissile material, expressed in terms of k_{eff}.

k_{eff}	**Criticality condition**	**Neutron-balance**
$= 1$	critical	Steady-state
> 0	Supercritical	Increasing
< 0	Subcritical	Decreasing

2.1.9 The concept reactivity

The behaviour of the ratio between the number of neutrons in two successive generations in a fissile system, can be expressed in terms of (1) the effective neutron multiplication factor k_{eff} and (2) the reactivity, ρ, which is defined as,

$$\rho = \frac{k_{\text{eff}} - 1}{k_{\text{eff}}} \tag{2.4}$$

The power $P(t)$ of a fissile system as a function of time, t, depends on the reactivity, ρ, in the manner shown in Table 2.3.

Table 2.3: The state of a system with fissile material, expressed in terms of the reactivity ρ.

$\boldsymbol{\rho}$	**Description**	**Power vs time, $\boldsymbol{P(t)}$**
$= 0$	Zero reactivity	Steady-state
> 0	Positive reactivity	Increasing power
< 0	Negative reactivity	Decreasing power

As can be noted in Table 2.2:, to have a non-zero steady-state neutron population in a fissile system (containing no fixed sources), the reactivity should be zero, i.e., k_{eff} must have the value 1. The insertion of negative reactivity ($\rho < 0$) into a fissile system decreases the neutron population and hence the power $P(t)$, while the insertion of positive reactivity ($\rho > 0$) increases the neutron population and power; if this remain uncontrolled, it will lead to a criticality excursion.

It is imperative to maintain a (non-reactor) system containing fissile material in a subcritical state, with an adequate margin of sub-criticality. This will ensure the safety of processes involving fissile material, such as the PUREX process. Nevertheless, as highlighted in Chapter 1, despite all efforts to ensure the safety of criticality systems, there often exist a chance of a sudden increase in the neutron-population, leading to a criticality excursion. The possible adverse change of the neutron population in a fissile system is a function of the parametric factors as expounded in § 2.2, which can be remembered at the hand of two handy initialisms — MERMAIDS and MAGIC MERV.

2.2 The factors affecting the criticality of a fissile system

As highlighted in § 1.3, the parameters driving a nuclear fission chain reaction underlying a potential nuclear criticality accident, can be conceptualised with the abbreviation MERMAIDS — Mass, Enrichment, Reflection, Moderation, Absorption, Interactions, Density and Shape. Alternatively, the initialism MAGIC MERV — Mass, Absorption, Geometry, Interactions, Concentration, Moderation, Enrichment, Reflection and Volume, can be used. These physical factors are functionally inter-connected, as expounded below. The acronym MERMAIDS will be used for presentation in this subsection.

2.2.1 Mass

The mass parameter for a system expresses the fact that a minimum mass of the $^{235}\mathrm{U}$ fissile isotope must be present before criticality can be reached. If a higher mass of $^{235}\mathrm{U}$ is present, attaining criticality is, generally speaking, easier. The more fissile material present in the system, the higher the probability that a free neutron will interact with $^{235}\mathrm{U}$ and cause nuclear fission. The mass of $^{235}\mathrm{U}$ required to support a fission chain reaction at $k_{eff} = 1$, for a given geometry, enrichment and moderation configuration of a fissile system, is known as the critical mass.

2.2.2 Enrichment

Three uranium isotopes are found in nature; these isotopes and their natural isotopic abundances are shown in Table 2.4.

Table 2.4: Average natural isotopic abundance in terrestrial uranium (Meija et al., 2016).

Isotope of Uranium	**Mass-percentage of isotope** (%)
U-238	99.27417
U-235	0.72041
U-234	0.00540

It is very difficult to reach criticality using natural uranium, because the natural mass fraction of the fissile isotope, $^{235}\mathrm{U}$, is so low. If un-enriched uranium is used in nuclear reactors, only graphite and heavy water can normally be used as moderator and reflector materials, because using light water as moderator and coolant will absorb too many neutrons and make reactor operation impossible. Even with the use of graphite or heavy water, fuel cycle lengths with the use of natural uranium, are in the order of 4 to 6 weeks, which makes continuous, online refuelling necessary. All these difficulties and operational agony can be averted by enriching the uranium to e.g., 4.75% in the fissile isotope $^{235}\mathrm{U}$. With the use of enriched uranium, a batch of fuel can serve as long as 18 months in a commercial PWR power reactor.

Today, all civilian reactors operate with LEU — low enrichment uranium, i.e., the mass-enrichment in the isotope $^{235}\mathrm{U}$ is below 20%. When waste material from an old facility that produced HEU is processed to recover enriched uranium, it is this HEU that will be recovered. Therefore uranium enrichments as high as 90% or even 93% may be encountered in a PUREX process facility.

2.2.3 Reflection

A neutron reflector can reflect neutrons that would otherwise escape from the system, back into the system. The most efficient neutron reflector materials are characterised by a high ratio,

$$\frac{\sigma_s(E)}{\sigma_a(E)},$$

over a wide neutron energy range. Here σ_s denotes the neutron scattering cross-section and σ_a the absorption cross-section. Only a few reasonably affordable materials are high-efficiency neutron reflectors, namely, $\boxed{^{2}\mathrm{H}}$, $\boxed{^{9}\mathrm{Be}}$, $\boxed{^{\mathrm{nat}}\mathrm{C}}$ $\boxed{^{16}\mathrm{O}}$ and $\boxed{^{90}\mathrm{Zr}}$. Figure 2.13 shows the favourable ratio $\frac{\sigma_s(E)}{\sigma_a(E)}$ for the interactions of $^{9}\mathrm{Be}$ with neutrons; ENDF/B-7.1 nuclear data in the JANIS-4 GUI[16] system (Soppera *et al.*, 2013).

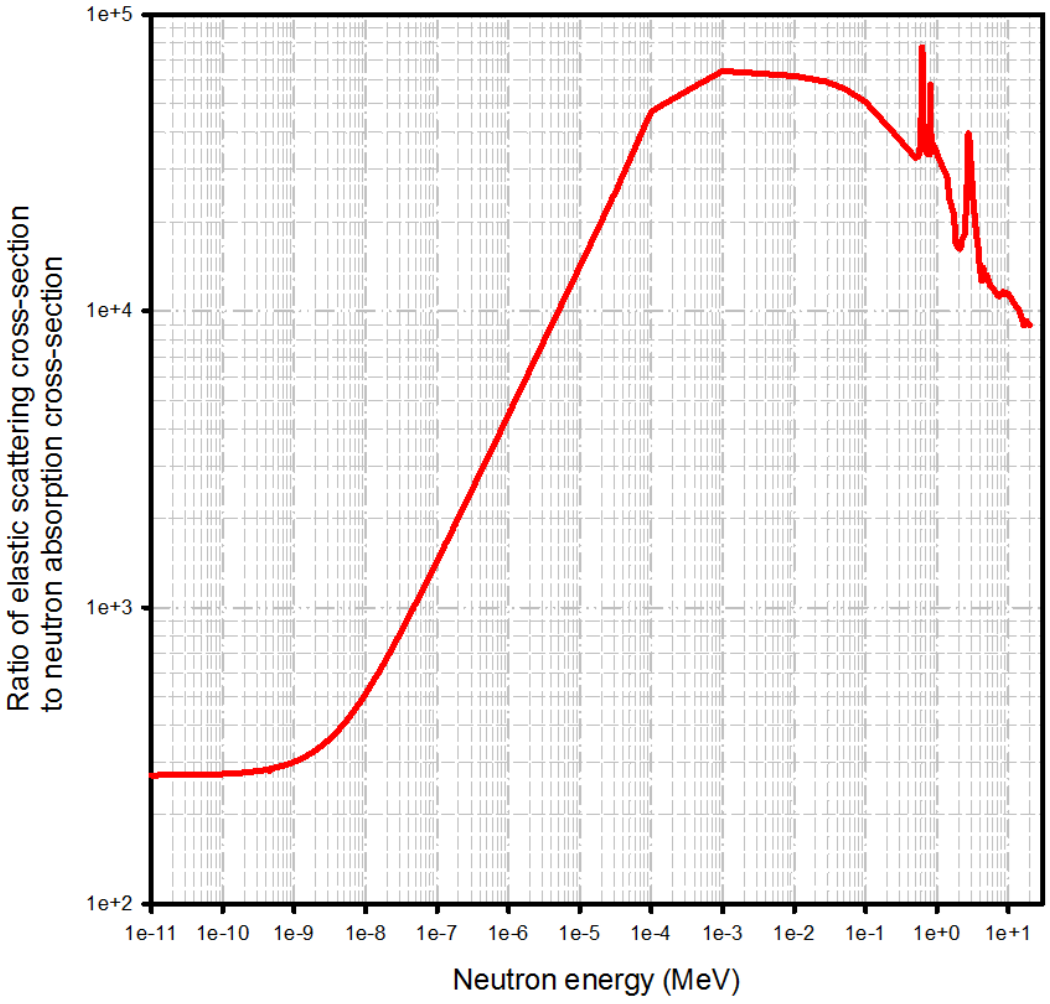

Figure 2.13: High ratio of the cross-section for neutron scattering (σ_s) to neutron absorption (σ_a), of the element beryllium.

[16] JANIS is a Graphical User Interface for accessing and plotting nuclear data; the initialism JANIS stands for "JAva Nuclear Information System". It was developed at the NEA OECD in Paris, France.

Figure 2.13 shows that the probability of neutron scattering in $^{9}\mathrm{Be}$ will be between 200 and 80,000 times higher than the probability of neutron absorption, i.e., Be is excellent at returning neutrons back into the fissile system, i.e., it is a high-efficiency neutron reflector. Only a handful of isotopes, as listed above, show such excellent neutron reflector properties.

Natural hydrogen, $^{1}\mathrm{H}$, is an excellent neutron moderator, and a second-tier neutron reflector. Materials such as, $^{\mathrm{nat}}\mathrm{Be}$, $^{2}\mathrm{H}_2{}^{\mathrm{nat}}\mathrm{O}$ and $^{2}\mathrm{H}_2{}^{\mathrm{nat}}\mathrm{C}$ and graphite are first-tier neutron reflectors. Materials such as ordinary (i.e., light) water, ordinary concrete, polyethylene, silicon dioxide, lead and iron are second-tier neutron reflectors.

2.2.4 Moderation

The neutrons born in the fission process have high energies and are called fast neutrons. The fission cross section of fissile isotopes, $\sigma_{(n,f)}(E)$, for fast neutrons, are very low. Fission and therefore a self-sustaining fission chain reaction, becomes far more achievable if the neutrons are slowed down by a neutron moderator. The best and most affordable neutron moderators are light water, heavy water and graphite. Via scattering interactions with the moderator, neutrons are slowed down, and a portion of the free neutron population becomes thermalised, i.e., they reach thermal equilibrium with the material in which they move. Thermalised neutrons van a Maxwellian energy distribution and their average energy is related as follows to the temperature of the material medium: $E_{av} = \frac{3}{2}k_B T$, where E_{av} is the average neutron energy, k_B is the Boltzmann constant and T is the temperature (expressed in the SI unit Kelvin) of the material medium. This equation is amazing in that it couples the sub-microscopic world of particle motion with the macroscopic world of temperature.

Let $\boxed{A = \frac{m_{\mathrm{scatterer}}}{m_n}}$ be the ratio of the mass, denoted as $m_{\mathrm{scatterer}}$, of the mono-isotope that elastically scatters neutrons. Then the number $n(A, E', E_{\mathrm{th}})$ of elastic neutron scattering collisions with the mono-isotopic scattering medium that is required to thermalise an incident neutron with initial energy E', down to the thermal energy range, $E_{\mathrm{th}} = 0.0253\ \mathrm{eV}$, is given by equation (2.5),

$$n(A, Q, E', E_{\mathrm{th}}) = \mathrm{ceil}\left(\frac{\log\left(\frac{E'}{E_{th}}\right)}{\log\left(\frac{E'}{E_{\mathrm{exp}}(A, E')}\right)}\right) \tag{2.5}$$

Where

$$E_{\exp}(A, E') = \left(\frac{1+\alpha(A)}{2}\right) E'$$

and

$$\alpha(A) = \left(\frac{A-1}{A+1}\right)^2.$$

In the above expressions (2.5) (Müller, 1986), E' is the energy of the incident, fast neutron, and $E_{th} \approx 0.0253\ \mathrm{eV}$ is the energy of a thermal neutron, m_n is the mass of the neutron. Because fission neutrons are born at an average energy of 2 MeV (Cranberg *et al.*, 1956), therefore, $E' = 2\ \mathrm{MeV}$. The number of elastic scattering collisions required for the thermalisation of fission neutrons, in mono-isotopic materials, are summarised in Table 2.5.

Table 2.5: Number of elastic scattering events required to thermalise a fission neutron.

Scattering Isotope	**Number of elastic scattering events required to thermalize a typical fission neutron**
^{1}H	27
^{2}H	31
^{9}Be (beryllium metal)	92
^{12}C (graphite)	118
^{16}O	154

It is seen that ^{1}H is a very efficient moderator, i.e., degrader of neutron energy. This fact makes it clear why water-ingress into a volume containing fissile material, is a serious safety concern — the presence of ^{1}H will scatter neutrons into the energy domain where the fission cross-section of $^{235}\mathrm{U}$ is high.

2.2.5 Absorption

Absorption is the process whereby free neutrons are removed from the system without fission occurring, thereby reducing the neutron fluence rate $\varphi(E)$ and hence the probability of nuclear fission reactions. The more neutron absorbers are present in a system, the higher the mass of the fissile isotope $^{235}_{92}\mathrm{U}$ required to achieve criticality. This means that introducing neutron absorber materials can serve to lower the k_{eff} of a fissile system, i.e., protect against criticality. Neutron absorbing materials are sometimes referred as neutron poisons. The most potent neutron poisons that can be used to control and prevent criticality are cadmium, boron and gadolinium. The second-tier neutron absorbers include lithium-6, indium and silver. Boron is by far the most affordable neutron absorber. The specific isotopes of B, Gd and Cd that absorb neutrons very well, are $^{10}\mathrm{B}$, $^{157}\mathrm{Gd}$ and $^{113}\mathrm{Cd}$.

2.2.6 Interaction

Interaction (also referred to as reaction) is the process whereby there is exchange of neutrons between two or more systems containing fissile isotopes such as $^{235}\mathrm{U}$. Placing one or more vessels containing fissile $^{235}\mathrm{U}$, closer to each other, raises the k_{eff} of the overall system.

2.2.7 Density

In nuclear criticality safety, the density and concentration of the fissile isotopes are both measured in mass per unit volume, and are therefore used interchangeably. This translate to the dictum: the denser the concentration of fissile material in the solution of a highly moderated system, the higher will the k_{eff} parameter become, i.e., the more one is "tickling the tail of the dragon". Conversely, lowering the concentration of the fissile isotopes in a system will lower the value of the k_{eff} parameter, which means that the system is further from criticality.

2.2.8 Shape

For the purpose of nuclear criticality safety, the terms "shape" and "geometry" of a fissile system have identical meanings. The shape and size of a system can be designed to make a criticality excursion impossible or very unlikely. One design principle is the use of high-leakage geometries such as flat pans or thin pipes. High-leakage geometries have large surface-to-volume ratios, which makes it easy for neutrons to leak out of the system and be un-available for further fission reactions. Avoiding or minimising neutron reflection is another design-principle for high-leakage geometries.

2.3 Nature of a nuclear criticality accident in aqueous fissile media

If a fissile system is supercritical on only the basis of the small fraction of DFNs, then the period of the system will be in the order of several seconds, i.e., the system called delayed-supercritical and is still controllable. Once a fissile system is critical on the contribution of PFNs alone, it is said to be prompt critical, and its period can be as short as $10^{-5}\ s$, i.e., it has become prompt-supercritical and is no longer controllable.

The fertile $^{238}\mathrm{U}$ in an aqueous, homogeneous solution of, e.g., uranyl nitrate, undergo spontaneous fission reaction at a low frequency – through which each fission reaction releases approximately two neutrons. Whilst the fissile $^{235}\mathrm{U}$ in an aqueous, homogeneous solution of, e.g., uranyl nitrate, can accidentally accumulate to a critical mass. The released free neutrons may interact with the critical mass of the fissile $^{235}\mathrm{U}$ and subsequently cause fissioning and releases more electrons, which may lead to a prompt supercritical state (i.e., $k_{\mathrm{eff}} > 1$), and if this is not prevented, the result will be a

criticality accident (Duderstadt and Hamilton, 1976; Johnson, 2017; Lamarsh and Baratta, 2017; Lewis, 2008; Skinner, 2017; Stacey, 2018; DOE-HDBK-1019/1-93 DOE (US), 2015; DOE-STD-1136-2017 DOE (US), 2017 and IAEA-TECDOC-1601, 2019). The resultant (prompt) supercriticality can be described as a sudden, unplanned power increase over a very short period of time — for a prompt supercritical system, the power doubling time can be below milliseconds, i.e., a timescale that cannot possibly be controlled by any conceivable control system. That is, the power $P(t)$ will increase exponentially in an extremely short time to an initial, single power-spike, also called the initial pulse, the initial burst or initial power peak. This may be followed by a succeeding quasi-steady-state or transient-state of decreasing power, and even a termination of criticality as a result of some fissile $^{235}\mathrm{U}$ having been forced out of the system by e.g., splashing. The initial criticality burst also produces neutron poisons such as $^{135}\mathrm{Xe}$. The first burst will usually release between circa 10^{15} and 10^{18} fissions. It can be potentially followed by subsequently oscillatory spikes of somewhat lower power, when compared to the first power-spike. The power of later spikes is suppressed by the evolution of gas bubbles and neutron poisons.

The first spike of a nuclear criticality accident can increase the temperature of a fissile solution containing $^{235}\mathrm{U}$. Such heating may lead to evaporation or possible splashing and redistribution of the fissile $^{235}\mathrm{U}$ solution within the critical system, and consequently decrease the density of the fissile material. This will in turn decrease the ability of a moderator to moderate and reflect neutrons into the volume of fissile material. This may terminate the nuclear criticality excursion without an additional series of later follow-up power spikes.

In instances where the HEU is not removed from solution by the initial power burst, the fission products generated in the excursion will cause gas evolution by radiolysis, or bubbles of steam, which decreases the reactivity of the fissile solution. After the gas and steam bubbles escape, a critical configuration may again be attained, leading to yet another supercritical state, i.e., a succession of follow-up pulses. This is characterised by oscillating spikes of relative lower fission yield when compared to the first prompt critical burst. Figure 2.14 on page 40 presents a typical example of the power-spikes, i.e., the function $P(t)$, over a period of time, for a fissile solution undergoing a criticality accident.

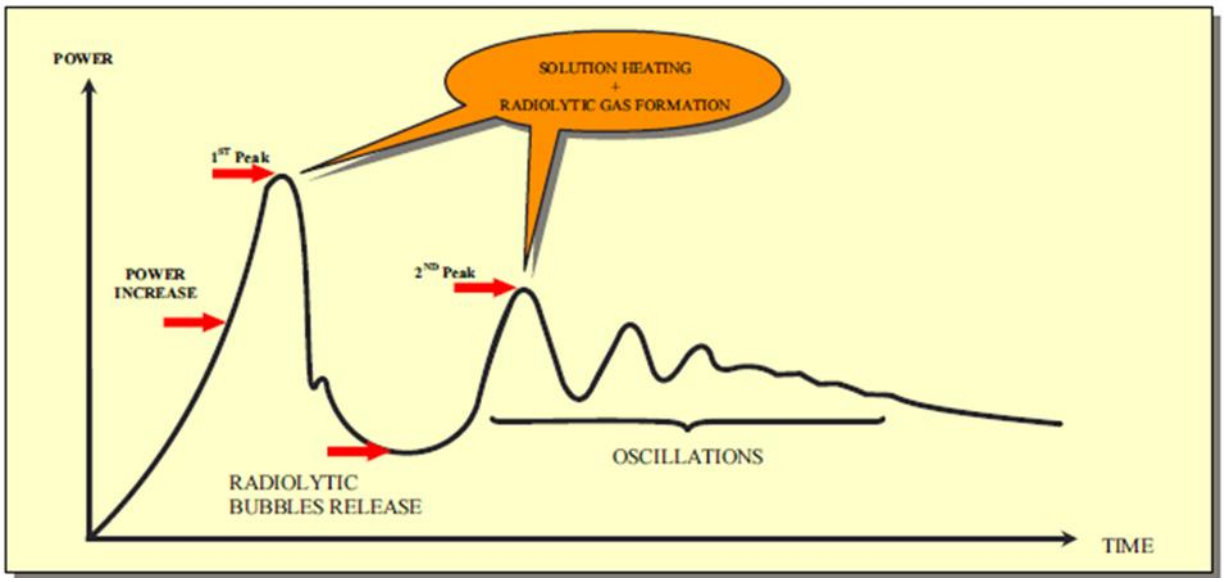

Figure 2.14: The power excursion for a fissile solution (IAEA-TECDOC-1601, 2008).

The critical power excursion shown in Figure 2.14, is not a single pulse but rather a substantial initial pulse followed by a succession of waning "tailing" pulses of criticality.

The focus in this study falls on radiation doses from neutrons and photons generated during the initial burst — the assumption is that this initial pulse is detected by a CAAS and that the area is then promptly evacuated, before the secondary train of pulses begins (there is typically a time-gap of some minutes between the first and the second power spike, which will give time for evacuation). McLaughlin *et al.* (2000) states that only 2 out of 22 criticality accidents were characterised by an extended duration — the 1962 criticality accident at Handford in the USA lasted about 37.5 hours, while the Tokai-mura accident in 1999 in Japan, lasted around 20 hours before it was terminated by emergency intervention.

In Table 1.1 on page 3, some approximate radii of non-survivability for an unshielded criticality excursion, are listed. In general, people positioned within a few metres from the epicentre of the volume of fissile material, have no chance of survival. For this reason, engineered and administrative criticality controls are imperative, to ensure that workers will never encounter the dreaded "blue flash of death" that characterises a criticality excursion.

2.4 Health risk to persons exposed during a nuclear criticality excursion — acute radiation syndrome (ARS)

As explained in Chapter 1, a nuclear criticality accident leads to the prompt emission of potentially lethal levels of intense ionising radiation. The radiation is typically emitted in a short flash, i.e., it is classified as an acute exposure, i.e., a high dose over a short period of time. The health effects from

acute radiation exposure are referred as acute radiation syndrome (ARS); the popular press usually refers to it as “radiation sickness” or “radiation poisoning”.

The clinical manifestation of acute exposure may become manifest within approximately an hour and may last for several months. Table 2.6 presents a summary of acute radiation syndrome (ARS) for the exposure of adults to high doses of whole-body penetrating ionising radiation (ICRP, 2007; ICRP, 2012; Zankl *et al*., 2018).

Table 2.6: The effects of acute radiation exposure on human health — acute radiation syndrome (ARS).

Degree of ARS	**Dose** (mSv)	**Effect on organ (and/or tissue)**	**Time to develop effect**
Sub-clinical	100 – 1000	Bone marrow syndrome No manifest illness No medical care required	30 – 60 days
Mild	1000 – 2000	Bone marrow syndrome Mild manifest illness Medical care required	30 – 60 days
Moderate	2000 – 4000	Bone marrow syndrome Moderate manifest illness Medical care required Usually survivable	30 – 60 days
Severe	4000 – 6000	Gastro-intestinal syndrome; Stem cells in small intestines severely depleted; Intensive medical care required; Usually fatal	6 – 9 days
Severe	4000 – 6000	Pneumonitis, i.e. damage to the lungs Medical care required Potentially fatal	1 – 7 months
Very severe	6000 – 8000	Gastro-intestinal syndrome; Stem cells in small intestines wiped out; Intensive medical care required; Non-survivable; always fatal	6 – 9 days
Lethal	> 8000	Whole body exposure	Death before day 10

2.5 Shielding the ionizing radiation emitted in a criticality excursion

2.5.1 Introduction

The ionising radiation emitted during a criticality excursion, is identical to the radiation emitted by nuclear fission reactors. Since the late-1940s, humanity has developed vast experience and a robust conceptual understanding of radiation shielding design for nuclear reactors. This knowledge can be directly applied to shielding design to mitigate the health effects of potential criticality accidents. A radiation shield that protects of people against high radiation doses, is called a biological shield.

2.5.2 Rational selection of materials for radiation shielding

When a large space is available for the placement of shielding materials, cost considerations dictate the use of ordinary concrete as principal shielding material. In rare cases such as when a facility has already been built, and shielding needs to be retro-fitted into a tight space, one may have to resort to more optimal shielding materials, i.e., materials that will give a larger dose attenuation per unit shield thickness. The materials of choice would, in such a case, typically be iron and borated poly-ethylene. Over the past centuries, iron (Fe) has consistently been the cheapest metal per unit mass, followed by lead (Pb). Of all neutron absorbers, boron is by far the cheapest and safest; terrestrial boron contains approximately 20% $^{10}\mathrm{B}$, which is the boron isotope responsible for this element's neutron absorption properties. Boron is readily available in many chemical forms, of which boron oxide and boron carbide are particularly suitable for admixture into e.g., polyethylene or paraffin wax, to enhance the shielding properties.

2.5.3 Engineered radiation safety system

When there is a possibility that high radiation doses may be encountered, an engineered radiation safety system has to be designed. The more intense and dangerous the sources of ionising radiation that are used, the higher the reliance on engineered radiation safety systems must be.

The three pillars of an engineered radiation safety system, are:

- A radiation-containment system.
- A radio-nuclide-containment system (radio-active material containment system).
- An access-control system to control access to radiation areas, e.g., prevent human entry into radiologically dangerous areas.

The above mentioned system of protection are expounded below.

Radiation-containment system

A radiation-containment system is an engineered system that counteracts, prevents, and limits high dose-rates and doses of ionising radiation in areas where people and sensitive equipment can be present. It has to maintain dose-rates and doses below ethical limiting values. A radiation-containment system has passive and active features.

Passive radiation-containment system

An example is: fixed, static radiation shielding, e.g., thick concrete shielding walls, shielding doors and entrance-labyrinths, are designed, and constructed to reduce dose-rates and doses to acceptable levels.

Active radiation-containment system

An examples is: movable, motorized plug-shields and isolation-shields move into place, based on readings from Area Radiation Monitoring System (ARMS) detectors, sensors and instructions from the safety-program which oversees the safety interlock system.

Radio-nuclide-containment system (containment system for radio-active material)

The function of the *radio-nuclide-containment system* is to prevent radio-nuclides from leaking out, that is, escaping out of controlled structures and areas. Further technical details are beyond the scope of this investigation.

Access-control system

The function of an access-control system is to prevent unauthorised people, as well as higher mammals, from entering area or workplace of relative high risk radiation level. Further technical details are beyond the scope of this investigation.

2.6 CAAS — criticality accident alarm system

In general, ionizing radiation cannot be sensed by the sensory organs. This means that radiation detectors have to be used to detect and measure the dose or dose rate. There are two categories of radiation detectors — passive and active. An example of a passive detector of radiation is a TLD — a thermoluminescent dosimeter. The passive dosimeter faithfully integrates the dose rate to record the time integral of the dose rate, i.e., the dose. Because it is passive, it cannot warn workers about high doses. An active, i.e., electrically powered radiation detection system that can warn workers and managers about a radiologically unsafe situation, is required. In the case of a facility where dose rates are normally low, but the possibility of a nuclear criticality excursion exists, a CAAS must be installed — a criticality accident alarm system. An example of facilities with CAAS installed are Tokai-

mura reprocessing plant in Japan, the Oak Ridge Y-12 enrichment plant in the United State, the pilot plant spent fuel reprocessing in China, and Trombay PUREX in India.

The technical requirements for a CAAS in a facility that processes fissile material, are specified in the standard ANSI/ANS-8.3 (Reed, 1991). Some of these specifications for a CAAS are:

- If the mass of fissile material in any single workstation exceeds
  - 700 g of ^{235}U, or
  - 450 g of ^{239}Pu, or
  - 500 g of ^{233}U, or
  - 450 g of any combination of these fissile isotopes,

  then a CAAS must be installed, and provide coverage of specific areas within the facility.
- The CAAS must be able to reliably and quickly detect an equivalent dose of 200 mSv at a distance of 2 m from the system where the critical excursion occurs.
- The CAAS must incorporate audible and visual alarms to warn the workforce to immediately evacuate the facility.
- The facility management has to develop emergency evacuation procedures; routine evacuation and mustering practice drills are essential.

2.7 Energy released in a nuclear criticality excursion of realistic magnitude

As an illustration consider a magnitude $\mathrm{CA}(10^{17}\mathrm{f})$ criticality excursion in a system containing HEU and 100 litres of water — certainly a realistic amount. The criticality excursion generates 10^{17} fissions in a matter of seconds. The recoverable energy release per fission event is $E_f = 200$ MeV (Lamarsh and Baratta, 2017). The total energy release will therefore be $E \approx 10^{17} \times 200\ \mathrm{MeV}$ which calculates to 3200 kJ. This is the amount of energy produced by a typical 2.5 kW large domestic oil-heater over circa 22 minutes of full-power operation. If all the energy released by 10^{17} fissions is deposited in 100 litres of water, the temperature of the water will be raised by just below 8 °C, which is certainly not excessive. An energy release of this magnitude into a large volume such as HEU in 100 litres water, is below the “explosive” range, i.e., the principal visible sign of the nuclear criticality excursion will be a characteristic flash of blue light, along with some agitation in the fluid, but not an outright explosion. This means that a typical nuclear criticality excursion is intensely radiative, but minimally explosive, in nature.

2.8 The correct way to quantify k_{eff} in Monte Carlo simulations, to ensure an adequate margin of subcriticality

When a Monte Carlo code such as MCNP is used to quantify the effective neutron multiplication factor k_{eff} of a system that contains fissile material, the answer is given along with a 1σ relative standard deviation estimate of the relative error. The code developers have repeatedly stated that this purely statistical estimate of the error, underpredicts the true error by a factor of 5 to 10 (Blomquist, 2006; Brown, 2009; Yamamoto and Miyoshi, 2004). Another factor at play, is that a 2σ (nominally a 95% confidence interval), and not merely a 1σ error estimate[17], has to be given for criticality analyses. The correct method for giving a responsible estimate for the k_{eff} of a system in technical reports, is therefore to specify the value,

$$k_{\text{eff}} = k_{\text{eff}} + (k_{\text{eff}}) \times (2 \times 10 \times \sigma) \tag{2.6}$$

To prevent misunderstandings, this is the value that has to be specified in reports to facility operators, as the k_{eff} of a system. As stated above, this conservative best estimate of k_{eff} must be below 0.95, under the worst possible realistic accident scenario, such as extensive water ingress, to ensure system safety. Maintaining the value of $k_{\text{eff}} \leq 0.95$ under serious accident conditions, is referred to as maintaining the *margin of subcriticality.*

2.9 Interpretation of calculated dose-rates and doses

When one hear that a car was driven at a certain speed on a given stretch of road, one evaluate this statement by reference to known reference speeds. As socialised citizens, we know, e.g., that the speed limit in urban areas typically ranges between 40 and 60 km/h, and that the speed-limit on highways is typically in the range between 100 to 120 km/h. This knowledge about reference values of a quantity, enables us to respond appropriately to information. One can call such reference values "beacon values" because they serve as guiding beacons without which we cannot respond appropriately to information. Knowing such beacon-values is an important facet of domain-knowledge.

In interpreting calculated dose-rates and doses from ionizing radiation, the following reference or beacon values must always be used, to ensure a proper perspective:

- The present average natural background dose rate (NBDR) on the surface of planet earth, is in the order of 1.1E-7 Sv/h, i.e., 0.11 μSv/h. Calculated and measured dose-rates in zones with human occupancy should be expressed as ratios $\frac{\text{DR}}{\text{NBDR}}$ in order to comprehend whether

[17] In the case of dose-rate calculations, the norm is to quote 1σ error estimates.

the dose-rate is within the “design-limits” of the human body, or far beyond what our bodies are designed to tolerate from nature in the terrestrial biosphere.

- The average annual natural background effective dose (ANBD) for people dwelling on the surface of planet earth, is in the order of 2.5 mSv per year (Cho *et al.,* 2017). Calculated doses D should be conceptually expressed as ratios $\frac{D}{\mathrm{ANBD}}$ in order to understand whether the accrued dose falls within the “design limits” of the human body, or far beyond what the body is designed to naturally receive per annum.
- The present dose-limit for the effective dose to occupationally exposed radiation workers (DL_{RW}), is 20 mSv per year (ICRP, 2007). Calculated effective doses D should be conceptually expressed as ratios $\frac{D}{\mathrm{DL_{RW}}}$ in order to understand whether the accrued dose is within the regulatory acceptable dose-limit regime, or far beyond the dose limits recommended by the International Commission on Radiological Protection — the ICRP.
- The average health risk per unit effective dose, is a 4% risk of serious detriment — mainly radiation related cancer — per 1000 mSv of dose received. The ICRP-2007 risk coefficient for radiation-related cancer is therefore $\frac{4\%}{\mathrm{Sv}}$ (ICRP, 2007). This is an average for both genders and all ages. The gender-difference is smallish, while the age-difference is substantial — the same dose to an 18-year old person is approximately 8 times more carcinogenic than to a 65-year old person (Zhang *et al.,* 2005).
- Approximately 17% of all women who die of disease, are expected to die from cancer, while approximately 29% of all men who die of disease, are expected to die from cancer; around 56% of people who die of sickness are diagnosed with cancer during their lifetimes (Cologne and Preston, 2000; ICRP, 2004; Kodama *et al.*, 2012; Ozasa *et al.,* 2011; Preston *et al.*, 2008).
- The threshold dose for deterministic tissue reactions from exposure to penetrating ionising radiation such as emitted during a criticality excursion, is circa 1000 mSv (ICRP, 2007).
- A dose above circa 3000 mSv can be lethal in circa 50% of exposed persons, within 60 days after exposure (i.e., $LD_{50/60} \approx 3000$ mSv); all doses above circa 5000 mSv are usually lethal (ICRP, 2007).

The above information is now used in an example of how to interpret calculated doses.

Suppose that an exposed male person received a dose of 1500 mSv during an accidental criticality excursion. This dose is interpreted as follows:

- The dose is $\frac{1500\ \text{mSv}}{\text{ANBD}\approx 2.5\ \text{mSv}} \approx 600$ times higher than the annual natural background dose, i.e., it is a serious over-exposure; the dose will overwhelm many natural defences of the human body.
- The dose is, furthermore, $\frac{1500\ \text{mSv}}{\text{DL}_{\text{RW}}=20\ \text{mSv}} \approx 75$ times higher than the recommended annual dose limit for occupationally exposed radiation workers, underscoring is classification as a serious over-exposure.
- The dose exceeds the threshold dose of 1000 mSv for deterministic tissue-reactions, i.e., the person will experience a definite degree of acute radiation syndrome.
- The dose is survivable in the short term, but in the long term the person's cancer risk is substantially raised.
- The nominal risk of radiation related cancer mortality from the dose, is

  $$\frac{1500\ \text{mSv}}{1000\ \text{mSv}} \times 4\% = 6\%,$$

  That is, the dose entails a 6% risk of radiation-related cancer mortality. The exposure will nominally raise the man's total cancer mortality risk from the 29% background cancer risk for non-exposed males, to a nominal total lifetime risk of $29\% + 6\% = 35\%$ of dying from cancer.

2.10 Dose limits, dose constraints, practices and interventions

The ICRP recommends dose limits, based on the best available quantitative knowledge of the detrimental impact of ionising radiation of human health. The ICRP's dose limits are revised every circa 15 to 20 years, and are based on the quantification of health risk as a function of dose, along with social judgement. The present dose limit on effective dose is 20 mSv per annum, and this is based on the finding that a person runs a 4% risk of radiation-related cancer mortality for every 1000 mSv of effective dose accrued. Over a working life of 50 years (from age 18 to 68), a person who receives 20 mSv of effective dose per year, every year, will receive a 1000 mSv effective dose in total. That person will therefore be burdened with a 4% risk of radiation-related cancer mortality. A social judgement is made that a 4% lifetime causation-of-death risk is acceptable because the worker had benefitted from having been employed and paid a salary for 50 years. Every job has health risks, and a 4% lifetime mortality risk is judged to be ethical; nothing is worse than being unemployed for a lifetime.

Even though the "official" annual dose limit is e.g., 20 mSv, an organisation is free to make a rule that they will set the annual limitation on effective dose at e.g., 12 mSv. This rule may not be called a dose limit, but is classified as a *dose constraint.* An organisation may set additional constraints, e.g., that no worker may receive more than 2 mSv in any given month.

The above dose limits and dose constraints are in force for normal operations, called *practices.* During radiological emergencies, however, life-saving *interventions* may be needed and then the restrictive dose limits for practices no longer apply as rigorously. During interventions such as was necessary at Fukushima or Chernobyl, workers may be allowed to receive doses of e.g., 100 mSv over days, weeks or a few months, as long as they act as volunteers or as military personnel. During interventions, the lowest risk will be achieved by asking older people to do the dangerous work, because the excess relative risk of radiation related cancer drops by a factor of more than 5 between age 18 and 60 as the age-at-exposure (the agex parameter in mathematical risk models (Preston *et al.*, 2003)).

The above presentation is mainly based on ICRP-2007 (2007) and Cho *et al*. (2018).

2.11 The code MCNP

This section discuss briefly an introduction to the code MCNP. A more in-depth discussion of the theory of radiation transport and the MCNP calculation models developed for this investigation, is presented in Appendix A on page 112 − 136.

MCNP is a general-purpose Monte Carlo N-Particle radiation transport code. The development of this code date as back as the 1940s; new versions are released approximately every 5 year. MCNP runs under a variety of operating systems, e.g., LINUX and Windows-10. The present release of the code is MCNP6.2 (LANL, 2018); in 2019, all previous versions of the MCNP code have been declared obsolete and unsupported by LANL. The code is shipped along with ENDF/B-8.0 (Brown *et al.*, 2018) as well as older nuclear data which have all been processed into ACE format (Conlin *et al.*, 2018). Thermal neutron scattering data compiled by (Parsons, 2018) should be used where possible, to ensure the accurate calculation of thermal neutron spectra.

MCNP tracks individual particles such as neutrons, photons, electrons over a range of energies from birth until they are terminated by absorption or physical escape from the system boundaries. MCNP uses pointwise cross-section data on a very fine energy grid — so fine that it can be called continuous-energy (CE) nuclear data. In KCODE mode, the code can be used to calculate the effective neutron multiplication factor, k_{eff}, of configurations of fissile material. Tallies may be specified to request the calculation of particle fluence values, or doses. In this way, the code can be used to design shielding that will lower doses to values below, e.g., dose limits.

In the case of a criticality excursion, the calculated radiological quantity is the dose (and not the dose-rate). The parameter that defines the magnitude of a criticality accident, is the number of fissions (and not the number of fissions per unit time), so that it is dose (as opposed to dose rate) that is calculated.

When the source is, e.g., an ensemble of radionuclides, the parameter that defines the radiological magnitude of the source, is activity, which is a “per second” rate-quantity, so that it is the dose rate (as opposed to the dose) that is calculated.

The user interacts with the code MCNP by developing a calculation model of the system. The code is then instructed to read this calculation model and simulate radiation transport in the system defined by means of the calculation model.

2.12 The code FISPACT-II

This section discuss briefly an introduction to the code FISPACT-II 3.0. Technical detail about the FISPACT-II calculation model used to calculate the post-excursion inventory of radionuclides, is presented in Appendix A.5 − A.6 on page 131 − 136.

FISPACT-II 3.00 (Sublet *et al.*, 2015, 2016, 2017) is an inventory and source-term code system which quantifies the radionuclide inventory in a system irradiated by e.g., neutrons. Usually the projectile particle is the neutron, but the code can also operate with either protons, photons, deuterons or alpha-particles as projectiles.

FISPACT solves a system of ODEs, specified in Eq. (2.7).

$$\frac{dN_i}{dt} = -N_i(\lambda_i + \sigma_i\phi) + \sum_{j\neq i} N_j(\lambda_{ij} + \sigma_{ij}\phi) \qquad (2.7)$$

where:

$\frac{dN_i}{dt}$ = Rate of change of the number of atoms of nuclide i.

N_i = Number of atoms of nuclide i at a given time t.

λ_i = Total decay constant for the radioactive transitions of nuclide i.

σ_i = Cross-section for reactions on nuclide i.

ϕ = Total neutron fluence-rate in $\mathrm{cm}^{-2}\ \mathrm{s}^{-1}$.

N_j = Number of atoms of nuclide j at a given time t.

λ_{ij} = Transition (decay) constant of nuclide j to nuclide i.

σ_{ij} = Cross-section for reactions on nuclide j producing nuclide i. For fission reactions, this will be a product of the fission cross-section and the fission-product yield function.

FISPACT-II uses a very accurate and numerically stable solver for ordinary differential equations (LSODEs), developed at Lawrence Livermore National Laboratory (LLNL) in the USA, to solve the set of ODEs. FISPACT-II was executed using TENDL-2019 (Koning *et al.*, 2019) nuclear data.

In the FISPACT-II calculation model, all possible physics was turned on; this includes neutron-induced fission as well as spontaneous fission.

3 The PUREX process and facility layout

3.1 Introduction

This chapter presents the nuclear facility where the PUREX process is used to recover non-irradiated, enriched uranium.

The utilisation of the PUREX chemical process to recover uranium nuclear material is important to prevent available enriched uranium resources on site, from not being economically utilised. The aim of the PUREX process is to recover enriched uranium and form these into uranium metal ingots, which can subsequently be used to fabricate molybdenum target-plates[18] for the production of medical radioisotopes. The ingots are HEU metal cylinders with diameter 9 cm, height 10.6 cm and a mass-density in the order of $18.5\ \mathrm{g\ cm^{-3}}$. The mass per HEU ingot is ~ 12.5 kg.

The PUREX chemical process constitutes several interconnected processing workstations which involves specific operations with fissile material. Because enriched uranium is processed, there is always a possibility of a sudden nuclear criticality excursion, which involves high doses as well as the creation of fission products, i.e., residual radionuclides, that will make post-accident clean-up operations more difficult.

3.2 The PUREX process

3.2.1 Facility

The PUREX facility is housed in a large processing hall with reasonably thick outer walls made of ordinary concrete. These outer walls function as a biological shield that has to contain any possible radiation from, e.g., a criticality excursion inside the processing hall, to protect workers outside the facility.

3.2.2 Process flow

The recovery of uranium is carried-out in several interconnected workstations, as shown in Figure 3.1 on page 51 — like the process, the facility is divided into separated units of operation, as shown in Figure 3.2, page 54.

[18] To manufacture fuel plates (FPs) for research reactor fuel assemblies, is not nearly as easy as manufacturing target plates (TPs) — in TPs, uranium is used in the metallic form (alloyed with Al), but for reactor fuel plates, the uranium must first be converted into uranium silicide (U_3Si_2) which is then hot-rolled with Al-powder into plates. U_3Si_2 powder often contain particles with sharp edges that can scar the thin Al-alloy cladding of the fuel plates.

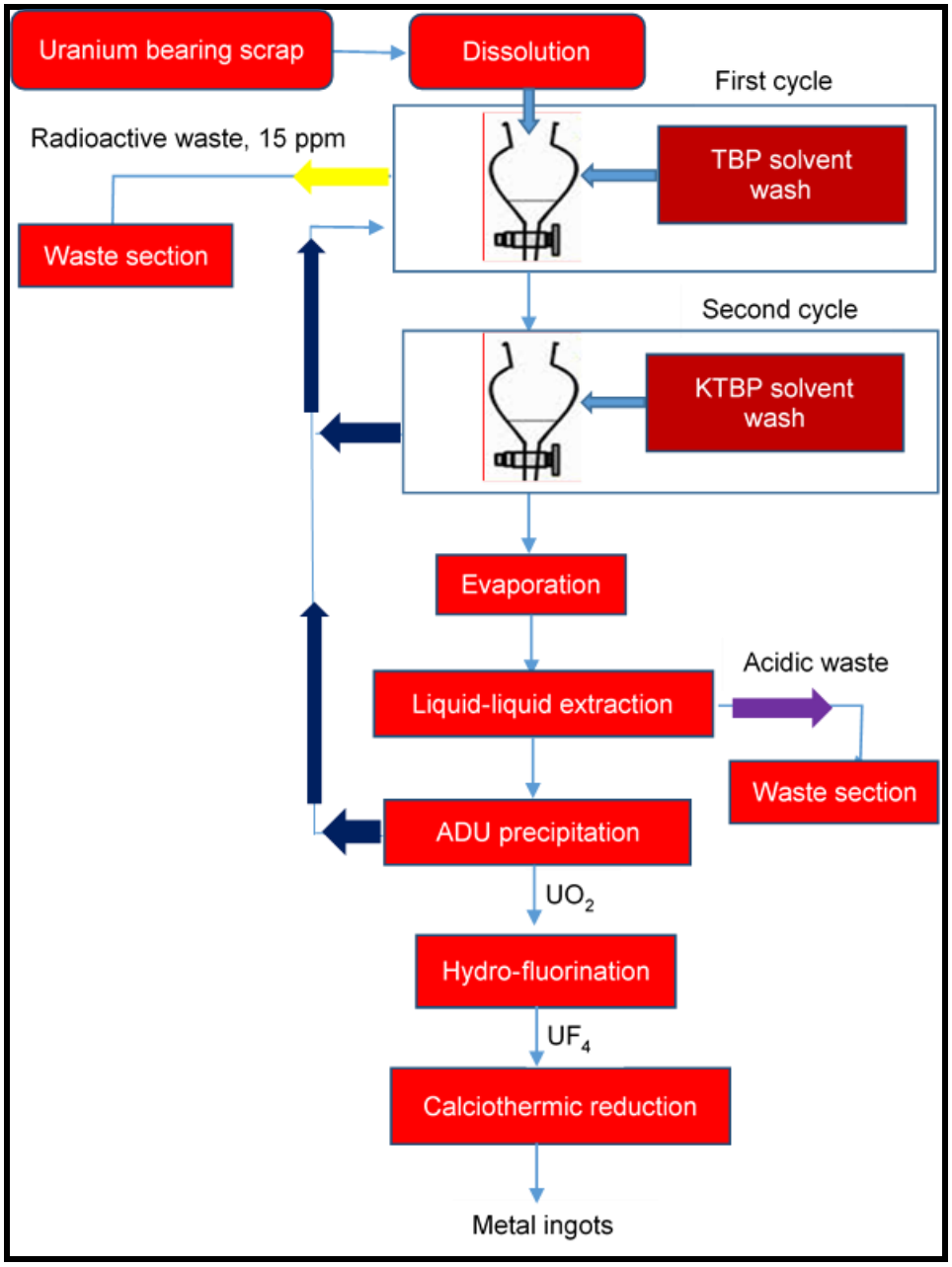

Figure 3.1: The summarized flowsheet of the PUREX process.

3.2.3 Preparation of feed material and dissolution

Uranium-bearing materials are machined in the workshop to cut/shave it into small pieces. Batches are measured to ensure no batch will contain more than $350\ \mathrm{g}$ of uranium, before being processed inside wet glove-boxes. The uranium-bearing material is then dissolved in nitric acid. The dissolved material is transferred to the manual liquid extraction glass funnels containing tributyl phosphate (TBP) organic solution.

3.2.4 Manual liquid extraction

In this step, the received material is processed in a fume cupboard. This material is placed in 2-litre separation glass funnels containing TBP organic solution. The solution is mixed and allowed to separate. The uranium solution is scrubbed and re-extracted by employing tributyl phosphate in inert purified kerosene (KTBP) diluents in separation containers, which are stirred. The uranium is then stripped with 1% nitric acid from the solvent phase, as uranyl nitrate. Thereafter, the solution is transferred to the liquid evaporation workstation to be concentrated. The waste is analysed and if the uranium concentration is less than$15\ \mathrm{ppm}$, it is transferred to the waste handling workstation.

3.2.5 Liquid evaporation

The liquid evaporation is performed with a criticality-safe horizontal evaporator, to concentrate the dilute uranyl nitrate solution. The evaporator consists of a horizontal cylinder made of borosilicate glass; the vessel internal diameter (ID) is approximately $100\ \mathrm{mm}$ while the height is close to 400 mm. It is closed off at each end and has a volume below 5 litres. This borosilicate glass (i.e., “Pyrex glass”) has good heat resistance. The solution boils at about $90°\mathrm{C}$. The solution is concentrated into the range $100 - 170\ \frac{\mathrm{grams}}{\mathrm{litre}}$ of uranium per evaporator. The concentrated uranium is removed from each evaporator and placed into a 5-litre dedicated container — this container may contain up to $1.2\ \mathrm{kg}$ of uranium. This concentrated of uranium solution is sent for further liquid-liquid extraction processing.

3.2.6 Liquid-liquid extraction

The concentrated uranyl nitrate solutions are received from the evaporation workstation and purified by a counter current liquid-liquid extraction process. The purification of the uranic solution is carried out by extraction with tributyl phosphate solvent in kerosene diluents in a stirred tanks. The impurity removal and uranium recovering from the organic phase is performed with diluted acids to re-extract the uranium resulting in a pure uranyl nitrate aqueous solution for further processing.

3.2.7 Ammonia precipitation

The received uranyl nitrate solution is placed in a $5l$ beaker and heated up to 35°C and sparged with ammonia gas while being stirred. The ammonia gas is received via stainless steel pipeline from the ammonia storage plant. The uranium in the solution precipitate as ammonium di-urinate (ADU). The solution is filtered and the resulted uranium concentration is transferred to the hydro-fluorination workstation for further processing.

3.2.8 Hydro-fluorination and calciothermic reduction

The transferred ADU is placed in an oven where the fluorination is performed. The oven is situated inside protective cupboards made of aluminium and perspex. This aluminium and perspex cupboards serve as shielding to protect the operator from airborne contamination and possible hydrogen fluoride vapour. The process convert the ADU to uranium tetrafluoride (UF_4). The UF_4 (commonly known as the green salt) is blended with calcium metal and iodine crystals to provide the reduction mixture. This mixture is placed in a reduction crucible made of magnesium oxide and sealed in an Inconel reactor where the uranium metal ingots are produced.

At the precipitation, hydro-fluorination and calcination workstations the prevailing risk is contamination which is related to the powder processing. Therefore the radiological protective system is important and so is the functional ventilation system. The imbalance in exchange columns and unexpected precipitation can lead to unwanted accumulations of uranium mass, in turn lead to a build-up which can cause criticality accident.

3.3 The PUREX process facility: Initial, “naive”, baseline floor-plan

The original design of the proposed PUREX facility, was conceived by a person with no knowledge of nuclear criticality accidents or radiation shielding principles. This design is called the baseline or modification-0 (MOD0) design. This design will be used as a point of departure. An MCNP model will be developed, executed and then the original design will be improved, step by step, as described in Chapter 4.

The top-view layout of the naïve or baseline or MOD0 design of the PUREX facility, is shown in Figure 3.2. The dark grey areas denote ordinary concrete walls, with a mass-density of $\rho = 2.30\ \mathrm{g\,cm^{-3}}$ and the standardised composition of Regulatory Concrete, as defined by the US NRC (Rearden and Jessee, 2020). Figure 3.2 shows the facility layout. The thick, outer perimeter wall is 60 cm thick, the thinner inner partitioning walls are 30 cm thick and the roof is a 30 cm thick slab of concrete. The distance between the concrete floor and the bottom of the roof slab, is 400 cm. In the initial design, the inner partitioning walls do not reach all the way to the roof, but a gap of 50 to 100 cm was left.

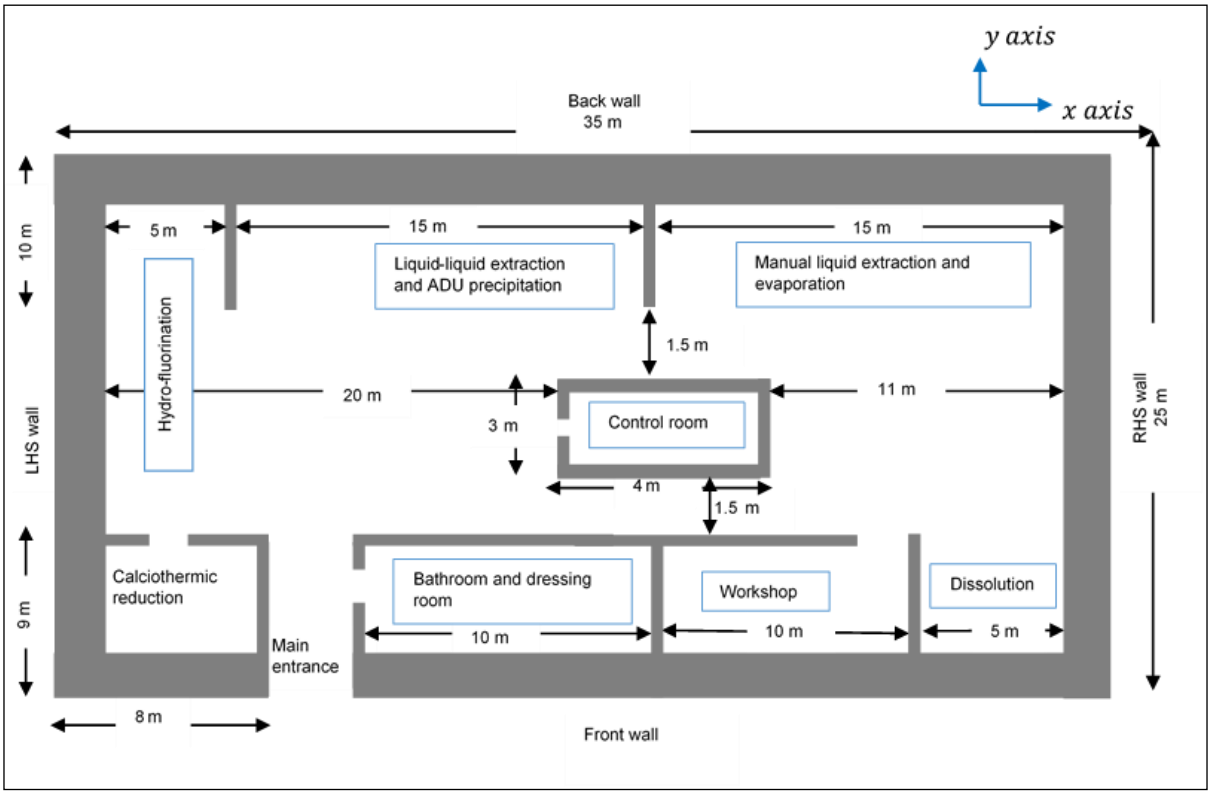

Figure 3.2: Top-view, i.e., x-y plane view of the originally planned layout of the PUREX uranium processing facility, showing the processing workstations, administrative areas and the biological shielding walls, made of ordinary concrete.

In the original design, some attempt was made to place short and thin partitioning shielding walls between the individual workstations, as seen in Figure 3.2. All inner partitioning walls are only 300 or 350 cm high, i.e., there is a gap of either 100 cm or 50 cm between the top of the partitioning walls and the underside of the roof slab. The internal doors leading to the calciothermic[19] reduction area, bathroom and dressing room, workshop and control room, are all standard, commercial wooden doors; these doors are 1 m wide. The main door leading to the facility is based on lead shielding sandwiched between two sturdy steel plates. The Pb layer is 5 cm thick and the door is 2 m wide. The x and y axes are oriented as indicated in Figure 3.2, while the z axis protrudes vertically upwards from the page.

[19] Calciothermic reactions are thermic chemical reactions which use calcium metal as the reducing agent (i.e. electron donor) at high temperature. Calciothermic processes are used to obtain metals such as uranium and thorium from their oxide forms.

3.4 The specification of the design-basis moderated HEU volume and criticality excursion

The evaporation step in the PUREX process is the most criticality accident prone process-step, because (1) enriched uranium is being concentrated while (2) an abundance of moderator (water) is still present in the fissile material solution.

The exact configuration of the fissile material volume is of minor and secondary importance from a radiation dose calculation perspective, because the magnitude of the excursion is imposed in the MCNP calculation model of the accident, by the analyst, as a $\mathrm{CA}(10^{17}\mathrm{f})$ event. The essence is to model a realistic quantity of well-moderated fissile uranic material to be marginally supercritical, and impose a $\mathrm{CA}(10^{17}\mathrm{f})$ magnitude on the excursion by specifying the tally multiplication factor (specified in the FM card and also as the numerical argument of the FACTOR keyword in FMESH tallies) in the MCNP model, at the value $\boxed{2.50\mathrm{E}17}$, i.e., the number of fission neutrons emitted during the design-basis accident. Next, the MCNP model is executed in KCODE mode, and doses are tallied in specified humanoid detector phantoms filled with tissue-equivalent material (TEM) as well as in approximately 20,000 mesh-tally voxels, as spatial dose distributions in the x-y and the x-z plane. This dose contour data can then be visualized in order to obtain visually intuitive pictures of the dose distribution in the PUREX facility, which will enable informed decisions on improving the design.

The fissile volume was fixed as being a right circular cylinder (RCC) with radius 15.5 cm (i.e., a diameter of 31 cm) and a height of 28 cm, inside a SS-316L vessel with a wall thickness of 0.5 cm. The vessel containing the aqueous fissile material rests on a table with a thickness of 5 cm and a CH_2 material composition; the table surface is 100 cm above floor level. The MCNP surface-cards for the fissile material and the stainless steel vessel that contains this fissile process mass, are:

```
02  RCC  0  0  +100.5     0  0  +28        +15.5     $ Cyl, HEU90 in water, MLE-Evaporator
03  RCC  0  0  +100.0     0  0  +30        +16.0     $ O/S of SS-316 Wall of MLE-Evaporator Vessel
```

The fissile material was allocated a mass-density of $\rho = 1.2\ \mathrm{g\ cm^{-3}}$ and the following material-card:

```
c HEU90 dissolved in water:
M02          1001      -8.39296
             8016      -69.5993
             92235    -19.8070
             92238    -2.20078
MT02       H-H2O.80T   U-UO2.80T   O-UO2.80T
```

This fissile system has a total mass of 23.75 kg and contains 5.94 kg HEU_{90} and 17.81 kg H_2O. The $^{235}\mathrm{U}$ mass is therefore $0.9 \times 5.94\ \mathrm{kg} = 4.70\ \mathrm{kg}$.

This combination of (1) vessel size and (2) fissile material composition, ensured a neutron multiplication factor of $1.01 \leq k_{\mathrm{eff}} \leq 1.02$, i.e., a marginally supercritical system. Because the correct

value of k_{eff} was the criterion of validity for the model, the above dimensions were arrived at by trial and error.

It is important to realize that the exact chemical form of the HEU_{90} solution is irrelevant — isotopes of e.g., nitrogen, found in uranyl nitrate, will merely be bystander or spectator isotopes in a fission excursion. The essence of the above specification of the design-basis criticality excursion, is that (1) a specified number of neutrons (2.5×10^{17}) neutrons will be released in a fissile system that (2) contains $4.70\ \text{kg}$ of ^{235}U and (3) enough water to ensure a realistic degree of moderation of the neutrons that will exit the vessel. Both the radiation dose and fission product yield are both direct functions of the number of fissions, which is a fixed, imposed, user-specified quantity. As long as (1) the number of fissions is fixed, and (2) the HEU fissile system is actually marginally supercritical, the exact uranium enrichment, chemical concentration and chemical form, as well as the exact size and shape of the fissile process mass, will have only a minor and secondary impact on radiation doses and the post-accident fission product inventory — "fission is fission" and 10^{17} fission events will always release $\nu \times 10^{17}$ neutrons.

In the MCNP6.2 calculation model, smaller, sub-critical quantities of HEU were also located at other workstations. In the neutronic simulation, neutrons from the epicentre of the excursion will enter these HEU materials and cause additional fissions, which would add to the dose received by operators at these workstations. The MCNP surface cards for the uranic materials are as follows:

```
25  RCC    -1600   +1000  +0100     0  0  +08       +05          $ Cyl, Uranic Stuff, H-F
26  RCC   -400     +1100  +0100     0  0  +08       +05          $ Cyl, Uranic Stuff, L-L-E-ADU-P
27  RCC    +1000   +1100  +0100     0  0  +28       +16.0        $ Cyl, Uranic Stuff, MLE-Evap     <<==
28  RCC    +1600  -1100   +0100     0  0  +08        +05          $ Cyl, Uranic Stuff, Dissolution
```

The corresponding cell-cards are:

```
25  02  -5.00          -25                    imp:n,p=1      $ Uranium Material in H-F
26  02  -5.00          -26                    imp:n,p=1      $ Uranium Material in L-L-E-ADU-P
27  01  -1.10          -27                    imp:n,p=1      $ Uranium Material in MLE-Evap     <<==
28  02  -5.00          -28                    imp:n,p=1      $ Uranium Material in Dissolution
```

The sub-critical fissile material at each of the 3 "spectator" workstations, was modelled as a cylinder of HEU_{100} in a UF_4 chemical form with mass-density $\rho = 5.0\ \text{g cm}^{-3}$, $10\ \text{cm}$ in diameter and $8\ \text{cm}$ high. These three subcritical volumes of HEU_{100} will generate additional fission neutrons when hit by neutrons coming from the site of criticality, and serve the purpose of making calculated doses in adjacent workstations more conservative.

In summary: A realistic design-basis criticality excursion in a realistic fissile system have been defined. The criterion of realism was marginal supercriticality in the MCNP simulation of the system. Calculated doses and post-accident radionuclide inventories will therefore be realistic.

4 Designing robust radiation shielding for the PUREX facility

4.1 Principal goal

The overall goal of this chapter is to improve the radiological safety of the PUREX facility by re-designing it step by step, on the basis of a series of MCNP simulations of a criticality excursion at one selected workstation in the facility. The MCNP simulations serve to quantify radiation doses at selected location, as well as facility-wide spatial dose distributions. This quantification and data visualisation enables an informed redesign of the PUREX plant, so that workers will have the benefit of significantly more robust radiation protection, in the event of a criticality excursion.

4.2 Methodology

The "naïve" original facility design seen in Figure 3.2 on page 54 is used as a point of departure. A series of MCNP6.2 calculation models are developed, successively, to calculate radiation dose distributions caused by the criticality excursion. The radiation shielding design is improved step by step, until a design is reached where high doses will be highly localised and will affect only a small portion of the floor-space inside the PUREX facility.

The criticality accident will involve 10^{17} fission events, which will produce a substantial activity of radionuclides (mainly fission products) inside the fissile process mass. This radionuclide inventory, i.e., the (nuclide, activity)-matrix, that is, (N_i, A_i) matrix, will be quantified by passing the neutron fluence spectrum $\Phi(E)$ calculated by MCNP6.2, to a calculation model developed for the nuclide inventory code, FISPACT-II 3.00 (Sublet *et al.*, 2015 and 2016; Fleming *et al.*, 2018).

4.3 Convergence of criticality calculations in MCNP6.2

The fissile material in the criticality system was located in each of the four workstations in the PUREX facility. These workstations are (1) dissolution, (2) manual liquid extraction and evaporation, (3) liquid-liquid extraction and ADU precipitation, and (4) hydro-fluorination as highlighted in §3.2 on page 50. All uranic material is assumed to have a right circular cylinder (RCC) shape and are placed on table-tops with vertical height $z = 100\ \mathrm{cm}$; all table-tops are assumed to be 5 cm thick and have the chemical composition $\mathrm{CH_2}$. The density of the table material was selected as $1\ \mathrm{g\,cm^{-3}}$. The material composition of the table is seen to be capable of moderating and reflecting neutrons back into the fissile material.

The criticality system in the manual liquid extraction and evaporation step — where the criticality accident is assumed to occur — was modelled as a larger volume with RCC geometry, as described in §3.4 on page 55.

The material composition of the aqueous uranic solution undergoing the criticality excursion, was calculated with a calculation model that is embedded in Appendix A.4. Based on the literature study, the number of fission events, i.e., the fission yield, of the design-basis accident (DBA), was set at 10^{17}; it should be noted that MCNP in particular, and non-military codes in general, cannot calculate this quantity, i.e., it has to be ***imposed*** upon an MCNP calculation model (McLaughlin, 2001b; McLaughlin, 2003; McLaughlin *et al.,* 2000) by specifying a tally multiplication factor $TMF = 2.5 \times 10^{17}$ which equals the number of fission neutrons produced in the excursion, at the *imposed magnitude*. The KCODE card specified in the series of MCNP calculation models, is discussed on page 121 in Appendix A.1.

Figure 4.1 shows the convergence of (MCNP's collisional estimate of) k_{eff}, as a function of the number of cycles of code execution. The code MCNP was executed over 550 cycles with 2.0E5 source neutrons per cycle; the results calculated in the first 50 cycles were disregarded, in order to allow the fission source to converge to the fundamental mode (technical terms used here, are explained in Appendix A).

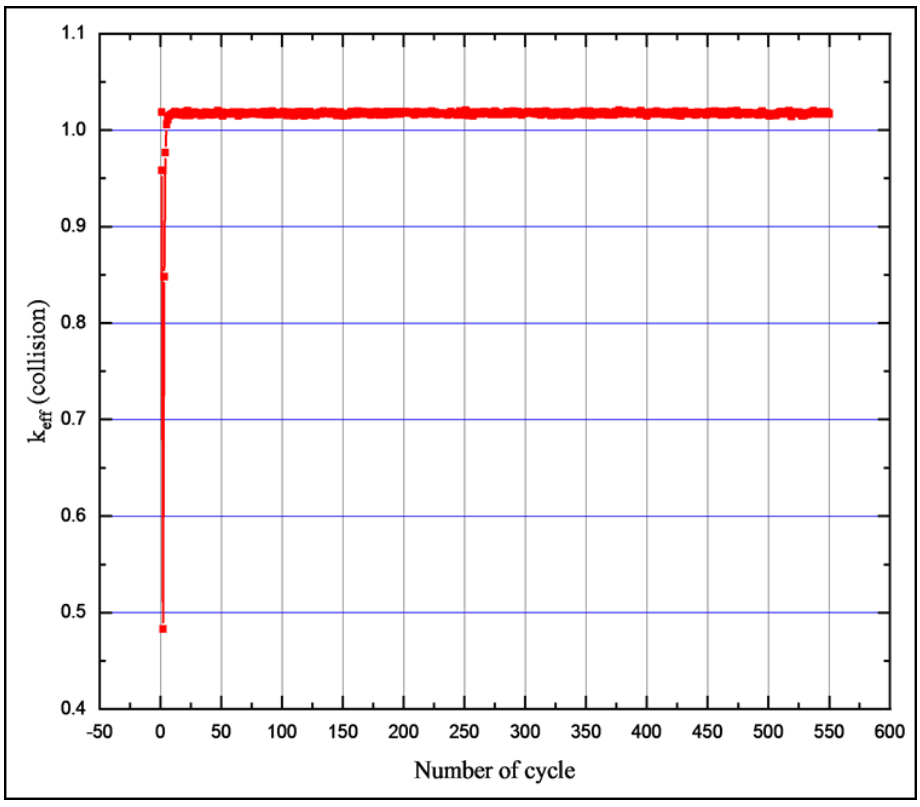

Figure 4.1: The convergence of the effective neutron multiplication factor, k_{eff}, as a function of the number of cycles ran in the MCNP simulation.

It is evident from Figure 4.1 that there is a prominent initial fluctuation of the value of k_{eff} over the first few cycles. Over, e.g., the first 5 cycles, the minimum value of k_{eff} is 0.483 while the maximum is 1.006, i.e., the parameter it is still fluctuating quite wildly. As the number of cycles increases, the magnitudes of the fluctuations decrease. The remaining "ripple" observed in Figure 4.1, is characteristic of the statistical Monte Carlo simulation process.

In criticality calculations, MCNP6.2 also calculates the *Shannon entropy* of the system. This parameter is a measure of the information disorder. An MCNP6.2 criticality model that had converged to a stable solution, will be characterised by a well-converged Shannon entropy. The code reports the Shannon entropy value for every calculational cycle, so that one is able to plot this parameter as a function of the number of cycles. In all MCNP calculations for the system under assessment, the Shannon entropy took less than 25 cycles to stabilise; it was therefore decided to specify, conservatively, that the first 50 cycles of the criticality calculation must be disregarded as "throw-away cycles", while only the results of the last 500 cycles should be used to quantify k_{eff} as well as radiation doses. In other words, the number of up-front throw-away cycles was specified as 50 while the number of active cycles was set at $550 - 50 = 500$.

With this KCODE card specification, k_{eff} converged well to 1.01750 ± 0.00003; it is seen that the 1σ relative standard error was calculated by the code to be $\sigma = 0.00003$. The code goes on to specify the 68%, 95% and 99% confidence intervals.

Table 4.1: MCNP's summary of the results of a KCODE type criticality calculation.

```
 the final estimated combined collision/absorption/track-length keff = 1.01750 with an estimated standard deviation of 0.00003

 the estimated 68, 95, & 99 percent keff confidence intervals are 1.01746 to 1.01753, 1.01743 to 1.01756, and 1.01741 to 1.01758

 the final combined (col/abs/tl) prompt removal lifetime = 1.0515E-03 seconds with an estimated standard deviation of 1.1422E-07

 the average neutron energy causing fission = 4.0473E-03 mev
 the energy corresponding to the average neutron lethargy causing fission = 3.6596E-08 mev

 the percentages of fissions caused by neutrons in the thermal, intermediate, and fast neutron ranges are:
         (<0.625 ev):  96.99%          (0.625 ev - 100 kev):   2.78%          (>100 kev):   0.23%

 the average fission neutrons produced per neutron absorbed (capture + fission) in all cells with fission = 1.4706E+00
 the average fission neutrons produced per neutron absorbed (capture + fission) in all the geometry cells = 1.0176E+00

 the average number of neutrons produced per fission = 2.430
```

The code reports the value of the fission neutron yield, for the modelled mixture of fissile isotopes, to be $\nu = 2.430$. This is typical of a fissile system with HEU_{90}. The simulation found that circa 97% of fissions were produced by thermal neutrons, 2.78% by intermediate energy neutrons and only 0.23% by fast neutrons — also typical of a well-moderated, aqueous HEU_{90} fissile system.

One responsible value of k_{eff} to report to the operational management of a facility, is the *upper boundary* of the 99% confidence interval, in this case $k_{\text{eff}} = 1.01758$. This value is calculated as follows by MCNP6.2:

$$k_{\text{eff}}^{99\%\text{CI}} = k_{\text{eff}}^{\text{MCNP}} + k_{\text{eff}}^{\text{MCNP}} \times 2.621(\sigma^{\text{MCNP}})$$

It is important not to confuse operational management with excessive statistical jargon, but simply to report a single, conservative number.

Based on published literature, it is even better to report the best estimate of the true value of k_{eff} as follows to operational management:

$$\boxed{k_{\text{eff}}^{\text{real}} = k_{\text{eff}}^{\text{MCNP}} + k_{\text{eff}}^{\text{MCNP}} \times 20(\sigma^{\text{MCNP}})}.$$

The convergence of fission source spatial distribution was further confirmed by analysing the Shannon entropy, i.e., the entropy of the fission source.

Initially, the Shannon entropy of the fission source fluctuates to an upper value of 4.8969, before settling down to a mean of 4.5281 and a standard deviation of 0.0012666, during the active KCODE cycles.

The convergence of the Shannon entropy of the fissile system, is shown in Figure 4.2 by plotting the deviation from the source entropy from the converged mean entropy over all active KCODE cycles, against the cycle counter, n.

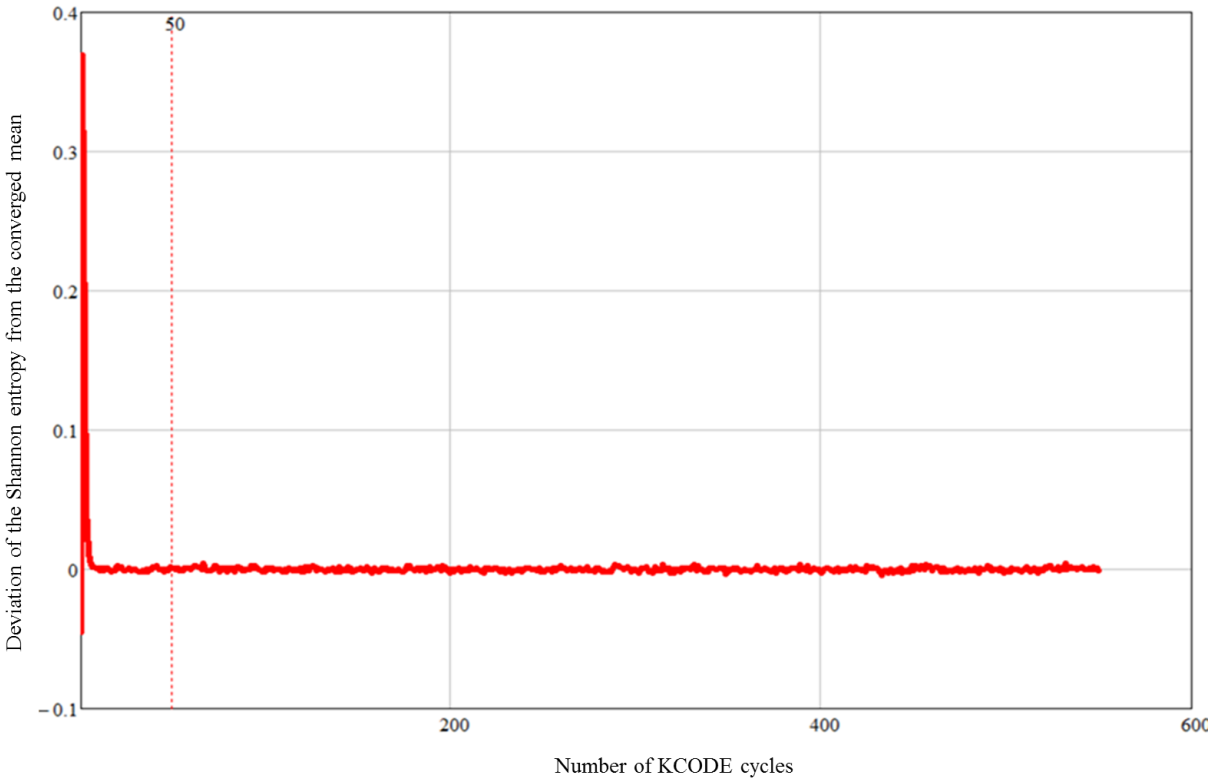

Figure 4.2: Deviation of the Shannon entropy of the fission source, from the converged mean entropy.

As expected, Figure 4.2 displays a significant fluctuation in the Shannon entropy for the first few cycles.

An expanded view of the entropy in the fission source, over the first 10 cycles, is given in Figure 4.3:.

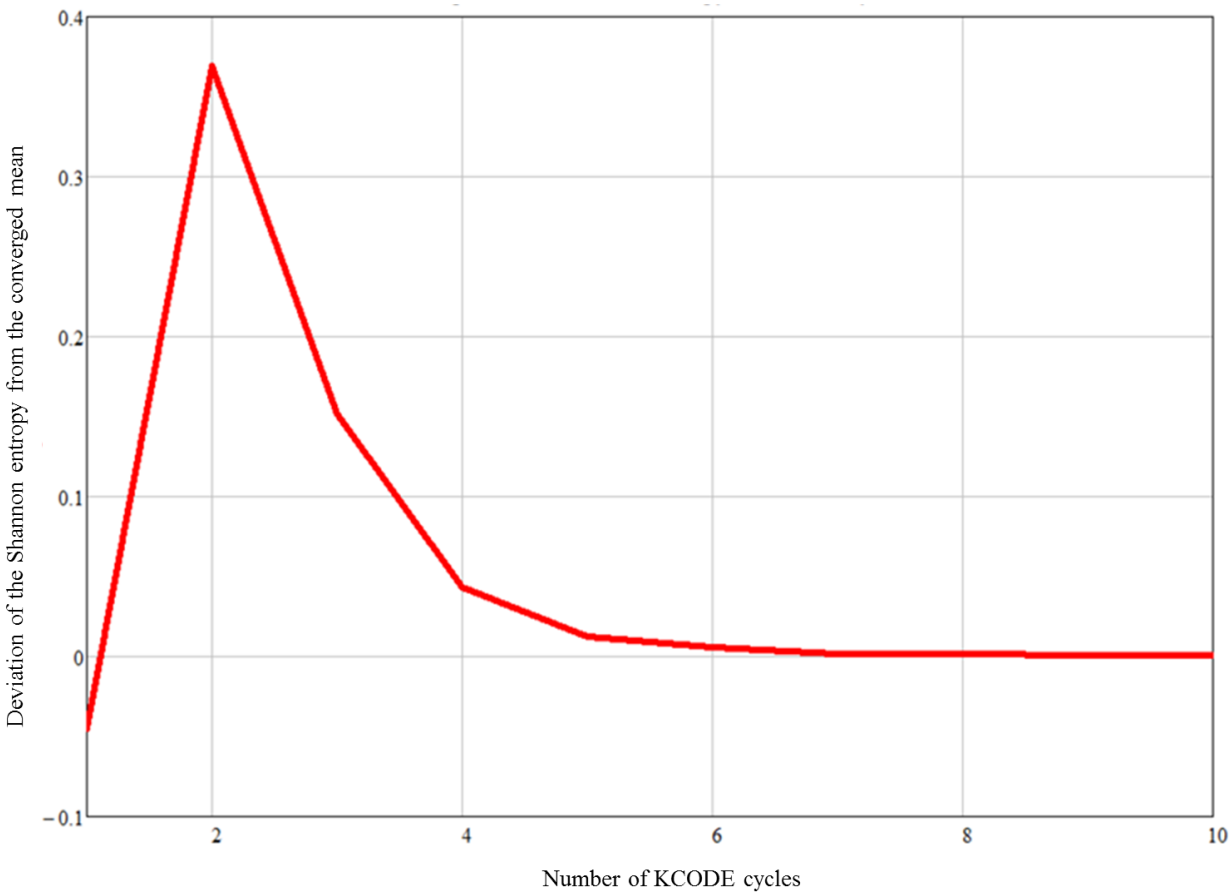

Figure 4.3: Expanded view of the entropy in the fission source, over the first 10 KCODE cycles.

Figure 4.3*:* makes it clear that the fission source has converged after 10 KCODE cycles. Likewise, Figure 4.1 shows that the value of k_{eff} has also converged within 10 KCODE cycles. The specification of the number of throw-away cycles at 50, is therefore (1) justified and (2) conservative — the fission source has, in fact, converged well before cycle $n = 50$.

4.4 MCNP calculation model of the baseline, MOD0 design of the PUREX facility

A top-view (x-y plane view) geometry of the MCNP model for the MOD0 layout of the PUREX facility is shown in Figure 4.4.

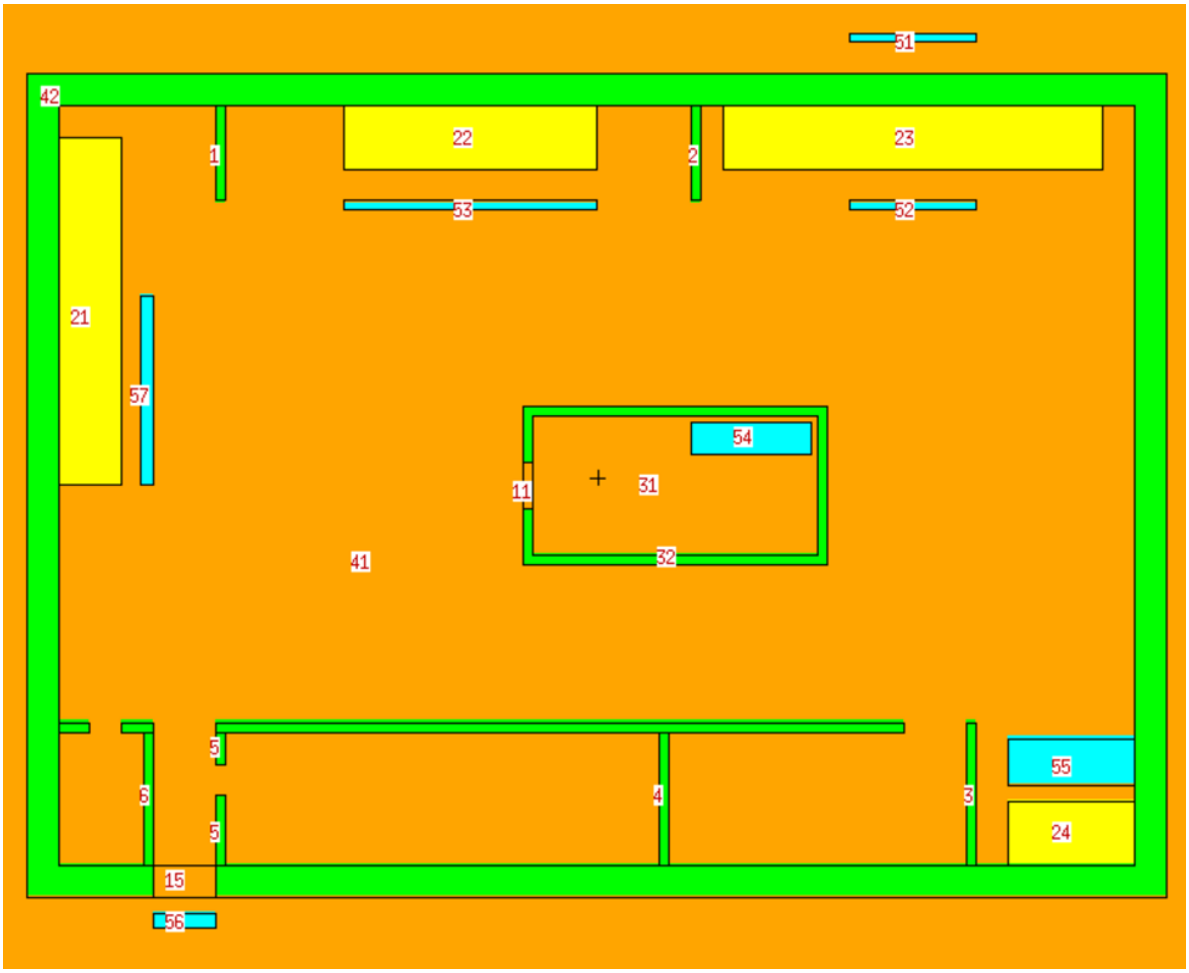

Figure 4.4: Top-view geometry of the MCNP model for the MOD0 layout of the PUREX facility, showing walls, tables and calculational detectors.

Colour-coded shown in Figure 4.4 represents: orange = air, yellow = table-top, blue = TEM, and green = ordinary concrete shielding walls. The red numbers seen in Figure 4.4 are the MCNP cell numbers. The yellow rectangles are table-tops where process vessels are situated. The blue rectangles are TEM-detectors[20], which all stretch from $z \in [50; 150]$ cm, i.e., the vertical domain of normal human occupancy where the most radiation-sensitive organs in the human body is located[21], and also the vertical range where radiation doses are expected to be highest, given that the all HEU batches are on tabletops 100 cm above the floor level.

Figure 4.5 shows the 4 locations of HEU process batches in the facility; three are small and subcritical while one (towards the upper RHS of the diagram) is significantly larger and well moderated, causing it to become marginally supercritical, and gives rise to a $\mathrm{CA}(10^{17}\mathrm{f})$ excursion.

[20] TEM = tissue equivalent material.

[21] From Table on page 124 it is clear that all the radiosensitive organs in the human body are located in this vertical domain.

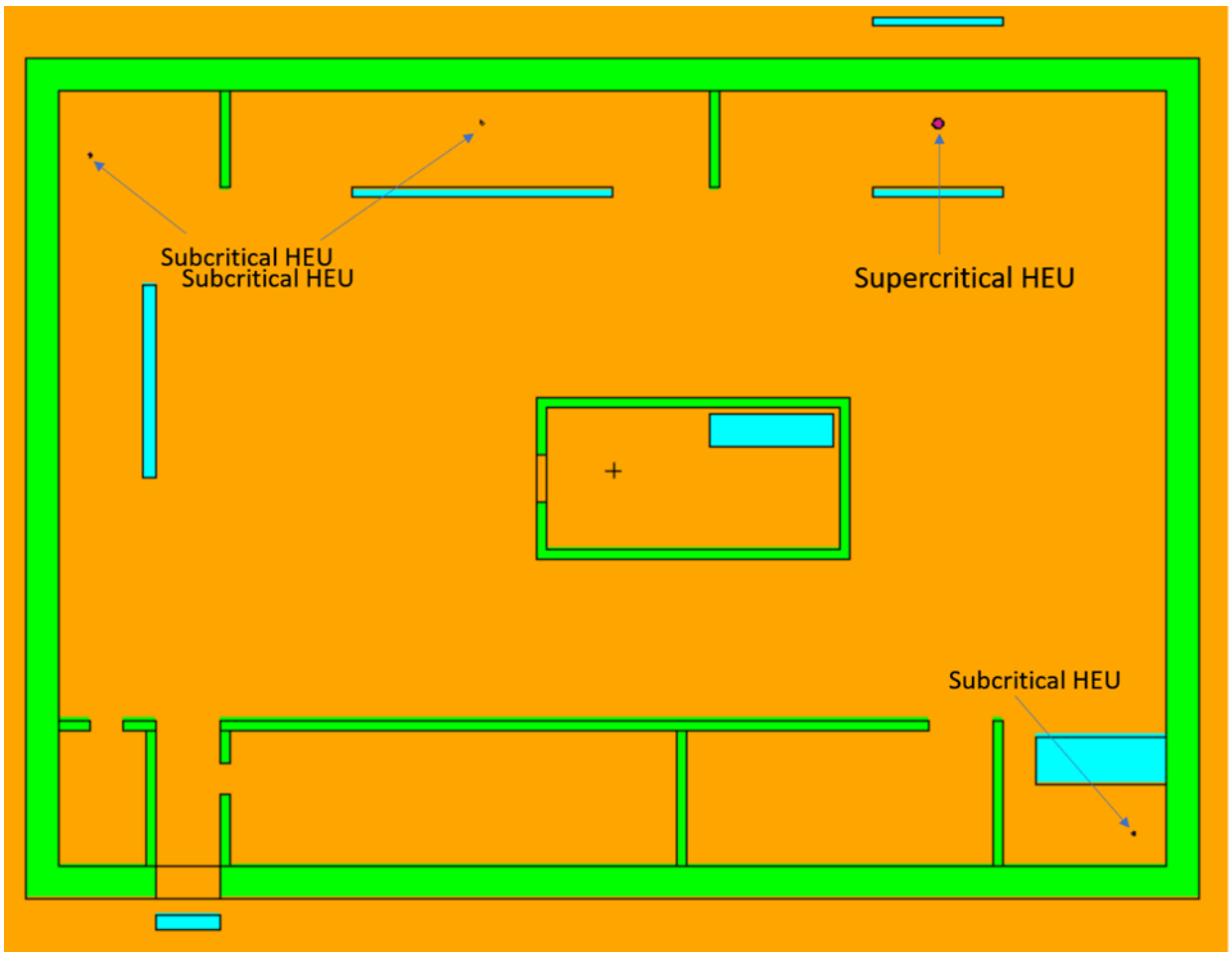

Figure 4.5: The 4 locations of HEU process batches in the PUREX facility; three are small and subcritical while the one towards the upper RHS of the diagram, is significantly larger and well moderated, causing it to become marginally supercritical and precipitate a CA(10^{17}f) excursion.

The colour-coded legend are as defined in Figure 4.4. Figure 4.6 shows a side-view (in the $\boldsymbol{x}$-$\boldsymbol{z}$ plane) of the PUREX facility; note that the inner partitioning walls do not reach to the roof, but leaves a substantial gap through which radiation can stream.

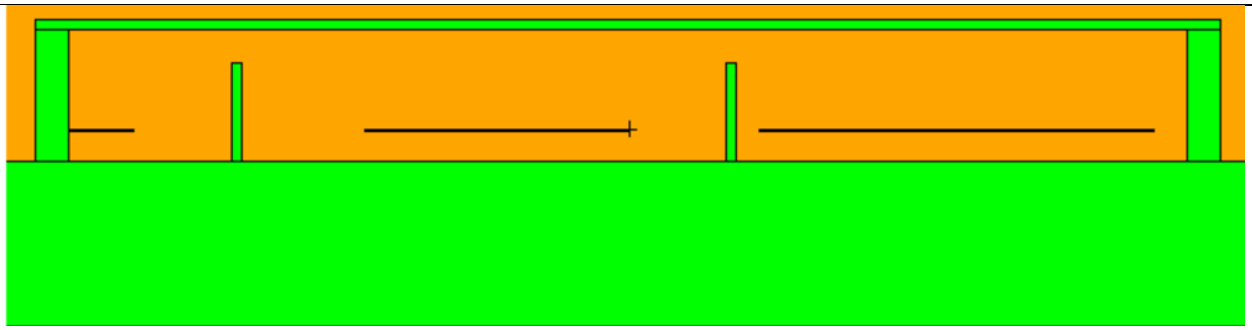

Figure 4.6: Side-view in the $\boldsymbol{x}$-$\boldsymbol{z}$ plane, of the PUREX facility, showing the gap between the inner partitioning walls and the roof slab; radiation can stream through this gap.

Of worthy to note, the thin horizontal “lines” in Figure 4.6 are the table-tops. Figure 4.7 shows the x-y mesh that is imposed on the radiation transport theatre, to calculate doses in a $\sim 20{,}000$ mesh, via an FMESH mesh tally.

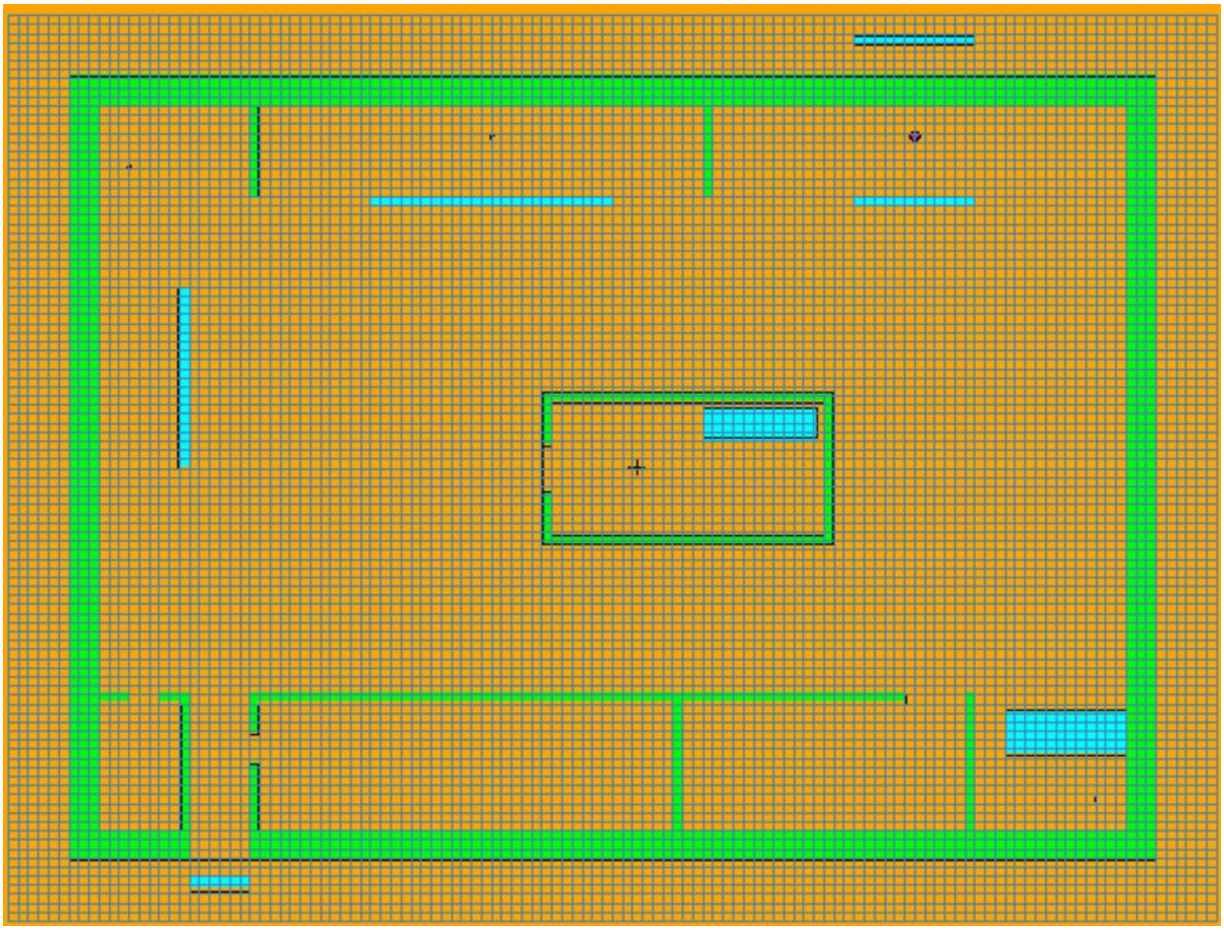

Figure 4.7: Mesh tally used to obtain contour plots of the dose distribution, in order to diagnose weaknesses in the radiation shielding design.

Figure 4.8 presents an augmented diagram of the facility in its *“naive”* MOD0 configuration, with emphasis on the placement of TEM detectors relative to the HEU process volumes. Seven calculational detectors are shown Figure 4.4, 4.5, 4.7 and 4.8; an eighth detector, Det_8, is located on the rooftop, directly overhead of the HEU material where the $\text{CA}(10^{17}\text{f})$ excursion occur – the criticality excursion is shown by a big red dot symbol towards the top RHS in Figure 4.8.

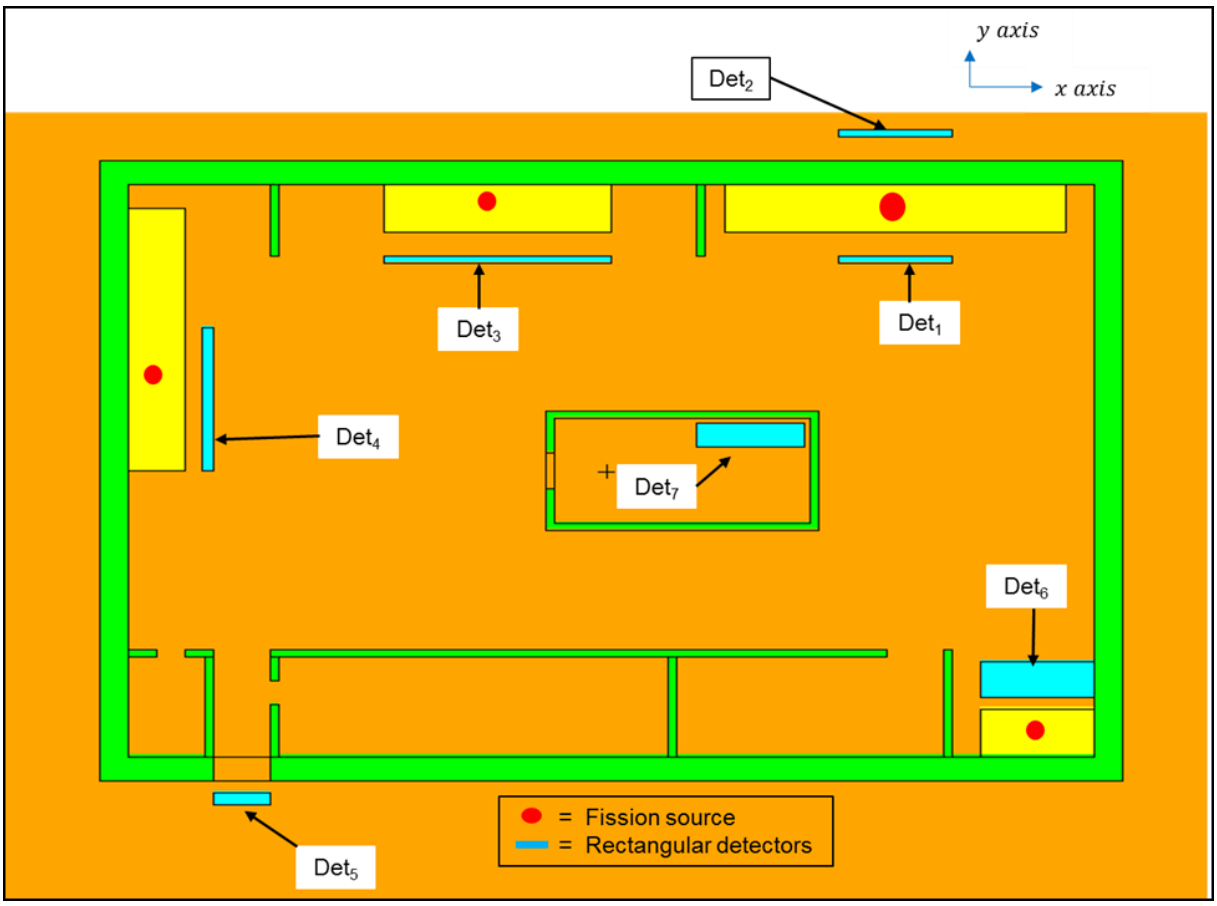

Figure 4.8: Top-view of the PUREX facility, showing the TEM detectors in relation to the HEU material.

4.5 Diagnostic and remedial decision-making logic to arrive at a viable PUREX facility design

4.5.1 Design MOD0

The plan

An initial, naïve facility design produced by a designer in an office for engineering drawings, was used as baseline design. As mentioned before, the designer had no knowledge of criticality excursions and radiation shielding principles. Design MOD0 is shown in Figure 4.9. The perimeter concrete wall is 60 cm thick, while the inner partitioning concrete walls are very short and only 30 cm thick. Ordinary concrete, i.e., NRC regulatory concrete, is used in the calculation model, as explained in §1.7.

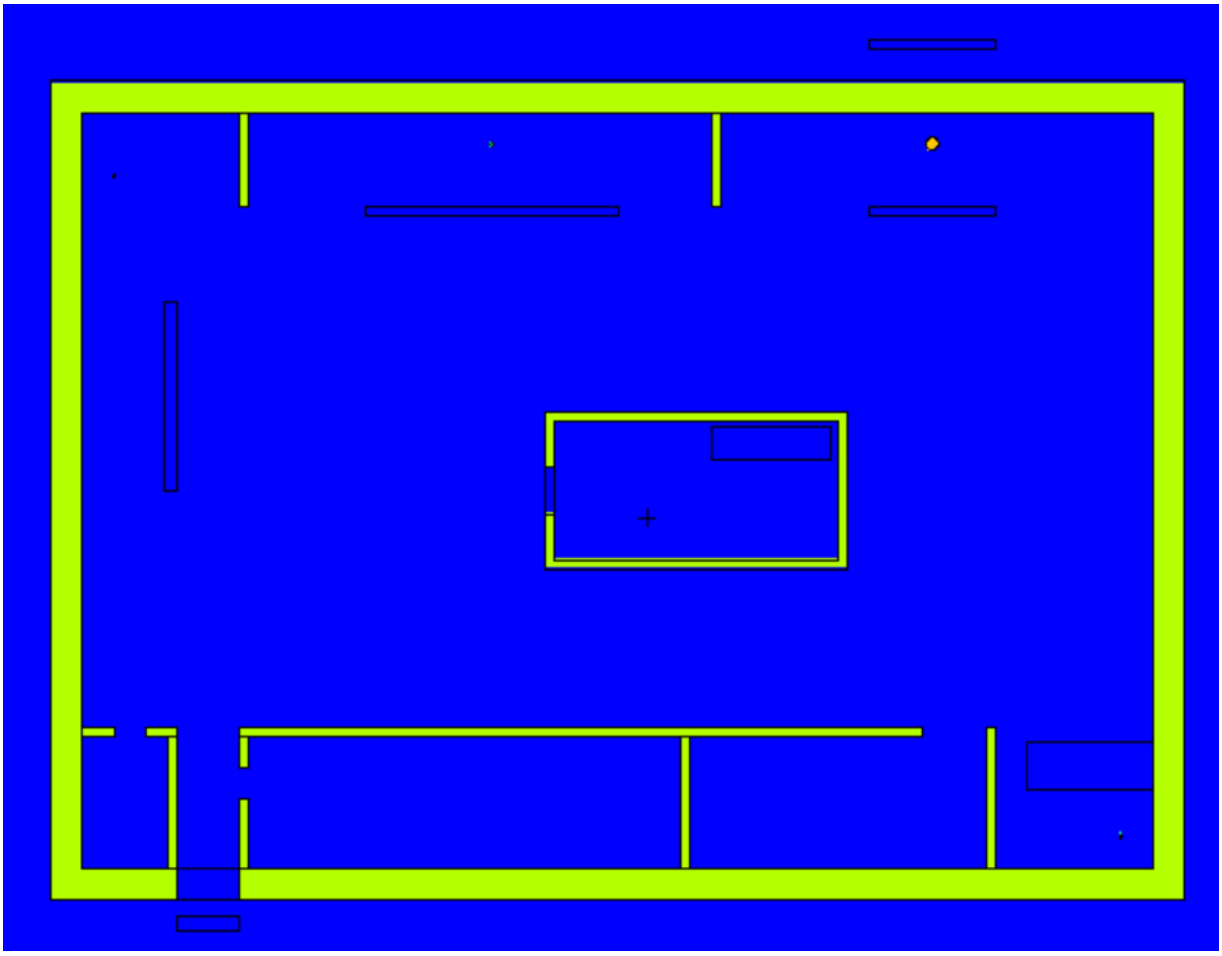

Figure 4.9: PUREX facility design modification MOD0 — the baseline, "naïve" design.

The dose contours

Figure 4.11 presents the calculated equivalent neutron and photon equivalent doses (NED and PED, respectively) mesh tally for the basic geometric facility layout.

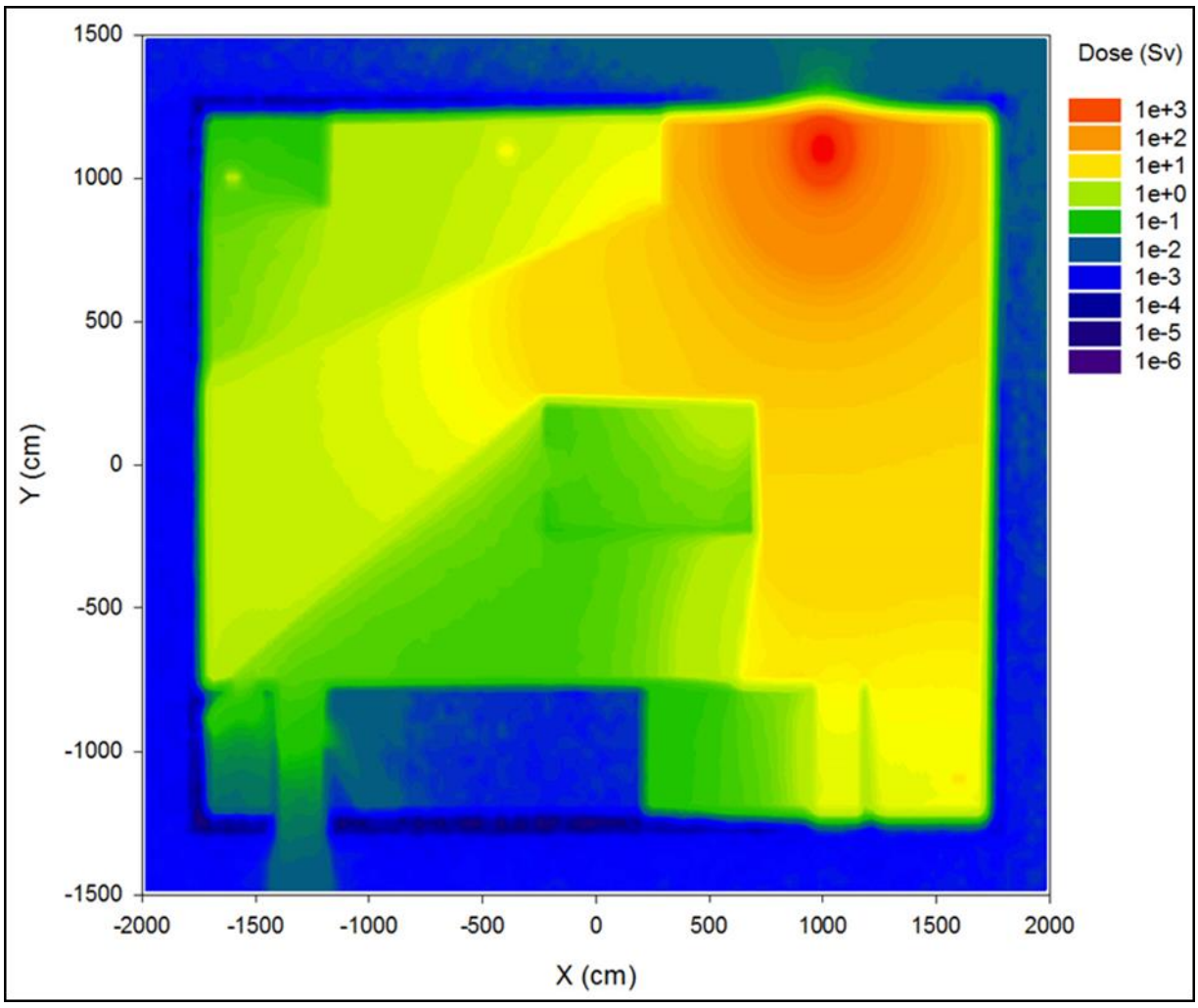

Figure 4.10 : The calculated NED(x,y) dose distribution contours for a CA(10^{17}f) criticality accident in facility design MOD0.

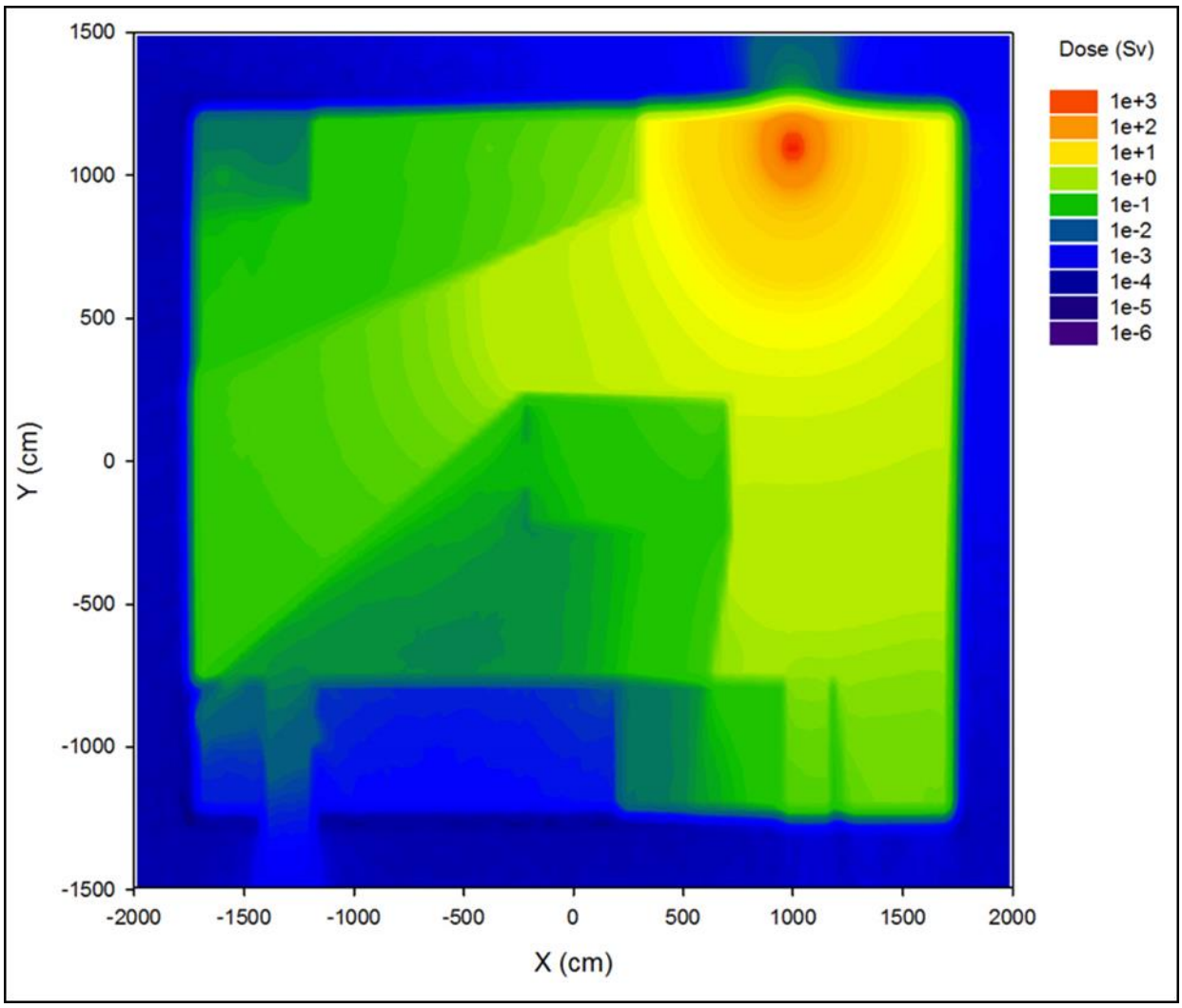

Figure 4.11 : The calculated PED(x,y) dose distribution contours for a CA(10^{17}f) criticality accident in facility design MOD0.

Figure 4.12 shows the calculated $TED(x, y)$ dose contours for the MOD0 facility.

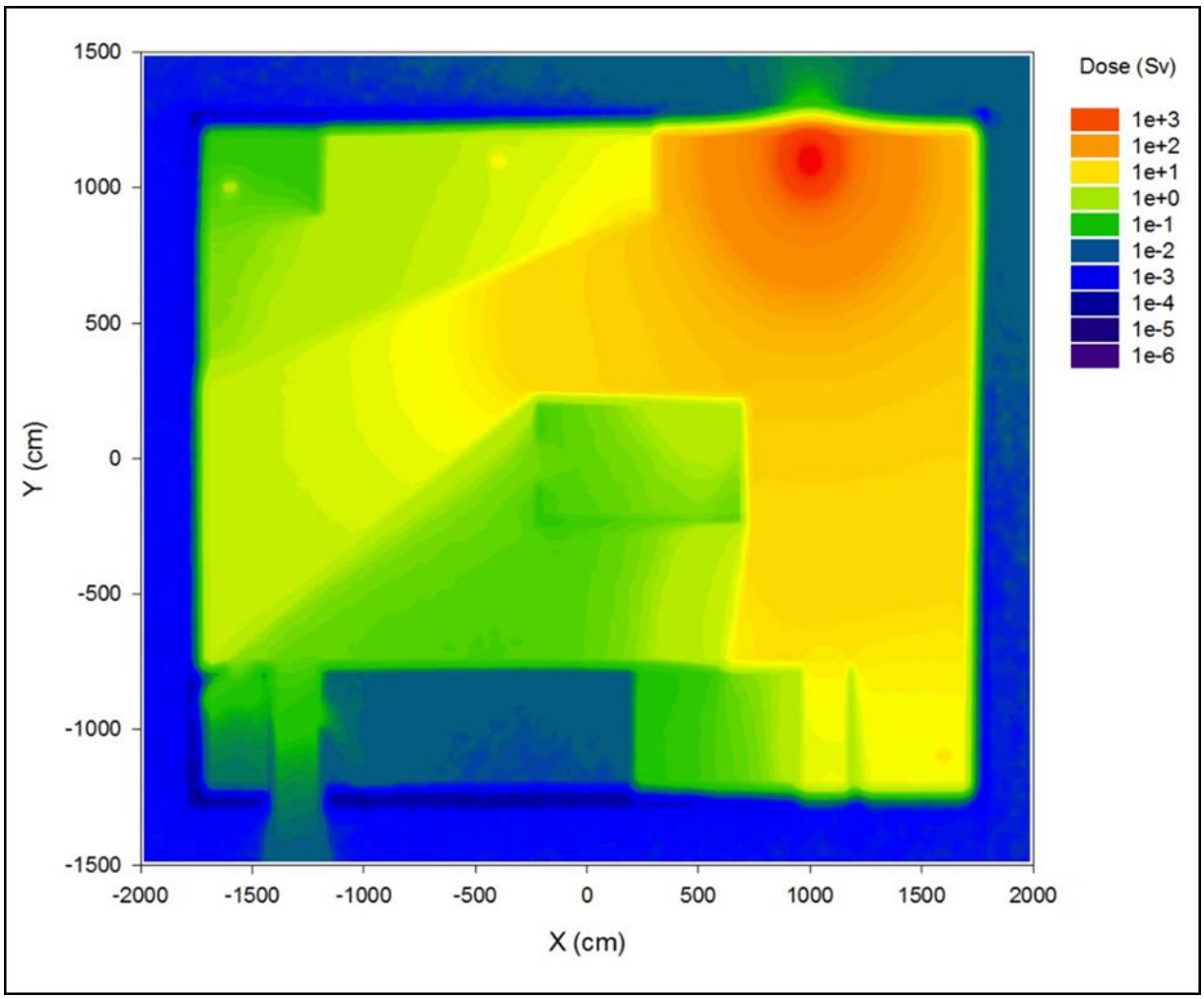

Figure 4.12: The contours of the total equivalent dose (TED) resulting from a CA(10^{17}f) event in the MOD0 facility.

In Figure 4.11 and Figure 4.12, as well as all other dose contours presented in this chapter section, the "human health outcome" interpretation that must be given to the colours of the dose contours, is summarised in Table 4.2.

Table 4.2: "Human health outcome" interpretation of the colours in all dose contour plots in this chapter.

Non-survivable; ARS
Non-survivable; ARS
Non-survivable; ARS
Survivable with ARS
No ARS
No ARS
Trivial dose

The diagnosis

The dose contour plots calculation for $\mathrm{CA}(\mathrm{MOD0}, 10^{17}\mathrm{f})$ shows that this design does not protect workers. The facility becomes a theatre of unmitigated death and horror in the event of a criticality excursion. Radiation streams freely and un-attenuated from the locale of the excursion, to other workstations. Operators in the control room will barely survive. Design MOD0 does not conform to the optimization principle in radiation protection (also called the ALARA principle). The radiation field is not confined and contained, because there is a complete lack of inner shielding structures to prevent radiation streaming from one process area to other areas. Almost all staff in the facility will receive either lethal radiation doses, or will be massively overexposed above the annual dose limit of 20 mSv/h. Workers who survive the acute radiation syndrome (ARS) will suffer substantial adverse affected health outcomes such as additional, above-background cancer risks as high as 12%. The design MOD0 is ethically unacceptable.

4.5.2 Design MOD1

The plan

An attempt was made to address the weaknesses in the baseline MOD0 design; this design modification or perturbation is called MOD1 and is shown in Figure 4.13.

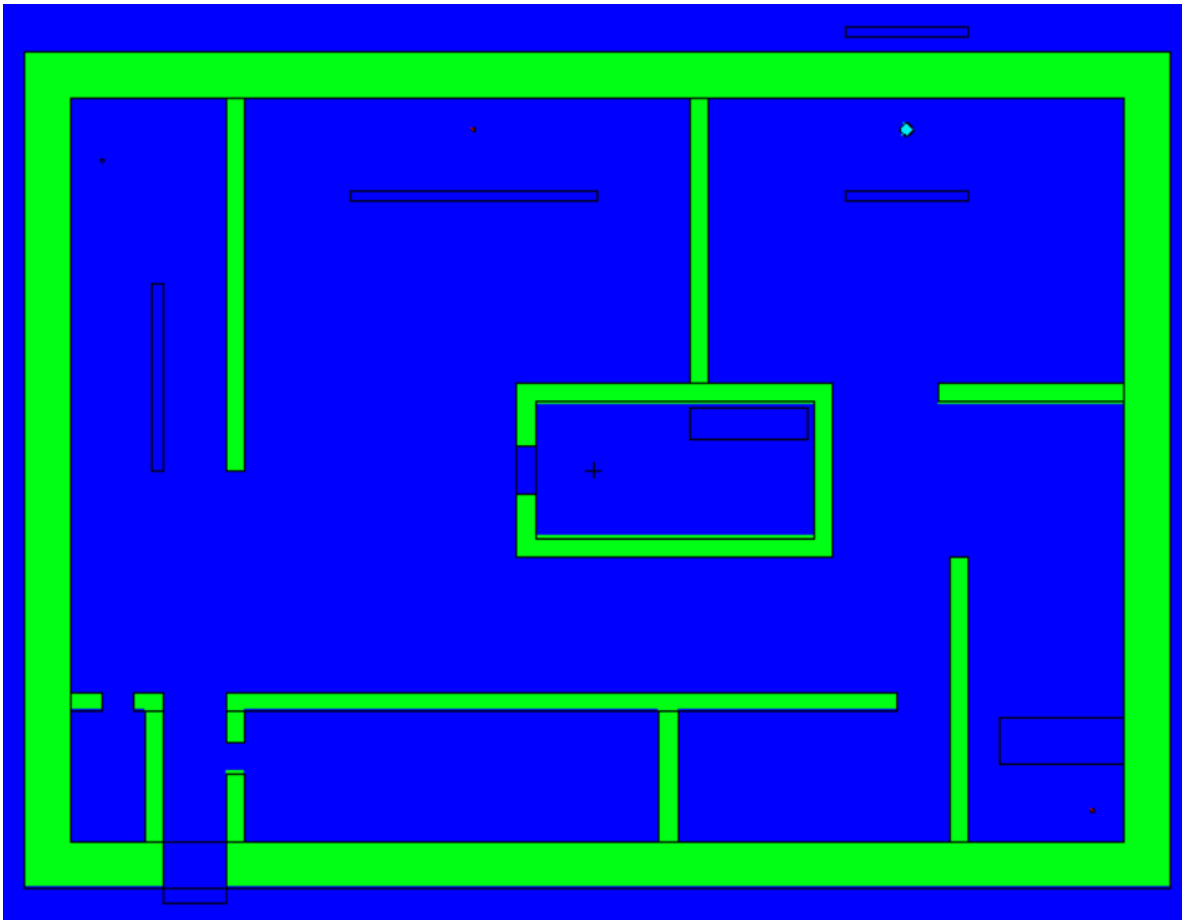

Figure 4.13: PUREX facility design modification MOD1.

The essence of design modification MOD1 is that (1) the perimeter wall is now 150 cm thick, while all inner walls are now 60 cm thick. Inner walls around process workstations were substantially lengthened in an attempt to provide better radiological isolation between workstations.

The dose contours

From this point onward, only the contours of the total equivalent dose (TED) will be shown; as always, $TED = NED + PED$.

Figure 4.14 shows the $TED(x, y)$ dose contours for design MOD1.

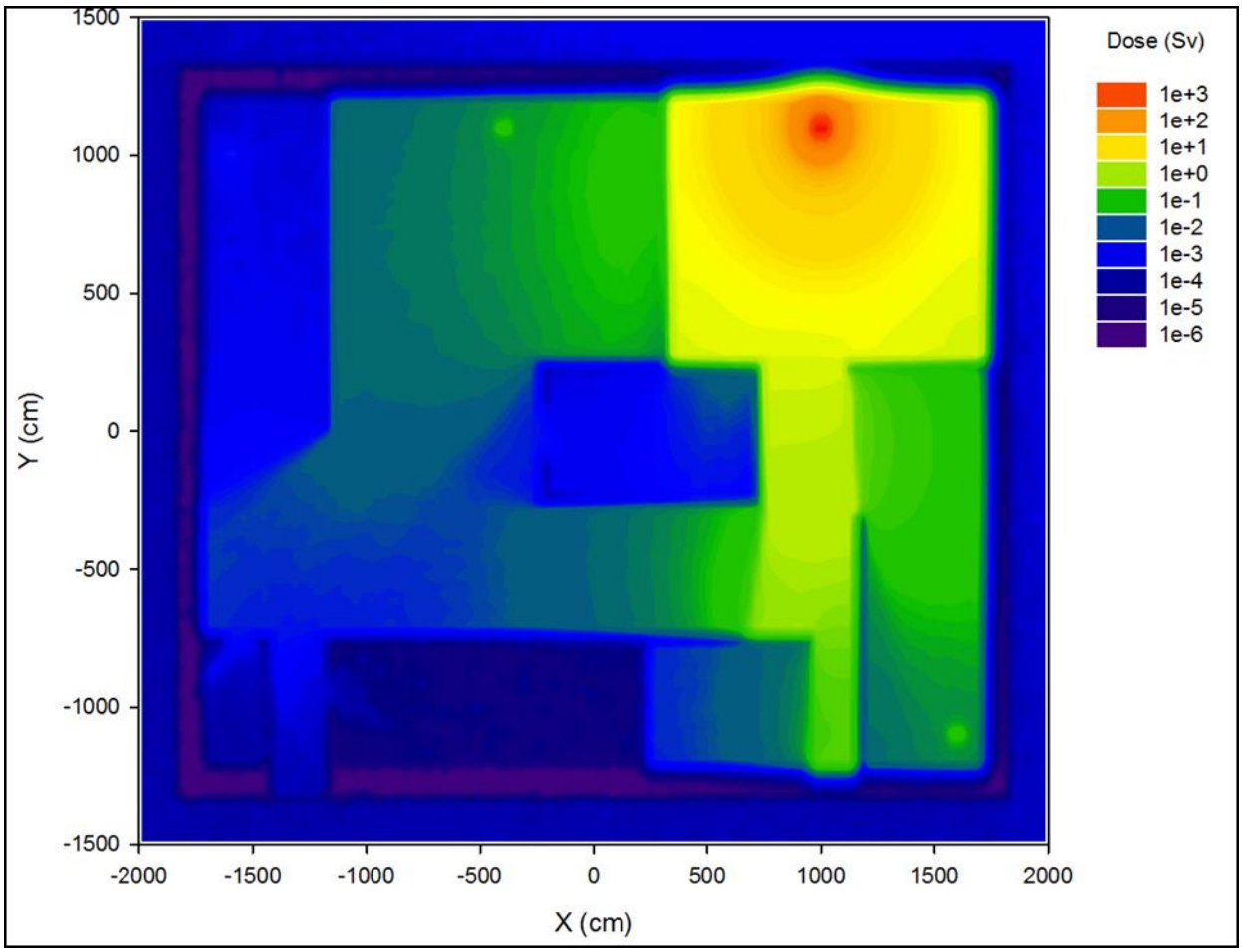

Figure 4.14: The contours of the total equivalent dose (TED) resulting from a CA(10^{17}f) event in facility design modification MOD1.

The diagnosis

The dose contours for $\mathrm{CA}(\mathrm{MOD1}, 10^{17}\mathrm{f})$ in Figure 4.14 are diagnosed as follows:

- Design modification MOD1 is a substantial improvement over the naïve, baseline design MOD0.
- Workers in the control room are far better protected against overexposures — MOD1 managed to lower the TED in the control room from hundreds of mSv to only 10 mSv.
- There are two major flaws in MOD1, however: (1) There is still an unacceptable degree of radiation streaming from the CA workstation to other workstations, and (2) the outer wall thickness of 150 cm is excessive — the peak dose outside the facility, directly opposite the location of the CA, is low at 1.2 mSv/h, and elsewhere it reaches the natural background dose level. It will be more economical to only give the perimeter wall a 150 cm thickness *only* around the most CA prone workstation, and to maintain its general thickness at a more affordable 60 cm.

4.5.3 Design MOD2

The plan

In design modification MOD2, the shortcomings that disqualified MOD1, were addressed. Design modification MOD2 is shown in Figure 4.15.

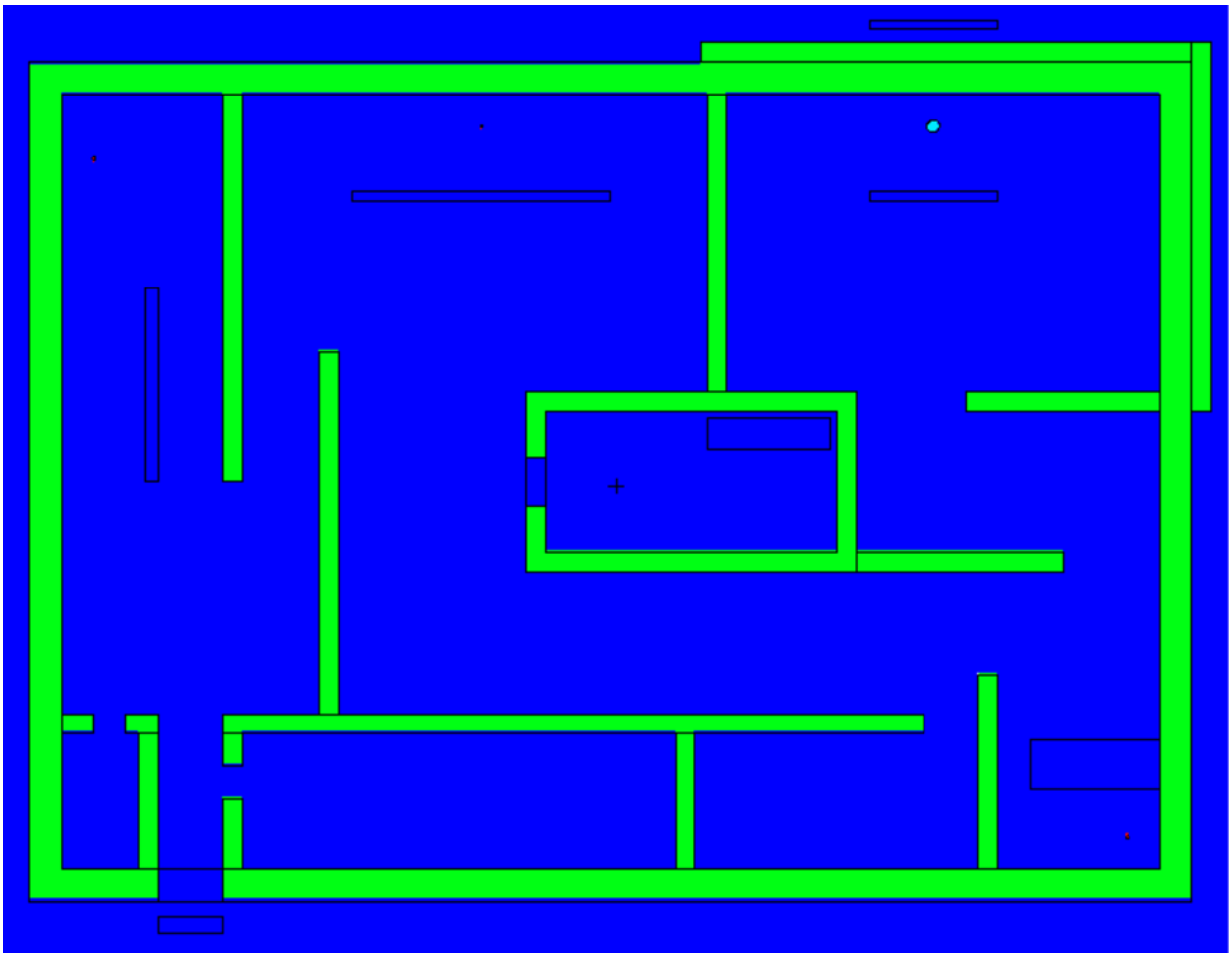

Figure 4.15: PUREX facility design modification MOD2.

The perimeter concrete wall of the PUREX process hall, is now 60 cm thick, with an additional 90 cm of concrete added around the CA prone workstation on the upper RHS — the increased concrete thickness is now local and not general, i.e., the deployment of concrete has been is radiologically and financially optimized. In addition, the inner shielding walls are now arranged in a labyrinthine fashion to properly "shadow" radiation streaming from the CA hotspot/epicentre — seen as a small green disk at the upper RHS of Figure 4.15.

The dose contours

Figure 4.16 shows the $TED(x, y)$ dose contours for design MOD2.

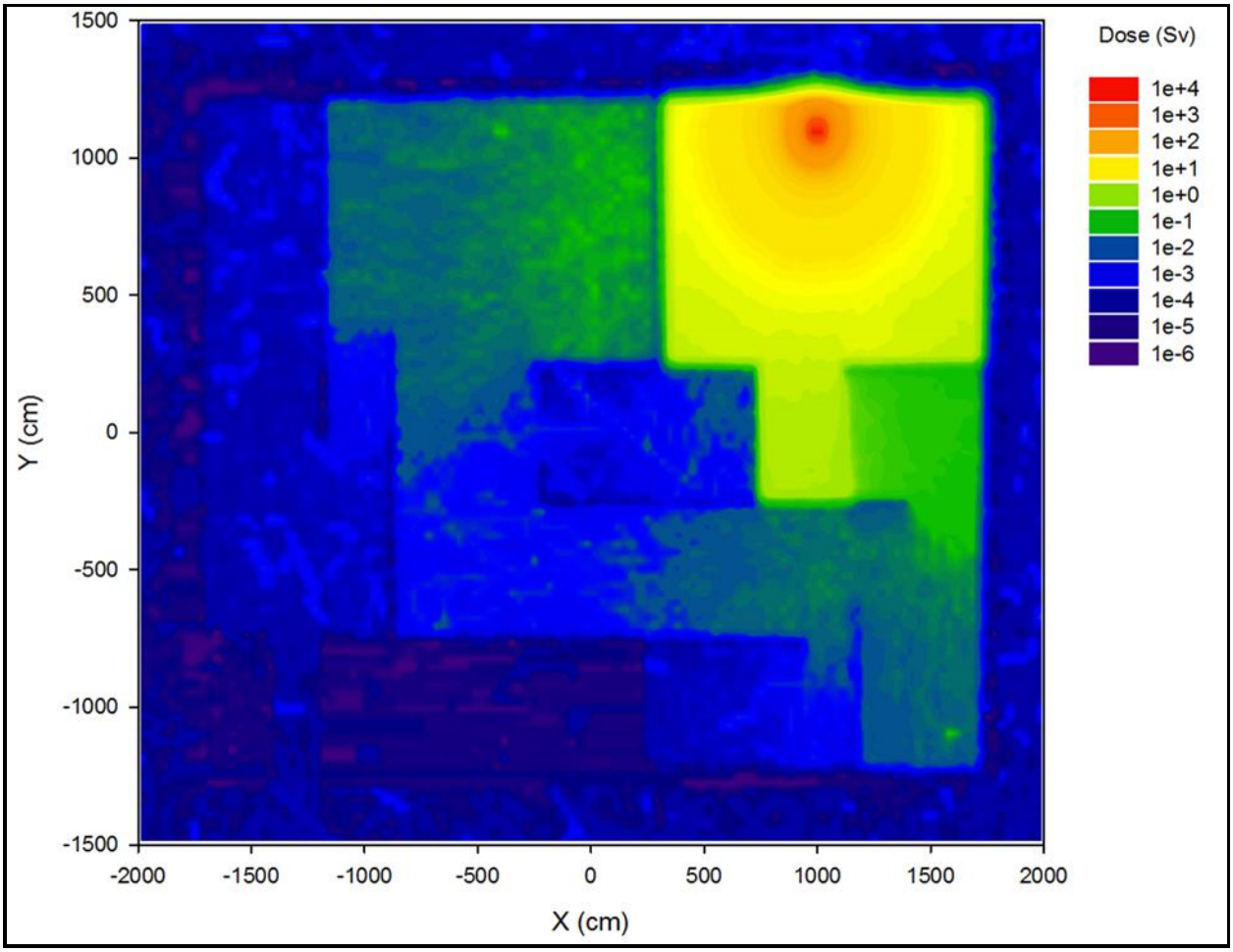

Figure 4.16: The contours of the total equivalent dose (TED) resulting from a CA(10^{17}f) event in the PUREX facility design MOD2.

The diagnosis

The dose contours for $\mathrm{CA}(\mathrm{MOD2}, 10^{17}\mathrm{f})$ in Figure 4.16 are diagnosed as follows:

- Doses calculated for MOD2 are substantially better than obtained with MOD1.
- MOD2 is, overall, a significant step forward towards an ethical facility design based on an "engineered survivability" philosophy.
- There is now a significant degree of radiological de-coupling between workstations. The high dose field is now confined to the CA workstation alone, while staff in other workstations are protected against lethal exposures. The layout is no longer an open floorplan, but based on individual shielded cubicles.
- There is still a shortcoming in MOD2: The calculated dose in the cubicle to the direct left of the accident cubicle, is above 50 mSv — completely survivable but still almost a factor

3 higher than the 20 mSv annual dose limit for occupational radiation exposure. Something is still wrong in the design, and this radiation streaming has to be stopped.

4.5.4 Design MOD3

The plan

Design MOD3 is a "shot in the dark" to try to address the above shortcoming in design MOD2 — doses in adjacent cubicles still exceeding the annual dose limit of 20 mSv. The inner concrete wall to the LHS of the CA cubicle, retains its 60 cm thickness, but is now made of a heavy concrete with better shielding properties compared to ordinary concrete. The concrete of this wall now contains 2% $^{10}\mathrm{B}$ and 14% Fe by mass. The aim of this perturbation in the concrete composition, is to test whether the offending high dose is sensitive to the perturbation. Iron (Fe) is able to degrade neutron energies very effectively via inelastic scattering, while $^{10}\mathrm{B}$ is a strong absorber of lower-energy neutrons. The photon shielding ability of Fe is better than that of the dominant oxygen and silicon in ordinary concrete. The neutron absorber $^{10}\mathrm{B}$ also suppresses the production of energetic photons from (n,γ) reactions, i.e., it can lower the PED as well. If direct transmission through the concrete wall had been the cause of the excessively high doses in the adjacent cubicle, the doses will be found to be greatly affected by the perturbation in the material composition.

Horizontal dose contours for MOD3

Figure 4.17 shows the $TED(x,y)$ horizontal dose contours for design MOD3.

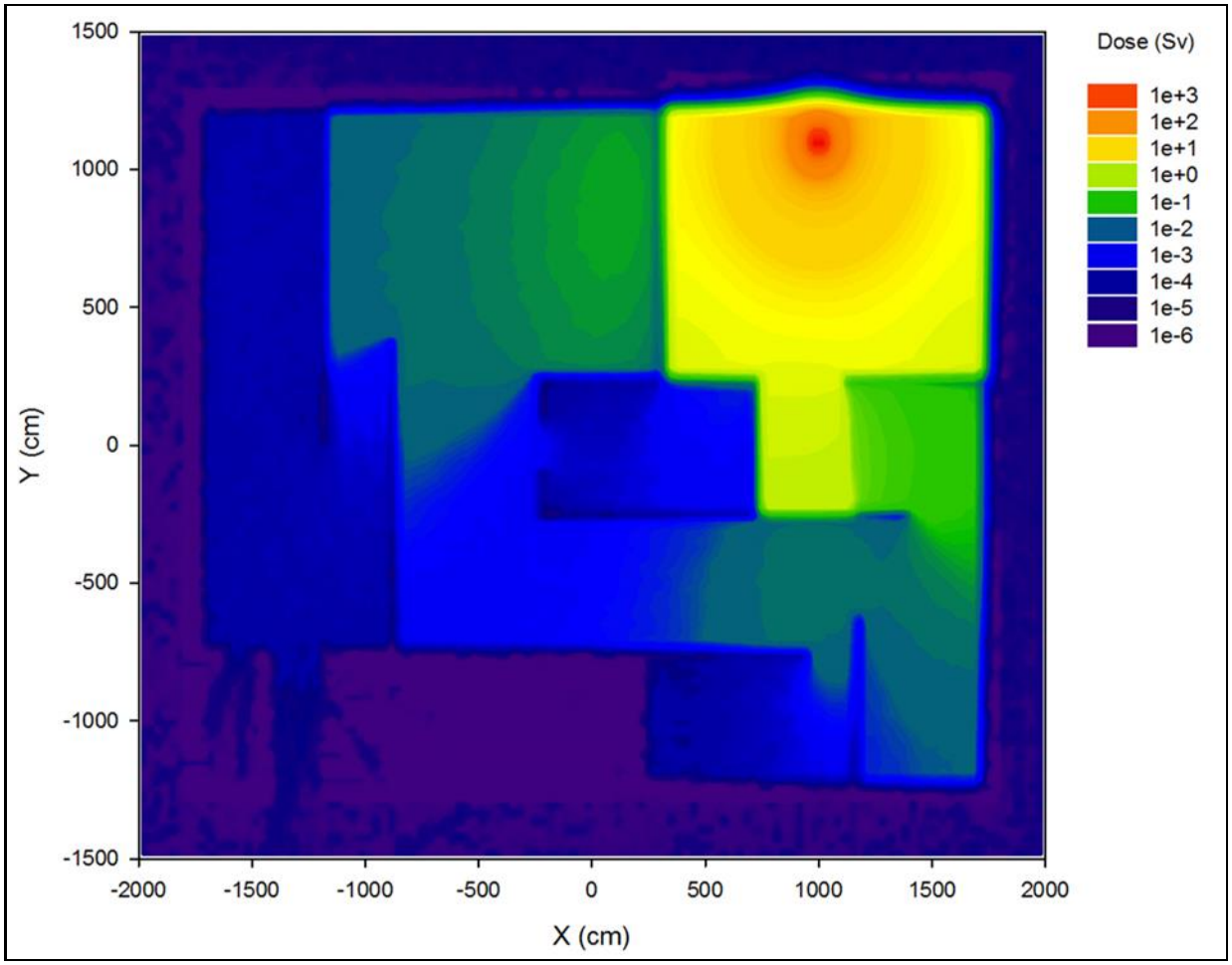

Figure 4.17: The horizontal dose contours of the total equivalent dose, TED(x,y) in the event of a CA(10^{17}f) excursion in the PUREX facility with shielding design MOD3.

The diagnosis of MOD3

The horizontal dose contour plot of $TED(x,y)$ for $\mathrm{CA}(\mathrm{MOD3}, 10^{17}\mathrm{f})$ in Figure 4.17 is diagnosed as follows:

- Disappointingly, the modified concrete composition appeared to only marginally lower doses in the adjacent cubicle. The NED was only lowered from 50.5 mSv to 48 mSv, while the PED was only lowered from 7.1 mSv to 6.4 mSv. The dose reduction that was achieved was marginal and does not rectify the shortcoming.
- The offending dose was found to be frustratingly insensitive to the addition of a substantial amount of Fe as well as the slow neutron absorber $^{10}\mathrm{B}$, in the shielding wall between the two workstations.
- The above finding means that the radiation does not reach the neighboring workstations via direct penetration through the partitioning wall(s), but via another route. This route has to be identified and then eliminated.

Vertical dose contours for MOD3

In a quest to discover how the radiation crosses over from the accident cubicle to the adjacent cubicles, the vertical dose distribution $NED(x,z)$, $PED(x,z)$ and $TED(x,z)$ were visualised as contour plot; the dose distribution $TED(x,z)$ is displayed in Figure 4.18.

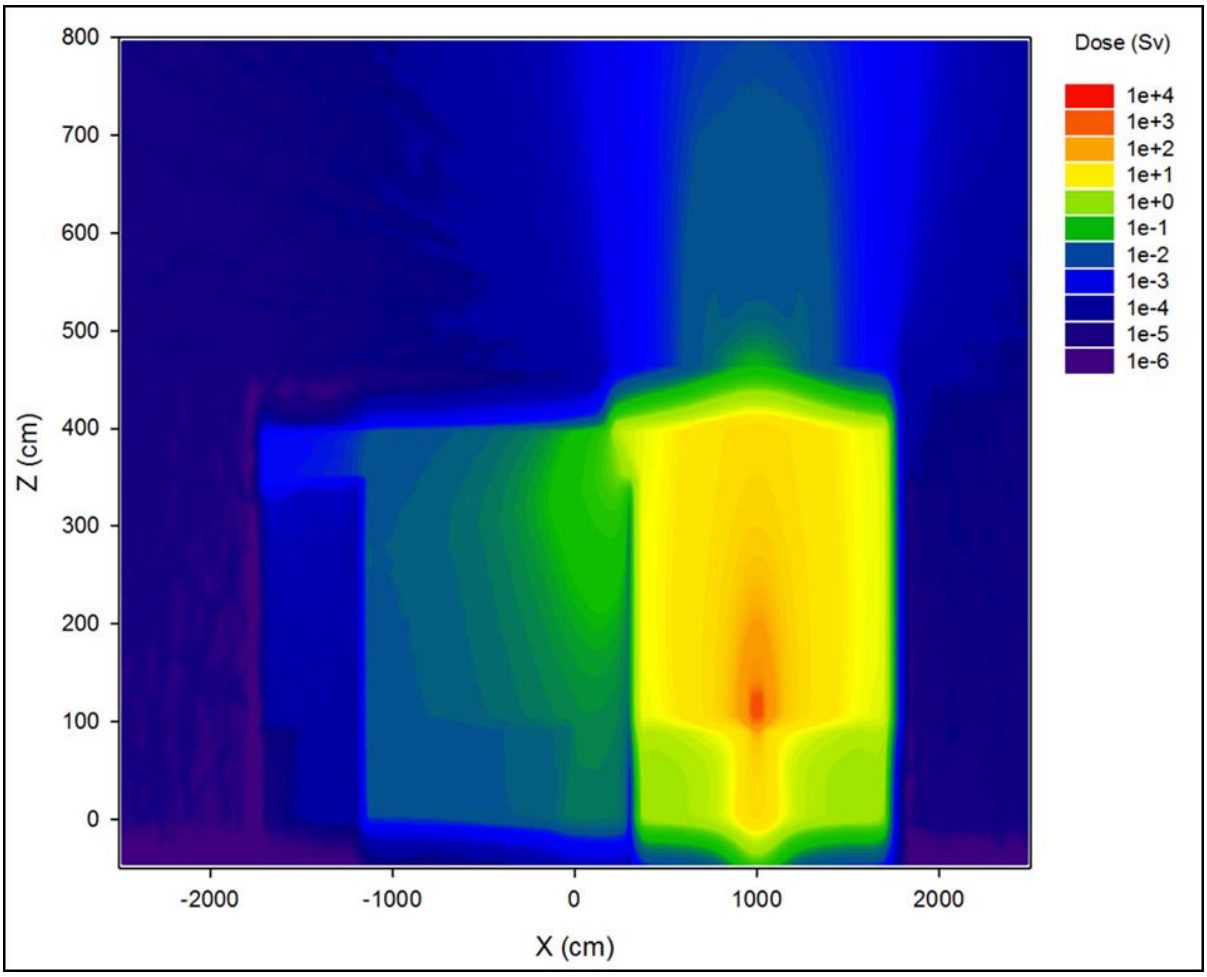

Figure 4.18: The vertical dose contours of the total equivalent dose, TED(x,z) in the event of a CA(10^{17}f) excursion in the PUREX facility having shielding design MOD3.

The diagnosis

The vertical dose contours plot of $TED(x,z)$ for $\mathrm{CA}(\mathrm{MOD3}, 10^{17}\mathrm{f})$ in Figure 4.18 is diagnosed as follows:

- The high doses seen in adjacent cubicles, are not caused by direct transmission through the partitioning walls, but via radiation streaming through the substantial gap between the top of the inner partitioning walls and the underside of the concrete roof slab.

It should be noted that the ability to rapidly diagnose the problem, rests strongly on data visualization. Without data visualization, diagnosis and rectification would have been more difficult.

4.5.5 Design MOD4

The plan

In MOD0, MOD1, MOD2 and MOD3, the inner walls do not reach to the roof, but end 100 cm below the bottom of the concrete slab roof. This is clearly seen in Figure 4.19.

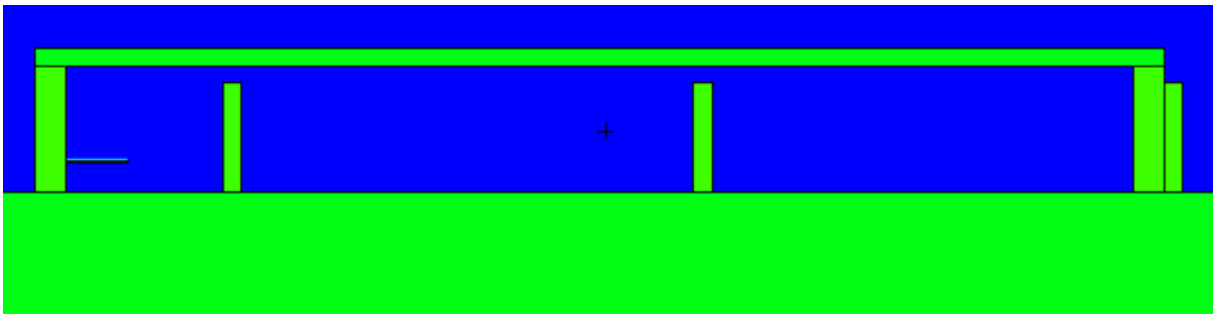

Figure 4.19: In facility designs MOD0, MOD1, MOD2 and MOD3, there is a gap between the top of the inner partitioning walls, and the bottom of the roof slab.

Radiation, specifically neutrons, were found to stream significantly through these gaps, and then "rain down" from above on workers — this is evidently visible in Figure 4.18. In design modification MOD4, the inner partitioning walls were modified to reach all the way to the roof, i.e., there is no more gap. The purpose of modification MOD4 is to achieve better radiological isolation between workstation cubicles, by closing a major streaming pathway. Figure 4.20 shows the MOD4 rectification of this major shortcoming in the original design.

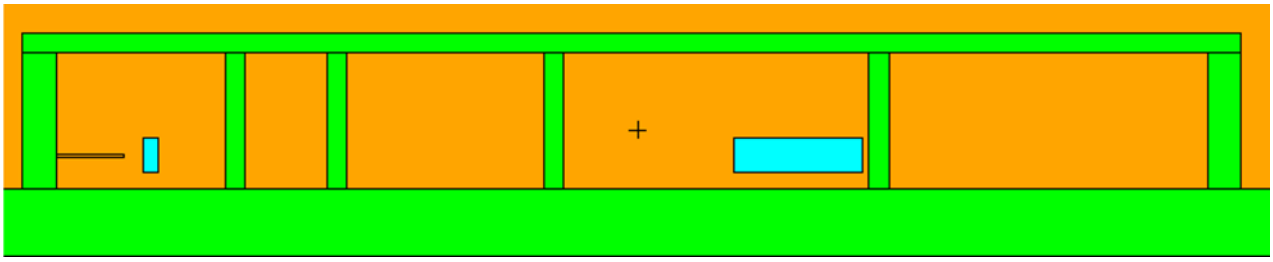

Figure 4.20: MCNP6.2 plot of design modification MOD4 to the PUREX facility — all inner partitioning walls now reach to the underside of the roof slab; the gap had been eliminated.

Calculated dose distributions for design MOD4

A lengthy[22] MCNP simulation proved MOD4 to be very successful — the offending high NED was lowered from circa 50 mSv to only 1.3 mSv — a spectacular improvement. The offending high photon dose was lowered from circa 7 mSv to only 0.93 mSv — another spectacular improvement. In fact,

[22] The better the shielding becomes, the longer the simulation needs to run, to converge doses to the typical convergence criterion that the 1σ relative error estimate should be below 5%.

these improvements are “too good”, and the design can be made more affordable by adjusting the thickness and composition of the one “overdesigned” partitioning wall.

Dose contours for MOD4 are visually almost indistinguishable from that of MOD6 — the recommended final PUREX facility design and dose contours are shown in Figure 4.21 and Figure 4.22, respectively.

4.5.6 Design MOD5

This modification has, since its original execution, been subsumed into MOD4, and is therefore briefly explained in this subsection. The thickness of the inner partitioning wall directly to the left-hand side of the workstation-cubicle where criticality accident is assumed to have occurred – is reduced to 30 cm. this is expounded in §4.5.7 for the final model, MOD6.

4.5.7 Design MOD6

The plan

In MOD6, the thickness of the inner partitioning wall directly to the LHS of the cubicle where the excursion happens, is lowered to its original thickness of 30 cm, because the root cause of the high dose, as seen with MOD3, was not a lack of shielding wall thickness, but rather radiation streaming through the gap between the top of the inner walls and the roof. Another facet of design modification MOD6 is that the ferrous & boron additions to the specific partitioning wall to the direct left of the excursion workstation, were abandoned. The partitioning wall is now composed of ordinary concrete, which entails that it will be cheaper to build.

A top view of the recommended, final facility design, namely MOD6, is shown in Figure 4.21.

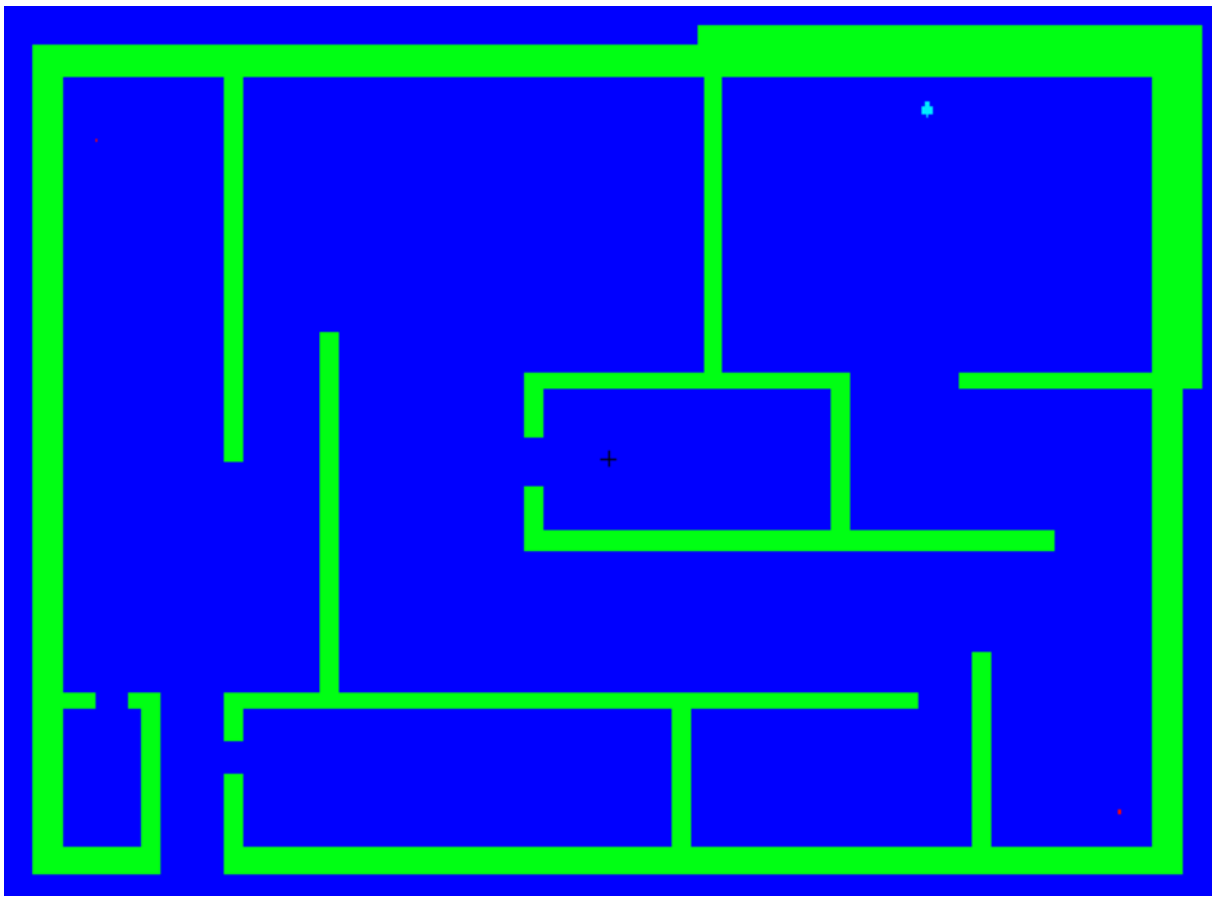

Figure 4.21: Top-view of the recommended, final PUREX facility design — MOD6.

Calculated doses for MOD6

With MOD6, the NED in the adjacent LHS cubicle was calculated to be 2.7 mSv and the PED was quantified as 1.6 mSv. The sum, TED, of these doses remains comfortably below the annual dose limit of 20 mSv and is therefore acceptable. Using a special heavy concrete for this wall will therefore be a wasteful and pointless expenditure, because safe doses are achieved with a 30 cm thick ordinary concrete wall.

In the MOD6 design, all workers in the process hall will easily survive a $\mathrm{CA}(10^{17}\mathrm{f})$ excursion, without even exceeding half of the 20 mSv limit on the annual effective dose. Workstations are radiologically decoupled. Only persons present in the CA cubicle, will accrue lethal doses — this is considered unavoidable until the process is fully automated and controlled remotely from the control room.

The MOD6 design is robust enough to even make a $\mathrm{CA}(10^{18}\mathrm{f})$ excursion survivable for all workers present in the PUREX facility, except those located in the CA cubicle.

Calculated horizontal dose contours for MOD6

The horizontal dose contours $TED(x,y)$ for design modification MOD6 are plotted in Figure 4.22.

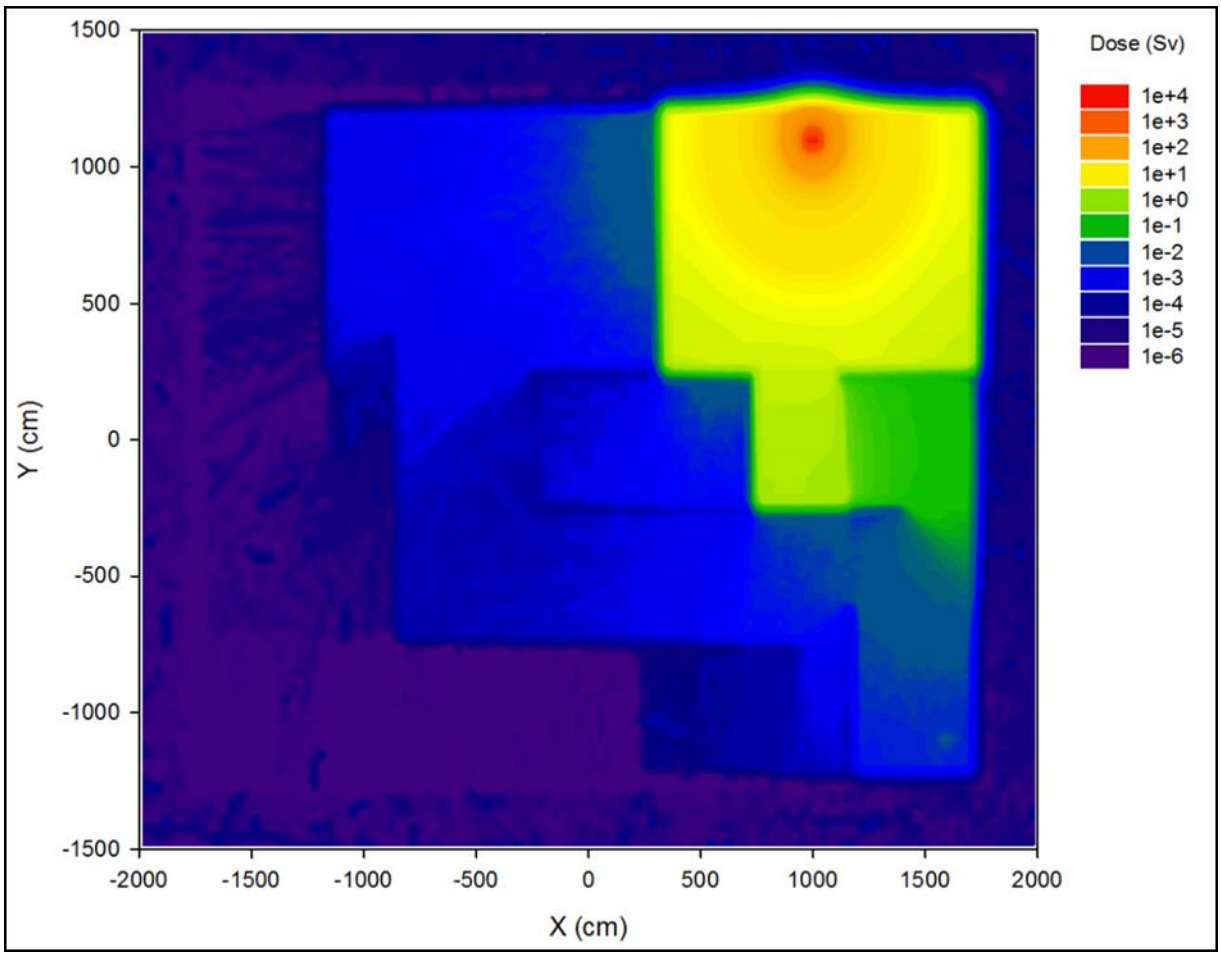

Figure 4.22: PUREX facility layout MOD6 — TED distribution in the x-y plane.

Calculated vertical dose contours for MOD6

The vertical dose distribution, $TED(x,z)$, for the MOD6 design, is shown in Figure 4.23.

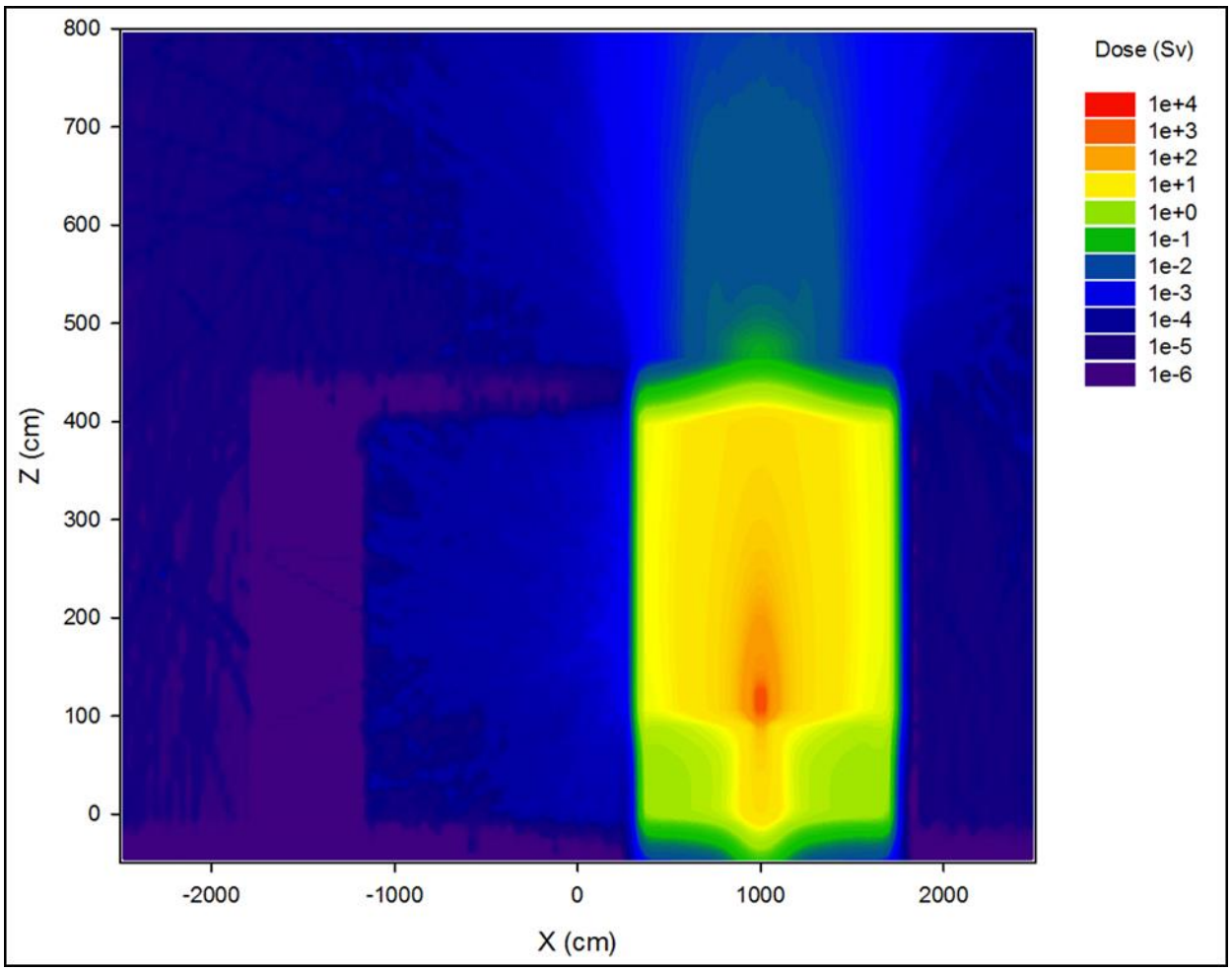

Figure 4.23: The vertical dose distribution, TED(x,z), for the MOD6 facility design.

The vertical dose contours in Figure 4.23 confirms that the excursion is confined and contained in a single cubicle, with minimal inter-cubicle streaming. The streaming pathway observed in the MOD3 design (as highlighted earlier in Figure 4.17 and Figure 4.18) has been (literally) plugged in the MOD6 design.

Figure 4.23 indicates a substantial dose on the rooftop, directly overhead of the epicentre of the excursion. The root cause is that the concrete roof slab is only 30 cm thick, whereas the horizontal shielding walls are at least 60 cm thick.

Dose on the rooftop

The calculated dose on the rooftop of the MOD6 design of the PUREX plant, directly overhead of the process mass experiencing the design-basis excursion, is given in Table 4.3.

Table 4.3: Calculated maximum radiation doses on the rooftop of the PUREX facility, in the event of a hypothetical CA(MOD6, 10^{17}f) criticality excursion.

NED on rooftop (Sv)	**PED on rooftop** (Sv)	**TED on rooftop** (Sv)
0.0196	0.0187	0.0383

The total equivalent dose (TED) on the roof is in the order of 1.92 times higher than the ICRP's recommended annual dose limit for workers involved with practices (ICRP, 2007).

The total equivalent dose on the roof is in the order of only 3.9 % of the threshold dose for the onset of acute radiation syndrome (ARS) and only circa 1.2% of a typical fatal dose (here assumed to be 3.5 Sv).

The above relatively high, but completely sub-clinical, dose registered on the rooftop is, of little practical concern, given that the human occupancy factor on the building's roof is exceedingly low. A brief probabilistic assessment makes it clear. Assumption is therefore made that the roof occupancy factor is around 1 hour per year, i.e., circa 1.0E-4. Assumption is also made that the annual probability of a criticality excursion accident, is e.g., 1.0E-5. Because these events are uncorrelated, the probability of human occupancy during a criticality excursion, calculates to $10^{-4} \times 10^{-5} = 10^{-9}$. To construct a more expensive, say 45 cm thick roof slab, for an event with a best-estimate probability of 1 in a billion, is not justified.

Analytic judgement Design MOD6

The dose contours of Figure 4.22 and Figure 4.23 as well as the calculated doses in the TEM detectors (refer to §4.6 on page 84), lead to the following decision on the efficacy of the MOD6 design:

- Adequate radiological decoupling between adjacent process workstations, has been achieved. Non-survivable doses are only encountered in the accident cubicle. At all other workstations, doses are easily survivable for the design basis accident.
- Far less neutrons from the accident cubicle will stream to other fissile material volumes at other workstations, i.e., the degree of neutronic decoupling between fissile process-masses inside the plant, has been greatly improved.

4.5.8 Further optimization of the design for the PUREX facility

From an economical perspective, the MOD6 design can be fruitfully subjected to further optimization. Some concrete walls, where dose rates in the event of a $\mathrm{CA(MOD6,10^{17}f)}$ excursion are below, e.g.,

1 mSv, can be made somewhat thinner. Lowering the thickness of the Pb layer in the entrance door from the present 5 cm thickness to, e.g. 3 cm, can also be tabled, because the calculated dose at this position (for the MOD6 design), is very low. These “final tweaks” to the material-cost facets of the facility design is best left to the detailed engineering-design phase of the PUREX project, and are considered far beyond the scope of this study.

4.6 Dose reduction at selected detector positions, from the initial design MOD0 to the final design MOD6

The doses calculated in the TEM detectors deployed in, around and on top of the PUREX facility, as well as their magnitudes relative to perspective-giving “beacon” quantities, as summarized in Table 4.4 below. The doses for the naïve MOD0 design are juxtaposed against the doses achieved with the MOD6 design, to highlight the degree of improvement in radiological safety that was achieved by progressing from MOD0 (naïve design) to MOD6 (final design). The dose on the rooftop is not listed, because it stays essentially the same for all design modifications.

Dose-reduction achievements are highlighted in green while doses and ratios that are cause for concern, and must be brought to the attention of responsible managers and safety committees, are highlighted in light red. A few special symbols are used in Table 4.4:

- D_ICRP: Annual limit on the effective dose for radiation workers, i.e., 20 mSv.
- D_ARS: Approximate dose threshold for acute radiation syndrome (ARS), i.e., 1 Sv.
- D_fatal: Approximate dose threshold for fatalities, i.e., 3 to 3.5 Sv.

Table 4.4: Calculated radiation doses for the MOD6 design, juxtaposed against doses for the naïve MOD0 PUREX facility design.

Detector cell-number in MCNP model	**Detector location**	**NEDR(MOD0)** (Sv)	**NEDR(MOD6)** (Sv)
151	Directly opposite excursion, outside perimeter wall	2.49E-03	2.95E-05
152	Excursion workstation, where manual liquid extraction and evaporation is performed	2.26E+01	2.28E+01
153	Workstation for liquid-liquid extraction and ADU precipitation	3.17E-01	2.65E-03
154	Inside control room	1.09E-01	4.84E-03
155	Workstation for dissolution	6.17E-01	6.99E-03
156	Entrance door to facility	2.00E-03	1.69E-06
157	Workstation for hydro-fluorination	1.91E-01	1.22E-06

Detector cell-number in MCNP model	Detector location	PEDR(MOD0)	PEDR(MOD6)
151	Directly opposite excursion, outside perimeter wall	1.77E-03	3.91E-05
152	Excursion workstation, where manual liquid extraction and evaporation is performed	3.08E+00	3.11E+00
153	Workstation for liquid-liquid extraction and ADU precipitation	3.73E-02	1.58E-03
154	Inside control room	3.05E-02	3.67E-03
155	Workstation for dissolution	7.48E-02	2.01E-03
156	Entrance door to facility	2.86E-04	5.48E-07
157	Workstation for hydro-fluorination	2.51E-02	5.40E-06

Detector cell-number in MCNP model	Detector location	TEDR(MOD0)	TEDR(MOD6)	Dose reduction factor $\frac{\text{TEDR(MOD6)}}{\text{TEDR(MOD0)}}$
151	Directly opposite excursion, outside perimeter wall	4.26E-03	6.86E-05	62.1
152	Excursion workstation, where manual liquid extraction and evaporation is performed	2.57E+01	2.60E+01	1.0
153	Workstation for liquid-liquid extraction and ADU precipitation	3.54E-01	4.24E-03	83.6
154	Inside control room	1.40E-01	8.51E-03	16.4
155	Workstation for dissolution	6.92E-01	9.00E-03	76.9
156	Entrance door to facility	2.29E-03	2.24E-06	1019
157	Workstation for hydro-fluorination	2.16E-01	6.63E-06	32569

Detector cell-number in MCNP model	Detector location	Ratio TEDR(MOD0)/ D_ICRP	Ratio TEDR(MOD0)/ D_ARS	Ratio TEDR(MOD0)/ D_fatal
151	Directly opposite excursion, outside perimeter wall	2.13E-01	4.26E-03	1.22E-03
152	Excursion workstation, where manual liquid extraction and evaporation is performed	1.28E+03	2.57E+01	7.33E+00
153	Workstation for liquid-liquid extraction and ADU precipitation	1.77E+01	3.54E-01	1.01E-01
154	Inside control room	6.98E+00	1.40E-01	3.99E-02
155	Workstation for dissolution	3.46E+01	6.92E-01	1.98E-01

156	Entrance door to facility	1.14E-01	2.29E-03	6.53E-04
157	Workstation for hydro-fluorination	1.08E+01	2.16E-01	6.16E-02

Detector cell-number in MCNP model	Detector location	Ratio TEDR(MOD6)/ D_ICRP	Ratio TEDR(MOD6)/ D_ARS)	Ratio TEDR(MOD6)/ D_fatal
151	Directly opposite excursion, outside perimeter wall	3.43E-03	6.86E-05	1.96E-05
152	Excursion workstation, where manual liquid extraction and evaporation is performed	1.30E+03	2.60E+01	7.42E+00
153	Workstation for liquid-liquid extraction and ADU precipitation	2.12E-01	4.24E-03	1.21E-03
154	Inside control room	4.26E-01	8.51E-03	2.43E-03
155	Workstation for dissolution	4.50E-01	9.00E-03	2.57E-03
156	Entrance door to facility	1.12E-04	2.24E-06	6.41E-07
157	Workstation for hydro-fluorination	3.31E-04	6.63E-06	1.89E-06

Some notable doses and ratios observed in Table 4.4 are now discussed:

- A dose reduction of between 16.4 and 32569 is achieved by progressing from design MOD0 to design MOD6. This points to a very successful redesign.
- With design MOD6, the design-basis accident is survivable in all workstations except at the accident workstation.
- With design MOD0, the design-basis accident will impart doses that are a factor 7 to 18 times higher than the ICRP's recommended annual dose limit of 20 mSv, at almost all the non-accident detector positions. This indicates that the MOD0 design is radiologically not acceptable — it clashes head-on with the *optimization principle* of radiation protection, which is of fundamental importance in the ICRP's system of radiological protection.
- With design MOD0, a $CA(10^{18}f)$ excursion, i.e., an event 10 times more severe than the design-basis accident, can be fatal to staff located at a total of three process workstations.
- With design MOD6, the design-basis accident will impart doses that are far below the ICRP's recommended annual dose limit of 20 mSv, at all the non-accident TEM-detector positions. This indicates that the MOD6 design is radiologically optimised — it conforms to the

optimisation principle of radiation protection, which is of fundamental importance in the ICRP's system of radiological protection.

- With design MOD6, a $CA(10^{18}f)$ excursion, i.e., an event 10 times more severe than the design-basis accident, will still be comfortably sub-fatal to all staff except those present in the accident cubicle.

4.7 The placement of CAAS detectors at the PUREX facility

The selection and placement of criticality accident alarm system (CAAS) detectors, must be based on several factors, including the dose distributions $NED(x,y,z)$ and $PED(x,y,z)$ that will prevail during the most probable criticality accident.

The neutron dose-rate distributions in the recommended (MOD6) facility design, in the event of a magnitude $\mathrm{CA}(10^{17}\mathrm{f})$ criticality excursion in the fissile material undergoing concentration by evaporation, is shown in Figure 4.24. The $PED(x,y)$ dose distribution is analogous to $NED(x,y)$.

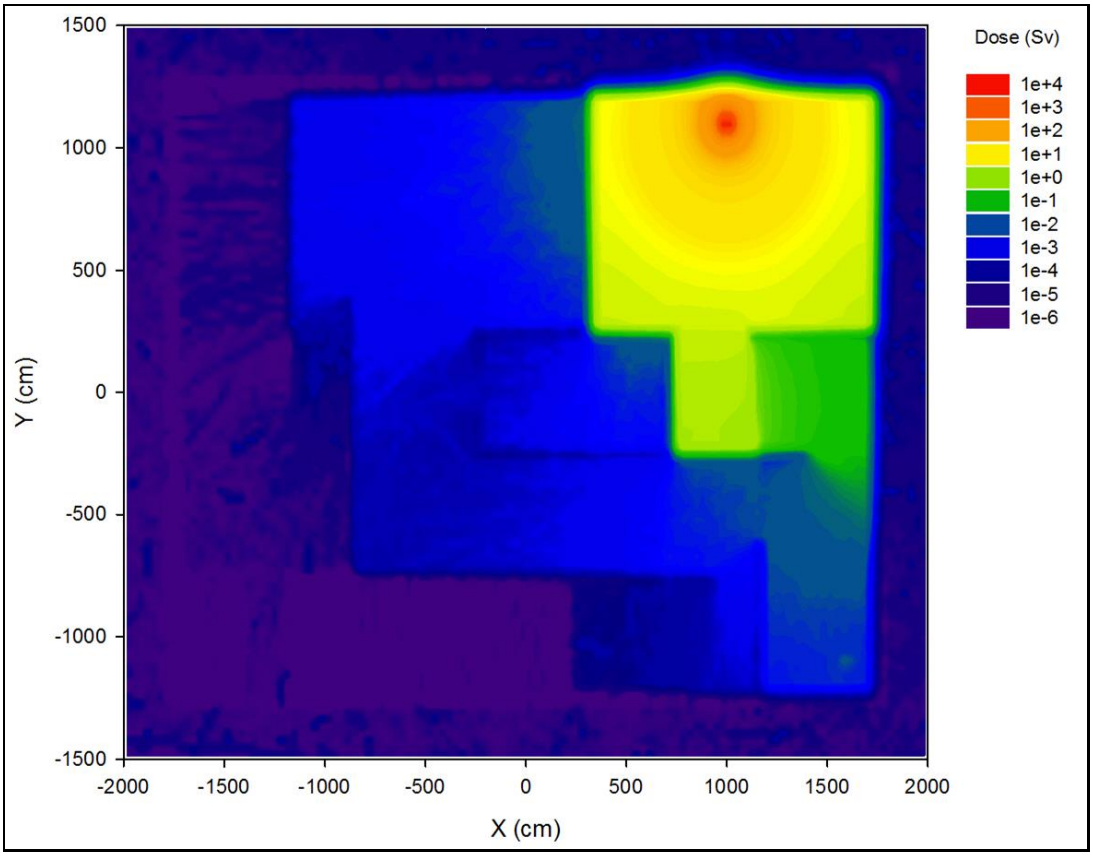

Figure 4.24: The neutron and photon dose-rate distributions in the recommended (MOD6) facility design, in the event of a criticality excursion in the fissile material undergoing concentration by evaporation.

The following conclusions regarding the placement of CAAS detectors can be drawn from the dose distributions.

1. The radiation detectors must be reliable dose integrators that can respond within for example a second.
2. The radiation detectors must be able to detect and correctly register dose pulses as low as 1 mSv and as high as, e.g., 50,000 mSv, that is, a wide dose range must be covered.
3. Using neutron detectors in the CAAS system will impart greater rejection of false alarms. Many portable γ-sources exist, whereas practically no portable neutron sources exist. A Radiation Protection Officer (RPO) entering the facility with a small, portable ^{137}Cs test-source, may trigger a false alarm if only γ-detectors are deployed. If, on the other hand, 6 neutron detectors and 6 γ-detectors are deployed, and the Area Radiation Monitoring System (ARMS) uses a logic that only registers an alarm condition if at least 1 neutron detector and 1 γ-detector registers a dose pulse, this to say:

```
IF
    HighDoseRate (≥1 neutron detector)
  AND
    HighDoseRate(≥1 γ-detector)
THEN
  TRIGGER ALARM
```

   then the probability of a false criticality alarm becomes very small.
4. Radiation detectors must be placed at every workstation.
5. Radiation workers in a PUREX facility must wear (passive[23]) personal dosimetry badges capable of (1) recording the photon dose, (2) the neutron equivalent dose.

Delving deeper into CAAS detector systems and their deployment, falls beyond the scope of this dissertation. These issues are treated in many available references (Baker *et al.*, 1994; Greenfield, 2009; Gross, 2018; Kiedrowski, 2012; Miller and Peplow, 2013; Peplow and Petrie, 2010)[24].

---

[23] Note by co-supervisor TJvR: A *passive* personal dosimetry badge is a "voiceless" dose integrator "without a battery"; it will faithfully record the magnitude of a dose that will kill a worker, but it cannot warn the worker of the danger of the situation. An *active* radiation detector such as an EPD (electronic personal dosimeter) has a battery which powers it; it is equipped with a numerical read-out as well as an audible alarm. An EPD records doses and can also sound an audible warning when the dose-rate or dose exceeds pre-set alarm levels. Only passive personal dosimeters are accepted as *dosimeters of legal record,* because active dosimeters have too many failure modes (e.g. flat batteries and electronic malfunctions).

[24] Note by co-supervisor TJvR: Both MCNP6 and the SCALE system are well suited for computations related to a CAAS. The advantage of MCNP6 is that it naturally produces secondary photons from neutron interactions. The disadvantage of the latest available release of SCALE (i.e., 6.2) is that its criticality codes (KENO-5a and KENO-6) function transport only neutrons; the concept "photon" is utterly alien to KENO. In dose calculation with SCALE 6.2 for CAAS simulation, the criticality excursion has to be modelled with KENO.

The control sequence MAVRIC then runs a built-in correlation to (artificially) add γ-radiation with a reasonably correct yield and energy-spectrum, into the fissile material. This source-term is then passed to another code in SCALE, the Monte Carlo code MONACO, which can natively transport neutrons as well as photons. The big advantage of SCALE 6.2 is its highly automated, elegant and efficient variance reduction capability, which is "in another class" compared to the awkward and laborious variance reduction schemes that the hapless MCNP user has to resort to, when having to simulate deep-penetration radiation transport.

5 Quantification of the radionuclide inventory, source term and post-accident dose rates caused by the criticality excursion

5.1 Pre-accident isotopic composition of the fissile material volume in which the postulated excursion happens

The initial sections focus on radioactivity content of the fissile process-mass, and does not consider radioactivity produced in SSC (structures, systems and components) by neutron activation.

The radionuclide inventory (fission products) subsequently to the postulated criticality accident was calculated using the inventory and source term computer code system, the FISPACT II. The geometric configuration of the criticality system is exactly the same as defined for the MCNP input deck. That is, the uranic parametrically mixture is defined in the cylinder of 15.5 cm radius and 28 cm height; and the density of the solution is $\rho = 1.2\ \mathrm{g/cm^3}$. The atomic density of each nuclide in the uranic solution for the FISPACT II input deck is shown in Table 5.1.

Table 5.1: Number of atoms of each nuclide in the aqueous uranic solution undergoing a criticality excursion.

Nuclide	Number of atoms
Hydrogen ($^{1}_{1}\mathrm{H}$)	2.4263×10^{27}
Oxygen ($^{16}_{8}\mathrm{O}$)	1.2678×10^{27}
Uranium ($^{235}_{92}\mathrm{U}$)	2.4552×10^{25}
Uranium ($^{238}_{92}\mathrm{U}$)	2.6936×10^{24}

The fission commands in the FISPACT II such as USEFISSION and FISYIELD was employed to simulate the fissioning process of the aforementioned criticality system.

5.2 Results obtained with the FISPACT-II model for the calculation of the radionuclide inventory in the fissile process mass

A FISPACT-II calculation model was developed to calculate the radionuclide inventory in the fissile process mass. The model is embedded in Appendix A.5 and A.6 on page 131 − 136. The FISPACT computational code used for quantification of radionuclide inventory following the criticality excursion did not give meaningful uncertainty estimates for the initial quantification of fission product activities at $T = 0$—and that the uncertainty in the activities at $T_{cool} = 1\ \mathrm{yr}$ are given by FISPACT as $1\sigma \approx 4.9\%$. The latter 1σ value only incorporates uncertainties in half-life data of fission products, that is,

the uncertainty information produced by fission product is incomplete and therefore quite nominal. A snapshot of uncertainty estimates is presented below in Table 5.2.

Table 5.2: The uncertainty estimates from the FISPACT computational code.

UNCERTAINTY ESTIMATES (cross sections only)

Uncertainty estimates are based on pathway analysis for the irradiation phase

Total Activity is	3.56875E+09	+/-	1.73E+08	Bq.	Error is 4.85E+00 % of the total.
Total Heat Production is	8.62241E-07	+/-	4.78E-09	kW.	Error is 5.54E-01 % of the total.
Total Gamma Dose Rate is	2.34034E-09	+/-	1.72E-10	Sv/hr.	Error is 7.35E+00 % of the total.
Total Ingestion Dose is	5.36933E+01	+/-	1.54E+00	Sv.	Error is 2.86E+00 % of the total.
Total Inhalation Dose is	7.72502E+03	+/-	5.30E+01	Sv.	Error is 6.87E-01 % of the total.
Total Gamma Heat Prod is	7.60731E-08	+/-	6.58E-10	kW.	Error is 8.65E-01 % of the total.
Total Beta Heat Prod is	1.64879E-07	+/-	4.15E-09	kW.	Error is 2.52E+00 % of the total.

Figure 5.1 presents the time-dependence of the total radionuclide activity in the process volume, shown is the graphs of quantity as a function of cooling time, $A(t)$. This total activity is made up of (1) the activity of the uranium isotopes initially present, (2) the added activity of fission products formed by the 10^{17} fission events, and (3) the activity of radionuclides produced by neutron activation in the fissile process mass.

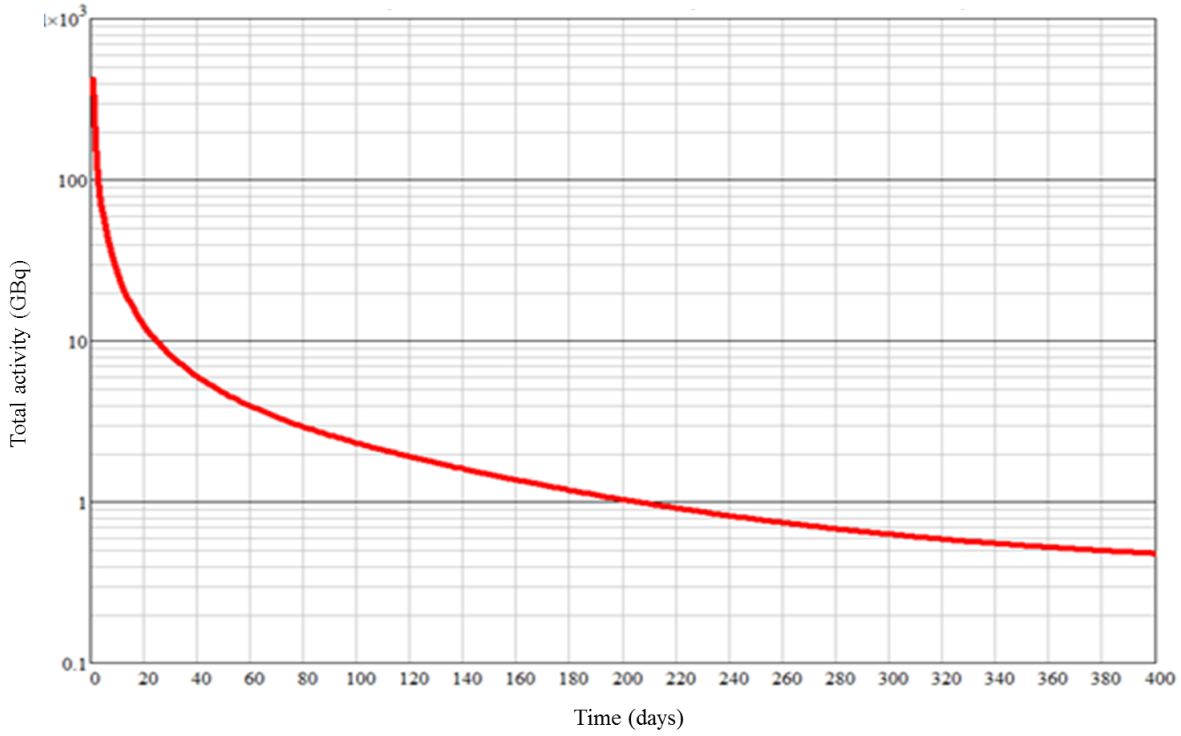

Figure 5.1: Time dependence of the total activity from all radionuclides present after the criticality excursion.

Prior to the criticality excursion, the initial, baseline activity in the fissile process mass calculates to 8.6989E8 Bq. Figure 5.1 shows that, immediately after the excursion, this value is upped by a factor 4000. One year after the excursion, the activity is still a factor 4.5 times higher than the initial, pre-accident activity.

Figure 5.2 expresses the post-accident activity $A_{\mathrm{post}}(t)$ as a multiple of the pre-accident activity, A_{pre}, that is, graphical presentation of the ratio $\frac{A_{\mathrm{post}}(t)}{A_{\mathrm{pre}}}$.

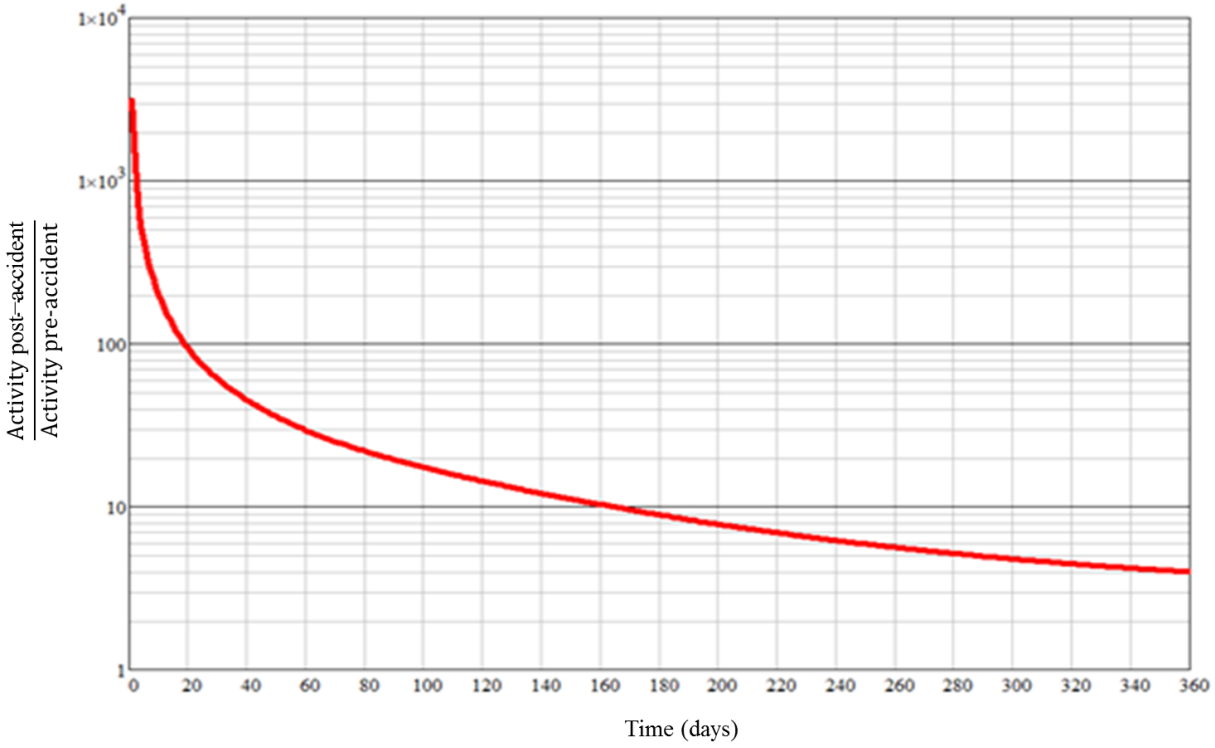

Figure 5.2: The post-accident activity as a multiple of the pre-accident activity.

The following information can be gleaned from Figure 5.2:

- The $\mathrm{CA}(10^{17}\mathrm{f})$ excursion, abruptly raises the activity inventory by a factor of circa 4000.
- After 25 days of "cooling", the ratio $\frac{A_{\mathrm{post}}}{A_{\mathrm{pre}}}$ has decreased to circa 100.
- It takes approximately 200 days for the ratio $\frac{A_{\mathrm{post}}}{A_{\mathrm{pre}}}$ to reach the value 10.
- After 1 year of cooling, the ratio $\frac{A_{\mathrm{post}}}{A_{\mathrm{pre}}} \approx 4.5$.

The nuclide inventory 1 day after the excursion, is summarised in Table 5.3; the total activity is $A(1\ \mathrm{day}) = 3.49\mathrm{E}12\ \mathrm{Bq}$.

Table 5.3: Radionuclide inventory at 1 day after the excursion involving 10^{17} fissions.

Radionuclide	**Activity** (Bq)
Nb97	3.0340E+11
Zr97	2.8130E+11
Nb97m	2.6770E+11
I133	2.4860E+11

Y93	2.3050E+11
Sr91	1.8380E+11
Ce143	1.7810E+11
I135	1.5690E+11
Mo99	1.4600E+11
Tc99m	1.2980E+11
Y91m	1.1830E+11
Y92	9.4870E+10
I132	8.4570E+10
Te132	8.2080E+10
Pr145	7.2050E+10
La141	4.1100E+10
Ba140	3.4810E+10
Pm149	3.4690E+10
Rh105	3.4220E+10
I131	2.4530E+10
Pm151	1.8460E+10
Te131m	1.7310E+10
Nd147	1.5260E+10
Ce141	1.2840E+10
Te129	1.2710E+10
La140	1.2170E+10
Pr143	1.1300E+10
Sb129	1.0720E+10
Ru105	9.6130E+09
Sr92	9.0210E+09
Zr95	8.2790E+09
Rb88	7.4960E+09
Sr89	6.4750E+09
Y91	5.7140E+09
Ru103	5.3470E+09
Rh103m	5.2890E+09
Sm153	4.9800E+09
Te131	4.5410E+09
Sb127	4.4550E+09
Te127	3.2140E+09
Np239	2.9070E+09
Rh105m	2.7320E+09
Pd109	1.9090E+09
Ag109m	1.9090E+09

Ag112	1.7070E+09
Sb128	1.5870E+09
Pd112	1.4690E+09
Pr144	1.3500E+09
Ce144	1.3490E+09
Sn121	1.2090E+09
In115m	9.9330E+08
Cd115	9.4380E+08
Sm156	8.6160E+08
U235	7.6620E+08
Te129m	5.6900E+08
Eu157	5.5580E+08
Br83	5.0900E+08
Ge77	4.9160E+08
As77	3.9130E+08
Ag113	3.6940E+08
Th231	3.6700E+08
Ag111	3.2290E+08
Nb96	1.8540E+08
Sn125	1.7460E+08
Gd159	1.6210E+08
Nb95	1.6110E+08
La142	1.3830E+08
Ce142	1.3830E+08
In117	1.0570E+08
Eu156	1.0520E+08
In117m	1.0320E+08
Ru106	9.5350E+07
Rh106	9.5350E+07
Nd149	9.4990E+07
U234	8.9470E+07
Cs136	8.6110E+07
Ba139	5.6820E+07
Cs137	5.0150E+07
Ba137m	4.7490E+07
I130	4.5640E+07
Sr90	3.8140E+07
Sn127	3.7570E+07
Br82	3.0750E+07
Cd117	2.9210E+07

Cd117m	2.8190E+07
Nb95m	1.7430E+07
Zn72	1.6530E+07
Sb126	1.6020E+07
Y90	1.4230E+07
Ga72	1.3320E+07
U238	1.3240E+07
Pr144m	1.2880E+07
Ga73	1.2520E+07
Ge73m	1.2330E+07
Pm147	1.1220E+07
Tb161	1.0370E+07
Ba136m	9.5360E+06
As78	5.4250E+06
Te127m	5.1690E+06
U237	4.6370E+06
Cd115m	3.7540E+06
Sb125	3.2420E+06
Rb86	2.8340E+06
Sn123	2.5200E+06
Eu155	2.3120E+06
Pd111m	1.8820E+06
Ag111m	1.8340E+06
Pd111	1.4790E+06
Se77m	1.3020E+06
U236	9.3800E+05
Y89m	6.2420E+05
Dy166	5.9370E+05
Ga72m	5.8270E+05
Sm151	5.2030E+05
Eu151	5.2030E+05
Sn117m	4.4190E+05
Ge78	4.1380E+05
I134?	4.0890E+05
Th234	3.7550E+05
Pa234m	3.7500E+05
Cu67	3.2700E+05
Ho166	3.0130E+05
Sb124	2.9220E+05
Sn119m	2.7490E+05

Cu66	2.3980E+05
Ni66	2.3950E+05
I132m	1.9490E+05
Ba135m	1.7310E+05
Pm150	1.6900E+05
Cs134m	1.6530E+05
Sb122	1.3560E+05
Te133m	8.3450E+04
Y90m	7.8100E+04
Pr142	6.2070E+04
As76	5.2580E+04
Sb128m	5.1730E+04
Dy165	4.3900E+04
Ho167	4.3540E+04
Sn128	4.2620E+04
Sr87m	4.1270E+04
Ge75	2.9960E+04
Te125m	2.7580E+04
Er169	2.7150E+04
Zn71m	2.6030E+04
Rh106m	2.6000E+04
Er171	2.2600E+04
Te133	1.7780E+04
Cs134	1.5080E+04
Sn121m	1.3770E+04
Er172	1.0750E+04
Tm173	8.9800E+03
I133m	8.3580E+03
Br80	6.3660E+03
Br80m	5.9410E+03
Cd113m	5.8450E+03
Cs132	5.3170E+03
Er167m	5.1940E+03
Pm148	4.7170E+03
Ni65	3.7400E+03
Rb84	3.3150E+03
Pm148m	3.0490E+03
Tm172	2.9250E+03
Zn69	2.7490E+03
Zn69m	2.5600E+03

Yb175	2.1190E+03
I126	1.4170E+03
Tc99	1.0700E+03
Nb92m	1.0330E+03
Se81	1.0130E+03
Sb120m	9.9840E+02
Sb119	8.2890E+02
Te134	7.8880E+02
Pa234	7.6400E+02
Ce139	7.5940E+02
Zr93	7.1180E+02
Se81m	6.8680E+02
Nb98m	4.6100E+02
Cs135	4.3450E+02
Y88	3.1430E+02
Lu177	2.6600E+02
Pu239	2.5880E+02
U235m	2.5270E+02
Tb160	2.3440E+02
Te123m	2.2580E+02
Ba133m	2.2500E+02
In118	2.0860E+02
Cd118	2.0820E+02
Cs131	2.0750E+02
Lu179	2.0510E+02
Sr85	1.3650E+02
Sn126	1.0600E+02
Sb126m	1.0600E+02
Fe59	9.3390E+01
Tm171	8.2010E+01
La135	7.7780E+01
Te121	7.4300E+01
Sb126n	7.1000E+01
Np240m	4.3010E+01
U240	4.2650E+01
Se79	3.9560E+01
Ta184	3.9460E+01
Pa233	3.6800E+01
Eu154	3.6340E+01
Ce137	3.4900E+01

Ce137m	3.1500E+01
Ag110m	2.8430E+01
Sb130	2.5850E+01
I125	1.5180E+01
Mn56	1.4710E+01
Tc97m	1.2770E+01
Hf181	1.2620E+01
Te121m	1.2360E+01
I129	1.2300E+01
Pa231	1.1780E+01
Sb118m	1.0660E+01

Noble gas isotopes were omitted from Table 5.3 because they will escape after the accident.

The nuclide inventory at 1 year after the excursion, is summarised in Table 5.4; the total activity is $A(1\,\mathrm{yr}) = 3.424\mathrm{E}9\ \mathrm{Bq}$. This value, $\frac{A(1\,yr)}{A_{\mathrm{pre}}}$, is still 3.93 times higher than the pre-accident activity of $A_{\mathrm{pre}} = 8.6989\mathrm{E}8\ \mathrm{Bq}$, but indicates that the excess activity introduced by the excursion, has largely decayed away after 1 year. As before, noble gas isotopes were omitted.

Table 5.4: Radionuclide inventory at 1 year after the excursion involving 10^{17} fissions.

Radionuclide	**Activity** (Bq)
Th231	7.6620E+08
U235	7.6620E+08
Pr144	5.5670E+08
Ce144	5.5660E+08
Nb95	3.4150E+08
Zr95	1.6100E+08
Pm147	1.4480E+08
Y91	9.4540E+07
U234	8.9470E+07
Cs137	4.9010E+07
Ru106	4.8370E+07
Rh106	4.8370E+07
Ba137m	4.6410E+07
Sr89	4.3930E+07
Y90	3.7240E+07
Sr90	3.7230E+07
Th234	1.3240E+07
Pa234m	1.3240E+07

Radionuclide	**Activity** (Bq)
U238	1.3240E+07
Ru103	8.6330E+06
Rh103m	8.5400E+06
Ce141	5.5570E+06
Pr144m	5.3150E+06
Sb125	3.8360E+06
Te127m	3.1670E+06
Te127	3.1020E+06
Eu155	2.0000E+06
Nb95m	1.8430E+06
Sm151	1.1760E+06
Eu151	1.1760E+06
U236	9.3800E+05
Te125m	9.2390E+05
Sn123	3.5760E+05
Te129m	3.1670E+05
Te129	1.9980E+05
Sn119m	1.1620E+05
Pa234	2.1190E+04
Pa231	1.6130E+04
Sn121m	1.3560E+04
Cd115m	1.3040E+04
Cs134	1.0810E+04
Sn121	1.0520E+04
Tc99	6.6980E+03
Cd113m	5.8310E+03
Sb124	4.4210E+03
Y89m	4.2350E+03
U235m	1.0360E+03
Pu239	1.0360E+03
Zr93	8.8680E+02
Th230	8.2210E+02
Cs135	6.8140E+02
Pr143	2.6480E+02
Ac227	2.5290E+02
Th227	2.1530E+02
Pb211	1.9860E+02
Bi211	1.9860E+02

Radionuclide	**Activity** (Bq)
Po215	1.9860E+02
Rn219	1.9860E+02
Ra223	1.9860E+02
Tl207	1.9800E+02
Ce139	1.2150E+02
Sn126	1.0600E+02
Sb126m	1.0600E+02
La140	1.0290E+02
Ba140	8.9430E+01
Sb126n	7.1000E+01
Tm171	6.4270E+01
Nb93m	4.3660E+01
Se79	3.9560E+01
Eu154	3.3530E+01
Y88	2.9490E+01
Te123m	2.7200E+01
I129	1.6080E+01
Sb126	1.4860E+01
Ag110m	1.0350E+01

There are two prominent radionuclides seen high up in Table 5.4, are ^{144}Pr (half-life below 18 minutes) and ^{137m}Ba (half-life below 3 minutes). These and many other short-lived radionuclides in Table 5.4 are continually produced by long-lived parent radionuclides such as $^{144}\mathrm{Ce}$ and $^{137}\mathrm{Cs}$.

The criticality excursion will produce a large ensemble of intense photon-emitting fission products. The $^{137}\mathrm{Cs}$ radionuclide, as mentioned above, is one of the significant contributor to photon radiation because of its relatively long half-life of 30 years and potential effects on human health. At any distance d from the point source of activity A and specific gamma-ray constant Γ, the dose-equivalent rate is mathematical given by equation (5.1)

$$\dot{D} = \frac{\Gamma \times A \times w_R}{d^2} \tag{5.1}$$

Where:

Γ = specific gamma-ray constant. For $^{137}\mathrm{Cs}$, $\Gamma = 0.33(\frac{\mathrm{Rm}^2}{\mathrm{Cihr}})$

A = the point source of activity in Curie (Ci)

d = distance from the point source in m^2

w_R = radiation weighting factor. For photons, $w_R = 1$.

The health physics, i.e., the radiation protection discipline alternatively uses traditional and international system of units (SI), therefore a conversion between traditional and SI units is, 1R (rem) = 0.01 sievert (Sv); and 1 Curie (Ci) = 37 $\times 10^9$ Bq.

If the entire process mass involved in the criticality event is simplified to an unshielded point source such as, ^{137}Cs – in order to obtain a qualitative measure of the dose rate without having to perform countless laborious transport calculations, the photon dose-rate at a reference distance of 1 m from the ^{137}Cs source, prior to the accident, would be $77.5\ \mu Sv/h$, which is quite low. Figure 5.3 shows the ratio between the post-accident unshielded photon dose-rate and the pre-accident unshielded dose-rate, as a function of time, up to 1 year after the excursion. The dose rate presented in Figure 5.3 is at 1 meter from the source term (criticality system) within the PUREX facility.

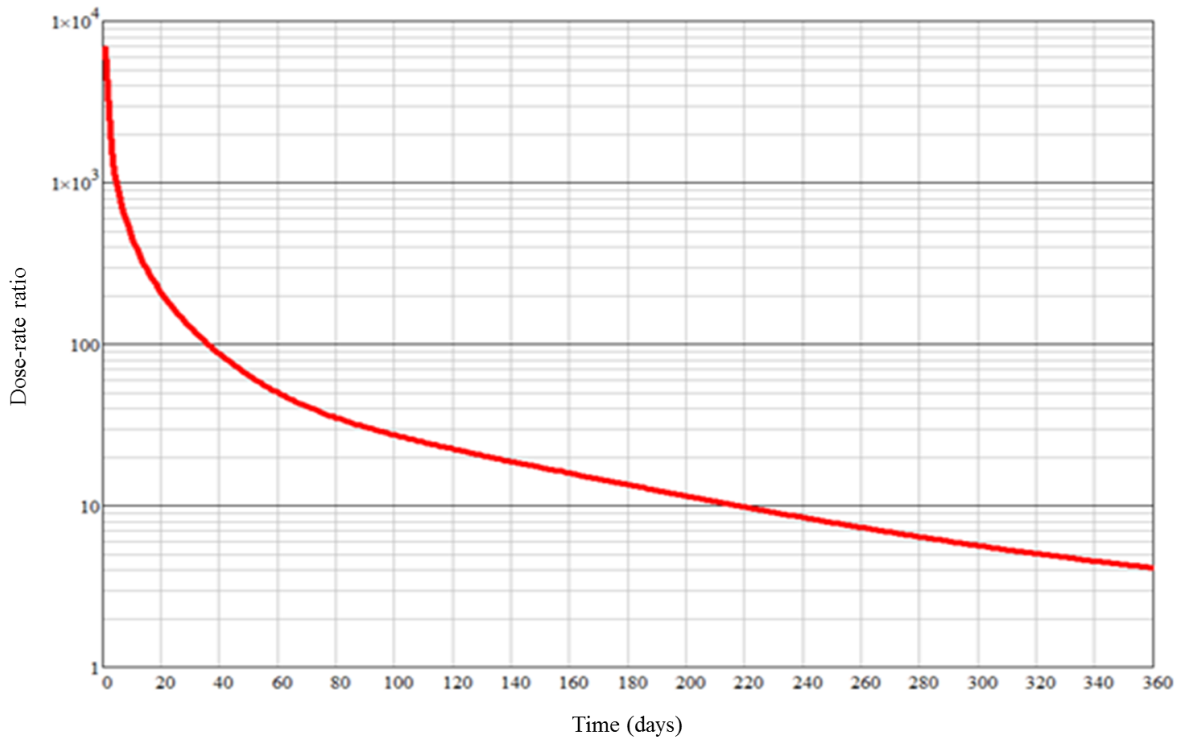

Figure 5.3: The ratio of the unshielded photon dose-rate after the criticality accident, to the unshielded photon dose-rate prior to the accident, as a function of elapsed time.

Figure 5.3 indicates that the unshielded photon dose-rate, in the immediate aftermath after the accident, will be almost 4 decimal orders of magnitude higher than the dose-rate prior to the excursion. Within 40 days, this $\frac{\text{post-accident}}{\text{pre-accident}}$ dose-rate ratio drops to a less dooming value around 100. At 220 days post-accident, the unshielded dose-rate is still 10 times higher than the pre-accident dose-rate. At $T_{\text{cool}} = 1\ \text{yr}$, the dose-rate is still around 4 times higher than the pre-accident radiation level. One can conclude that it will be beneficial to postpone clean-up operations and re-

commissioning of a facility that had suffered an excursion, to circa 1 year after the accident. If clean-up operations are performed in haste, unwarranted high radiation doses will be received.

5.3 Nuclide inventory and dose-rates produced by neutron activation during the excursion

The focus now shifts to radioactivity produced in SSC (structures, systems, and components) by neutron activation, which is by fission neutrons produced during the criticality excursion.

The engineering structure that will experience the highest neutron fluence Φ during the CA, is the wall of the process vessel in which the excursion happens. Assumption are made that this vessel is made from stainless steel 316L (SS-316L), and has a reference mass of 10 kg. An MCNP6.2 model of the fissile volume and its SS-316L vessel wall was executed, and the neutron spectrum tallied in the vessel wall was ported to the FISPACT-II calculation model. The integral fluence in the vessel wall calculated to $\Phi = 6.37\text{E}12\ \text{cm}^{-2}$. The first phase of the FISPACT-II calculation was to collapse TENDL-2019 (Koning *et al.,* 2019) neutron reaction cross-sections from 709 neutron energy groups, to a 1-group form. Next, FISPACT-II executed the main activation model. The total mass of SS-316L (which is 10 kg) as well as the mass-percentage of each element in SS-316L[25], was given as input, and is reproduced in Table 5.5.

Table 5.5: material composition of SS-316L, as specified in the FISPACT-II calculation model.

MASS	10.00	10
C	00.03	
N	00.10	
SI	00.70	
P	00.04	
S	00.03	
CR	17.00	
MN	01.80	
FE	64.40	
NI	13.00	
MO	02.90	

The calculated (N, A) matrix[26], produced by neutron activation, at $T_{cool} = 1\ \text{day}$ post-accident, is given in Table 5.6.

[25] An online engineering reference was consulted regarding the elemental composition of SS-316L. https://www.sandmeyersteel.com/images/316-316l-317l-spec-sheet.pdf

[26] (Nuclide, Activity) matrix.

Table 5.6: The calculated (Nuclide, Activity) matrix, produced by neutron activation, at a cooling time of 1 day after the criticality excursion.

Isotope	**Activity** (Bq)
Cr51	7.3510E+07
Mn56	6.4890E+07
Co58m	1.9690E+07
Mo99	5.5970E+06
Tc99m	4.9760E+06
Co58	1.9090E+06
Fe55	1.5560E+06
Fe59	9.4750E+05
Ni65	3.9160E+05
P32	1.8150E+05
Mn54	1.5120E+05
Ni63	3.2450E+04
Nb92m	2.5710E+04
Si31	1.9990E+04
Ni57	3.3680E+03
Co57	2.1150E+03
S35	1.1410E+03
Zr89	6.5480E+02
Co60	6.5420E+02
Y89m	6.5410E+02
Nb96	6.4140E+02
Nb95m	5.3570E+02
Nb95	2.6020E+02
Ni59	2.5140E+02
P33	1.5130E+02
Nb91m	9.5650E+01
V49	6.5300E+01
C14	6.3530E+01
Co61	3.4210E+01
Nb97	2.5790E+01
Zr97	2.3900E+01
Nb97m	2.2740E+01
Zr95	2.2430E+01
H3	1.3610E+01
Mo93m	1.0760E+01
Mo93	3.7900E+00

The calculated (N, A) matrix, produced by neutron activation, at $T_{cool} = 1\ \text{year}$ post-accident, is given in Table 5.7.

Table 5.7: The calculated (Nuclide, Activity) matrix, produced by neutron activation, at a cooling time of 1 year after the criticality excursion.

Isotope	*Activity (Bq)*
Fe55	1.2098E+06
Mn54	6.7375E+04
Co58	5.7273E+04
Ni63	3.2234E+04
Cr51	8.1418E+03
Fe59	3.2655E+03
Co57	8.4314E+02
Co60	5.7387E+02
Ni59	2.5140E+02
S35	6.3850E+01
C14	6.3523E+01
V49	3.0398E+01
H3	1.2866E+01
Mo93	3.7892E+00
Nb91m	1.5143E+00
Nb95	1.1601E+00

Of important to note, the several nuclides in Table 5.7 — principally ^{55}Fe, ^{63}Ni, ^{59}Ni, ^{14}C and ^{3}H — do not emit high-energy penetrating γ-photons.

Figure 5.4 displays the total activity of radionuclides produced by activation, as a function of time, over the 1st year after the $\text{CA}(10^{17}\text{f})$ excursion.

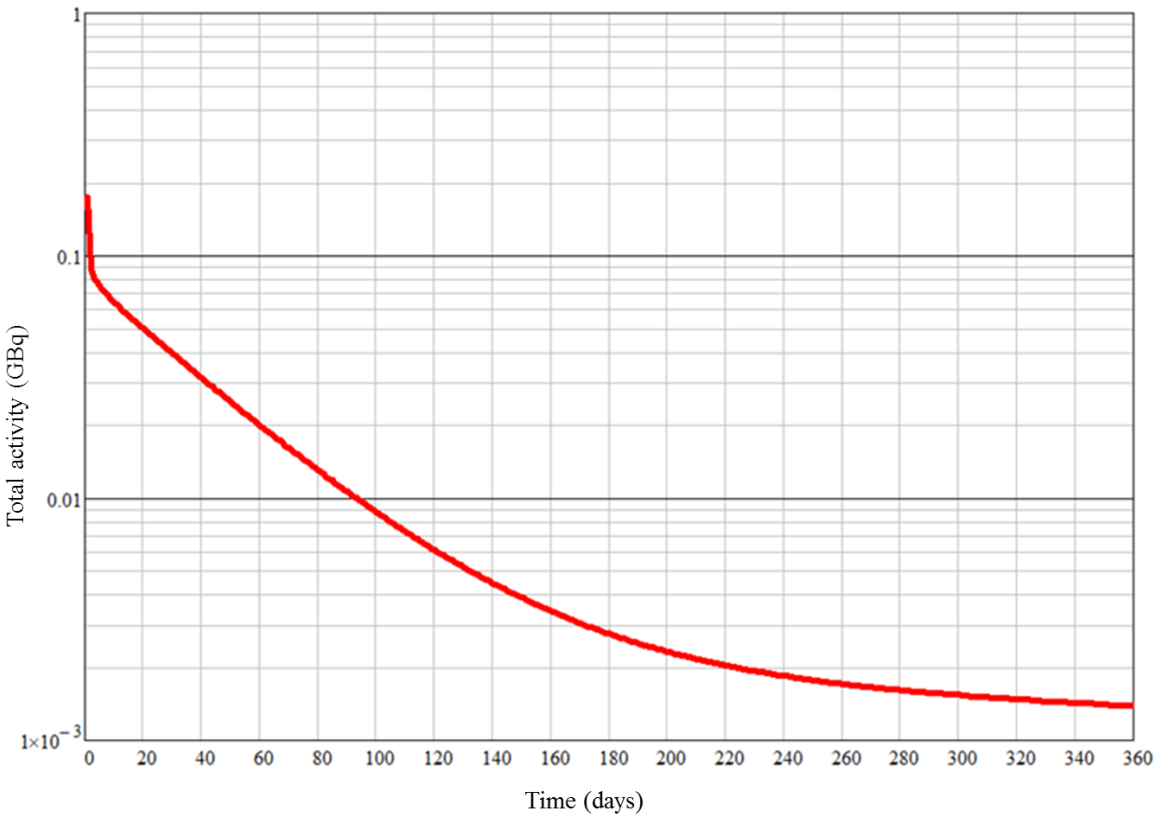

Figure 5.4: Total activity $A_{act}(t)$ of radionuclides produced by neutron activation in the SS-316L vessel containing the fissile material, as a function of time, over the 1st year after the CA(10^{17} f) excursion.

For proper perspective, it is necessary to graphically presents the ratio $\frac{\mathrm{A_{act}(t)}}{\text{Activity present before excursion}}$. The activity present before the excursion, was contributed by the activity of the uranium isotopes present in the fissile mass. The pre-excursion activity is $\boxed{8.70\mathrm{E}8\ \mathrm{Bq}}$. The above ratio is shown in Figure 5.5.

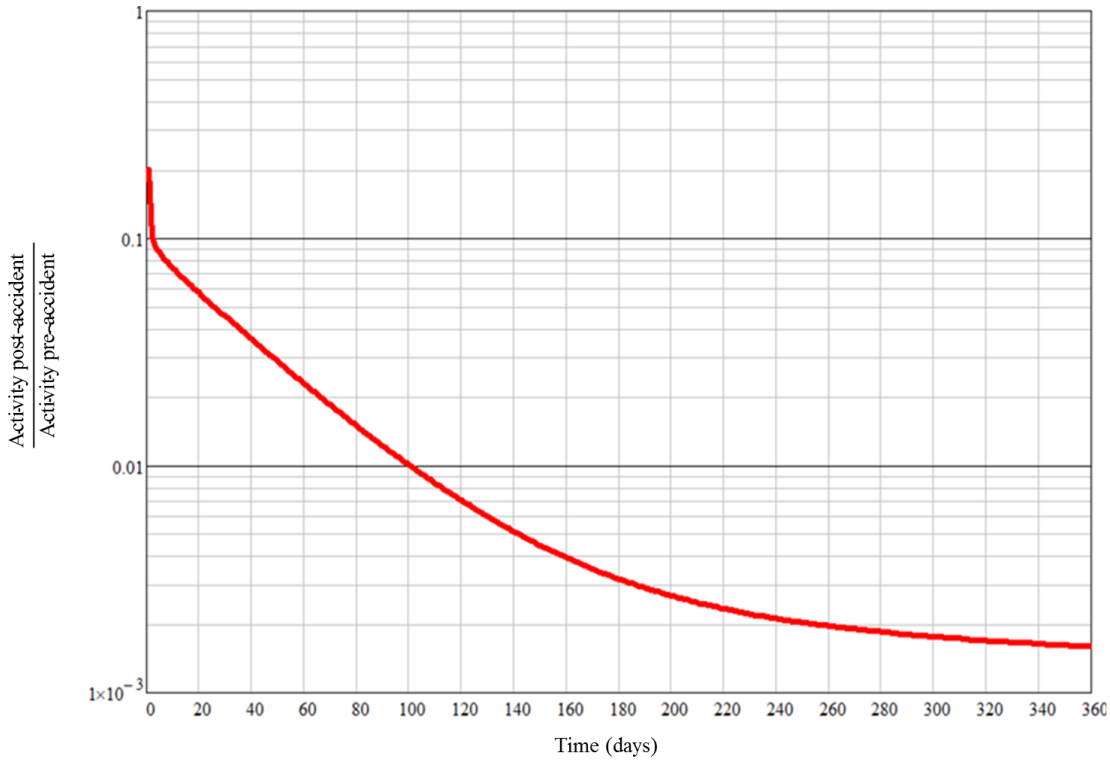

Figure 5.5: The ratio between activity induced via neutron activation, and the activity of the uranium isotopes present before the excursion.

Figure 5.5 immediately shows that the activation source term is negligible — it is completely dwarfed by the activity of the initially present uranium isotopes, and will also be completely swamped by the activity of fission products formed during the excursion. FISPACT calculations also showed that the dose-rate from the activation source term will be approximately $1\ \mu\mathrm{Sv/h}$ at 1 day after the excursion, and will reach the natural background dose-rate level of approximately $0.1\ \mu\mathrm{Sv/h}$ after 150 days post-accident. Dose-rates in this range are of no safety concern.

The dose rates mentioned above were calculated using a built-in mathematical function in FISPACT, the mathematical function is presented in equation (5.2).

$$\dot{D} = \sum_i \sum_g \frac{\Re_\gamma(E_g) A_i Y_{i,g}}{4\pi r^2} \tag{5.2}$$

Where

$\dot{D}$ = the dose rate

$\Re_\gamma(E_g)$ = the fluence-rate to dose-rate response function

A_i = the activity of nuclide i

$Y_{i,g}$ = the emission yield of photon number g emitted by radioisotope i

$r = 1\,m$ = the distance from the point source where all the radioactivity is assumed to be concentrated

Conclusion remarks

Neutron activation will be the least of concerns following a criticality excursion. The neutron activation source term produced in process vessels and concrete walls in the facility will be very low and will drop below the natural background dose rate within less than 6 months.

Maodi (2020) performed a systematic review of the neutron activation of all non-gaseous elements in the Periodic Table, for atomic numbers in the domain $Z \in [1; 83]$. For the timescales at stake in a NCA, the top-activator chemical elements are arranged in Table 5.8 — the chemical elements are read from left hand side to right hand side column.

Table 5.8: Most problematic neutron activator chemical elements, for a criticality accident, arranged from most to least dose-contributing.

Chemical elements		
Ir	Rb	Cd
Sc	In	**Mo**
Eu	Ge	Ti
Tb	Re	Tl
Ta	Nd	Nb
Co	Te	Br
Cs	**Ni**	Er
Sb	**Zn**	Ar
Ag	Sm	As
Hf	**Zr**	Rh
Yb	**Fe**	Y
Lu	Ba	**Ca**
Os	Sr	**Mn**
Au	Sn	**Cu**
Ru	W	Ga
Tm	La	**Na**
Ce	Pd	Pr
Se	K	Bi
Hg	Dy	V
Gd	Ho	Te
Cr	Pt	

Noteworthy chemical elements that may be found in stainless steel, lead bricks concrete and electrical wiring, are highlighted red in Table 5.8. SS-316L contains Fe, Cr, Ni, Mn, Mo, that is, it will be a fairly high activator. In other words, if the activation of SS-316L is negligible, practically all other materials will also be found to undergo negligible neutron activation during a criticality excursion.

6 Conclusions

This study focused on a hypothetical nuclear criticality excursion in a PUREX processing facility for the recovery of non-irradiated enriched uranium, which are present in scrap material from historical operations. The entire facility, including the fissile process-mass there the hypothetical excursion takes place, the concrete biological shielding walls, and roof, was modelled in a series of calculation models for the execution of the radiation transport code, MCNP6.2. ENDF/B-8.0 nuclear data (Brown *et al., 2018*; Conlin *et al.,* 2018) was used, and special thermal treatment of scattering kinetics was requested wherever possible, to accurately quantify the impact of the bound state of nuclides, on the thermal neutron energy spectrum. The calculation models were developed to quantify the neutron and photon doses at a number of "human detector" positions places inside and around the PUREX facility, resulting from the criticality excursion. The design basis criticality accident is an excursion involving 10^{17} fission events, which is denoted as a $\mathrm{CA}(10^{17}\mathrm{f})$ accident.

The calculation model of a "naïve", baseline facility design was used to quantify the neutron and photon doses in the baseline facility design. This design was denoted as "modification zero" or MOD0. The conclusion was that the baseline design carries an unacceptable radiological risk — a nuclear criticality excursion inside this baseline facility design was able to typically kill every person within a circa 10 m radius from the epicentre of the fissile process mass where the excursion takes place, and also lead to acute radiation syndrome and a substantially elevated cancer risk in all survivors. This baseline design was unable to contain the pulse of ionising radiation, because there was a lack of partitioning shielding walls inside the facility. Radiation therefore streamed freely between processing workstations. Step-by-step facility design modifications, denoted as MOD1, MOD2, unti MOD6, were then introduced in order to arrive at a significantly safer facility design, from a personnel exposure perspective. The goal of the stepwise improvements was to compartmentalise the facility into well shielded cubicles, with a shielding wall geometry and thickness able to localise the lethal dose to a single workstation compartment/cubicle, whilst maintaining the doses in all other compartments near or below the ICRP's recommended annual dose limit of 20 mSv for occupational exposure, which is a factor 50 times below the threshold dose of 1000 mSv for the onset of acute radiation syndrome. It is practically unavoidable that the person(s) in the cubicle where the excursion takes place, will receive a lethal dose, that is to say, the aim of the improvements was to ensure that staff in adjacent workstations, the control room, workshop, and ablution facilities, as well as persons outside the main processing hall, at a position directly opposite the fissile volume hosting the excursion, would receive effective doses at or below the annual dose limit for normal occupational exposure. The analysis also showed that all the inner partitioning walls must reach all the way to the roof; if this is not done, a significant amount of streaming from the accident cubicle to adjacent cubicles, was observed. This shielding design methodology that proved fruitful and ultimately

successful, can be called the radiological de-coupling of process workstations from each other, via an improved placement of inner partitioning concrete walls of adequate thickness and height. The shielded workstations are designed so that the radiation from a criticality excursion is contained and confined to the accident workstation; lethality is localised and the PUREX plant is rescued from being "one large coffin".

In the final design of the facility, the highest effective dose recorded in passages and workstation cubicles adjacent to the accident cubicle, ranged from a minimum of 1 mSv to a maximum of 50 mSv, this means, the design modifications to achieve radiological decoupling of sub-spaces, via an improved design of partitioning walls, was successful. In the control room, workshop and ablution cubicle, doses were well below 20 mSv — the present dose limit on effective dose for radiation workers. The dose on top of the concrete roof, directly overhead the vessel hosting the postulated $\mathrm{CA}(10^{17}\mathrm{f})$ excursion, was just below 40 mSv; this is considered acceptable because the human occupancy factor on the roof is essentially zero. The above radiological compartmentalisation was achieved with ordinary concrete shielding walls, this being the cheapest possible concrete, with which structural engineers and building contractors are also most familiar.

The next step was to quantify the inventory of fission products produced in the 10^{17} fission events. The neutron fluence spectrum as well as the integral neutron fluence inside the fissile process mass, were ported to the code FISPACT-II 3.00 to calculate the inventory of radioactive fission products produced by the excursion; the latter code was executed using TENDL-2019 nuclear data (Koning *et al.*, 2019).

As a last step, the inventory of radioisotopes products produced by neutron activation by the $\mathrm{CA}(2.5 \times 10^{17}\mathrm{n})$ excursion, was calculated. The neutron fluence-rate spectrum $\varphi_n(E)$ as well as the integral neutron fluence-rate $\varphi_n = \int_0^\infty \varphi_n(E)\, dE$ inside the stainless-steel vessel containing the fissile process mass, were calculated, and ported to FISPACT-II, to calculate the inventory of radioactive isotopes that would be produced in the SS-316L alloy by neutron activation. As before, FISPACT-II was executed with TENDL-2019 nuclear data. Results showed that the activities of, and dose-rates from, fission products will completely dominate the neutron activation source-term. It is also shown that the facility may have to be sealed off for as long as 1 year before decontamination and either decommissioning or re-commissioning work should commence. If human entry is allowed before $T_{\mathrm{cool}} \approx 1\ \mathrm{yr}$, an unnecessarily high dose will be received by the decontamination crew.

If the MOD6 design for the PUREX facility is approved and constructed, workers will work in a facility where a severe criticality accident will be confined and isolated in only on workstation. At all other workstations, doses are easily survivable. This knowledge may improve worker confidence and lower the overall work-stress.

The quantification of doses for the design-basis accident, $\mathrm{CA(MOD6, 10^{17}f)}$, enables a better conformance to a variety of laws or Acts pertinent to nuclear industries — not only the 1999 *Nuclear Energy Act*[27] and the 1999 *National Nuclear Regulator Act*[28], but also the Occupational Health and Safety Act ("OHS Act") 85 of 1993, which requires that workplace hazards be accurately communicated to workers. Article 13(a) of the latter act states the *Duty to Inform* in the following terms: "The employer must make every employee conversant with any health and safety hazards attached to work, production, processing, handling, storing, transporting, and with precautionary measures."

A corollary (associated truth) of this investigation is that the local nuclear sector will struggle to survive the social and political trauma posed by a nuclear criticality accident, and that it is therefore imperative to prevent such events by designing systems, structures, and components as well as administrative processes so that the probability of criticality accidents is driven to practically zero.

[27] Nuclear Energy Act 46 of 1999.

[28] National Nuclear Regulator Act 47 of 1999.

Appendix A

A.1 How the code MCNP is used to calculate the effective neutron multiplication factor, k_{eff}, of a system containing fissile material

The first step in the use of the code MCNP6.2 to calculate the value of k_{eff} of a system containing fissile and fissionable material, is to specify the geometry and material composition of the system to high accuracy, in an MCNP ***calculation model.*** The code needs to know the spatial location of matter in space, which can be expresses mathematically as $N_i(\vec{\boldsymbol{x}})$, where N_i denotes the number density of nuclide i as a function of the spatial vector $\vec{\boldsymbol{x}}$. The need to specify $N_i(\vec{\boldsymbol{x}})$ is seen by referring to the Boltzmann transport equation (BTE). A key function of the calculation model is to specify the spatial distribution of matter, to the radiation transport code.

It must be stressed that a Monte Carlo code such as MCNP does not "solve" the BTE numerically, but rather models the stochastics of the very physical processes that led to the derivation of the mathematical formulation of the BTE. This "equivalence" between a stochastic code and the BTE, means that one can use the mathematical form of the BTE to conceptualise Monte Carlo simulation codes, specifically their user-input specifications.

In operator notation, the time-independent or steady-state Boltzmann transport equation, which is an integro-differential equation, may be written as

$$\mathbb{B}\psi = Q$$

where the linear Boltzmann transport operator (BTO) is, in its simplest form,

$$\mathbb{B} \equiv \vec{\boldsymbol{\nabla}} \cdot \hat{\boldsymbol{\Omega}} + \mu_t(\vec{\boldsymbol{x}}, E) - \int_0^\infty dE' \int_{\hat{\boldsymbol{\Omega}}} d\hat{\boldsymbol{\Omega}}\, \mu_s(\vec{\boldsymbol{x}}, E' \to E, \hat{\boldsymbol{\Omega}}' \to \hat{\boldsymbol{\Omega}})$$

The function Q is known as the source-term of the BTE[29]. If there are non-zero terms in Q that are independent of the solution, ψ, of the BTE, then $\mathbb{B}\psi = Q$ is an inhomogeneous operator equation, with the source-term Q "driving" the system. In the BTO, $\hat{\boldsymbol{\Omega}}$ denotes the direction of movement of a radiation particle, μ is the linear interaction coefficient, μ_t is the total linear interaction coefficient, μ_s is the linear interaction coefficient for scattering transfer, $\vec{\boldsymbol{x}}$ is the spatial position of the particle and E its energy. More information about the BTE and its interpretation can be found in Henry (1975).

[29] Note by co-supervisor TJvR: The symbol Q was used by German-speakers such as Boltzmann, in an age when German was still the pre-eminent language of physics, because the German word for source is *Quelle.* This word is related to the Latin term for water, aqua, which in turn derives from a Semitic root, QaW, (pronounced as "qau") for a gathering of water. Words such as quality and equality originated from "aquality", i.e., water-like behaviour, namely being gravitationally self-gathering and self-levelling.

The source-term of the BTE can be expanded into two terms: a so-called "fixed source" term, which is independent of the directional fluence-rate of neutrons, ψ, and a fission source, which does depend on ψ:

$$Q(\vec{\boldsymbol{x}}, E, \hat{\boldsymbol{\Omega}}) = Q_{\text{fixed}}(\vec{\boldsymbol{x}}, E, \hat{\boldsymbol{\Omega}}) + Q_{\text{fission}}(\vec{\boldsymbol{x}}, E, \hat{\boldsymbol{\Omega}})$$

where

$$Q_{\text{fission}}(\vec{\boldsymbol{x}}, E, \hat{\boldsymbol{\Omega}}) = \frac{\chi(E)}{4\pi} \int_0^\infty dE' \int_{4\pi} d\hat{\boldsymbol{\Omega}}\, \nu(E')\, \mu_f(\vec{\boldsymbol{x}}, E')\, \psi(\vec{\boldsymbol{x}}, E', \hat{\boldsymbol{\Omega}})$$

Here $\chi(E)$ is the energy spectrum with which fission neutrons are emitted, μ_f the linear interaction coefficient (alias "macroscopic cross-section" for fission, ψ the angular neutron fluence-rate, $\vec{\boldsymbol{x}}$ the spatial variables, E the energy and $\hat{\boldsymbol{\Omega}}$ the unit-vector in the direction of movement of the particle, and ν the (energy dependent) multiplicity or yield of fission neutrons.

For real-life radiation sources and material configurations, the BTE, $\boxed{\mathbb{B}\psi = Q}$ has to be solved by computer codes running on powerful digital computers. The user develops a *calculation model,* which serves as user-input to the code. The code reads the *calculation model*, which is an ASCII text file containing many keywords and numbers, in which the user specifies the identities and spatial positions of materials (most generally: isotopes) and fixed sources as well as tallies, i.e. the quantities to be calculated.

The nuclear cross-section data used by MCNP6.2 (LANL, 2018) spans many Gigabytes (GBs) of nuclear data files, which are either shipped with the code or downloaded by the user and then made available to the code by editing the code's XSDIR ("cross-section directory") file[30], which resides in the DATA folder.

An important concept in understanding the input to MCNP, is that several terms in the BTE contain linear interaction coefficients μ, also known as "macroscopic cross-sections" Σ. The linear interaction coefficient μ is defined as

$$\mu(\vec{\boldsymbol{x}}, E) = \sum_i N_i(\vec{\boldsymbol{x}})\sigma_i(E)$$

where $N_i(\vec{\boldsymbol{x}})$ denotes the number-density of nuclide i as a function of the spatial vector $\vec{\boldsymbol{x}}$, and $\sigma_i(E)$ is the energy-dependent cross-section or "microscopic cross-section" of nuclide i. The bottom-line is that (1) values of $\sigma_i(E)$ are read from extensive nuclear data compilations available to the code,

[30] Note by co-supervisor, TJvR: For quality management purposes, the addition of cross-sections and attendant editing of the XSDIR file is typically only done by or under the guidance of the code's custodian(s) in an organisation.

as an automatic background process, whereas (2) the user has to explicitly specify $N_i(\vec{x})$, i.e., the spatial positions of different materials. Typically, up to 90% of an MCNP calculation model deals with the user's specification of the identities i and the 3D spatial location $N_i(\vec{x})$ of all nuclides i, within the system of interest. The specification of $N_i(\vec{x})$ is spread over all three subdivisions of an MCNP6.2 calculation model — the surface cards[31], cell cards and the material cards.

Instead of attempting to solve the full, time-dependent form of the BTE, a criticality calculation with MCNP6 conceptually uses the steady-state BTE. (This is a practical necessity, because the code MCNP typically executes at least 10 decimal orders of magnitude slower than real-time.) The material system is bombarded with a starting-spectrum of "starter" neutrons, which then cause fissions to occur. By using an eigenvalue formalism, the code determines whether the neutron population grows or shrinks with succeeding cycles or generations, and calculates k_{eff} as a ratio between the neutron population in successive generations. The statistical average of the ratio

$$\frac{\text{number of neutrons in generation N} + 1}{\text{number of neutrons in generation N}}$$

over, e.g., 1000 cycles of 1E6 source-neutrons per cycle, is taken as the value for k_{eff}. The code also attempts to calculate an estimate for the relative standard error in k_{eff}, but in the case of MCNP6, this purely statistical quantity is known to underpredict the true uncertainty in k_{eff}, by a factor of roughly 5 to 10 (Blomquist, 2006; Brown, 2009; Yamamoto and Miyoshi, 2004). In the case of nuclear criticality safety calculations, the international best practice is, furthermore, to specify the 2σ uncertainty (i.e., the 95% confidence interval) and not merely the 1σ uncertainty (i.e., the 68% confidence interval) (IAEA, 2014). Let σ_{true} denote the real relative uncertainty in the quantification of the value of k_{eff} and let σ_{MCNP6} be the relative uncertainty, i.e., 1σ standard deviation of k_{eff}, reported by an MCNP6 calculation. Because $\sigma_{\text{true}} \approx 10\sigma_{\text{MCNP6}}$, the operational norm is therefore to write criticality-related safety reports according to the principle that the values of k_{eff} reported to the management of a nuclear facility such as, e.g., a PUREX plant, is not merely the k_{eff} value(s) obtained from the output of an MCNP run, but rather the value

$$k_{\text{eff}} + (2 \times 10)\sigma = k_{\text{eff}} + 20\sigma.$$

For a processing plant that has to be maintained in a subcritical state under all conditions, this conservative reporting practice strives to eliminate misunderstandings and misinterpretations. In practice, then, the quantity that must always be safely below the upper limit of 0.95, is not the k_{eff} value reported by the MCNP calculation, but rather $\boxed{k_{\text{eff}} + 20\sigma}$. A corollary (i.e., an associated,

[31] Note by co-supervisor, TJvR: Technically, the surface cards are the second part of an MCNP input, yet they have to be developed first, because the cell-cards (section 1 of an MCNP input) are entirely dependent of the surface definitions.

dependent truth) is that MCNP criticality safety calculations have to be run with enough cycles and neutrons per cycle, to yield low values of σ. Values of $\sigma_{\text{MCNP6}} \approx 0.1\%$ will produce $\sigma_{\text{true}} \approx 2\%$ which is acceptable (LANL advises that the relative standard deviation must be below 5%)[32].

We now return to the Boltzmann transport operator, in order to ascertain what input the user has to specify to the code MCNP.

1. The term $\boxed{\vec{\nabla} \cdot \hat{\Omega}}$ is known as the ballistic term or streaming term in the BTE; it represents the laws of the transport of radiation in the absence of matter (i.e., in a classical vacuum) and requires no user-input.

2. The term $\boxed{\mu_t(\vec{x}, E)}$ is known as the outscattering term in the BTE; the variable μ_t represents a sum over all nuclides, $N_i(\vec{x})$ in the 3D spatial system, i.e., the user has to specify the identity i and 3D spatial position of every nuclide in the system. (The energy-dependence of the cross-sections is read from the circa 40+ GByte of nuclear data that ships with MCNP6, but this is an automated background process). The physical interpretation of this term is that *any* (hence the total cross-section) interaction at spatial position $\vec{x}$ will remove a neutron travelling in the infinitesimally small cone of directions $d\hat{\Omega}$ around $\hat{\Omega}$**,** and in the infinitesimally small energy-band dE around E, to a direction of travel and an energy outside this domain of phase-space.

3. The term $\mu_s(\vec{x}, E' \to E, \hat{\Omega}' \to \hat{\Omega})$ is known as the inscattering integral of the BTE; it is also a linear interaction coefficient (i.e. a macroscopic cross-section), and therefore requires exactly the same user-supplied information as necessitated by the total linear interaction coefficient term, μ_t, as discussed above — namely the specification of $N_i(\vec{x})$ where N_i is the number density of every isotope of interest, inside the spatial volume of interest, i.e., the spatial "radiation transport theatre". This term deals with the ability of matter to scatter neutrons moving in other directions, and having other energies, into the infinitesimally small cone of directions $d\hat{\Omega}$ around $\hat{\Omega}$**,** and into the infinitesimally small energy-band dE around E, at the infinitesimally small spatial cell $d\vec{x}$ around $\vec{x}$.

4. The term $\boxed{Q_{\text{fixed}}(\vec{x}, E, \hat{\Omega})}$ requires the user to specify the spatial location (variable: $\vec{x}$), energy spectrum (variable: E) and directionality (variable: $\hat{\Omega}$) of all "fixed sources", i.e., sources that do not depend on the fluence-rate.

---

[32] Note by co-supervisor TJvR: At present (2020) the goal of reaching $\sigma_{\text{MCNP6}} \leq 0.1\%$ within the timespan of overnight MCNP simulations, requires the use of workstation class computers with multi-core processors, ideally having core-counts of at least 32.

5. The fission source term, $\boxed{Q_{\text{fission}}(\vec{\boldsymbol{x}}, E', \hat{\boldsymbol{\Omega}})}$ contains yet another linear interaction coefficient, $\mu_f(\vec{\boldsymbol{x}}, E)$, which, in principle, requires the user to specify the spatial location $N_i(\vec{\boldsymbol{x}})$ of all fissile and fissionable material in the physical system; information such as the energy-dependence of fission cross-sections σ_f and fission neutron yields ν, are read from the code's multi-GB database of nuclear data, i.e., the user does not need to supply this. During a stochastic simulation of radiation transport, the identity and energy spectrum of emitted fission neutrons, will be sampled from linear interaction coefficients functions of the form $\mu(E)$; the code performs this in an automated fashion.

Conclusive remarks

By analysing the Boltzmann Transport Equation (BTE) it becomes clear that, in an MCNP6 calculation model, the identities and spatial locations $N_i(\vec{\boldsymbol{x}})$ of all nuclides i, as well as the spatial placement, energy spectrum and angular emission characteristics of all fixed sources $Q_{\text{fixed}}(\vec{\boldsymbol{x}}, E, \hat{\boldsymbol{\Omega}})$ have to be defined. The balance of a typical MCNP input is composed of tally definitions (i.e., output requests) along with a handful of "housekeeping" cards.

The above discussion has now presented the background needed to interpret a simple MCNP6 calculation model for the calculation of the k_{eff} of a sphere of HEU_{50} surrounded by water. The calculation model is reproduced in Table *A-1*.

Table A-1: Calculation model to determine the k_{eff} of a metallic sphere of HEU_{50} in air.

```
Metallic sphere of 50% U-235 and 50% U-238
c CELL CARDS
1  1   -19.10    -1        IMP:N=1   $ HEU50
2  2   -1.2E-3   -2  +1    IMP:N=1   $ Air
3  0                +2    IMP:N=0   $ External Void = UmWelt
c ====================================================================

c ====================================================================
c Surface cards
1 SPH     0   0    0         +12.2   $ HEU50 Sphere
2 SPH     0   0    0        +500.0   $ Surrounding medium
c ====================================================================

c ====================================================================
c Data Cards
MODE  N
c
SDEF   POS   = 0  0  0
       PAR   = N
       ERG   = D4
       X     = D1
       Y     = D2
       Z     = D3
       CELL  = 1
       EFF   = 0.001
```

```
c
c
#       SI4       SP4
        L         D
        1E-9      0.20
        1E-6      0.20
        0.001     0.20
        0.1       0.20
        3.0       0.20
c
SI1  H    -10   +10
SP1  D  0     1
c
c
SI2  H    -10   +10
SP2  D  0     1
c
c
SI3  H    -10   +10
SP3  D  0     1
c
c
c Material definitions:
M1    92235  -50                $ U-235
      92238  -50                $ U-238
c
c
c Air with 1% water (Neutron Transport Runs):
M2      1001     -0.00111967185672092
        1002     -3.58077068509439e-007
        2003     -7.01300681482183e-013
        2004     -6.93002257732448e-007
        6000     -1.269899924930E-04
        7014     -0.744226018468389
        7015     -0.00293093736342699
        8016     -0.238274132603651
        8017     -6.338532733037E-04
        10020    -1.188009929771E-05
        18036    -3.8063224269139e-005
        18038    -7.57346759599989e-006
        18040    -0.0126264625590237
        36078    -9.80896820559013e-009
        36080    -6.47380864579173e-008
        36082    -3.3656973211545e-007
        36083    -3.37936500433013e-007
        36084    -1.69483116165613e-006
        36086    -5.26125375559769e-007
        54124    -3.55783232684075e-010
        54126    -3.37976986796745e-010
        54128    -7.36915932270391e-009
        54129    -1.02645376834607e-007
        54130    -1.59506563063874e-008
        54131    -8.38324527235628e-008
        54132    -1.07054801524348e-007
        54134    -4.21479276142738e-008
        54136    -3.63078420449797e-008
MT2     H-H2O.80T
c
c
c Pure Water:
```

```
M3    1001      +1.99976      $ H-1  in H2O
      1002      +0.00024      $ H-2  in H2O
      8016      +0.99757      $ O-16 in H2O
      8017      +0.00243      $ O-17 in H2O
MT3   H-H2O.80T
c
c
KCODE  1E5  2.2   50   100   20E5
c ======================================================================
```

The surface cards

```
c Surface cards
1 SPH     0   0    0         +12.2   $ HEU50 Sphere
2 SPH     0   0    0        +500.0   $ Surrounding medium
```

specify two spheres; sphere 1 has a radius of 12.2 cm, while sphere 2 has a radius of 500 cm.

The cell cards

```
1  1   -19.10    -1        IMP:N=1   $ HEU50
2  2   -1.2E-3   -2  +1    IMP:N=1   $ Air
3  0                +2    IMP:N=0   $ External Void = UmWelt
```

refer to the surface cards as well as to the material cards

```
c Material definitions:
M1    92235  -50                $ U-235
      92238  -50                $ U-238
c
c
c Air with 1% water (Neutron Transport Runs):
M2     1001     -0.00111967185672092
       1002     -3.58077068509439e-007
       2003     -7.01300681482183e-013
       2004     -6.93002257732448e-007
       6000     -1.269899924930E-04
       7014     -0.744226018468389
       7015     -0.00293093736342699
       8016     -0.238274132603651
       8017     -6.338532733037E-04
       10020    -1.188009929771E-05
       18036    -3.8063224269139e-005
       18038    -7.57346759599989e-006
       18040    -0.0126264625590237
       36078    -9.80896820559013e-009
       36080    -6.47380864579173e-008
       36082    -3.3656973211545e-007
       36083    -3.37936500433013e-007
       36084    -1.69483116165613e-006
       36086    -5.26125375559769e-007
       54124    -3.55783232684075e-010
       54126    -3.37976986796745e-010
       54128    -7.36915932270391e-009
       54129    -1.02645376834607e-007
       54130    -1.59506563063874e-008
       54131    -8.38324527235628e-008
       54132    -1.07054801524348e-007
```

```
        54134    -4.21479276142738e-008
        54136    -3.63078420449797e-008
MT2     H-H2O.80T
c
```

Cell card 1,

```
1  1   -19.10    -1        IMP:N=1   $ HEU50
```

states that cell 1 contains material 1, i.e., metallic HEU_{50}. The mass-density of material 1 is $19.1\ \mathrm{g\ cm^{-3}}$; all space inside surface 1, i.e., the sphere with radius 12.2 cm, is filled with HEU_{50}. The importance of neutron transport in this cell is 1.

Cell card 2,

```
2  2   -1.2E-3   -2  +1    IMP:N=1   $ Water
```

states that cell 2 contains material 2, i.e., the material specified in material card m2, i.e., air. The mass-density of material 2 (air) is $1.2 \times 10^{-3}\ \mathrm{g\ cm^{-3}}$; the intersection of all space that is inside surface 2 but outside surface 1, is filled with air. The importance of neutron transport in cell 2 is 1.

The specification of the isotopic composition of materials to MCNP as in

```
c Air with 1% water (Neutron Transport Runs):
M2      1001     -0.00111967185672092
        1002     -3.58077068509439e-007
        2003     -7.01300681482183e-013
        2004     -6.93002257732448e-007
        6000     -1.269899924930E-04
        7014     -0.744226018468389
        7015     -0.00293093736342699
        8016     -0.238274132603651
        8017     -6.338532733037E-04
        10020    -1.188009929771E-05
        18036    -3.8063224269139e-005
        18038    -7.57346759599989e-006
        18040    -0.0126264625590237
        36078    -9.80896820559013e-009
        36080    -6.47380864579173e-008
        36082    -3.3656973211545e-007
        36083    -3.37936500433013e-007
        36084    -1.69483116165613e-006
        36086    -5.26125375559769e-007
        54124    -3.55783232684075e-010
        54126    -3.37976986796745e-010
        54128    -7.36915932270391e-009
        54129    -1.02645376834607e-007
        54130    -1.59506563063874e-008
        54131    -8.38324527235628e-008
        54132    -1.07054801524348e-007
        54134    -4.21479276142738e-008
        54136    -3.63078420449797e-008
MT2     H-H2O.80T
```

uses ZAID, i.e., ZA-ID identifiers of isotopes/nuclides. A "regular" ZAID is $\boxed{ZAID = 1000Z + A}$, i.e., ${}^{2}_{1}\mathrm{H}$ is, for example, specified as $\boxed{1000 \times 1 + 2 = 1002}$ while ${}^{235}_{92}\mathrm{U}$ is, for example, specified as $\boxed{1000 \times 92 + 235 = 92235}$. The negative number following the ZAID is the mass-fraction or mass-percentage of the isotope (Z, A) in the material; a positive number would denote a number-of-atoms fraction.

A utility code, ELIS_APP (Van Rooyen, 2018), was used to convert elemental chemical compositions to detailed isotopic compositions, for materials with unperturbed, natural terrestrial isotopic abundances. The code ELIS_APP reads the NUBASE-2016 database of isotopic masses (Audi *et al.*, 2017) as well as IUPAC's 2016 database of the present natural isotopic abundances of terrestrial elements (Meija *et al.,* 2016). The composition for material 2 is copied from the output of the code ELIS_APP ("EL$_{\text{ement}}$ to IS$_{\text{otope}}$") and pasted into the MCNP calculation model.

Next, we consider the statement $\boxed{\text{MODE N}}$ at the start of the data card section of the MCNP calculation model. This simply means that only neutron transport is considered in the model.

The starting neutron source is specified as follows:

```
SDEF   POS   = 0  0  0
       PAR   = N
       ERG   = D4
       X     = D1
       Y     = D2
       Z     = D3
       CELL  = 1
       EFF   = 0.001
c
c
#      SI4       SP4
       L         D
       1E-9      0.20
       1E-6      0.20
       0.001     0.20
       0.1       0.20
       3.0       0.20
c
SI1  H    -10   +10
SP1  D  0     1
c
c
SI2  H    -10   +10
SP2  D  0     1
c
c
SI3  H    -10   +10
SP3  D  0     1
c
```

Source neutrons $(\mathrm{par} = \mathrm{n})$ are randomly generated at (x, y, z) points inside a 20 cm × 20 cm × 20 cm cubic volume centred around the point $(x, y, z) = (0,0,0)$, but then only source-points inside cell 1,

are accepted in accordance with the criterion $\boxed{\text{CELL} = 1}$; this is called cell-rejection. Cell-rejection allows one to specify a simple rectangular sweep-volume by using cartesian spatial source distributions D1, D2 and D3. The source neutrons are "fission arson" neutrons and their energy spectrum, specified in distribution D4, is chosen rather arbitrarily simply to "set neutronic fire" to the fissile system, by initiating many fission events in cycle 1. The code MCNP subsequently generates the fission neutron spectra $\chi(E)$ and fission neutron multiplicities $\nu(E)$ correctly, from sampling built-in spectrum functions $\chi(E)$ and neutron yield functions $\nu(E)$, for fissile and fissionable isotopes in the system. In energy distribution D4 shown above, 20% of starter-neutrons are generated at $E = 10^{-9}$ MeV, 20% at $E = 10^{-6}$ MeV, 20% at $E = 10^{-3}$ MeV, 20% at $E = 10^{-1}$ MeV, and 20% at 3.0 MeV. This simple, discrete energy spectrum for fission-initiating "arson"-neutrons works well; it is deliberately arbitrary.

The card $\boxed{\text{MT2 H-H2O.80T}}$ requests the detailed, special thermal treatment of ^1H bound in light water. This is a request that, at neutron energies below, e.g., 4 eV, neutron scattering off the isotope ^1H bound in H_2O molecules should not default to the default assumption that all isotopes are in a free-gas form, but should use $S(\alpha,\beta)$ bound-state thermal scattering cross-section data for ^1H in material 2. At sub-4-eV energies, neutron scattering is not with free-gas ^1H but rather with an entire $^1\text{H}_2\text{O}$ molecule, and this substantially impacts the kinematics of the neutron scattering process, because the effective mass-number A of the scattering species is no longer $A(^1\text{H}) = 1$, but rather

$$A(^1\text{H}_2\text{O}) = 2A_H + A_O$$
$$= 18.$$

Requesting $S(\alpha,\beta)$ bound-state thermal-range neutron scattering treatment, ensures a more accurate quantification of the magnitude and energy spectrum of the neutron fluence-rate $\varphi(E)$ in the neutron energy domain $E \leq 4\ \text{eV}$, which will improve the accuracy of the calculated system safety parameter k_{eff}, which depends sensitively on the sub-4 eV part of the function $\varphi(E)$, because both fission cross-sections $\sigma_{\text{f}}(E)$ and absorption cross-sections $\sigma_{\text{a}}(E)$ are large in this energy range.

A very important card in an MCNP calculational model for quantifying the value of k_{eff} of a fissile system, is the KCODE card, e.g.

```
KCODE  1E5  2.2   50   100   20E5
```

The first parameter (here 1E5) specifies the number of source neutrons per cycle. The second number (here 2.2) is a starter guess value for k_{eff}; it is usually chosen deliberately large, because it also serves as a memory-reservation specifier; a guess-value of 0.5 will reserve 5 times less computing memory than a guess-value of 2.5. The next number (here 50) is the number of "throw-away cycles". The fluence-rate solutions of the first 50 cycles are disregarded in the calculation of k_{eff} because the intent of these initial cycles is to allow the shape of $\phi(x,y,z)$ to *settle to the*

fundamental mode that characterises the fissile system, which is functionally equivalent to the requirement that the Shannon information-entropy must stabilise. Only the solutions of $\psi(\vec{\boldsymbol{x}}, E)$ of cycles 51 to 100 (the latter being the second-last number in the above KCODE card) will be used to enumerate k_{eff}, the relative statistical error estimate σ, radiation doses, etc. The final value in the KCODE card (here 20E5) is optional, because it only acts as a memory-reservation number; experience has taught that specifying a value of 20 × {number of cycles}, i.e. 20 times the first number in the KCODE card, usually leads to stable, error-free code execution. If this last number is not specified explicitly, and the code's internally calculated, default memory allocation is accepted, code execution may be more prone to failure[33] (usually midway through the calculation).

A.2 MCNP6 dose calculations for criticality excursions

Conceptual foundation

Conceptually, a dose calculation with a radiation transport code proceeds by first solving the steady-state Boltzmann transport equation $\mathbb{B}\psi = Q$, which quantifies the directional fluence-rate function, $\psi(\vec{\boldsymbol{x}}, E, \widehat{\boldsymbol{\Omega}})$. Whereas the transport of radiation depends intimately on the directional variable, $\widehat{\boldsymbol{\Omega}}$, the average biological effect of ionising radiation on a target such as a biological cell in a human, is, on average, independent of $\widehat{\boldsymbol{\Omega}}$. In simple language, the means that a biological cell in the body will, on average, suffer the same magnitude of deleterious effect, irrespective of whether it is hammered by radiation impinging from the left, right, top or bottom. Therefore the scalar fluence-rate $\varphi(\vec{\boldsymbol{x}}, E)$ is calculated by integrating $\psi(\vec{\boldsymbol{x}}, E, \widehat{\boldsymbol{\Omega}})$ over the domain of the angular variable $\widehat{\boldsymbol{\Omega}}$., i.e., over 4π steradians. Next, the biological response R is calculated as

$$R = \int_V d\vec{\boldsymbol{x}} \int_0^\infty dE\, \varphi(\vec{\boldsymbol{x}}, E)\, \mathfrak{R}(E)$$

where V is the volume of the human body that acts as volume-extended receiver, and $\mathfrak{R}(E)$ is the response function. The above notation is now simplified by introducing the notation of inner product brackets from the mathematical discipline of linear spaces (Akhiezer and Glazman, 1993). The calculation of the impact of radiation, i.e. the *response* to radiation, is now written as the linear functional

$$R = \langle \varphi, \mathfrak{R} \rangle$$

where the inner product brackets denote integration over the continuous variables and summation over the discrete variables of phase-space. R is the response, which is positive real number; a dose or a dose-rate are examples of responses that are real functionals. The function $\mathfrak{R}(E)$ is the

[33] Note by co-supervisor TJvR: The older code, MCNPX, was quite prone to this failure mode — it was focused on high-energy calculations and not on KCODE calculations, for which MCNP5 used to be the code of choice. It is possible that this failure mode has been eliminated in MCNP6.

response function; fluence-to-dose factors are examples of response functions. Note that the real functional $\langle \varphi, \Re \rangle$, here signifying mathematical integration over the variable E, i.e., particle energy, maps two functions, $\varphi(E)$ and $\Re(E)$, to a real value, i.e., a scalar. The conceptual formalism for a dosimetric calculation with a radiation transport code, can therefore be formulated as follows:

Step 1: Solve the BTE

$$\mathbb{B}\psi = Q$$

so as to quantify ψ, and then obtain φ by integration[34].

Step 2: Calculate the response R to the radiation field φ as

$$R = \langle \varphi, \Re \rangle$$

using the appropriate response function(s), $\Re(E)$.

Radiation dose

The base-line dose definition is that of absorbed dose, which is the amount of ionising radiation energy absorbed per unit mass in a "receiver" volume. Let the absorbed dose from radiation type r that is absorbed in organ T be denoted by $D_{r,T}$. The SI unit of absorbed dose is the gray (Gy), where $1\,\mathrm{Gy} = 1\,\frac{\mathrm{joule}}{\mathrm{kg}}$.

Absorbed dose does not correlate well with the risk of radiation-related cancer, because it is not only the $\frac{\mathrm{joule}}{\mathrm{kg}}$ parameter of energy deposition that determines the risk of the neo-genesis of radiation-related cancer. The most carcinogenic radiation-related lesion in the human body, is double-stand breaks (DSBs) in DNA in cellular nuclei — DSBs are complex, clustered, and essentially non-repairable lesions. Low-LET radiation types such as ionising photons, tend to cause mostly highly repairable single-strand breaks (SSBs) in DNA, whereas high-LET types of ionising radiation, e.g., neutrons, cause non-repairable DSB lesions in DNA. It has been found that a given absorbed dose from neutrons or alpha-particles can be up to 20 times more carcinogenic than the same dose from γ-photons. This has led the ICRP (ICRP, 2007) to define the radiation weighting factor w_r and introduce the quantity equivalent dose. The equivalent dose to an organ or tissue T, is

$$H_T = \sum_r w_r D_{r,T}$$

where w_r is the radiation weighting factor of radiation type r, which quantifies the ability or radiation type r to cause irreparable, potentially carcinogenic DNA lesions. The SI unit of the equivalent dose is the Sievert (Sv).

[34] Note: this integration is an automated background process in MCNP.

Absorbed dose is the correct dose quantity for, e.g., quantifying damage to polymers, simply because such “rubbers and plastics” do not contain cells, cell nuclei or DNA and cannot develop cancer. In contrast, absorbed dose is an inadequate and deficient dose quantity for quantifying the deleterious impact of ionising radiation on living organisms such as humans; the equivalent dose is a far better dose quantity for the expression of detriment to humans.

A final refinement in the definition of radiation dose is required because some organs are more radiosensitive and more prone to radiation-related carcinogenesis than other organs. The effective dose E to the entire human body is defined as (ICRP, 2007)

$$E = \sum_T w_T H_T$$

$$= \sum_T w_T \left(\sum_r w_r D_{r,T} \right)$$

where w_T is the tissue weighting factor of organ T, which quantifies this organ’s relative susceptibility to the development of primary, radiation-related cancers. The SI unit of the effective dose is the Sv. The tissue weighting factors are listed in the 2007 Recommendations of the ICRP (ICRP, 2007) and are reproduced in Table on page 126. Like the radiation weighting factors w_r, the tissue weighting factors w_T are revised by the ICRP every 15 to 20 years, based on new research findings in radiobiology, radio-epidemiology, and radiation oncology.

Important: In Monte Carlo calculations for radiation protection purposes, the calculated quantity is often not the effective dose, because this would require the use of a bio-realistic humanoid voxel-phantom, which is impractical, except for research work. The quantity that is calculated is closer to the equivalent dose.

Radiation weighting factors, w_R

Compilations of the best published radiation weighting factors (year 2020), are embedded Table . It must be noted that the ICRP-2007 (ICRP, 2007) radiation weighting factors for three groups of charged particles — protons, alpha-particles and light ions — have all been thoroughly superseded by new values determined by National Aeronautics and Space Administration (NASA), in preparation for manned interplanetary space missions (Cucinotta, 2015; Sato, 2016; Sato *et al.,* 2013). Double-click on the icons of the embedded files in Table A-2 on page 125, and open them with e.g. NP++ or VSCODE.

Table A-2: Best published radiation weighting factors for the quantification of equivalent dose with radiation transport codes, available in 2020.

Particle types	**Radiation weighting factor, w_r** (Sv/Gy)
Protons, α-particles and Fe nuclei	
Neutrons	

The radiation weighting factor functions for neutrons, as defined in ICRP-2007 (ICRP, 2007), still holds, i.e., the more recent research by NASA did neither disproved nor improved The ICRP-2007 definition of $w_R^n(E)$ by the ICRP. This function, $w_R^n(E)$, is displayed in *Figure A-1*.

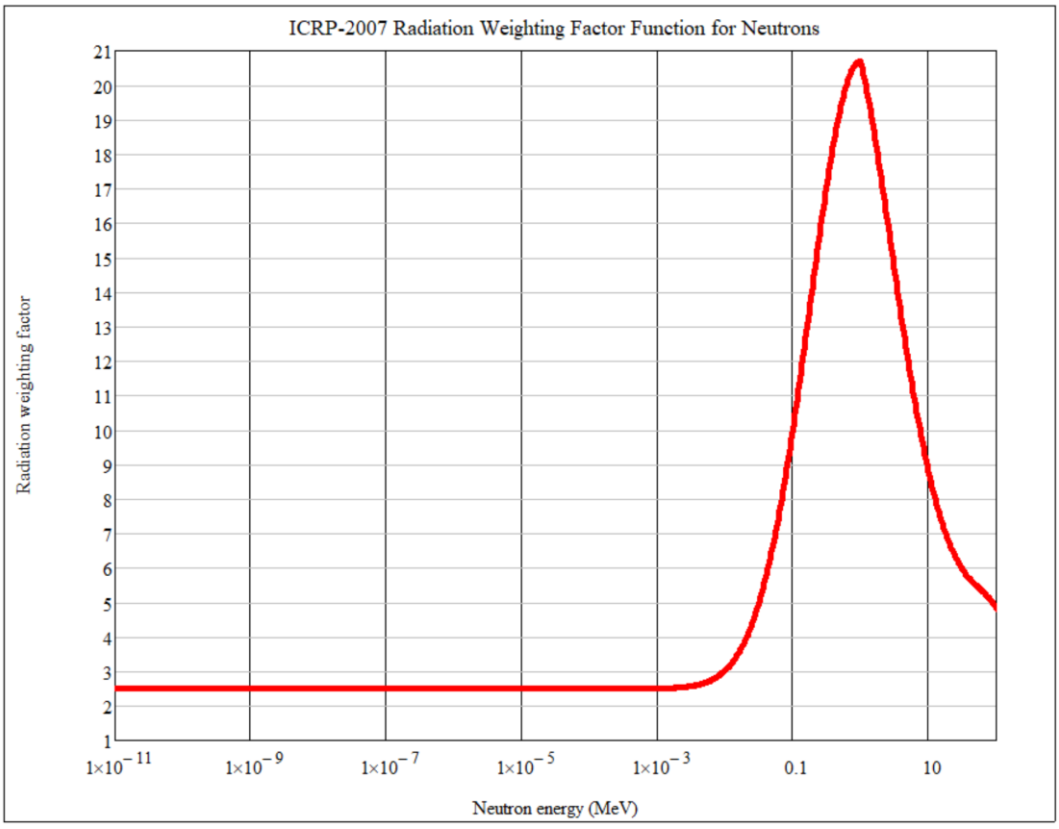

Figure A-1: The radiation weighting function $w_R(E)$ for neutrons (ICRP, 2007).

The radiation weighting factor function for neutrons, $w_R^n(E)$ equals 2.5 up to circa 1 keV; it then rises steadily to a value $w_R \approx 20.6$ at $E = 1\,\mathrm{MeV}$, and then slowly drops to reach the value 5 at

$E = 200$ MeV, from where it eventually tends to 2.5 at very high energies. The fact that the function $w_R^n(E)$ for neutrons peaks at $E = 1$ MeV does *not* mean that neutrons are most dangerous at 1 MeV, but that the ratio $\frac{\text{NED}}{\text{NAD}}$ (unit: $\frac{\text{Sv}}{\text{Gy}}$) peaks at 1 MeV; here NED denotes the neutron equivalent dose and NAD the neutron absorbed dose. The curve $\mathfrak{R}_n(E)$ is displayed in Figure A-2 on page 128 and indicates that the biological hazard per unit fluence of neutrons is essentially a monotonically rising function of neutron energy over the energy range

$$10^{-11}\ \text{MeV} \leq E \leq 1000\ \text{MeV}.$$

Tissue weighting factors

The values of the tissue weighting factors, $w_{T,}$ in the 2007 Recommendations of the ICRP (ICRP, 2007), are listed in Table A-3.

Table A-3: Tissue weighting factors (ICRP-2007).

Tissue/Organ	**Tissue weighting factor,** w_T
Bone marrow, Breast, Colon, Lung, Stomach	0.12
Gonads	0.08
Bladder, Esophagus, Liver, Thyroid	0.04
Bone surface, Brain, Salivary glands, Skin	0.01
Remainder tissues	≈ 0.009 each

The values of the tissue weighting factors are a quantification of the susceptibilities of different tissues to the development of primary[35] radiation-related cancers. Tissue weighting factors are based on cancer incidence data, and takes account of the lethality rate, the years of life lost and of a weighted contribution from the non-fatal cancers and from hereditary disorders. The values of w_T are normalised to add up to 1, i.e., the numerical values of w_T have only relative meanings and no absolute meaning.

Table indicates that bone marrow, the colon, the (young) female breast[36], the stomach and the lungs are the organs most susceptible to the development of primary radiation-related cancers, whereas the bone surface, brain, salivary glands, skin and the remainder tissues are relatively insensitive to

[35] Note by co-supervisor TJvR: Primary, i.e., as opposed to metastatic.

[36] Note by co-supervisor TJvR: After menopause, the radiosensitivity of the female breast drops from 0.12 to circa 0.04.

radiation-associated carcinogenesis. An interesting observation from the ratios between the TWFs in Table , is that a radiation worker "must worry 12 times more about his stomach than his brain". The ratios between the TWFs can be directly used for the design of shadow-shields for radiation workers.

Pre-calculated response functions

When MCNP is executed, realistic doses to humans can be calculated either by means of an F4 tally or an F6 energy-deposition tally. We will here focus on the use of F4 tallies. To use the F4 tally for a realistic dose calculation to a human, one can, e.g., specify a "pillar-phantom" as a "basic human shape" using a surface card such as

```
01 RCC  0  0  20   0  0  175   12
```

for a radiation worker standing on a floor. The geometry specification RCC defines a right circular cylinder, i.e., a pillar shape. The vertical extent of the "pillar phantom" is from $z = 20\,\mathrm{cm}$ to $z = 175\,\mathrm{cm}$, which is the vertical extent of the radiosensitive part of the human body of a person with a typical length. That is, the vertical extent of the radiosensitive part of the body can be inferred from the tissue weighting factors in (ICRP, 2007) — as transparent in Table . This pillar phantom is now filled with tissue-equivalent material[37] at a low mass-density of, e.g., $\rho = 0.01\,\mathrm{g\,cm^{-3}}$. This is a valid methodology, because absorbed dose is an intensive and not an extensive quantity (joule/kg), i.e. when the density is 100 times less than a reference value, 100 times less energy will be absorbed into a mass that is also 100 times lower, i.e., the quotient $\frac{\text{absorbed energy}}{\text{mass}}$ will be stable and essentially invariant. In the MCNP calculation model, fluence-to-dose response functions $\mathfrak{R}(E)$ are specified at a selection of energies E_i as $\boxed{DE\ \ DF}$ dose-function tables. The low mass-density for the TEM in the humanoid-shaped detector eliminates self-shielding and shadow-shielding effects (e.g., one phantom detector shielding another phantom detector) and therefore leads to conservative results. The latest fluence-to-dose response functions $\mathfrak{R}(E)$ for a neutrons and ionising photons, are specified in (ICRP and ICRU, 2017) and are shown in *Figure A-2*.

[37] The MCNP material card for tissue-equivalent material is embedded here: MCNP TEMPLATE - MATERIAL - TEM - TI (https://en.wikipedia.org/wiki/Composition_of_the_human_body).

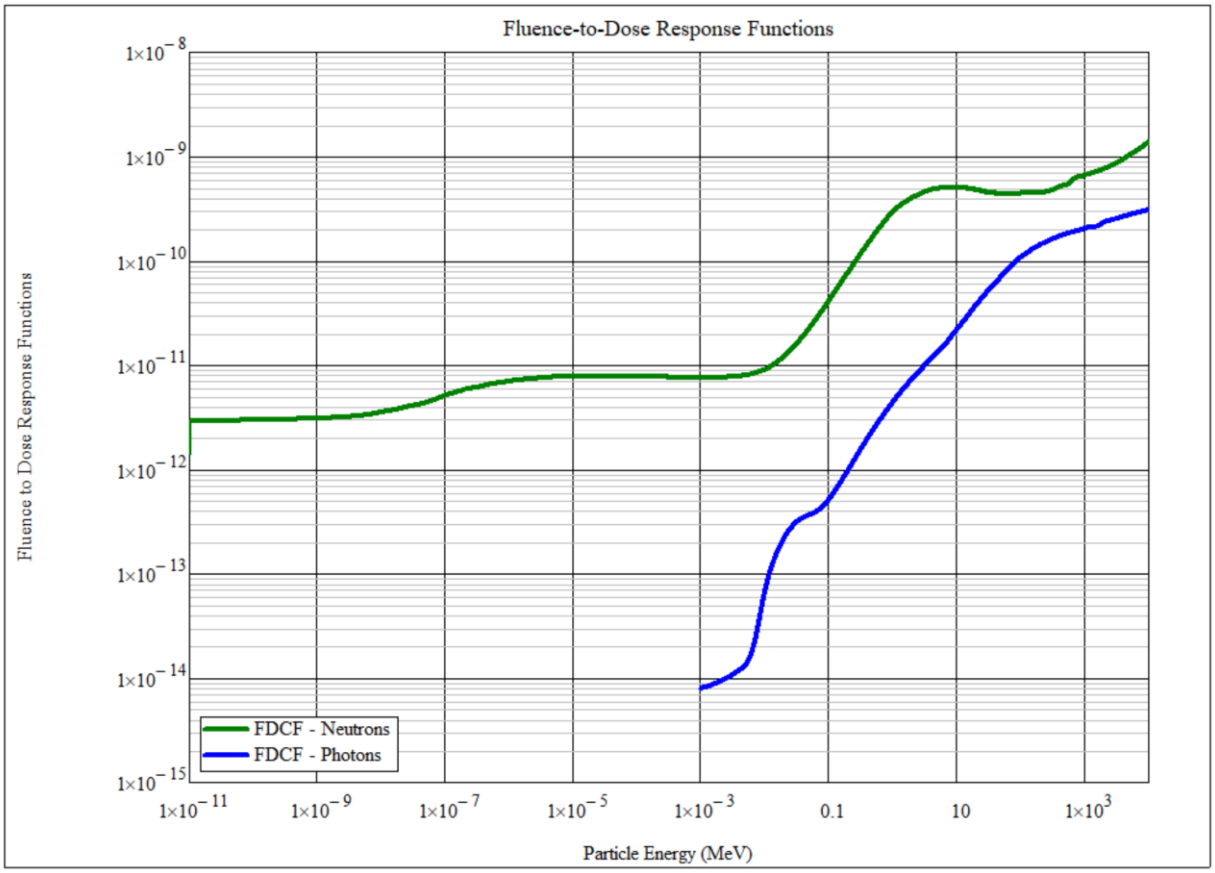

Figure A-2: Fluence-to-dose response functions $\mathfrak{R}(E)$ for neutrons (green line) and photons (blue line) (ICRP and ICRU, 2017)

From *Figure A-2* it is evident that, at every energy in the energy-domain of interest in this work, i.e., $E \in [10^{-11}; 20]\ \mathrm{MeV}$, the neutron is a significantly more biologically hazardous particle than the photon — the green curve for the biological hazard of neutrons is notably higher than the blue curve for the biological hazard of photons. Photons at $E < 10^{-3}\ \mathrm{MeV}$ impart an insignificant dose, whereas the neutron remains biologically dangerous[38] right down to $E = 10^{-11}\ \mathrm{MeV}$.

Examples of quantitative information that can be gleaned from the data graphed in Figure A-2, are:

- A given fluence of 10 MeV neutrons is 66 times more carcinogenic[39] than the same fluence of 1 keV neutrons.

[38] Note by co-supervisor TJvR: The biological hazardousness of thermal neutrons has much to do with the reaction ${}^{14}_{7}\mathrm{N}(\mathrm{n},\mathrm{p}){}^{14}_{6}\mathrm{C}$ being exothermic at $Q = 625.87\ \mathrm{keV}$ (https://www.nndc.bnl.gov/qcalc/qcalcr.jsp), i.e., thermal neutron capture in the nitrogen in amino acids in the skin and subcutaneous structures, leads to the emission of protons at energies of circa $E_{\mathrm{proton}} \approx 0.6\ \mathrm{MeV}$. It is mainly these secondary protons emitted from the above thermal neutron reaction with nitrogen that make thermal neutrons biologically harmful.

[39] Note by co-supervisor TJvR: In the approximate dose range $H \in [0; 100\ \mathrm{mSv}]$, the dominant health concern is a risk of radiation related cancer, which is approximately 40 times higher than the risk of hereditary ill health (Grant et al., 2015; ICRP, 2007).

- A given fluence of 2 MeV neutrons is 54 times more carcinogenic than the same fluence of 1 keV neutrons.
- A given fluence of 1 MeV neutrons is 67 times more carcinogenic than the same fluence of 1 MeV photons.

The fluence-to-dose dosimetric response functions $\mathfrak{R}_n(E)$ and $\mathfrak{R}_\gamma(E)$, as displayed in Figure A-2, were calculated by an international task-force over the span of several years, using the most accurate and complete available anthropomorphic voxel phantoms, defined in calculation models in several Monte Carlo codes, including MCNP[40], TRIPOLI[41] and FLUKA[42] (ICRP, 2010; ICRP and ICRU, 2017).

A.3 Normalization of MCNP calculations executed in KCODE mode

The following unpublished report, directed to the community of MCNP users,

MCNP - Normalization in KCC,

states that doses calculated with MCNP criticality calculations, executed in KCODE mode, have to be divided by the value of k_{eff} to be correctly normalised. (The referenced report is embedded above, because it cannot always be located with ease on the Internet.)

In all criticality calculations in this work, which modelled a marginally supercritical system, the calculation model was designed (by using trial and error to home in on a marginally supercritical volume and material composition for the fissile system), to restrict k_{eff} inside a narrow band of values

$$1.01 \leq k_{\text{eff}} \leq 1.02$$

which means that no renormalisation of calculated doses was necessary in this work.

A.4 MCNP calculation models

The six MCNP6.2 calculation models developed for the different layouts (MOD0, MOD1, until MODE6) of the PUREX facility, are embedded[43] in Table A-4.

[40] https://mcnp.lanl.gov/

[41] https://www.cea.fr/energies/tripoli-4/tripoli-4

[42] http://www.fluka.org/fluka.php

[43] To open a calculation model file, the reader simply double-clicks the icon and, if necessary, elects to open the file with a text editor such as NP++, VSCODE, ATOM, Sublime, Brackets, etc.

Table A-4: MCNP6 calculation models developed in this study.

Design MODification number	**MCNP6 calculation model**	**Brief description of calculation model**
MOD0	 00MOD00_PUREX_BaseLine_OrdCRT_OW	Baseline model, “naïve” facility layout, very limited inner partitioning shielding walls to radiologically de-couple workstations in the facility.
MOD1	 01MOD01_PUREX_OW150_IW60_LIW.INP	Original partitioning walls made wider and longer No walls added. Entire perimeter concrete wall now 50% thicker.
MOD2	 02MOD02_PUREX_OW100_Labyrinth.INP	Additional partitioning walls are added to radiologically de-couple workstations, from each other. Outer wall thickness decreased to 100cm; 150 cm wall thickness retained around highest-risk cubicle
MOD3	 03MOD03_PUREX_CRT-10B2-Fe14.INP	Same wall layout as MOD2 Material composition of the most important inner partitioning shielding wall is improved by using a higher-density shielding concrete with 14% Fe and 2% ^{10}B.
MOD4	 04MOD04_PUREX_NoTopGap_LHS80.INP	Same wall layout and materials as MOD3 All inner partitioning shielding walls now reach to the roof, to eliminate a problematic radiation streaming path. The most important partitioning shielding wall is dimensionally improved by making it 80 cm thick
MOD5	 05MOD05_PUREX_LHS60.INP	Same layout and materials as MOD4, but the most important shielding wall is given its original thickness of 30 cm.
MOD6	 06MOD06_PUREX_OrdCRT.INP	Same layout and materials as MOD6, but the most important inner partitioning shielding wall is now made of ordinary concrete.

These MCNP calculation models comprises elemental composition of US NRC regulatory concrete – an example of elemental composition is shown in Table A-5.

Table A-5: Elemental composition of US NRC regulatory concrete.

```
c US-NRC REGULATORY CONCRETE, Specification for low-energy P E Runs:
M04    1000    -01.00
       8000    -53.20
       11000   -02.90
       13000   -03.40
       14000   -33.70
       20000   -04.40
       26000   -01.40
c Note: The US-NRC requests that all radiation shielding transport calculations involving concrete, be standardised to REGULATORY
CONCRETE.
```

```
c
c US-NRC REGULATORY CONCRETE, Specification for Neutron Runs:
M04    1001    -0.009996802968762650
       1002    -3.197031237352260E-6
       8016    -0.530588536334774000
       8017    -0.000214228120751659
       8018    -0.001197235544474060
      11023    -0.029000000000000000
      13027    -0.034000000000000000
      14028    -0.309613753235242000
      14029    -0.016282998492026800
      14030    -0.011103248272731500
      20040    -0.042531188975811100
      20042    -0.000298038140943721
      20043    -6.366957663197520E-5
      20044    -0.001006638966754470
      20046    -2.018025984862260E-6
      20048    -9.844631387389200E-5
      26054    -0.000790378165836526
      26056    -0.012866214257972400
      26057    -0.000302465885119295
      26058    -4.094169107181630E-5
MT04   H-H2O.40T  SiO2.40T  AL-27.40T  Fe-56.40T
c
```

Nominally, the elemental composition of US NRC REGULATORY CONCRETE is presented on page 7-191 in the SCALE 6.2.4 User's Manual (Rearden and Jessee, 2020). The material reg-concrete is a standard composition available in SCALE 6.2. From a shielding perspective, it is a deliberately conservative, transmissive material with a sand and sandstone dominated composition and a density of 2.3 g/cm^3.

A.5 Description of the FISPACT-II 3.00 calculation model developed to calculate the radionuclide inventory produced by the criticality excursion, inside the fissile process mass

The FISPACT-II 3.00 code (Sublet *et al.,* 2015) was used to calculate the nuclide inventory and, by extension, the ionising photon emission intensity and energy-spectrum of the radionuclides produced by the criticality excursion.

FISPACT-II 3.00 requires input from a transport code such as MCNP in order to calculate the above system parameters. In particular, the code requires the energy-spectrum of the neutron fluence-rate, $\varphi_n(E)$, averaged in the material volume in which the nuclear fission takes place, the duration

T_{ca} of the exposure, the integral fluence-rate, $\varphi_n = \int_0^\infty \varphi_n(E)\,dE$, and the numbers[44] of all initially present isotopes in the volume of interest. In practice, the magnitude of a hypothetical, licensing-case criticality accident is decided upon on the basis of a literature survey. In the case under assessment, an excursion involving 10^{17} fissions, was selected as the design-basis accident — denoted as $\mathrm{CA}(10^{17}\mathrm{f})$. The number of neutrons emitted during the excursion has to be specified to MCNP, and is obtained by multiplying the number of fissions, by ν — the fission neutron yield or multiplicity. The value $\nu = 2.5$ was selected, based on MCNP BURN(up) calculations, i.e., the normalisation factor specified to MCNP was 2.5E17 — this is the total number of neutrons released by the modelled $\mathrm{CA}(2.5 \times 10^{17}\mathrm{n})$ excursion. In the case of KCODE calculations with MCNP, the normalisation factor is specified in the FM tally normalisation cards and also (when necessary) with the FACTOR keyword in FMESH mesh-tally cards. The MCNP code reads the calculation model and quantifies, by simulation, the integral fluence-rate φ_n in the fissile material volume where the accident occurs. In the case under assessment, the result was $\varphi_n = 1.425\mathrm{E}13\ \mathrm{cm}^{-2}\ \mathrm{s}^{-1}$; this value of φ_n is passed to FISPACT-II for the isotopic inventory calculation. The MCNP calculation model quantified the neutron spectrum $\varphi(E)$ as displayed in Figure A-4 — this is a typical neutron spectrum where the neutrons are born from fission events, having the source-neutron energy spectrum shown in Figure A-3. The Watt prompt-fission-neutron (PFN) spectrum formula, with parameters determined by (Cranberg *et al.*, 1956), is

$$Q(E) = 0.45283 \exp\left(\frac{-E}{0.965}\right) \sinh\sqrt{2.29E}$$

and is displayed on page 133.

[44] Note by co-supervisor TJvR: These are not number densities, but the aggregated number of atoms. The concept of space does not exist in nuclide inventory codes such as FISPACT and ORIGEN; these codes are classified as “point” codes, i.e. they operate with zero spatial dimensions. Because there is no concept of length in FISPACT, there will, by necessity, also be no concept of number density, because the latter concept depends on a more basic concept of space.

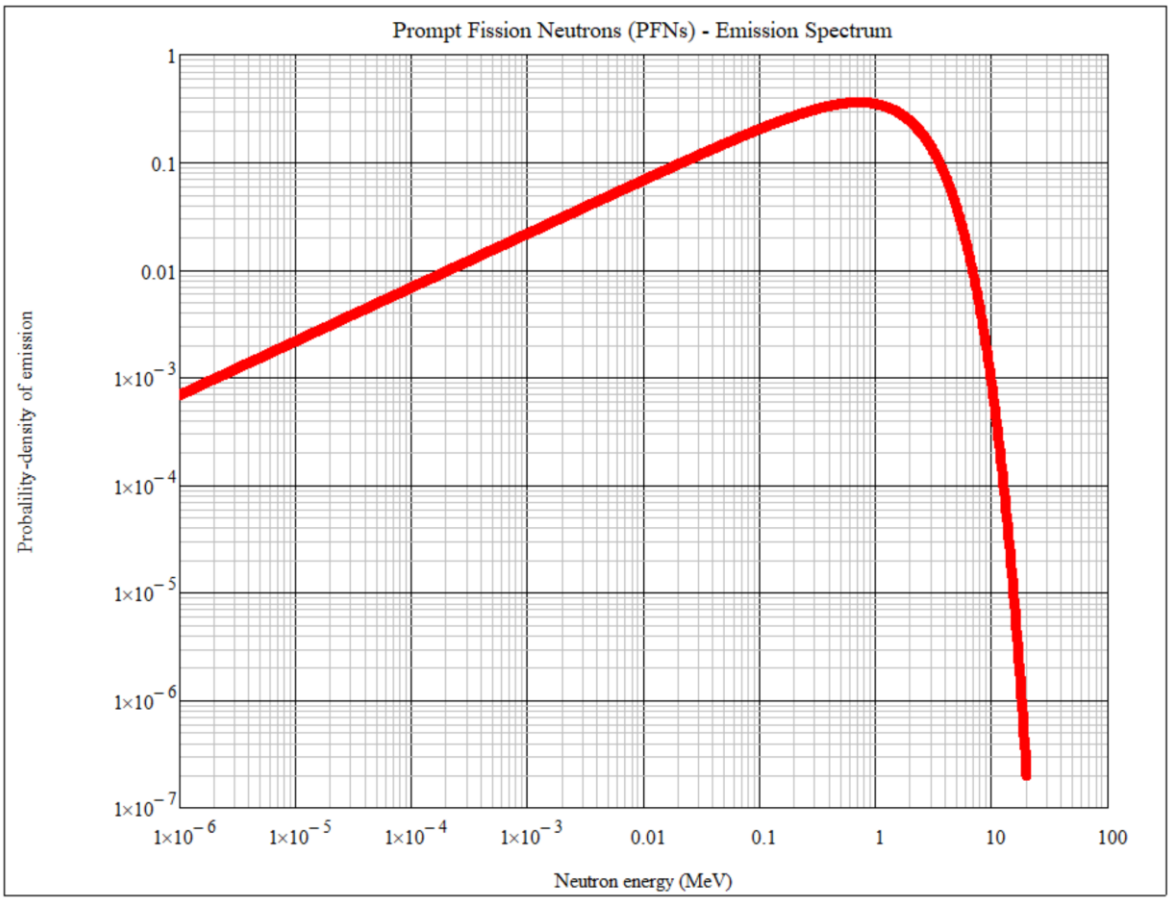

Figure A-3: Energy-spectrum Q(E) at which prompt fission neutrons are emitted when ^{235}U fissions (Cranberg et al., 1956).

The PFN spectra of other fissioning isotopes, are qualitatively similar to the spectrum seen in Figure A-3. The calculation model requests MCNP to calculate the group-integrated multigroup neutron spectrum φ_g in e.g. 172 or 180 groups. Each of these 180 values of φ_g are then divided by the energy-width of each energy interval, and $\frac{\varphi_g}{\Delta E_g}$ is then interpolated as a function of E, to arrive at a reconstructed differential neutron spectrum, i.e., an approximation of $\varphi(E)$. A standardised calculational path for this procedure, which was given the name **Neutron_Spectrum_App**, has been developed for this purpose[45]. The calculated differential neutron spectrum, $\varphi(E)$, is shown in Figure A-4.

[45] By the co-supervisor, TJvR.

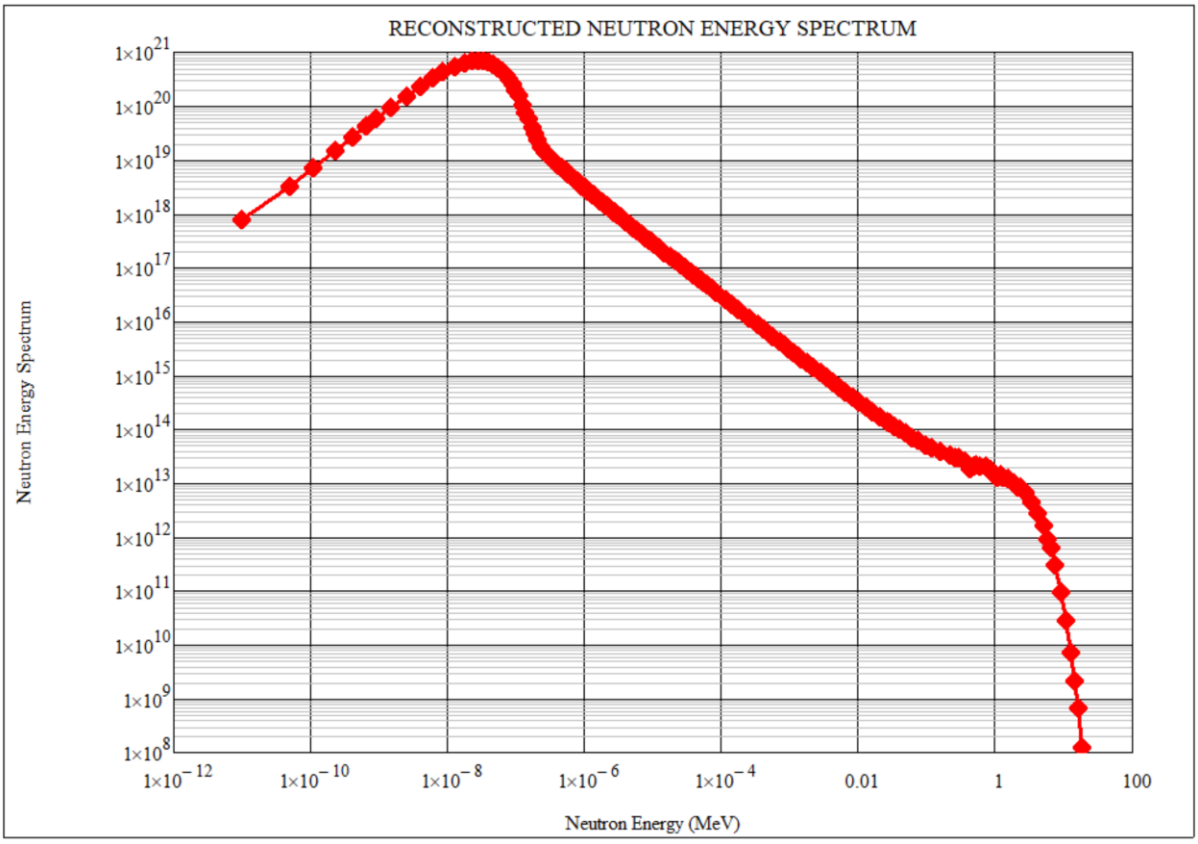

Figure A-4: Calculated neutron spectrum in the material in the process vessel where the postulated criticality excursion takes place.

It is evident that the neutron spectrum of Figure A-4 contains, on the high-energy side, an "uncollided" portion of the PFN spectrum seen in Figure A-3. Below circa 0.9 MeV, a slowing-down spectrum that is characteristic of materials with an abundance of $^{1}\mathrm{H}$, is seen — in the absence of the latter isotope, the above characteristic shape (a straight line on a log-log graph) of the slowing-down spectrum would not have been observed. Below circa 0.625 eV, a Maxwellian thermal neutron spectrum shape is observed.

FISPACT-II 3.00 requires neutron spectra ported to it from transport codes, to be group-integral spectra in a standardised 709-group partition of the neutron energy interval $[10^{-11}\ \mathrm{MeV}; 1000\ \mathrm{MeV}]$; in more recent versions of FISPACT[46], the 709-group structure had been abandoned in favour of a 1102-group structure. The utility code Neutron_Spectrum_App calculates this multigroup spectrum by integrating the reconstructed, interpolated spectrum $\varphi(E)$ over the 709-group partition of the energy variable, which is defined in the FISPACT-II user manual.

[46] Note by co-supervisor TJvR: At an up-front cost of British Pound Sterling (GBP) 12,500 along with annual license fees of GBP 1500, it has become very difficult, if not impossible, to obtain updated versions of the code FISPACT. The above outlay does not buy an individual license, but a site-license for FISPACT-II.

(Note: To converge individual energy groups in a direct calculation of $\varphi(E)$ in a 709-group structure, would typically require MCNP runs of at 30 days, on an 18-core workstation — the best computing technology that had been available for this project. Converging MCNP runs directly in a 709-group partition of the neutron energy range, is beyond reach, unless one has access to a high performance computing (HPC) system. In contrast, the calculation of the neutron spectrum in 180-groups, converged very well over a 4-day calculation. The calculated neutron spectrum, which is also the spectrum shown in Figure A-4 is embedded here:

NS_NEUTRON_SPEC
TRUM.INP

(The above spectrum is a text file and can be opened with, e.g., NP++ or VSCODE.)

The initial isotopic numbers in the volume in which the criticality excursion takes place, was calculated and are shown in Table A-6.

Table A-6: Calculated initial isotopic numbers in the process volume in which the criticality excursion takes place.

Isotope	**Number**
H1	3.105714E27
O16	1.561714E27
U235	3.928355E24
U238	4.309706E23

The calculation of the above initial or input-inventory was done with the same utility worksheet used to calculate the MCNP material card for the process-volume in which the excursion happens. The calculational method used to calculate both the MCNP material-card and the initial isotopic numbers specified to FISPACT, is embedded here, as a PDF document:

Aqueous Uranyl
Nitrate - Composition

The three parts of the FISPACT-II calculation model used to enumerate the post-accident radio-nuclide inventory, are embedded in Table A-7.

Table A-7: The three parts of the FISPACT-II calculation model used to quantify the radioisotope inventory after the criticality excursion.

Description	**Embedded model**
CollapX model to collapse problem-independent 709-group reaction cross-sections to problem-dependent 1-group cross-sections, using the weighting spectrum of neutrons, supplied from an MCNP calculation.	 CollapX_PURex.i

Description	Embedded model
ArrayX input to incorporate emission-spectra of radionuclides and also model spontaneous fission.	 ArrayX.i
Main FISPACT-II calculation model that specifies, e.g., the projectile particle, fissioning nuclides, convergence criteria, material composition, neutron fluence as a function of time, cooling time and points in time where (N_i, A_i) must be written in the output file.	 CA_PUREX.i

A.6 FISPACT-II 3.00 calculation model developed to calculate the radionuclide inventory produced neutrons from the criticality excursion, causing neutron activation of nearby materials

The three parts of the FISPACT-II calculation model used to calculate nuclide inventories from neutron activation reactions, produced by neutron emitted in the criticality excursion, are embedded in Table A-8.

Table A-8: The three parts of the FISPACT-II calculation model used to quantify the radioisotope inventory in the SS-316L process vessel, produced from neutron activation by fission neutrons emitted during the criticality excursion.

Description	Embedded model
CollapX model to collapse problem-independent 709-group reaction cross-sections to problem-dependent 1-group cross-sections, using the weighting spectrum of neutrons, supplied from an MCNP calculation.	 CollapX_SS316L.i
ArrayX input to incorporate emission-spectra of radionuclides and also model spontaneous fission.	 ArrayX.i
Main FISPACT-II calculation model that specifies, e.g., the projectile particle, fissioning nuclides, convergence criteria, material composition, neutron fluence as a function of time, cooling time and points in time where (N_i, A_i) must be written in the output file.	 CA_PUREX_SS316.i

Glossary of technical terms

Note that technical terms belonging to the “general nuclear engineering knowledge” category, e.g. radiation, atom, radioactivity, activity, cross-section, barn, etc., will not be defined in this glossary. As a general rule, general concepts, quantities and units defined and used in the first 5 chapters of Lamarsh and Baratta (2017) will be accepted as common knowledge that warrants no additional elucidation.

Acute exposure

An exposure to ionising radiation that amounts to several multiples of the present annual dose limit of 20 mSv, received over a short period of time such as minutes, hours, or days.

Acute radiation syndrome

A collection of health effects caused to exposure to high doses of ionizing radiation (above circa 1000 mSv) over a short period of time. This syndrome is also known as radiation sickness or “radiation poisoning”; symptoms are dose-dependent and can begin within hours and may last for months.

Administrative control (of criticality)

A control measure to prevent criticality, that relies on human actions for its implementation. Administrative controls are human-based and subject to error in application.

Biological shield

A mass of material placed around an actual or potential source of ionising radiation, to absorb the radiation and lower dose-rates to levels close to or below the average terrestrial natural background dose-rate (NBDR) of circa 0.11 μSv/h.

Chain reaction

A reaction that initiates its own repetition. In a nuclear fission chain reaction, a fissile nucleus absorbs an incident neutron and fissions spontaneously, releasing multiple additional neutrons. These, in turn, can cause fission of other fissile nuclei, releasing still more neutrons. A fission chain reaction is self-sustaining when the number of neutrons released in a given time equals or exceeds the number of neutrons lost by absorption in non-fission reactions or by escape from the fissile system.

Criticality accident

An uncontrolled nuclear fission chain reaction. It sometimes referred to as a criticality excursion, a critical power excursion or a divergent chain reaction.

Criticality accident alarm system (CAAS)

A combination of nuclear criticality detectors, audible alarms, and electronic modules (comparator panel) that is deployed for the prompt detection of a criticality excursion and the immediate triggering of an audio-visual alarm to warn personnel.

Critical mass

The smallest mass of fissionable material that will support a self-sustaining chain reaction.

Criticality safety

A self-sustaining chain of fission events is termed 'nuclear criticality'. When a system is critical, the rate of generation of neutrons is equal to the rate of loss of neutrons and the effective neutron multiplication factor $k_{\mathrm{eff}} = 1$. The goal of criticality safety is to assure subcriticality – that is, $k_{\mathrm{eff}} < 1$ – for all conditions that a system outside of a reactor might encounter. Radioactive material containing fissile nuclides is typically termed *fissile material* and criticality safety during the handling of such material must be ensured in order to protect workers and the public from the radiological effects of an un-anticipated nuclear criticality event. The four major fissile nuclides, which are characterised by high cross-sections for fission induced by slow neutrons, and the absence of an energy threshold for neutron induced fission, are $^{233}\mathrm{U}$, $^{235}\mathrm{U}$, $^{239}\mathrm{Pu}$ and $^{241}\mathrm{Pu}$. A criticality safety assessment (CSA) is the term used to describe the process that must be undertaken to demonstrate that subcriticality will be maintained under both normal conditions and accident conditions. This chapter will provide an overview of the regulatory requirements for design and transport of packages that contain fissile material, address methodologies and approaches used to perform the criticality safety assessment, and discuss the complexities and challenges related to reliable assurance of criticality safety.

Dose, absorbed

The amount of energy of ionising radiation absorbed per unit mass. Let the absorbed dose from radiation type r that is absorbed in organ T be denoted by $D_{r,T}$. The SI unit of absorbed dose is the gray (Gy), where $1\,\mathrm{Gy} = 1\,\frac{\mathrm{joule}}{\mathrm{kg}}$.

Dose, equivalent

The equivalent dose to an organ or tissue T, is $H_T = \sum_r w_r D_{r,T}$, where w_r is the radiation weighting factor of radiation type r, which quantifies the ability or radiation type r to cause irreparable, potentially carcinogenic DNA damage. The SI unit of the equivalent dose is the Sv. (In Monte Carlo calculations for radiation protection, the calculated quantity is normally the equivalent dose.)

Dose, effective

The effective dose E to the entire human body is $E = \sum_T H_T = \sum_T \left(\sum_r w_r D_{r,T}\right)$ where w_T is the tissue weighting factor of organ T, which quantifies its relative susceptibility to the development of primary radiation-related cancers. The SI unit of the effective dose is the Sv. (Note: In Monte Carlo calculations for radiation protection purposes, the calculated quantity is normally not the effective dose, because this would require the use of a bio-realistic humanoid voxel-phantom, which is impractical, except for research work.)

Dose rate

In dose-rate calculations, the dose rate is usually $\frac{dH}{dt}$, also denoted as $\dot{H}$, with H denoting the equivalent dose.

Double-Contingency

The double-contingency principle states that *process designs should incorporate sufficient factors of safety (FoS) to require at least two unlikely, independent, and concurrent changes in process conditions, before a criticality accident becomes possible.*

Engineering control (criticality)

A physical design that reliably serves as a criticality safety control.

Excursion

A sudden, very rapid rise in the power level of a system containing fissile material, caused by super-criticality, i.e. the state when $k_{\text{eff}} > 1$.

External radiation

A source of ionizing radiation is located outside the human body.

Fertile material

An actinide isotope that is not fissile, that can be converted into a fissile material by neutron irradiation in e.g. a nuclear reactor. There are two main fertile isotopes, namely $^{238}_{92}\mathrm{U}$ and $^{232}_{90}\mathrm{Th}$. When $^{238}_{92}\mathrm{U}$ captures neutrons, it is converted into fissile $^{239}_{94}\mathrm{Pu}$; when $^{232}_{90}\mathrm{Th}$ captures neutrons, it is converted into fissile $^{233}_{92}\mathrm{U}$.

Fissile material

Actinide isotopes such as $^{233}\mathrm{U}, ^{235}\mathrm{U}, \mathrm{and}\ ^{239}\mathrm{Pu}$ that can be fissioned by thermal neutrons.

High enrichment uranium (HEU)

Uranium enriched to above a 20% mass percentage in the fissile isotope $^{235}\mathrm{U}$.

Lethal dose $\boldsymbol{LD_{50/30}}$

The dose of ionising radiation expected to cause the death of 50% of an exposed population within 30 days. Typically, $LD_{50/30}$ is around 3000 mSv with no medical intervention, and 4000 mSv with expert medical intervention (ICRP, 2007). (This notation is widely used in toxicology.)

Lethal dose $\boldsymbol{LD_{50/60}}$

The dose of ionising radiation expected to cause the death of 50% of an exposed population within 60 days. Typically, $LD_{50/60}$ is around 3000 mSv with no medical intervention, and 4000 mSv with expert medical intervention (ICRP, 2007). (This notation is widely used in toxicology.)

Moderator

A material, such as ordinary water, heavy wate, or graphite, that can slow down high-energy neutrons into the energy range of thermal equilibrium with the matter traversed by the roaming neutrons, thereby increasing the likelihood of fission.

Natural uranium

Un-enriched uranium that contains the average relative concentrations of isotopes presently found on earth — 0.72041% $^{235}\mathrm{U}$, 99.27417% $^{238}\mathrm{U}$, and $5.42\mathrm{E}\text{-}3\%$ $^{234}\mathrm{U}$ by mass (Meija et al., 2016).

Nuclear criticality accident

An uncontrolled nuclear fission chain reaction. It is sometimes referred to as a nuclear criticality excursion, critical power excursion, or divergent chain reaction. Criticality accidents can release potentially fatal radiation doses, if they occur in an unprotected (i.e. unshielded) environment.

Reactivity

The deviation of a criticality system from criticality, i.e. from $k_{\text{eff}} = 1$. A positive reactivity addition indicates a move toward supercriticality (a power increase). A negative reactivity addition indicates a move toward subcriticality (a power decrease).

Reflector

Material immediately surrounding a system of fissile material, that scatters back (i.e. reflects) into the system many neutrons that would otherwise escape. The returned neutrons can then contribute to fissions and improve the neutron economy of the fissioning system. Common reflector materials are graphite, beryllium, light water, heavy water, and natural uranium.

Risk

The combined answer to three questions:

(1) what can go wrong?

(2) How likely it is to go wrong?

(3) What will be the consequences if it goes wrong?

These three questions serve as aid to understand and quantify risk.

Source term

Consider a system having a radionuclide inventory (N_i, A_i) where N is the identity and A is the activity of radionuclide i. This inventory is called the nuclide-activity matrix of the system and we denote it by (N, A). Let radionuclide i emit radiation type j with the radiation emission yield function $Y_{i,j}(E)$. The total emission of radiation type j will then be $Y_j(E) = \sum_i Y_{i,j}(E)$. The concept "source term" refers to both (1) the (N, A) nuclide-activity matrix and (2) the radiation emission functions $Y_j(E)$ for ionising radiation types j that characterises a system.

Supercriticality

When the rate of fission neutron production in a system exceeds the total rate of all neutron losses from the system, the effective neutron multiplication ratio exceeds unity, i.e. $k_{\text{eff}} > 1$, i.e. the neutron population in the system will rise as a function of time. If it is only the contribution of delayed fission neutrons that is responsible for $k_{\text{eff}} > 1$, then the time period of the system can be the order of, e.g., 30 seconds or more, and the system can be controlled and classified as a "nuclear reactor". If, on the other hand, it is the contribution of prompt fission neutrons that is responsible for $k_{\text{eff}} > 1$, then the system is called "prompt critical" and its time period is in the order of 10^{-5} s, i.e. the fissile system cannot be controlled and constitutes an uncontrolled nuclear criticality excursion or accident.

SILENE

A French reactor system for experiments to quantify the behaviour of nuclear criticality excursions for the processing of solutions of fissile materials. The research work with the SILENE reactor has provided vital information in the field of nuclear criticality safety.

TRACY

The Japanese ***TRA****nsient Experiment* ***C****riticalit****Y*** *Facility* houses a research reactor used in experiments to quantify nuclear criticality excursion that may occur in the processing of fissile solutions. The research work at TRACY has provided important information in the field of nuclear criticality safety.

References

Abrefah, R.G., Essel, P.A.A., and Odoi, H.C., 2018. *Estimation of the dose rate of nuclear fuel of Ghana Research Reactor-1 (GHARR-1) using ORIGEN-S and MCNP 6*. Progress in Nuclear Energy 105, 309–317.

Akhiezer, N.I., and Glazman, I.M., 1993. *Theory of Linear Operations in Hilbert Space*. Dover Publications.

Anand, V.P., Rajeev, R., Velavendan, P., Pandey, N.K., and Kamachi-Mudali, U., 2018. *Modeling and Simulation of Diluent Recovery Unit in PUREX Solvent Regeneration System*. Progress in Nuclear Energy 104, 359–367. https://doi.org/10.1016/j.pnucene.2017.01.011

Aneheim, E.H.K., 2012. *Development of a solvent extraction process for group actinide recovery from used nuclear fuel*. PhD Thesis . Chalmers University of Technology, Gothenburg, Sweden.

Audi, G., Kondev, F.G., Wang, M., Huang, W.J., and Naimi, S., 2017. *The NUBASE2016 evaluation of nuclear properties*. Chinese Physics C 41, 1–138. https://doi.org/10.1088/1674-1137/41/3/030001

Badenhorst, J., Krieg, H.M., Meyer, W.C.M.H., and Van Rooyen, T.J., 2016. *Effect of α-Irradiation from Enriched Uranium on the Leaching Properties of PTFE*. Engineering Failure Analysis 74, 1–10. https://doi.org/10.1016/j.engfailanal.2016.12.003

Baker, J.S., Smith, J.A., and Berry, D.T., 1994. *Testing of the Y-12 Plant Criticality Accident Alarm System detectors at the Sandia Pulsed Reactor Facility*. Y-12 National Security Complex, Oak Ridge National Laboratory, Tennessee, USA.

Barbry, F., and Fouillaud, P., 2002. *Criticality Accident Studies and Research Performed in the Valduc Criticality Laboratory, France*. Report: IAEA-CN-82/26. International Atomic Energy Agency (IAEA), Vienna, Austria.

Barbry, F., Fouillaud, P., Grivot, P., and Reverdy, L., 2009. *Review of the CRAC and SILENE Criticality Accident Studies*. Nuclear Science and Engineering 161, 160–187.

Barbry, F.Y., 1993. *Review of the SILENE Criticality Excursions Experiments*. Report: SRSC-93. CEA Institut De Protection et de Surete Nucleaire, France.

Baumgärtner, F., and Ertel, D., 1980. *The modern PUREX process and its analytical requirements*. Journal of Radioanalytical and Nuclear Chemistry 58, 11–28.

Blomquist, R., 2006. *Source Convergence in Criticality Safety Analyses, Phase 1: Results of Four Test Problems*.

Brown, D.A., Chadwick, M.B., Capote, R., Kahler, A.C., Trkov, A., Herman, M.W., Sonzogni, A.A., Danon, Y., Carlson, A.D., and Dunn, M., 2018. *ENDF/B-VIII.0: The 8th Major Release of the Nuclear Reaction Data Library with CIELO-Project Cross Sections, New Standards and Thermal Scattering Data*. Nuclear Data Sheets 148, 1–142. https://doi.org/10.1016/j.nds.2018.02.001

Brown, F.B., 2009. *Review of Monte Carlo Criticality Calculations - Convergence, Bias, Statistics*. Report: LA-UR-086558. Los Alamos National Laboratory (LANL), Los Alamos, New Mexico, USA.

Cho, G., Hyun, J., Tae, K., Park, S., and Choc, K., 2017. *Proposing a Simple Radiation Scale for the Public: Radiation Index (RAIN)*. Nuclear Engineering and Technology 49, 598–608.

Cho, K.-W., Cantone, M.-C., Kurihara-Saio, C., Le Guen, B., Martinez, N., Oughton, D., Schneider, T., Toohey, R., and Zölzer, F., 2018. *Ethical foundations of the system of radiological protection*, Annals of the ICRP. SAGE, London.

Cologne, J.B., and Preston, D.L., 2000. *Longevity of atomic-bomb survivors*. The Lancet 356, 303–307. https://doi.org/10.1016/S0140-6736(00)02506-X

Conlin, J.L., Haeck, W., Neudecker, D., Parsons, K.D., and White, M.C., 2018. *Release of ENDF/B-8.0-Based ACE Data Files for MCNP*. Report: LA-UR-18-24034. Nuclear Data Team, XCP-5, Los Alamos National Laboratory (LANL), Los Alamos, USA.

Cranberg, L., Frye, G., Nereson, N., and Rosen, L., 1956. *Fission neutron spectrum of U 235*. Physical Review 103, 662.

Cucinotta, F.A., 2015. *Review of NASA approach to space radiation risk assessments for Mars exploration*. Health physics 108, 131–142.

DOE (US), 2017. *Good Practices for Occupational Radiological Protection in Uranium Facilities*. Report: Good Practice Guide DOE-STD-1136-2017. Department of Energy (DOE), USA.

DOE (US), 2015. *DOE-HDBK-1019/1-93 - DOE Fundamentals Handbook, Nuclear Physics and Reactor Theory, Volumes 1 and 2*. Report: DOE-HDBK-1019/1-93, DOE Technical Standards Program. Department of Energy (DOE), USA.

Duderstadt, J.J., and Hamilton, L.J., 1976. *Nuclear Reactor Analysis*, 1st edition. ed. WILEY, New York.

Durazzo, M., Saliba-Silva, A.M., Martins, I.C., De Carvalho, E.F.U., and Riella, H.G., 2017. *Manufacturing low enriched uranium metal by magnesiothermic reduction of UF4*. Annals of Nuclear Energy 110, 874–885.

Endo, A., 2010. *Dose Assessment in the Criticality Accident at Tokai-Mura*. Radiation Measurements 45, 1484–1490.

Fleming, M., Sublet, J.-Ch., and Kopecky, J., 2018. *Integro-Differential Verification and Validation, FISPACT-II & TENDL-2017 Nuclear Data Libraries* 532.

Fourie, M., Meyer, W.C.M.H., van der Westhuizen, D.J., and Krieg, H.M., 2016. *Uranium recovery from simulated molybdenum-99 production residue using non-dispersive membrane based solvent extraction*. Hydrometallurgy 164, 330–333.

Gama, J.S., Barry, J., and Crouse, P.L., 2018. *Batch adsorption study of uranium on various ion exchange resins as an alternative method to solvent extraction*.

Grant, E.J., Furukawa, K., Sakata, R., Sugiyama, H., Sadakane, A., Takahashi, I., Utada, M., Shimizu, Y., and Ozasa, K., 2015. *Risk of death among children of atomic bomb survivors after 62 years of follow-up: A cohort study*. The Lancet Oncology 16, 1316–1323. https://doi.org/10.1016/S1470-2045(15)00209-0

Greenfield, B.A., 2009. *Criticality Alarm System Design Guide with Accompanying Alarm System Development for the Radiochemical Processing Laboratory in Richland, Washington*. Masters . University of New Mexico, Albuquerque, New Mexico, USA.

Gross, C., 2018. *Technical Basis for the Uranium Processing Facility Criticality Accident Alarm System*. Y-12 National Security Complex, Oak Ridge National Laboratory, Tennessee, USA.

Henry, A.F., 1975. *Nuclear Reactor Analysis*. MIT Press Cambridge, Massachusetts.

Hodges, M.S., and Sanders, C.E., 2014. *Nuclear Criticality Accident Safety, Near Misses and Classification*. Progress in Nuclear Energy 76, 88–99. https://doi.org/10.1016/j.pnucene.2014.05.018

IAEA, 2019. *Homogeneous Aqueous Solution Nuclear Reactors for the Production of Mo-99 and other Short Lived Radioisotopes*. Report: IAEA-TECDOC-1601, TECDOC. International Atomic Energy Agency (IAEA), Vienna, Austria.

IAEA, 2014. *Criticality Safety in the Handling of Fissile Material*. Report: Specific Safety Guide SSG-27. International Atomic Energy Agency (IAEA), Vienna, Austria.

IAEA, 1999. *Recycle and Reuse of Materials and Components from Waste Streams of Nuclear Fuel Cycle Facilities*. Report: IAEA TECDOC 1130. International Atomic Energy Agency (IAEA), Vienna, Austria.

ICRP, 2012. *ICRP statement on tissue reactions and early and late effects of radiation in normal tissues and organs–threshold doses for tissue reactions in a radiation protection context*. Report: ICRP-118, Annals of the ICRP. International Commission on Radiological Protection (ICRP).

ICRP, 2010. *Conversion Coefficients for Radiological Protection Quantities for External Radiation Exposures*. Report: ICRP-116. Elsevier.

ICRP, 2007. *The 2007 Recommendations of the International Commission on 103*. Elsevier.

ICRP, 2004. *ICRP-099 - Cancer Risk from Low Doses of Ionising Radiation*. Report: ICRP ICRP-099, Annals of the ICRP. International Commission on Radiological Protection (ICRP).

ICRP and ICRU, 2017. *ICRU & ICRP - Draft Joint Report Operational Quantities for External Radiation Exposure - 2017*. ICRP and ICRU.

ICRU, 2011. *Fundamental Quantities and Units for Ionizing Radiation*. Report: Journal of the ICRU Vol 11 No 1 (2011) Report 85. International Commission on Radiation Units and Measurements, Bethesda, Maryland, USA. https://doi.org/10.1093/jicru/nd

INL, 1999. *Criticality Safety Basics: A Study Guide*. Idaho National Engineering and Environmental Laboratory, Idaho Falls, ID (US), Idaho Falls, Ihado, USA.

Irish, E.R., and Reas, W.H., 1957. *The PUREX Process: A Solvent Extraction Reprocessing Method for Irradiated Uranium*. Report: HW-49483 A, AEC Research and Development Report. Hanford Atomic Products Operation, Richland, Washington, USA.

Ishigure, N., Endo, A., Yamaguchi, Y., and Kawachi, K., 2001. *Calculation of the absorbed dose for the overexposed patients at the JCO criticality accident in Tokai-mura*. Journal of Radiation Research 42, S137–S148.

Johnson, T., 2017. *Introduction to Health Physics, Fifth Edition*, 5th edition. ed. McGraw-Hill Education / Medical, New York.

Kerr, G.D., and Tankersley, W.G., 2006. *External Radiation Dose Estimates For Individuals Near the 1958 Criticality Accident at the Oak Ridge Y-12 Plant*. Report: ORAUT-OTIB-0057.

Kiedrowski, B.C., 2012. *MCNP6 for Criticality Accident Alarm Systems - A Primer*. Report: LA-UR-12-25545. Los Alamos National Laboratory (LANL), Los Alamos, New Mexico, USA. https://doi.org/10.2172/1053540

Kodama, K., Ozasa, K., and Okubo, T., 2012. *Radiation and cancer risk in atomic-bomb survivors*. Journal of Radiological Protection 32, N51. https://doi.org/10.1088/0952-4746/32/1/N51

Koning, A.J., Rochman, D., Sublet, J.-C., Dzysiuk, N., Fleming, M., and Van Der Marck, S., 2019. *TENDL: Complete Nuclear Data Library for Innovative Nuclear Science and Technology*. Nuclear Data Sheets 155, 1–55. https://doi.org/10.1016/j.nds.2019.01.002

Lamarsh, J.R., and Baratta, A.J., 2017. *Introduction to Nuclear Engineering*, 4 edition. ed. Pearson, Hoboken, NJ.

LANL, 2018. *RSICC Code Package CCC-850: MCNP6.2: Monte Carlo N–Particle Transport Code System Including MCNP6.2 and MCNPDATA Libraries*. LANL, Los Alamos, USA.

Lewis, E.E., 2008. *Fundamentals of Nuclear Reactor Physics*. Elsevier.

Maodi, A.S., 2020. *Neutron activation characterization of the chemical elements in preparation for nuclear reactor decommissioning*. MSc . North-West University, Potchefstroom, South Africa.

Mathur, J.N., Murali, M.S., Natarajan, P.R., Badheka, L.P., Banerji, A., Ramanujam, A., Dhami, P.S., Gopalakrishnan, V., Dhumwad, R.K., and Rao, M.K., 1993. *Partitioning of actinides from high-level waste streams of PUREX process using mixtures of CMPO and TBP in dodecane*. Waste Management 13, 317–325.

Mathuthu, M., Mokhine, N.D., and Stassen, E., 2019. *Organic solvent extraction of uranium from alkaline nuclear waste*. Journal of Radioanalytical and Nuclear Chemistry 319, 687–693.

McKenzie, G.E., 2019. *Nuclear Criticality Safety Fundamentals*. Los Alamos National Lab.(LANL), Los Alamos, NM (United States).

McKibben, J.M., 1984. *Chemistry of the PUREX Process*. Radiochimica Acta 36, 3–16.

McLaughlin, Thomas P., 2003. *Process criticality accident likelihoods, magnitudes and emergency planning. A focus on solution accidents*.

McLaughlin, T.P., 2003. *Process criticality accident likelihoods, magnitudes and emergency planning. A focus on solution accidents*. Presented at the JAERI-CONF--2003-019-PT2, JAERI, Japan. http://dx.doi.org/10.11484/JAERI-Conf-2003-019-Part2

McLaughlin, T.P., 2001a. *Development and Application of Consensus Standards in Criticality Safety in the USA*. Los Alamos National Laboratory (LANL), Los Alamos, New Mexico, USA.

McLaughlin, T.P., 2001b. *Development and Application of Consensus Standards in Criticality Safety in the USA*. Los Alamos National Laboratory (LANL), Los Alamos, New Mexico, USA.

McLaughlin, T.P., Monahan, S.P., Pruvost, N.L., Frolov, V.V., Ryazanov, B.G., and Sviridov, V.I., 2000. *Review of Criticality Accidents - 2000 Revision*. Los Alamos National Laboratory (LANL), Los Alamos, New Mexico, USA.

McLaughlin, Thomas P., Monahan, S.P., Pruvost, N.L., Frolov, V.V., Ryazanov, B.G., and Sviridov, V.I., 2000. *A review of criticality accidents 2000 revision*. Los Alamos National Lab., NM (US).

Mechitoua, B., 2001. *Tokaimura Criticality Accident: Point Model Stochastic Neutronic Interpretation*. Transactions of the American Nuclear Society 84, 289–292.

Meija, J., Coplen, T.B., Berglund, M., Brand, W.A., De, B.P., Gröning, M., Holden, N.E., Irrgeher, J., Loss, R.D., Walczyk, T., and Prohaska, T., 2016. *Isotopic compositions of the elements 2013*

(IUPAC Technical Report). Pure and Applied Chemistry 88, 293–306. https://doi.org/10.1515/pac-2015-0503

Miller, T.M., Celik, C., Hopper, C., Duluc, M., Heinrichs, D., Kim, S., Brown, A., Wilson, C., and Troisne, M., 2018. *Update of the Nuclear Criticality Slide Rule Calculations: Studies with Common Shielding Materials*. Presented at the ANS RPSD 2018, Oak Ridge National Laboratory, Santa Fe, New Mexico, United States of America, p. 12.

Miller, T.M., and Peplow, D.E., 2013. *Guidance Detailing Methods to Calculate CAAS Detector Response and Coverage*. Oak Ridge National Laboratory, PO Box 2008, Oak Ridge, TN 37831-6170, USA.

Morsy, M.A., 2012. *Simple EPR/Alanine Dosimeter for Medical Application*. Open Journal of Radiology 2012, 7. https://doi.org/doi:10.4236/ojrad.2012.24022

Müller, E., 1986. *The Role of Scattering Kinematics in Neutron Slowing Down*.

Murazaki, M., Tonoike, K., and Uchiyama, G., 2009. *Re-evaluation of dose measurements under criticality accident conditions at SILENE and TRACY using TLDs*. Japan Atomic Energy Agency.

Nakajima, K., 2003. *Applicability of simplified methods to evaluate consequences of criticality accident using past accident data*.

Nakamura, T., Tonoike, K., and Miyoshi, Y., 2004. *Dose evaluation in criticality accident conditions using transient critical facilities fueled with a fissile solution*. Radiation Protection Dosimetry 110, 483–486.

Ozasa, K., Shimizu, Y., Sakata, R., Sugiyama, H., Grant, E.J., Soda, M., Kasagi, F., and Suyama, A., 2011. *Risk of cancer and non-cancer diseases in the atomic bomb survivors*. Radiation Protection Dosimetry 146, 272–275. https://doi.org/10.1093/rpd/ncr168

Parsons, D.K., 2018. *NJOY Processing of ENDF/B 8.0 Thermal Scattering Files*. Report: LA-UR-18-25096. Nuclear Data Team, XCP-5, Los Alamos National Laboratory (LANL), USA.

Peplow, D.E., and Petrie, L.M., 2010. *Criticality Accident Alarm System Modeling Made Easy With SCALE 6.1*, in: Transactions of the American Nuclear Society. Presented at the ANS-2010, Oak Ridge National Laboratory (ORNL), Oak Ridge National Laboratory, Tennessee, USA, pp. 297–293.

Physics Stack Exchange, 2020. Binding energy per nucleon. Last visited on 20 October 2020, from https://physics.stackexchange.com/questions/557583/binding-energy-per-nucleon.

Potgieter, M., Barry, J.C., van der Westhuizen, D.J., and Krieg, H.M., 2019. *Extraction of uranium from synthetic nuclear conversion plant waste*. Solvent Extraction and Ion Exchange 37, 360–375.

Potgieter, M., Van der Spoel Badenhorst, W.D., Barry, J.C., van der Westhuizen, D.J., and Krieg, H.M., 2020. *Feasibility of electro-reduction of U (VI) in oxalic acid using an electrolytic CEM-separated cell*. Journal of Radioanalytical and Nuclear Chemistry 1–6.

Preston, D.L., Cullings, H., Suyama, A., Funamoto, S., Nishi, N., Soda, M., Mabuchi, K., Kodama, K., Kasagi, F., and Shore, R.E., 2008. *Solid cancer incidence in atomic bomb survivors exposed in utero or as young children*. Journal of the National Cancer Institute 100, 428–436. https://doi.org/10.1093/jnci/djn045

Preston, D.L., Shimizu, Y., Pierce, D.A., Suyama, A., and Mabuchi, K., 2003. *Studies of mortality of atomic bomb survivors. Report 13: Solid cancer and noncancer disease mortality: 1950–1997*. Radiation Research 160, 381–407. https://doi.org/10.1667/RR3049

Putman, V.L., 2012. *Criticality Safety Basics for INL FMHs and CSOs*. Idaho National Laboratory (INL).

Ramanujam, A., 1998. *An Introduction to the PUREX Process*. IANCAS Bulletin 11–26.

Rearden, B.T., and Jessee, M.A., 2020. *SCALE Code System Version 6.2.4 Reference Manual*. Report: Report ORNL/TM-2005/39. Office of Scientific and Technical Information (OSTI), PO Box 62, Oak Ridge, TN 37831, USA.

Reed, D.A., 1991. *American National Standard Criticality Accident Alarm System*. Report: ANSI/ANS-8.3-1986. American Nuclear Society, USA.

Sato, T., 2016. *Issues on Radiation Weighting Factor*. Presented at the ICRP Symposium, Tokyo, Japan, ICRP.

Sato, T., Endo, A., and Niita, K., 2013. *Comparison of the mean quality factors for astronauts calculated using the Q-functions proposed by ICRP, ICRU, and NASA*. Advances in Space Research 52, 79–85. https://doi.org/10.1016/j.asr.2013.03.013

Skinner, C.M., 2017. *Evaluation of Energy Released from Nuclear Criticality Excursions in Process Solutions*. M.Sc. . University of New Mexico, Albuquerque, New Mexico, USA.

Sono, H., Yanagisawa, H., Ohno, A., Kojima, T., and Soramasu, N., 2001. *Measurement of Neutron and Gamma-Ray Absorbed Doses Under Criticality Accident Conditions at TRACY Using Tissue-Equivalent Dosimeters*. Nuclear Science and Engineering 139, 209–220. https://doi.org/10.13182/NSE01-A2232

Soppera, N., Bossant, M., Cabellos, O., Dupont, E., and Díez, C.J., 2013. *JANIS 4.0 JAva-based Nuclear Information System*. OECD Nuclear Energy Agency (NEA), Paris, France. https://doi.org/10.1051/epjconf/201714607006

Stacey, W.M., 2018. *Nuclear Reactor Physics*, 3 edition. ed. Wiley-VCH, Weinheim.

Stassen, L., and Suthiram, J., 2015. *Initial development of an alkaline process for recovery of uranium from 99 Mo production process waste residue*. Journal of Radioanalytical and Nuclear Chemistry 305, 41–50.

Stratton, W.R., and Smith, D.R., 1989. *Review of Criticality Accidents*. Lawrence Livermore National Laboratory, USA.

Sublet, J.-C., Eastwood, J.W., Morgan, J.G., Fleming, M., and Gilbert, M.R., 2015. *The FISPACT-II User Manual. Version 3.00*. UKAEA.

Sublet, J.-Ch., Eastwood, J.W., Morgan, J.G., Gilbert, M.R., Fleming, M., and Arter, W., 2017. *FISPACT-II: An Advanced Simulation System for Activation, Transmutation and Material Modelling*. Nuclear Data Sheets, Special Issue on Nuclear Reaction Data 139, 77–137. https://doi.org/10.1016/j.nds.2017.01.002

Sublet, J.-Ch., Fleming, M., Gilbert, M.R., Eastwood, J.W., and Morgan, J.G., 2016. *FISPACT-II: An Advanced Simulation Platform for Inventory and Nuclear Observables* 10.

Takada, J., 2012. *Chernobyl Nuclear Power Plant Accident and Tokaimura Criticality Accident*. Nippon Rinsho 70, 405–409.

Union Carbide Nuclear Company, 1958. *Accidental Radiation Excursion at the Y-12 Plant*. Report: Y-12-34. Union Carbide Nuclear Company, Oak Ridge, Tennessee, USA.

Van Rooyen, T.J., 2018. *ELIS_APP: A Utility Code to Calculate the Isotopic Compositions of Mixtures of Natural Terrestrial Elements*`. Report: RRT-VER-REP-18001. Radiation and Reactor Theory (RRT), South African Nuclear Energy Corporation (Necsa), Pelindaba, South Africa.

Vargo, G.J., 1999. *Brief History of Nuclear Criticality Accidents in Russia-1953-1997*. Health Physics 77, 505–511.

Watt, B.E., 1952. *Energy spectrum of neutrons from thermal fission of U 235*. Physical Review 87, 1037.

Yamamoto, T., and Miyoshi, Y., 2004. *Reliable Method for Fission Source Convergence of Monte Carlo Criticality Calculation with Wielandt's Method*. Journal of Nuclear Science and Technology 41, 99–107. https://doi.org/10.1080/18811248.2004.9715465

Zankl, M., Becker, J., Lee, C., Bolch, W.E., Yeom, Y.S., and Kim, C.H., 2018. *Computational phantoms, ICRP/ICRU, and further developments*. Annals of the ICRP 47, 35–44.

Zhang, W., Muirhead, C.R., and Hunter, N., 2005. *Age-at-exposure effects on risk estimates for non-cancer mortality in the Japanese atomic bomb survivors*. Journal of Radiological Protection 25, 393. https://doi.org/10.1088/0952-4746/25/4/003

Ziegler, J.F. and Biersack, J.P., 2008. SRIM-2008, Stopping power and range of ions in matter.